UNIVERSITY OF SOUTHAMPTON

SEDIMENTARY PROCESSES AND DEPOSITS ASSOCIATED WITH A COASTAL HEADLAND: PORTLAND BILL, SOUTHERN UK

Alex C. Bastos

Submitted to the University of Southampton
in fulfilment of the requirements for the
Degree of Doctor of Philosophy

School of Ocean and Earth Science
Faculty of Science

November 2002

UNIVERSITY OF SOUTHAMPTON

ABSTRACT

FACULTY OF SCIENCE
SCHOOL OF OCEAN AND EARTH SCIENCE

Doctor of Philosophy

SEDIMENTARY PROCESSES AND DEPOSITS ASSOCIATED WITH A COASTAL HEADLAND: PORTLAND BILL, SOUTHERN UK

by Alex C. Bastos

The present study investigates the sedimentary processes and deposits, associated with a coastal headland. The case study considered here is the continental shelf around Portland Bill (southern UK). A range of different scientific approaches was undertaken, in order to develop and expand upon the scientific understanding of such processes and deposits: (a) numerical modelling (including tidally-induced flow, sand transport and wave refraction); (b) *in situ* hydrodynamic measurements; and (c) geophysical surveys (side-scan sonar and using an high-resolution seismic profiler) and sediment sampling.

The presence of a sequence of sedimentary deposits, associated with a complex suite of bedforms and sedimentary facies, was observed. This sequence of deposits, described as headland-shelf deposits (HSD), have a reasonably symmetrical sigmoidal plan-view distribution, on both sides of the headland; they are described, sequentially, towards the headland, as: sand shoals, or "sand streams" (the Adamant and West Shoals); sandy/gravel flats, representing sand bypass zones (the East and West Flats); and sandbanks, associated with zones of sand convergence (Shambles and Portland Banks). The HSD are isolated laterally, but are connected longitudinally. Both shoals and banks have an asymmetric cross-section steeper towards the coast, being the main depocentres over the area.

The distribution of such facies and deposits is controlled by instantaneous gradients in bed shear stress and sediment transport rates; these are related to the transient development of headland-eddies and the associated bedload transport. Sediment transport, associated with a coastal headland, is defined by the occurrence of two conceptually-distinct zones: (a) an *inner zone*, showing sand transport towards the headland, following an increase in gradient in the sand transport rates; and (b) an *outer zone*, showing sand transport away from the headland, following a decrease in gradient in the transport rates. The boundary between these two zones defines a bedload convergence zone. At the tip of the headland, a scour zone (or zone of maximum erosion) is present.

The analysis of the sediment dynamics combined with the interpretation of the morphology and architecture of the HSD provide a significant new insight into the understanding of headland-associated sandbank formation and maintenance processes. The occurrence of such sandbanks is related to a larger sedimentary system than assumed previously. The sandbanks are the high-energy end-members of a HSD sequence. The formation of the sandbanks was found (within the present investigation) to be the result of the strong convergent component of sand transport, induced by instantaneous gradients in bedload transport rates throughout the tidal cycle. Their "tidally-induced" maintenance process is shown to be the combined result of two distinct hydrodynamic and sediment dynamic processes acting during the different phases of the tidal cycle.

An integrated analysis of sediment dynamics with morphological and architectural evidence, together with spatial distribution and nature of the bedrock, indicates that the formation, evolution and maintenance of HSD are hydrodynamically- and morphologically-controlled.

To Gabriel, my very little best friend and for someone else that might come in the near future

Wind on this ocean, rain on this land
three drops of water, one grain of sand
and I will tell you the story
as quick as I can
I've got nothing but time

Terry Callier (jazz/bluesman)

Acknowledgements

There are a lot of people that I would like to thank for their support and friendship over the last years.

I shall start with special thanks for my supervisor Prof. Mike Collins, not only for his friendly supervision, but also for his enthusiasm, "wine passion" and friendship during the last years and also for letting me "fly free". It was a great pleasure to have Dr. Neil Kenyon acting as my supervisor, as well. Thanks Neil for passing me your extensive experience and for sharing with me some good volleyball matches.

Thanks to my very good friend Dr. Doros Paphitis, for our endless discussions and for guiding me through the "small details" and the Cypriot cuisine. Dr. Adonis Velegrakis, thanks very much for your, always, insightful ideas.

This would never have been possible without the financial support provided by the Brazilian Government, through the National Council for Scientific and Technological Development – CNPq. Thanks also to the Standing Conference on Problems Associated with the Coastline (SCOPAC) for funding the fieldwork campaign.

Several organisations and Local Authorities are thanked for providing existing data: the Environmental Services of the Dorset County Council, in the name of Tim Badman; HRWallingford and Wessex Water, for making available the TELEMAC model results; BODC, for giving the wave data; Geological Survey of Canada, for providing the SEDTRANS model; Ambios Consultant, for providing current meter data; and BGS, for providing spreadsheets of sediment samples over Lyme Bay.

I want to thank everybody that helped me during the fieldwork campaign: a special thanks to John Davis, for his technical support and endless discussions about the geology of the Dorset Coast, Ana Paula, Andrey, Silvia, Oliver, Margarita, Valeria and Gabriel.

Thanks all the guys in the Sediment Dynamics Research group and the Brazilian "community" at the SOC, for sharing good and bad moments.

Thanks Chico, Tom, Vinicius, Cae, Gil, Joao, Zelia, Osvaldo, Frank, Terry and others, that inspired me during endless nights.

Thanks Mum and Dad, for showing me the way to get here: "If I've seen further, it is by standing on the shoulders of giants", *Sir Isaac Newton.*

Valeria and Gabriel, thanks for everything; you are ALWAYS there.

Assim como viver
Sem ter amor não é viver
Não há você sem mim
E eu não existo sem ***vocês***

(Tom & Vinicius)

Table of Contents

List of Figures

List of Tables

Chapter 2

Chapter 7

Chapter 1

Introduction

1.1 Background

The use of the coastal zone for recreation, tourism, port/shipping and industrial activities has increased significantly during the past decades. At the same time, it has become imperative that these areas had to be protected from being flooded, or eroded by the sea. In order to balance the necessity to protect property, without threatening the integrity of the natural coastline, scientific understanding of the marine, coastal and terrestrial processes acting over the coastal area is required; likewise, the use of creative coastal management solutions.

The management, planning and sustainable development of the coastal zone requires the understanding, by coastal managers and Authorities, of the physical processes acting and influencing the evolution of the coastal system. Within this context, studying the seabed sediment mobility and transport pathways over the inner continental shelf (water depth < 50 m), adjacent to the coast, is highly significant.

The inner shelf is considered to be dynamically, morphologically and sedimentologically contiguous with the beach and shoreface (Wright, 1995). The presence of sandbanks, sand shoals and shore-connected ridges, on the inner shelf, will have a substantial influence on regional sediment transport pathways (Whitehouse, 2001; and Williams *et al.*, 2000). Sandbanks alter significantly the hydrodynamic regime, influencing directly the physical processes along the coastline; they can create localised tidal current patterns and alter the wave propagation (Pattiaratchi and Collins, 1987).

The formation of a sandbank is associated with the accumulation of sand; this is a response to the regional sediment transport patterns and gradients (Dyer and Huntley, 1999). Moreover, once formed, sandbanks develop and can modify current patterns; in turn, they can also be modified by the prevailing current and wave regime, representing growth and maintenance processes (which can differ from the process of formation).

Sandbanks are important commercially, as potential source of material for the dredging industry. Conversely, they can be extremely important as a "sand-feed" source for the

coastline, as well as a natural coastal defence, refracting the approaching waves. At the same time, sandbank deposits can be important in providing evidence of regular and extreme events, within their internal structure. Alternating periods of deposition and erosion can be identified and related to the prevailing tidal currents and storms (Houthuys *et al.*, 1994). Moreover, within a geological time scale, sandbanks can exists as extensive oil reservoirs; hence, their characterisation and recognition in the stratigraphic records is of great interest.

A specific type of sandbank (Banner banks, or headland-associated sandbanks) occurs in association with coastal irregularities (capes or headlands) or islands. Such banks occur usually on tidally-dominated shelves and are very common around the British Isles. Their formation is considered to be related to the development of tidal eddies, due to the interaction of coastal headlands and oscillating tidal currents (Pingree, 1978; Signell and Harris, 2000).

The proximity of the sandbanks, to the coast, and their presence in shallow water areas make them: (a) a suitable focus for the dredging industry; (b) a possible site for an offshore wind farm (power generation); and (c) a risk for shipping and for the stability of pipelines and for submarine cables. Therefore, investigating such banks and their relationship to the regional sediment transport pathways is not only relevant, from a scientific perspective, but also of applied significance.

The successful outcome of such studies depends upon a well defined scientific framework (incorporating: geological and geomorphological setting; seabed morphology; unconsonlidated sediments; and hydrodynamic regime) followed by the proper application of different scientific methods (including: geomorphological and/or sedimentological indicators; field observations; and numerical simulation).

In order to investigate the formation, evolution and maintenance processes of a headland-associated sandbank, the present study distinguishes the regional context of the sandbank, in terms of its geological origin and evolution and the local and short-term hydrodynamic/sediment dynamic processes; likewise, the presence of the sandbank is discussed within the geological/sedimentological context of headland-associated sedimentary deposits, facies distribution and sand transport pathways.

1.2 The Present Study: Objectives and Methods

The present research programme involves the investigation of the sedimentary processes and deposits, associated with coastal headlands. The case study considered here is the continental shelf around the Isle of Portland, located in the English Channel (southern UK, Fig.1.1). The main objective of this study is to develop and expand the scientific knowledge of the sedimentary processes and deposits around coastal headlands, with a special emphasis on the occurrence of headland-associated sandbanks.

Towards this objective, the research has focused upon:

(i) characterising the seabed mobility and sand transport pathways over the continental shelf under investigation, for different (hydrodynamic) energy conditions;

(ii) examining sand transport processes around a coastal headland and the response of this process, in relation to the formation and evolution of tidally-induced transient eddies;

(iii) mapping the distribution of seabed sedimentary facies around the headland and examining their relationship to the prevailing hydrodynamic conditions;

(iv) investigating the morphology and internal structure of headland-associated sedimentary deposits and discussing their formation, in terms of the physical parameters that might be controlling their evolution.

At the same time, the present research aims also to interpret the sedimentary deposits, not only from a hydrodynamic or sediment transport perspective, but considering also the distribution and the morphological and sedimentological characteristics of the deposits.

Towards the objectives outlined above, a methodological framework was designed, based upon different scientific approaches; this provided various scientific insights on the study topic. The framework relies upon: (a) the application of numerical models (including a depth-averaged (tidal flow) hydrodynamic model (TELEMAC-2D), sediment transport model (SEDTRANS) and wave refraction model (RCPWAVE-CEDAS)), to simulate and predict the seabed mobility and sediment transport pathways around the headland, under different prevailing hydrodynamic regimes; (b) *in situ* hydrodynamic data collection, using a ship-

borne Acoustic Doppler Current Profiler, to determine the prevailing hydrodynamic processes over the sandbanks; (c) mapping the seabed, using side-scan sonar surveys and seabed sampling, in order to characterise the seabed sedimentary facies; and (d) use of a high-resolution seismic profiler, to identify the internal structure of the sedimentary deposits, in order to investigate their evolution and relationship to the basal substrate.

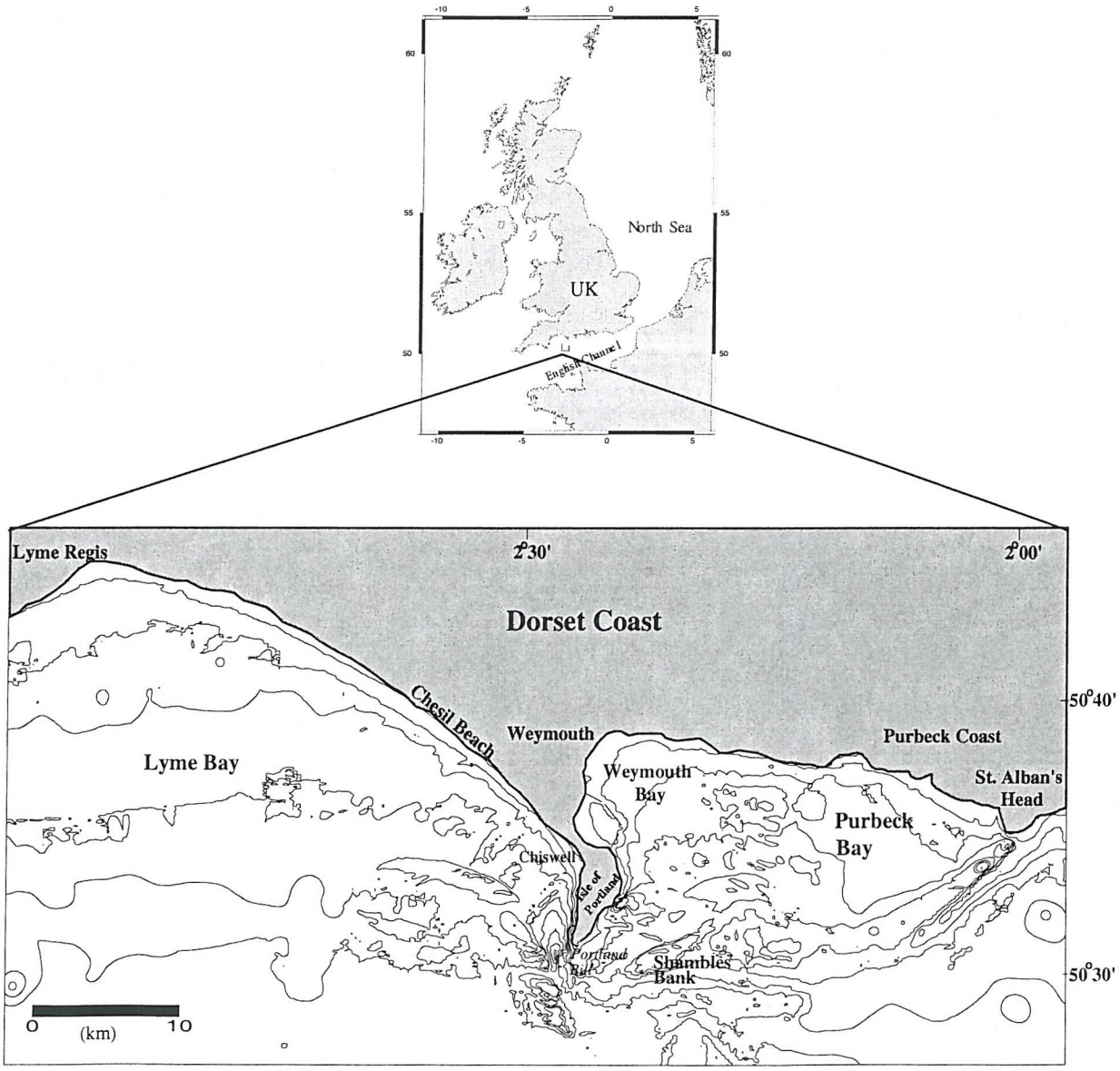

Figure1.1 Location of the study area.

1.3 Thesis Structure

The thesis is structured in three distinct parts: (i) background to the research (Chapters 2 and 3); (ii) results and discussion (Chapters 4 to 8, inclusive); and (iii) synthesis and conclusions (Chapter 9).

The first part, or the background to research, comprises Chapters 2 and 3. Chapter 2 reviews the general sedimentary processes and deposits over the inner continental shelf, together with the scientific concepts used and discussed throughout the research. Included also is the existing knowledge relating to water circulation around coastal headlands and the formation of headland-associated sandbanks. Chapter 3 introduces the regional geological, geomorphological and hydrodynamic settings of the study area, i.e. the Dorset coast and the adjacent inner continental shelf.

The results and discussion part of the thesis consists of Chapters 4 to 8; this is presented here as a collection of scientific articles and one technical report. Hence, in this part of the thesis, each Chapter has its own introduction and/or scientific background, methodology, results and discussion and/or conclusions. Chapters 4 to 8 are organised in a manner to describe sequentially the research findings of the present study. It must be noted that this sequence does not follow necessarily a chronological order of the results obtained. Hence, earlier Chapters (4, 5 and 6) may refer to a published article presented in a later Chapter (7).

Chapter 4 reviews the tidal flow patterns around headlands and explores the associated sand transport processes. Applying coupled hydrodynamic and sediment transport models, the results show a time-series of sand transport around a coastal headland, discussing the occurrence of sandbanks using patterns of water residual circulation and net bedload sand transport.

In Chapter 5, the short-term (12.4 hours tidal cycle) dynamics of a headland-associated sandbank (Shambles Bank) is investigated, by means of field measurements (synchronous data using an ADCP and side-scan sonar imaging) and hydrodynamic and sediment transport models. The process of sandbank maintenance is described in terms of along- and cross-bank velocity components, sand transport pathways and bedform asymmetries.

A seabed mobility and sand transport pathways study, using hydrodynamic, sediment transport and wave refraction models and seabed mapping techniques (side-scan sonar imaging and seabed sampling), is presented in Chapter 6. This approach explores the effect of different hydrodynamic conditions on the seabed sediment mobility and the resultant patterns of sediment transport. The application of various methods to investigate seabed mobility is discussed, together with how they increase the level of accuracy and confidence in establishing the (net and instantaneous) sand transport pathways.

In Chapter 7, the results derived from the application of numerical models are combined with morphological, sedimentological and geophysical field datasets; this is in order to relate the observed sedimentary facies distribution, around the coastal headland, with the prevailing hydrodynamic patterns. This Chapter presents also a generalised conceptual model for sedimentary processes around coastal headlands.

The morphology and architecture of the deposits, associated with the coastal headland, are examined in Chapter 8. High-resolution side-scan sonar and seismic profiles were used to investigate the bedform distribution and the internal structure of these deposits, respectively. This Chapter explores also the physical controlling parameters that can influence the evolution of such deposits.

The contribution made by the author and the different co-authors to the scientific articles is presented in a table, before each respective Chapter; this includes the following subjects: initiative for the research, data collection and analysis, interpretation and manuscript preparation.

A complete synthesis of the results obtained, throughout the investigation, is presented in Chapter 9. In this Chapter, the new findings are compared with the previous existing knowledge on the study subject; they are discussed in terms of their significance in developing and expanding the knowledge within this particular subject area. Final concluding remarks and unresolved problems, together with recommendations for future research, are presented also in this Chapter.

Chapter 2

Inner Continental Shelf Processes and Deposits: A Review

2.1 Shelf Sand Transport

The most important physical processes responsible for the transport and fluxes of sediment particles along and across the continental shelf are governed by tidally-induced currents, wave-orbital flows, wind-driven flows, buoyant plumes, density currents and internal waves (Nittrouer and Wright, 1994) (Fig.2.1).

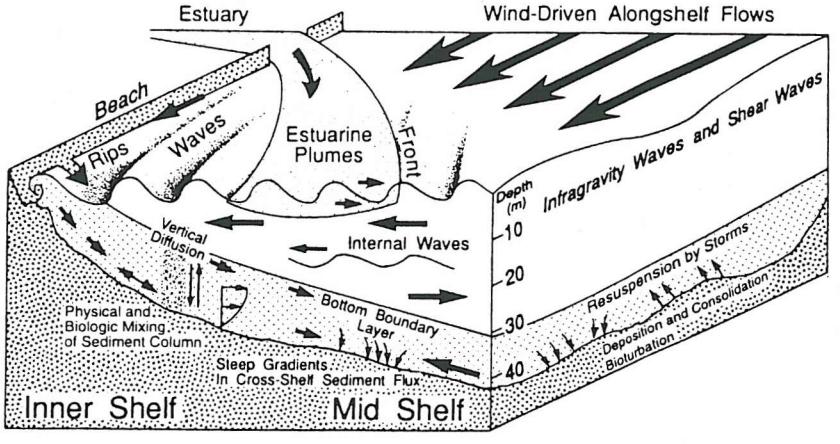

Figure 2.1 Synthesis of the physical transport processes acting on the inner shelf (Nittrouer and Wright, 1994)

In terms of flow regimes, the continental shelf can be divided into 3 regions (Fig.2.2): (a) the inner shelf; (b) the mid-shelf; and (c) the outer shelf. In a sense, the inner shelf is a frictionally-dominated flow zone, where surface and bottom boundary layers are mixed, in response to tide and wave action. The outer shelf zone (associated water depths > 100 m) is characterised by geostrophically-dominated flows, often showing a stratified water column. The mid-shelf region is considered to be a transition zone, showing increasing differentiation into surface and bottom (water) layers. Inner shelf environments can be defined as being the region lying to seaward of the surf zone, extending offshore to water depths about 30-60m. As described by Wright (1995), the inner shelf is dynamically, morphologically and sedimentologically adjoining with beaches and surf zones; secondarily, with estuaries, river mouths and tidal inlets.

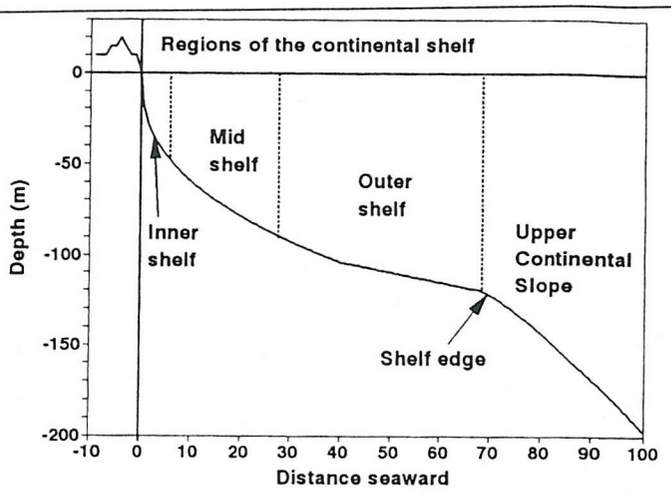

Figure2.2 Regions of the continental shelf, based upon flow regime and water depth (Wright, 1995).

Modern sedimentary processes acting along inner shelves are the result of the interaction between the flow (including waves and tidal currents) and the seabed sediments. The processes close to the bed are those of greatest significance in terms of sediment dynamics. Frictional forces are exerted by waves and currents on the seabed (bed shear stress, τ, Eq.2.1) through the boundary layer and, once the critical condition for initiation of sediment movement is exceeded (threshold of motion), sediment transport occurs (Fig. 2.3). Therefore, sediment transport is a response to the exchange of momentum between sediments and flow (Leeder, 1999).

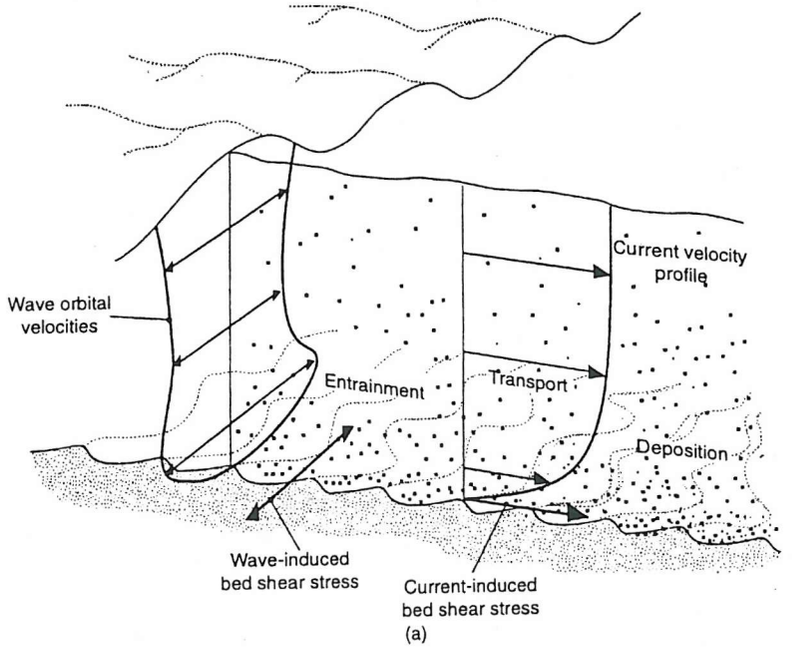

Figure 2.3 Schematic diagram of sand transport processes over the continental shelf (Soulsby, 1997).

For sediment dynamics investigations, the frictional force exerted by the currents per unit area of the seabed is, most probably, the most important parameter to be determined. This parameter is called the bed or bottom shear stress (τ), which can be described in terms of units of force per unit area (Nm^{-2}) or as units of velocity ($m\ s^{-1}$), known as friction or shear velocity (u_*). The bed shear stress and the shear velocity are defined by the equations presented below

$$\tau = \rho u_*^2$$
$$u_* = \sqrt{\tau/\rho} \qquad (2.1)$$

where u_* is the shear or friction velocity and ρ is the fluid density.

Sediment transport rates are termed the total amount of sedimentary particles moving on the bed and the water column, over a unit area, multiplied by the mean velocity of particles movement. Their spatial and temporal derivatives define the sediment dynamics. As a consequence, a combination of the processes of erosion, transport and deposition will produce the resulting morphological changes and the seabed morphology. The term morphodynamic implies the mutually-interdependent hydrodynamic processes, seabed morphology and sequences of change (Wright, 1995). The understanding and prediction of the morphodynamics is one of the most important objectives of sediment dynamic studies.

The transport of sediments, on continental shelves, is controlled by unidirectional, oscillatory and combined flows. Here, tidal currents are considered as unidirectional flows, whilst oscillatory flows are related to surface waves. A brief review on the mechanics of sediment transport under each type of flow is presented here; their distinct characteristics are described, in terms of bottom boundary layer and bed shear stress models, the threshold of movement and sediment transport rate calculations. The objective is an improved understanding of the limitations of sediment transport model application.

2.1.1 Sediment Transport under Unidirectional Flows

A fluid moving over a stationary boundary experiences frictional effects, leading to the formation of a vertical zone where a velocity gradient, orthogonal to the boundary, is formed. Within this zone, known as the boundary layer, the velocity increases from zero at the boundary ("no slip" condition) to a maximum value at the outer "free stream" zone, i.e. not

influenced by the frictional effects on the boundary. Assuming the moving fluid as a tidal current and the stationary boundary as the seabed, the processes relating to sediment transport can be described within the bottom boundary layer (BBL).

Considering the continental shelf environment, the discussion presented here assumes that the flow is turbulent, as laminar flows are rarely observed within this environment (Dyer, 1986). The parameter to establish the nature of the flow is the Reynolds Number (Re), which represents the effect of viscous to inertial forces.

$$\mathrm{Re} = \frac{Uh}{\nu} \tag{2.2}$$

Where U is the flow speed, h is the water depth and ν is the kinematic fluid viscosity ($\nu = \mu/\rho$, where μ is the molecular viscosity of the fluid and ρ is the fluid density).

The current-induced BBL can be up to tens of metres in thickness and, especially in shallow waters, can occupy the entire water column (Dyer, 1986). The BBL structure can be described in terms of the distribution of velocity, as a function of height above the bed, which is termed the current velocity profile. Hence, three regions can be recognised within the BBL (Fig. 2.4): (i) an inner region, which can be subdivided into a laminar sublayer, a viscous sublayer and a buffer layer; (ii) an overlap region or logarithmic layer; and (iii) an outer region or free stream layer.

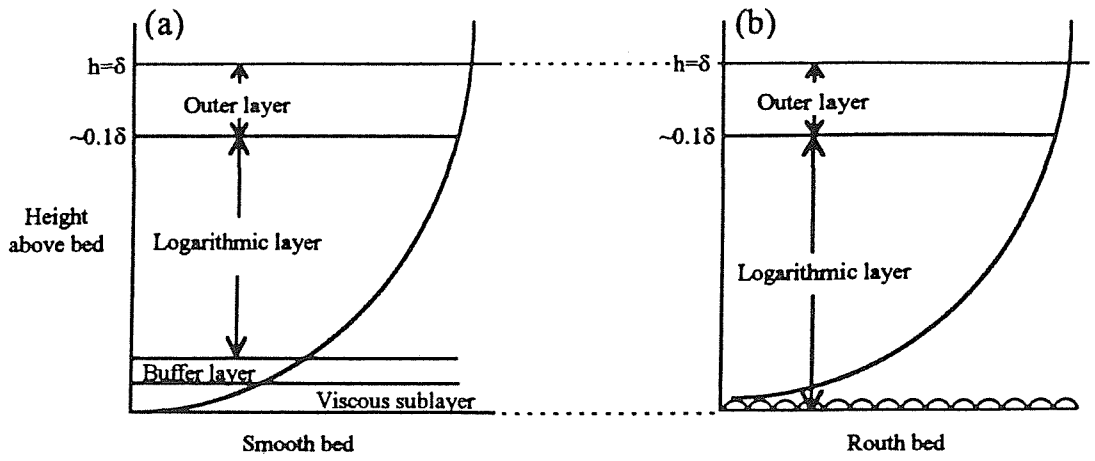

Figure 2.4 Velocity profile within the water column for an hydrodynamically-smooth bed (a) and an hydrodynamically-rough bed (b) (modified from Dyer, 1986).

In the inner region, the flow is dominated by the effects of molecular viscosity or by the roughness elements. The (turbulent) flow herein can be classified according to the roughness or grain Reynolds number, $Re_*= u_* k_s / \nu$, where k_s is the grain effective roughness height (see below). Re_* can be described as being proportional to the ratio of the grain diameter to the thickness of the viscous sublayer (δ) through the equation (Sleath, 1984),

$$\delta = 11.6 \frac{\nu}{u_*}$$
$$\mathrm{Re}_* = 11.6 \frac{k_s}{\delta} \qquad (2.3)$$

Therefore, the transition from smooth to rough turbulent flows is dependent upon the relationship between the scale of roughness elements and the thickness of the viscous sublayer.

Above the viscous sublayer, the velocity profile assumes a logarithmic form, making up the so-called logarithmic layer. Within the logarithmic layer, the speed U at a height z above the seabed, is expressed by the Prandtl-Von Karman equation,

$$U_z = \frac{u_*}{k} \ln\left(\frac{z}{z_0}\right) \qquad (2.4)$$

where k is the von Karman's constant (k=0.40, in clear water), z_0 is the seabed roughness length and u_* is the shear velocity. In rough turbulent flows, the viscous sublayer is absent and the logarithmic layer extends down to the bed. The tidal current speed can be calculated throughout the water column, by using an empirical formula (Soulsby, 1997),

$$U_z = \left(\frac{z}{0.32h}\right)^{1/7} \overline{U} \text{ , for } 0<z<0.5h \qquad (2.5)$$

$$U_z = 1.07\overline{U} \text{ , for } 0.5h<z<h \qquad (2.6)$$

This empirical relationship shows good agreement when compared to a variety of field measurements in: deep and shallow water; slow and fast currents; stratified and unstratified conditions; and flat beds and sandwaves (Soulsby, 1997). Moreover, tidal current speed can be referred as a depth-averaged current speed $\overline{U}$; this is related to the velocity profile trough

$$\overline{U} = \frac{1}{h}\int_0^h U_z dz \tag{2.7}$$

where h is the water depth, U_z is the current speed at height z and z is the height above the seabed. Above the logarithmic layer, the velocity and turbulent profile depend upon the nature of the free stream flow.

In consideration of the effects of roughness elements on the vertical structure of the flow velocity, it might be considered that the shear stress exerted on the bed is not only dependent on the flow speed, but also on the physical seabed roughness. Seabed roughness is described as the sediment properties (grain size) and the seabed morphology (bedforms). The influence of seabed roughness in the bed shear stress distribution is represented by the roughness length (z_0). It has been shown that the bottom roughness length, together with the drag coefficient and the threshold of motion (see below) may change as sand moves and ripples change their shape, during a tidal cycle (Dyer, 1980). The bed roughness can be obtained using the relationship proposed by Christoffersen and Jonsson (1985), based upon Nikuradse (1933) experimental results.

$$z_0 = \frac{k_s}{30}\left[1 - \exp\left(\frac{-u_* k_s}{27\nu}\right)\right] + \frac{\nu}{9u_*} \tag{2.8}$$

For hydrodynamically-rough flow, $z_0=k_s/30$, where k_s is the Nikuradse grain (skin friction) roughness.

The roughness length may be described as two roughness components of the seabed; the skin friction (z_{0sf}) and the form drag (z_{0fd}): $z_0 = z_{0sf} + z_{0fd}$

For hydrodynamically rough beds,

$$z_0 = z_{0sf} + z_{0fd} = \left(\frac{k_s}{30}\right) + \left(\frac{k_f}{30}\right) \tag{2.9}$$

The skin friction is produced by the sediment grains and can be measured by the Nikuradse, or grain, roughness (k_s). Nikuradse (1933) established $k_s=D_{50}$; however, several expressions were, subsequently, derived (see below).

Sleath (1991)	$k_s=2D_{50}$
Van Rijn (1993)	$k_s=3D_{90}$
Soulsby (1997)	$k_s=2.5D_{50}$

The form drag component expresses the influence of bedforms; it is produced by the pressure field associated with the flow over ripples or larger bedforms. It has been shown that τ increases, over the bedform, from the trough to the crest (Soulsby, 1997). Bedform roughness can be related to the height (η) and spacing (L) (or steepness, η/L) of the ripples (Soulsby, *op cit.*):

$$k_f = C\left(\frac{\eta^2}{L}\right), \text{ where } 1< C > 30 \qquad (2.10)$$

The roughness parameter plays an important role in the calculation of the total bed shear stress. The total shear stress may be expressed in terms of the sum of the two components; skin friction (τ_{sf}) and form drag (τ_{fd}). At very high flows, usually sheet flow conditions, a third roughness element might be taken in account, the sediment-transport contribution.

The sediment-transport contribution (τ_{st}), or bedload roughness (k_{bt} , Wiberg and Rubin, 1989; and Li *et al.*, 1997), is produced by the momentum extracted from the flow to move the grains (and by saltating grains), being related to the intensity of transport (Soulsby, 1997). In a flow transporting sediments, a portion of the flow is spent in overcoming the grain-to-grain friction force and maintaining a thin bedload transport layer (Li *et al.*, 1997). The bedload roughness may be described in terms of the thickness scale of the bedload layer (δ_{bl}), as hypothesised by Owen (1964). From Wiberg and Rubin (1989), $k_{bt} = 1.68\delta_{bl}$; or from Grant and Madsen (1982), $k_{bt} = 3.8\delta_{bl}$.

Effectively, the component that actually moves the sediments is the skin friction. However, to calculate the shear stress, assuming only the skin friction component, may overestimate the final calculations in sediment transport. Considering, for example, a current flowing over a rippled bed, the shear stress exerted on the bed is a function of the skin friction and the presence of ripples (form drag); this means that part of the shear stress acting on the bed, is

not directly related to transporting grains. The contribution of the form drag component, to the total shear stress, is shown schematically in figure 2.5.

Studies undertaken by several authors, in the laboratory or in the sea, indicate that form drag can represent up to 60% of the total applied stress (Bagnold,1963; Engelund and Hansen, 1972, Kapsdali and Dyer, 1986; and Powell, 1996). Li *et al.* (1997), based upon field observation, present a detailed discussion regarding the effect of the different roughness parameters (bedforms, saltating grains and bedload roughness) on the final calculation of the shear stress, comparing to predicted threshold values.

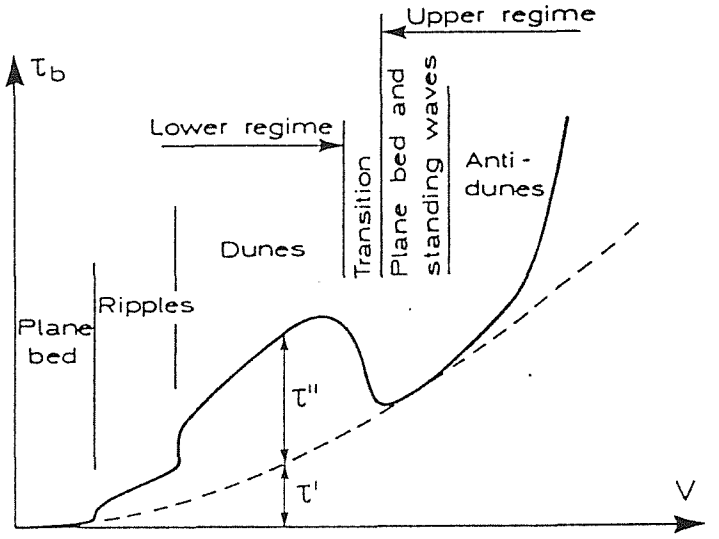

Figure 2.5 Relationship between (total) bed shear stress ($\tau_b = \tau'$ (skin friction) + τ'' (form drag)) and flow velocity, for different bed forms (Van Rijn, 1993).

Shear Stress Determination

Shear stress can be estimated by applying different methods: velocity profile; quadratic friction law; Reynolds stress; inertia dissipation method; and surface water (or total) energy slope. Here, the first three methods will be presented, due to their potential application within the present study.

The velocity profile method is based upon multi-level current speed measurements obtained within the logarithmic layer, usually using a velocity gradient rig. Current speeds are fitted to a logarithmic velocity profile curve and the roughness length (z_0) can be obtained graphically. Applying the logarithmic velocity profile equation, u_* is then calculated.

The quadratic friction law is, probably, the simplest technique available to calculate the shear stress; it is based upon a current measurement at a fixed height above the seabed, applying a quadratic friction law. In turbulent flows, it has been shown, experimentally, that the shear stress is proportional to the square of the current velocity and introducing a drag coefficient (Sternberg, 1972),

$$\tau = \rho C_D U_z^{\,2} \tag{2.11}$$

If the current is measured at 1m (100cm) above the seabed, then

$$\tau = \rho C_{100} U_{100}^{\,2} \tag{2.12}$$

where, C_D (C_{100}) is the drag coefficient, which relates the mean velocity near the bed to the applied stress. An investigation undertaken by Sternberg (1968), in the sea, has indicated that, for hydrodynamic-rough flows, the drag coefficient assumes a constant value related to the bed configuration. Hence, the shear stress can be calculated from a single measurement within the BBL, as the drag coefficient can be related to the roughness length (Sternberg, 1972). The drag coefficient is a function of the bed roughness and can be calculated through the equation (Soulsby, 1983):

$$C_D = \left(\frac{k}{\ln\left(z/z_0 \right)} \right)^2 \tag{2.13}$$

Soulsby (1983) has proposed typical values of z_0 and C_D for different bed types, based upon a large number of field measurements (Table 2.1).

The Reynold's stress or eddy correlation method is based upon measurements of the turbulent fluctuations in the velocities (Dyer and Soulsby, 1988). However, the concept of the Reynold's stress calculation is somewhat complex (see Heathershaw, 1988 and Soulsby, 1983); consequently, it will be introduced here.

Table 2.1 Mean values of z_0 and C_{100} for different bottom types (abstracted from Soulsby, 1983).

Bottom type	z_0 (mm)	C_{100}
Mud	0.2	0.0022
Mud/sand	0.7	0.003
Silt/sand	0.05	0.0016
Sand (unrippled)	0.4	0.0026
Sand (rippled)	6	0.0061
Sand/shell	0.3	0.0024
Sand/gravel	0.3	0.0024
Mud/sand/gravel	0.3	0.0024
Gravel	3	0.0047

Turbulent flows consist of random movements of eddies within the fluid, generating random fluctuations in the velocity field and in the stresses which are exerted upon the sediments (Heathershaw, 1988). Considering that the instantaneous velocities in the BBL are defined as $u+u'$; $v+v'$; $w+w'$ (where, u, v, w are the means in the x,y,z axes direction and u', v', w' are the turbulent deviations or fluctuations), then the Reynold's stresses are: $\tau_{xz} = -\rho\, u'w'$; $\tau_{yz} = -\rho v'w'$; $\tau_{xy} = -\rho u'v'$.

The xz plane is taken as the plane normal to the bed, whilst xy is the plane defining the horizontal flow direction. The τ_{xz} component defines the turbulent flux of momentum across the xz plane, which is, actually, the shear stress exerted by the moving fluid on the fluid at a lower level. An important feature, related to sediment transport, is that the contribution of $u'w'$ components to the Reynolds stresses (τ_{xz}) are large and highly intermittent (Heathershaw, 1988). This method of shear stress calculation requires high-frequency measurements, obtained, for example, by electromagnetic current meters or acoustic doppler velocimeters.

Threshold of sediment movement

As the shear stress is exerted over the bed, a critical point is reached when the sediments start to move. This critical point, when a slight increase in the applied stress will move the

sediment, is known as the threshold of sediment movement. The recognition of the sediment threshold is a very important parameter for use in the computation of sediment transport and seabed mobility.

Sediment grains begin to move when the combined resultant forces of the fluid (combined lift and drag forces) exceed the gravity force applied to the grain on the bed. This resultant force may move the grain, by lifting it over the bed or rotating the grain under a pivot angle (Middleton and Southard, 1984 and Li and Komar, 1986). In a general situation, the threshold is a function of the sediment characteristics (density, size, packing, sorting, shape), the fluid (density and viscosity) and the flow properties (velocity and shear stress) (Miller *et al.*, 1977).

Threshold curves, for the prediction of sediment transport processes and rates, have been published by several authors; these are based usually upon laboratory experiments, relating the threshold to the applied current speed or to the bed shear stress (Shields, 1936; Hjulstrom, 1939; Yalin, 1972; and others). Extensive reviews on threshold curves have been presented by Miller *et al.* (1977) and Paphitis (2001).

In an early investigation, Shields (1936) derived an experimental curve (known as Shields Diagram) after undertaking a dimensional analyses, combining sediment, fluid and flow function properties, for the definition of threshold. The Shields parameter (θ) defines the ratio of the bed shear stress acting on the grain, to the submerged specific weight of the grain; this was plotted against the grain Reynolds number, Re_* (Fig. 2.6a).

$$\theta = \frac{\tau}{(\rho_s - \rho)gD} = \frac{\rho u_*^2}{(\rho_s - \rho)gD} = f\left(\frac{u_* D}{\nu}\right) \tag{2.14}$$

Where ρ_s is the sediment density, ρ is the fluid density, g is the acceleration due to gravity (9.81m s^{-1}), D is the grain size and the relationship u_*D/ν is the dimensionless grain Reynolds number (Re_*)

The threshold condition for sediment movement is referred as the Shield criterion (θ_{cr}).

$$\theta_{cr} = \frac{\tau_{cr}}{(\rho_s - \rho)gD} \tag{2.15}$$

(Note: in this expression the shape of the grain is neglected and the curve is based upon the investigation of flat beds).

(a)

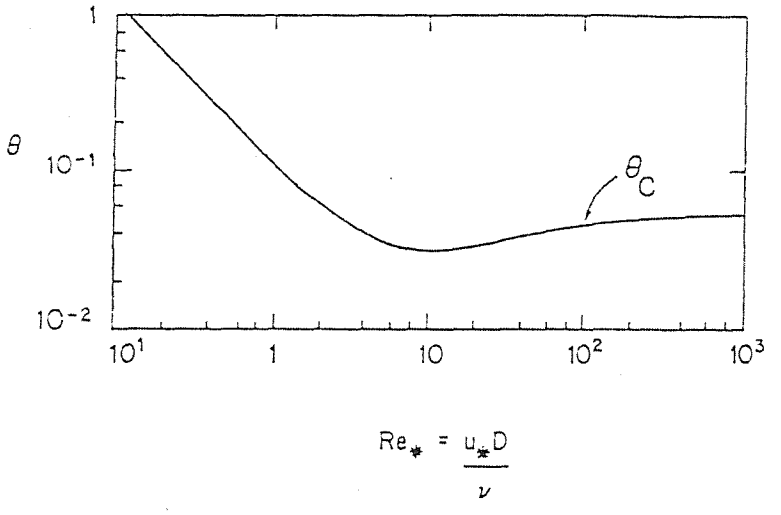

(b)

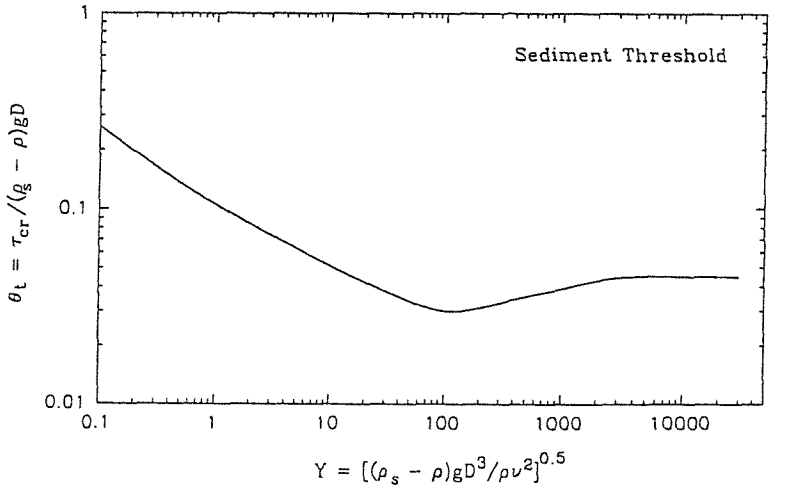

Figure 2.6 Threshold Curves: (a) Shields curve; and (b) Yalin's curve.

Miller et al (1977) have proposed a modification of the Shields curve, by reviewing experimental flume data from different sources. With these additional data, Miller *et al.*(*op cit.*) extended the curve by three orders of magnitude.

The Shields diagram has the disadvantage, in its utilisation, that u_* is presented on both axis; as such, this does not permit a direct determination of the threshold condition. Combining θ_{cr} and Re_*, to eliminate u_* from the abscissa, Yalin (1972) defined a paramater, Ξ (the Yalin

parameter), which retained only fluid and grain properties. The plot of θ_{cr} against Ξ shows a curve similar to the original curve of Shields (Fig. 2.6b)

$$\Xi = \frac{\mathrm{Re}_*}{\theta_{cr}} = \frac{(\rho_s - \rho) g D_{50}{}^3}{\rho \nu^2} \tag{2.16}$$

Consequently, a threshold condition (θ_{cr}) can be determined directly for known fluid and grain parameters, by calculating Ξ. Another alternative to the Use of Shields curve is the application of a dimensionless grain diameter (Van Rijn, 1993),

$$D_* = \left[\frac{R_*^2}{\theta_{cr}}\right] = \left[\frac{(\rho_s - \rho) g}{\rho \nu^2}\right]^{1/3} D \tag{2.17}$$

Grain-shape effects are not incorporated in the Shields diagram, despite being a very important characteristic of sedimentary particles; as such, an important parameter for use in threshold studies. An alternative approach is the use, in an expression, of the settling velocity (w_s) of a particle.

Collins and Rigler (1982) defined the Movability number (u_*/w_s), based upon the dimensionless analysis provided by Liu (1957). The Movability number, plotted against Re_*, has been used as an alternative to the Shields curve; this incorporates grain-shape effects into the determination of the threshold (Komar and Clemens, 1986; Paphitis *et al.*, 2002). Collins and Rigler (*op cit.*) deduced an empirical relationship:

$$\tau_{cr} = 1.24 w_s^{0.33} \tag{2.18}$$

Sediment threshold conditions for (non-flat) rippled beds were proposed by Kapdasli and Dyer (1986), based upon a Shields-type diagram curve provided by Bagnold (1963). Kapdasli and Dyer (*op. cit.*) showed that the Shields diagram can be applied to determine the threshold on rippled beds. In this approach, the skin friction shear stress component, at the crest, is considered instead of the total shear stress.

Van Rijn (1993) and Soulsby (1997) have presented solutions for the calculation of depth-averaged speed threshold, $\overline{U}_{cr}$. These solutions are most applicable for the consideration of

sediment transport, in depth-averaged hydrodynamic numerical models. It is assumed that the seabed is horizontal, flat and that no ripples are present. Soulsby (*op cit.*) presented the following equation:

$$\overline{U}_{cr} = 7\left(\frac{h}{D_{50}}\right)^{1/7}\left[g(s-1)D_{50}f(D_*)\right]^{1/2}$$
$$f(D_*) = \frac{0.3}{1+1.2D_* + 0.055\left[1-\exp(-0.02D_*)\right]} \qquad (2.19)$$
$$D_* = \left[\frac{g(s-1)}{\nu^2}\right]^{1/3} D_{50}$$

where s is the ratio of grain and water densities.

Sediment transport rates

Once threshold is reached, any slight increase in the applied stress (or current speed), will transport a certain amount of sediment downstream and create patterns on the seabed (bedforms). Subsequently, in sediment transport studies, sediment transport rates are investigated. Equations to calculate sediment transport rates are widely available; however, the selection of most suitable equation is still unclear (Heathershaw, 1981; Soulsby, 1997).

Existing equations relate sediment transport rates, to current speed or near-bed shear stress. Bedload transport rates can be expressed as volumetric transport rates (q_b= m^2 s^{-1}); mass transport rate (Q_b= $\rho_s q_b$, kg m^{-1} s^{-1}) and immersed weight transport rate (i_b= (ρ_s-ρ) $g q_b$, N $m^{-1}s^{-1}$).

Usually, transport rates are calculated based upon an excess shear stress or flow speed (see, for example, Heathershaw, 1988; van Rijn, 1993; Soulsby, 1997). Here, the concepts of Bagnold, Einstein (stochastic), Yalin and Engelund-Hansen will be presented, followed by the final derived equations.

Bagnold (1963). The concept of "stream power" defined by Bagnold (1956), relates the transport rate to the power expended by the fluid moving over the sediment-water interface, using an efficiency factor K.

$$q = \frac{\rho_s}{(\rho_s - \rho)g}(K\Omega) \tag{2.20}$$

The stream power parameter, Ω, is the power per unit area expended on the seabed, by the flowing fluid; it is given by

$$\Omega = \tau u_* = \rho u_*^3 \tag{2.21}$$

The efficiency factor, *K*, is dependent upon the sediment grain size and on excess shear stress; hence, *K* is a function of $(\tau - \tau_{cr})/\tau_{cr}$ for a particular sand size (Kachel and Sternberg, 1971). This modified Bagnold relationship showed good agreement with earlier flume data obtained from Guy *et al.* (1966). Gadd *et al.* (1978) removed *K*, by restructuring the velocity dependence of the Bagnold's stream power equation. Gadd *et al.* (*op cit*) obtained the following expression for (bedload) sediment transport calculation.

$$q = \beta(U_{100} - U_{cr})^3 \tag{2.22}$$

where β is a coefficient of proportionality taken from the Guy *et al.* (1966) flume experiment data. The data showed that β ranges from 1.73×10^{-3} to 7.22×10^{-5} for grain sizes of 0.18mm to 0.45mm.

Einstein (1950). The statistical approach of Einstein suggests that sediment transport is related to the turbulent behaviour of the flow, rather than to the mean velocity. This investigator describes the particle motion in terms of probability, relating the hydrodynamic lift force and particle weight (Note: Einstein does not consider a threshold condition). Another approach is the Einstein-Brown equation (Brown, 1950), which considers the particle settling velocity. This equation was obtained from flume experiments, under unidirectional flow, over well-sorted sediment (0.3-29mm).

$$q = 40 w_s D_{50} \left(\frac{\rho}{(\rho_s - \rho) g D_{50}} \right)^3 u_*^5 \tag{2.23}$$

Yalin (1972). Yalin's approach considers the average lift forces exerted on a sediment grain. The grains move by saltation and an increase in bedload discharge is not necessarily

associated to an increase in the number of grains, but an increase in the grain path length. Yalin's equation assumes a threshold condition for sediment movement.

$$q = 0.635\rho_s D_{50} u_* s\left[1 - \frac{1}{as}\ln(1+as)\right] \tag{2.24}$$

where $s=(\tau-\tau_{cr})/\tau_{cr}$, and a is given by

$$a = 2.45\left(\frac{\rho}{\rho_s}\right)^{0.4}\left(\frac{\tau_{cr}}{(\rho_s-\rho)gD_{50}}\right)^{1/2} \tag{2.24a}$$

Engelund-Hansen (1972). Engelund and Hansen (1972) approach is based upon flume experiments and it was, initially, derived for dune-covered beds. This method (which does not include a threshold condition) is widely used to calculate total load transport rates. The equation is:

$$q_t = \frac{0.04C_D^{3/2}U_{100}^5}{[g(s-1)]^2 D_{50}} \tag{2.25}$$

where U_{100} is the current speed at 100 cm above the bed.

2.1.2 Sediment Transport under Oscillatory Flows

Waves on the sea surface can be characterised by: (a) wave height (H), which is the vertical distance from trough to crest; (b) wave period (T), which is the time between two successive crests or troughs passing a fixed point; (c) wavelength (λ), which is distance between wave crests; and (d) wave celerity or speed, given by the relationship C = λ/T. Natural, or real waves in the sea, consist of a spectrum of wave heights, periods and directions. Statistical analysis of waves is used commonly for the calculation of sand transport, together into the modelling of coastal changes. A widely used statistical wave height is the significant wave height (Hs), defined as the average of the highest one third of the waves, measured over an interval of time. In terms of the wave period, the zero-crossing period (Tz) is the interval between successive crossings, in an upwards direction, of still water level.

Understanding the mechanics of wave transformation, from deep waters to shallow waters, implies the application of mathematical relationships to predict the speed of wave movement, changes in wave height with depth, and equations for the wave energy and power (Komar, 1976). In terms of sediment transport, wave theories are of great significance; these may describe the wave orbital motion and velocities near the bed, which are important parameters in the entrainment and transport of sediments. The linear "Airy" wave theory and the Stokes wave theory will now be summarised here. Wave theories for very shallow water or conditions close to breaking, e.g. solitary and cnoidal wave theories, will not be discussed here.

The linear Airy wave assumes waves of sinusoidal profile, with the wave height being much smaller than the wavelength. The theory shows that the water particles beneath the wave move in circular orbits, in deep water ($h/\lambda > 1/2$). In intermediate water depths ($1/4 > h/\lambda > 1/20$), the orbits become elliptical, with the size of the ellipses decreasing downward and becoming flat near the bed. In shallow waters ($h/\lambda < 1/20$), the ellipses have flattened to horizontal motions and the orbital diameter is constant and greater than the wave height (Komar, 1976). In shallow water, wave heights tend to increase as depth decreases. The orbital velocity is defined by:

$$U_w = \frac{\pi H}{T \sinh(\kappa h)} \tag{2.26}$$

where sinh is the hyperbolic sine function and $\kappa = 2\pi/\lambda$ is the wave number. For a list of wave equations derived from the linear theory see Komar (1976).

Stokes wave theory provides a better representation of the water particle motion in shallow water. However, it uses a more complex analysis. The theory assumes waves of (approaching) trochoidal profile, characterised by narrow crests and broad and flat troughs; this is more comparable to a wave profile moving into shallow water. Figure 2.7 shows a comparison of the theoretical bottom orbital velocity under Airy and Stokes waves.

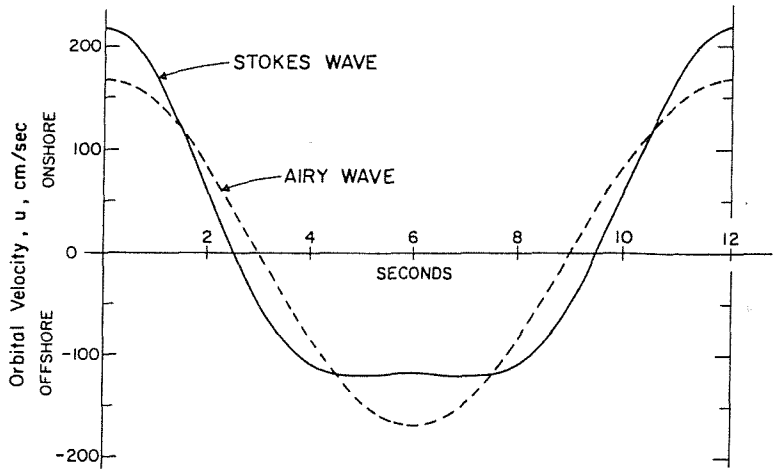

Figure 2.7 Comparison of the bottom orbital velocity under Airy and Stokes waves, using the same wave height and period (Komar, 1976).

A fundamental difference between the Stokes and the Airy theories is that, in the former, general solution for the wave profile accounts for the wave steepness, H/λ. Hence, as the waves approach shallow waters, the wave crest becomes more pronounced and the troughs flatter. Consequently, an asymmetry in the magnitude and duration of the orbital velocity is present beneath the crest and trough. Under the crests, this effect increases the magnitude, but shortens the duration of the velocity; under the troughs, the effect is reversed. This asymmetry is extremely significant for sediment transport studies, as it tends to drive sediment onshore. The orbital velocity under crests and trough is defined by:

$$U_{wc} = U_w \left[1 + \frac{3\kappa h}{8\sinh^3(\kappa h)} \frac{H}{h} \right] \tag{2.27}$$

$$U_{wt} = U_w \left[1 - \frac{3\kappa h}{8\sinh^3(\kappa h)} \frac{H}{h} \right] \tag{2.28}$$

where U_{wc} is the orbital velocity under the crest and U_{wt} is the orbital velocity under the trough. U_w is given by Equation 2.26.

As the waves move on the sea surface, frictional effects near the bed produce an oscillatory boundary layer; within this, the orbital velocity amplitude increases rapidly with height from zero at the bed to a value U_w at the top of the wave boundary layer (WBL) (Fig.2.8). The thickness of the WBL ranges from millimetres to few centimetres; this in turn, actually

enhances a much larger bed shear stress, compared to the stress produced by currents (Soulby, 1997).

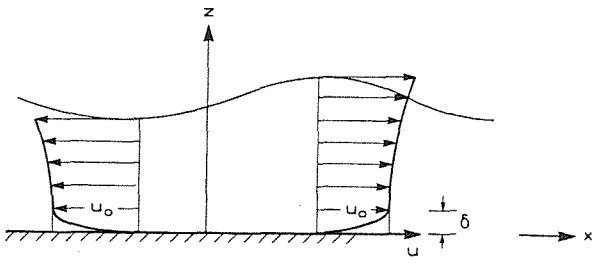

Figure 2.8 Schematic diagram of a wave boundary layer (Fredsoe and Deigarrd, 1992).

For sediment transport under waves, the parameter to be calculated or measured firstly, is the same as under current action, i.e. bed shear stress. Under waves, the shear stress is oscillatory in character and may be defined by means of a wave friction factor, f_w (Jonsson, 1966)

$$\tau_w = \frac{1}{2}\rho f_w U_w^2 \tag{2.29}$$

The wave friction factor is a coefficient relating the orbital velocity U_w, to the bed shear stress τ_w. The factor depends upon the wave Reynolds number (Re_w), i.e. whether the flow is laminar, smooth turbulent or rough turbulent and the relative roughness, r. Jonsson (1966) presents a detailed discussion of the wave friction factor and its relationship to flow properties.

$$\mathrm{Re}_w = \frac{U_w A}{\nu} \tag{2.30a}$$

$$r = A/k_s \tag{2.30b}$$

Where $A = U_w T/2\pi$ is the semi-orbital excursion and k_s is the Nikuradse equivalent grain roughness. As the occurrence of ripples is frequent under wave action, so the form drag component must be considered, in the calculation of the total wave shear stress.

The threshold of sediment movement under waves is described, usually, as a function of the near-bed orbital velocity, wave period, grain size and density. Komar and Miller (1974), defined two equations for the threshold orbital velocity:

$$U_{wcr} = [0.118g(s-1)]^{2/3} D^{1/3} T^{1/3} \text{ for D} < 0.5\text{mm} \quad (2.31)$$

$$U_{wcr} = [1.09g(s-1)]^{4/7} D^{3/7} T^{1/7} \text{ for D} > 0.5\text{mm} \quad (2.32)$$

Attempts to express the threshold of motion in terms of shear stress have also been proposed. The Shields-type diagram can be used to define the bedload threshold, by applying the wave friction factor to the shear stress (Komar and Miller, 1973 and 1974). Two relationships can be used to calculate the threshold of movement under oscillatory flows:

$$\frac{\rho U_w^2}{(\rho_s - \rho)gD} = 0.21(\frac{d_0}{D})^{1/2} \text{ for D<0.5mm} \quad (2.33)$$

$$\frac{\rho U_w^2}{(\rho_s - \rho)gD} = 0.46\pi(\frac{d_0}{D})^{1/4} \text{ for D>0.5mm} \quad (2.34)$$

where d_0 is the orbital diameter of the wave motion given by $(T/\pi)U_w$, based upon linear Airy wave theory.

Wave action on seabed sediments is related, principally, to the "stirring up" of the sediments. Net sediment transport will take place only when asymmetric velocities beneath the crest and trough occur. Hence, considering asymmetric motion, a certain amount of sediment will be transported. The net bedload transport is then defined by the difference between: (a) the half-cycle transport beneath the crest; and (b) the half-cycle transport beneath the trough (Soulsby, 1997).

2.1.3 Sediment Transport under Combined Flows

Mechanisms of sediment transport and seabed response over the continental shelf have been described, so far within the text, for unidirectional and oscillatory flows. Combined flows, i.e. waves and currents, may significantly affect the mechanisms of sediment transport, including the threshold, transport rates and net transport direction.

The complexity of combined wave and current flow arises as there is non-linear interaction between wave and current boundary layers; i.e. the shear stress exerted by the currents depends not only upon the seabed roughness, but also upon the wave boundary layer (Dyer and Soulsby, 1988). The combined wave-current BBL enhances a larger value of bed shear stress (τ_{wc}), compared to a simple linear addition of the wave-alone and current-alone stresses (Soulsby, 1997) (Fig. 2.9).

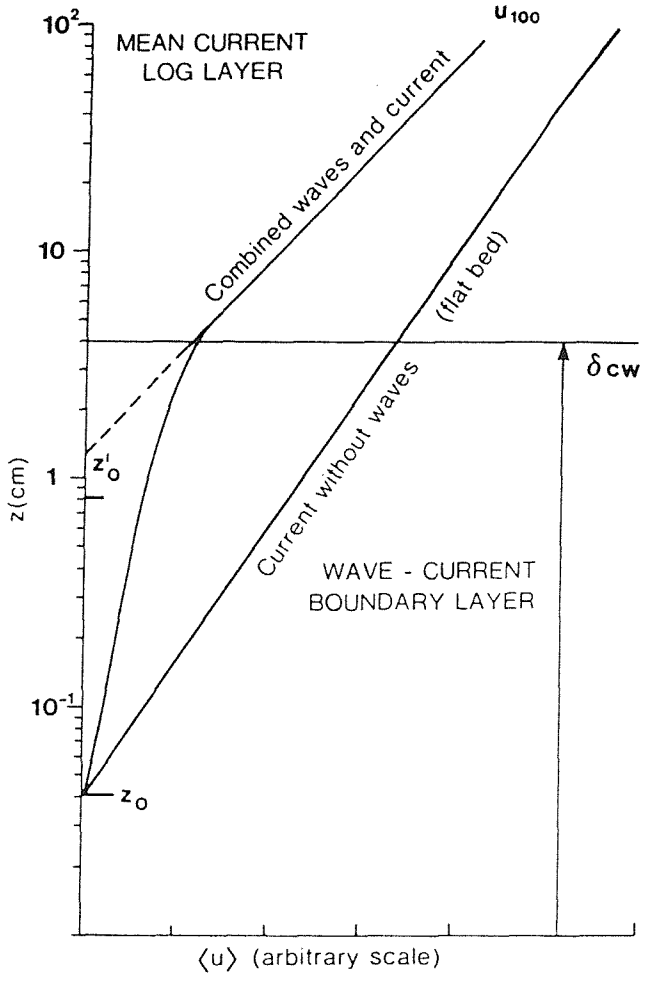

Figure 2.9 Schematic diagram showing the relationship between the current velocity profiles with or without the combination of waves (Wright, 1995).

Different theoretical approaches were applied to generate combined BBL models: (a) the eddy-viscosity distribution (Grant and Madsen, 1979 and Smith, 1977); (b) momentum-deficit integral (Fredsoe, 1984); (c) turbulent kinetic-energy closure (Davies *et al.*, 1988); and (d) mixing-length distribution (Bijker, 1967).

An intercomparision of eight different combined BBL models was undertaken by Soulsby (1993), by calculating the mean (τ_m) and maximum bed shear stresses (τ_{max}), during a wave cycle. The author found that differences between the models are usually 30-40%. Based on 61

laboratory values and 70 field values of τ_m, Soulsby (1995) tested the performance of the different parameterised models. The author found that Grant and Madsen (1979), Fredsoe (1984), Huynh-Thanh and Temperville (1991) and Davis *et al.* (1988) models gave a good performance.

Shelf sediment transport measurements, including estimates of bed shear stress, bed roughness and ripple migration, have provided a good agreement when compared to predicted results from modified Grant and Madsen (1979) and Smith (1977) models (Wiberg and Smith, 1983; Cacchione and Drake, 1990; Drake and Cacchione, 1992; and Li *et al.*, 1997). These models predicted the wave-current shear stress and the resultant near-bed velocity profiles in a combined flow, for unstratified conditions. Effects of stratified conditions, i.e. movable rough bed (bedload roughness) and suspended sediment stratification, were later considered and included (Grant and Madsen, 1982; Grant and Madsen, 1986; and Wiberg and Rubin, 1989)).

The Grant and Madsen (1986) model assumes a time-invariant eddy viscosity function, increasing linearly with z; it relates the eddy viscosity to the enhanced bottom shear stresses (shear velocity), within and above the wave-dominated portion of the combined BBL. Amongst other models, this model distinguishes three shear velocities: (a) u_{*c}, related to the mean current; (b) u_{*w}, related to oscillatory flows only; and (c) u_{*cw}, combined wave-current boundary layer flows. Hence, because of the non-linearity between current and wave friction, u_{*w} and u_{*cw} are mutually dependent and must be solved iteratively:

$$u_{*w}^2 = \frac{k u_{*cw} u_{b\max}}{\left\{\left[\ln\left(\frac{k u_{*cw}}{z_0 \omega}\right) - 1.15\right]^2 + \left(\frac{\pi}{2}\right)^2\right\}^{1/2}} \tag{2.35}$$

and

$$u_{*cw} = u_{*w}\left[1 + 2\left(\frac{u_{*c}}{u_{*w}}\right)^2 \cos\phi_{cw} + \left(\frac{u_{*c}}{u_{*w}}\right)^4\right]^{1/4} \tag{2.36}$$

where u_{bmax} is the maximum orbital velocity, ω is the radian frequency and ϕ_{cw} is the angle between waves and currents.

Sediment threshold under combined flows may be determined by the Shields parameter, as suggested by Amos *et al.* (1988), Cacchione and Drake (1990) and Soulsby (1995). Note that for rippled beds, only the skin friction component of total stress may be applied. Soulsby (*op cit.*) presents a Shields-type diagram for sediment threshold beneath waves and/or currents, showing that, providing the right calculation of shear stress and bed roughness, the Shields criterion is applicable for any flow condition.

The prediction of sediment transport rates under combined flows still requires further investigation and analysis in terms of defining a suitable transport formulae. Many of the formulae were derived originally for unidirectional flow conditions, i.e. not considering wave action. In a sense, sediment transport (bedload) is a result of the mean flow exceeding a threshold value, or of wave re-suspension and subsequent transport by the mean current (Bagnold, 1963). Therefore, not accounting for the presence of waves when estimating the shear stresses, i.e. ignoring the interaction of waves with currents, implies lower estimation of sediment transport rates (Wiberg and Smith, 1983).

An assessment of available formulae was undertaken by Pattiaratchi and Collins (1985), comparing measured transport rates (based on fluorescent sand tracer techniques), with 10 different transport equations. The results showed a significant variation in the transport rate prediction and, in general, that the predicted rates were lower than the measured rates. More recently, Powell (1996) compared ripple migration measurements to predicted rates from 10 different formulae. This author found that the results can differ by two or three orders of magnitude.

Attempts to compare measured (estimated, on the basis of ripple migration) *in situ* transport rates to predicted-formulae rates, were also undertaken by Amos *et al.* (1988), Cacchione *et al.* (1994) and Li *et al.* (1997). In general, good agreement was not found.

However, different methods have been proposed also to calculate sediment transport rates under wave and currents. Bijker (1967) presented a method based upon time-averaged variables, following the approach of Einstein (1950). Swart (1976) modified Bijker's model by assuming a function of bed roughness and using the wave friction factor from Jonsoon (1966). van Rijn (1993) and Soulsby (1997) have also proposed different equations to estimate transport rates, under combined flow conditions. Nevertheless, shelf process investigations have proven that an ideal or suitable transport formula is still required.

Although the prediction of sediment transport rates is still unclear for wave-current flows, this interaction is particularly relevant and applicable to shelf sediment transport studies. In relation to net sediment transport pathways, the wave component may influence both the rates and direction of net sediment movement. Pattiaratchi and Collins (1988) have demonstrated that, under wave action, principally storm conditions, sediment transport can reverse in comparison to tidal currents alone.

Therefore, wave action needs to be considered, even in relation to tidally-dominated shelves, in order to develop an improved understanding and prediction of long-term shelf sediment erosion-transport-deposition and coastal stability.

2.2 Shelf Sedimentary Facies

2.2.1 History of Research

The study of sediment distribution over continental shelves can be dated back to the beginning of last century. In 1919, the "profile of equilibrium" theory suggested by Johnson, based upon a grain size-graded shelf (sediment grain size decreasing seaward), was probably the first concept to describe a shelf sedimentation process. Later, Shepard (1932) and Emery (1952), showed the patchy distribution of different sediment textures over continental shelves, suggesting that this distribution is a product of Pleistocene sea-level changes, i.e. unrelated to modern processes. These deposits were denominated as *relict* sediments and, as such, they are in a non-equilibrium state in respect to the shelf modern processes.

A pioneering investigation, to relate seabed morphology and modern processes, was presented by Van Veen (1935) in studying the Southern North Sea. Van Veen described bedforms and associated them with prevailing tidal currents. About 30 years later, Stride (1963), Belderson and Stride (1966) and Kenyon and Stride (1970) presented the concept of "tidal current-swept shelf sediments", based upon sediment and bedforms distribution and their relationship to tidal currents. Swift (1970) recognised three shelf sedimentary facies based upon sediment characteristics: (a) shelf relict sands, which are associated with a very thin and discontinuous (transgressive) lag deposit overlying pre-Holocene deposits (relict sediments show no reworking by present hydrodynamic processes); (b) modern sand prism, consisting of nearshore sands, in equilibrium with present prevailing hydrodynamic conditions; and (c) a modern shelf mud sheet, associated with modern (fine-grained) sediment supplied from river deltas. Subsequently, Swift *et al.* (1971) introduced the term *palimpsest*, to sediments showing characteristics of modern and relict environments.

2.2.2 Facies and Bedforms

In general, continental shelves can be divided into tidally- and storm- (or wave) dominated shelves. The latter are described as those showing a low tidal range (usually < 2 m) and associated weak tidal currents. In terms of sedimentary regimes, two main types of continental shelf are recognised (Swift and Thorne, 1991): (a) an accommodation-dominated regime,

which is associated with high rates of sediment dispersal and is characterised by shoreface erosion and sediment bypass, seabed sediment reworking and modern deposits overlying a erosional transgression surface (e.g. English Channel and North Sea); and (b) a supply-dominated regime, which is characterised by high rates of sediment input, usually through deltaic river mouths (e.g. Louisiana and Amazon shelves). Considering the nature of the present study, this review will concentrate upon sedimentary facies and deposits in tidally-dominated shelves, associated with an accommodation-dominated sedimentary regime.

On tidally-dominated continental shelves, sands are swept by strong tidal currents, resulting in seabed erosion and bedload transport as longitudinal or transverse bedforms. The investigations of Stride (1963), Belderson and Stride (1966) and Kenyon and Stride (1970) have identified the net bedload sediment transport direction on the shelf around the British Isles, based upon: (i) the asymmetry of the surface peak currents, i.e. difference between the peak current speeds during an equal ebb and flood duration; (ii) the elongation of the tidal current ellipse; (iii)bedform distribution, considering the asymmetric profile of transverse bedforms with the steeper side showing the direction of transport (sandwaves) and the direction of longitudinal bedforms (sand ribbons); and (iv)sediment grain size distribution.

In terms of bedforms and their significance, in indicating net sand transport, Belderson *et al.* (1982) developed a model to predict the development of a suite of bedforms reflecting a decrease in the current strength (for both high and low levels of sand supply). A generalised model, disregarding sediment supply, corresponds to the following sequence, as the current speed decreases (Fig. 2.10): furrows and gravel waves → sand ribbons → large sand waves → small sand waves → rippled sand sheet and sand patches. In relation to a high sand supply model, the development of sandbanks is likely to occur.

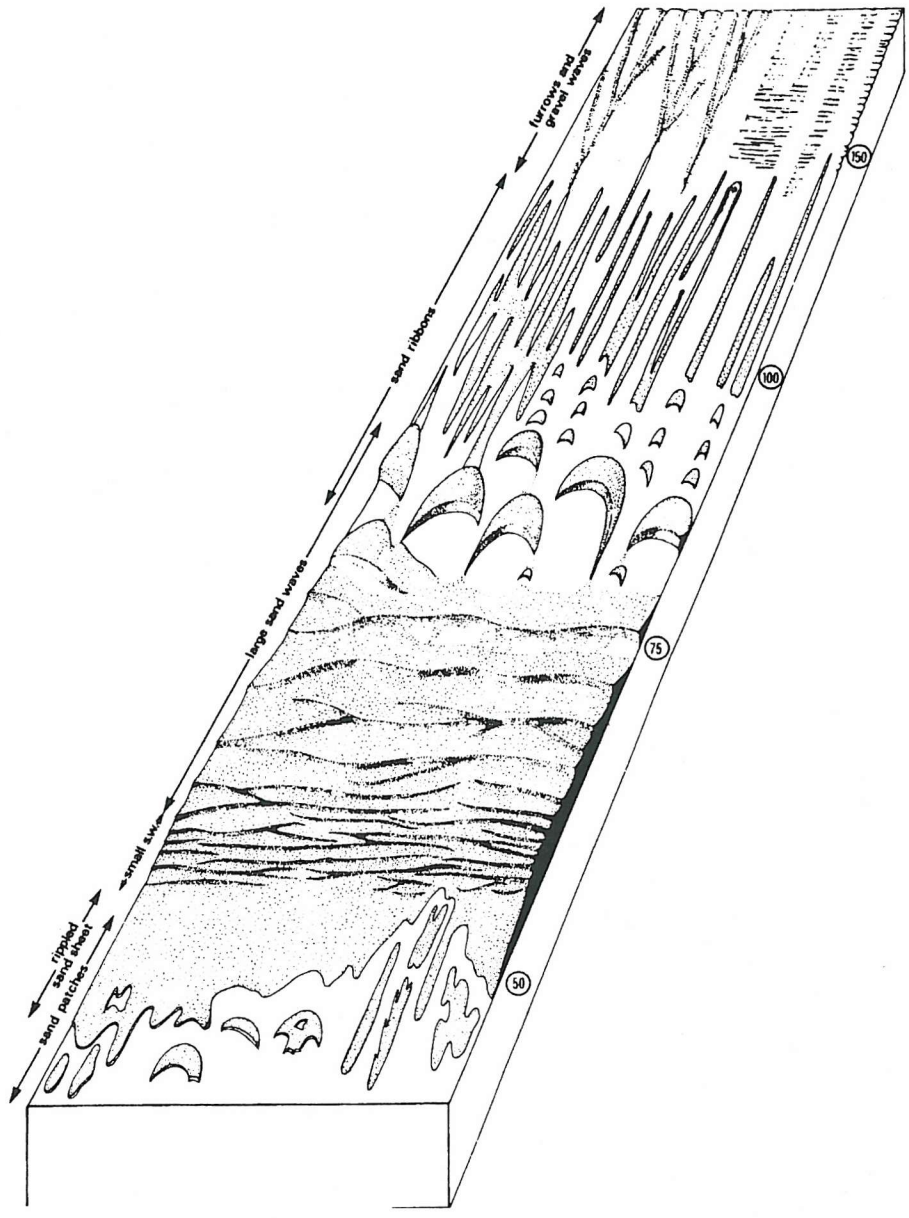

Figure 2.10 Diagram showing the "general" development of a sequence of bedforms as a function of (tidal) flow speed, on the continental shelf (Belderson *et al.*, 1982). The flow speed in the diagram indicates the peak surface current speed.

A conceptual model for sand dispersal around the British Isles, extended to more generally tidally-dominated environments, has been described by Stride and co-workers (Stride, 1963; Belderson and Stride, 1966; and Kenyon and Stride, 1970) in terms of divergent and convergent zones of transport. "Bedload parting zones" are referred to as zones of divergent sand transport, leading to seabed erosion, whilst "bedload convergence zones" are dominated by sand deposition. Pingree and Griffiths (1979) have shown that the distribution of the maximum and mean bottom stresses around the British Isles was very similar to the transport paths presented by Stride and co-workers. The former investigators concluded that the interaction of the M2 and M4 tidal constituents determines the sand transport pathways

around the U.K. Using a coupled hydrodynamic and sediment transport numerical model, Grochowski *et al.* (1993) predicted the sediment transport pathways for the English Channel; their results showed a very similar pattern of sand dispersal for the Channel, specially the existence of a bedload parting zone within the middle part of the Channel. These findings reinforced the conceptual model proposed earlier.

The concept of bedload parting zones refers to an eroded basal bed, associated with maximum current speeds, from where sediment is winnowed downstream and a depositional sequence of bedforms is generated, following a decrease in bottom stress. From such a zone, sand ribbons and scattered dunes are observed, grading into a sandwave field or linear sandbanks and, finally, to muddy sand sheet deposits.

Harris *et al.* (1995) have discussed the significance of bedload parting zones, suggesting a model for the development of scour zones, as a function of sediment supply and maximum bottom stress. Scours zones are produced by advective and/or diffusive processes, in association with maximum bottom stress; they are correlated always with the lag-gravel/bedrock members of a facies succession. The parting zones are associated with advective processes, related to asymmetries in the tidal wave; they do not necessarily correspond to a specific sedimentary facies. These investigators proposed a "staged" evolutionary model for scour zones: mutually evasive; incipient; partial; and complete. According to this analysis, a bedload parting zone is a special case of a scour zone, i.e. the complete one; here, the distribution of maximum bottom stress coincides with divergent sediment pathways.

Shelf Deposits

The floor of the inner continental shelf is subject to the combined processes of erosion, transport and deposition of sedimentary material. Modern inner shelf deposits are formed by the reworking of lowstand (or early transgressive) deposits, and/or sediment input from the coast. In general, two main types of modern sand deposits are found over the inner shelf, disregarding its hydraulic-dominated regime: (a) transgressive and tidal sand sheets; and (b) sandbanks and shore-connected sand ridges. The nature of these deposits is controlled by energy levels of the dominant hydraulic regime (tidally- or storm- dominated shelf) and

accretion/erosion rates associated with the sedimentary regime (supply- or accommodation-regime).

Tidal sand sheets are tabular sand bodies that occur over extensive areas of the seafloor. In the Southern Bight of the North Sea, it extends over 100 km and can reach up to 10 m in thickness (Stride *et al.*, 1982). They develop in association with bedforms (no sandbanks) and usually show a sequence of distinct bedforms in relation to the tidal current strength.

A more detailed review on sandbanks is presented in the next Section (see below).

2.2.3 Inner Shelf (Tidal) Sandbanks

Generally, sandbanks are the result of the combination between abundant sand availability and strong currents capable of moving sediments (Off, 1963); they are sedimentary bodies found on tidally and wave-dominated continental shelves and within coastal areas. The formation of a sandbank is associated with the accumulation of sand; this is, in fact, a response to the regional sediment transport pattern and gradients in the transport rates. Sand accumulation is likely to occur due to bedload convergence or a decrease in the bed shear stress along the transport pathway (Dyer and Huntley, 1999). However, once formed, sandbanks develop and can modify the associated current patterns; they can bed modified also by currents and waves, representing growth and maintenance processes, which can be different from the process of formation.

There are different types of banks, in relation to their morphology and regional setting (e.g. Off, 1963, Caston, 1972; Swift, 1975; Kenyon *et al.*, 1981; Collins *et al.*, 1995; and Berne *et al.*, 1994), as well as, different proposed mechanisms describing their origin and maintenance (e.g. Houbolt, 1968; Smith, 1969; Caston, 1972; Pingree, 1978; Huthnance, 1982 a,b; Pattiaratchi and Collins, 1987; and Hulscher *et al.*, 1993).

Off (1963) described rhythmic linear sand bodies caused by currents based upon world-wide occurrences. Swift (1975) distinguished two different types of sandbanks, based upon Off's description: estuarine or embayment ridges (parallel to the axis of the embayment or estuary) and ridges off capes and promontories (coast-parallel, tending to be elongated normal to the shore). A third type was described by Swift (*op. cit.*), as occurring on shelf edges.

Pattiaratchi and Collins (1987) described seven different categories of sandbanks, considering the orientation of the adjacent coastline and the direction of the prevailing currents: fields of sandbanks off open coastlines, lying parallel or oblique to the coastline and oblique to the tidal current direction; sandbanks adjacent to convergent and divergent coasts; sandbanks perpendicular to embayment heads or delta fronts; isolated sandbanks associated with coastline irregularities (capes, headlands); and spit derived banks of individual orientation..

Subsequently, in an extensive review of sandbank origin and classification, Dyer and Huntley (1999), suggested a generic classification based upon sandbank origin and development. These authors pointed out the necessity to distinguish the regional context of the bank, in terms of their geological origin and development, and the local and short-term hydrodynamic processes. Three different types were proposed: open shelf ridges (Type 1); estuary mouth (Type 2, ridges and tidal deltas); and headland-associated banks (Type 3, banner banks and alternating ridges).

Sandbanks are considered to be hydrodynamically-controlled systems, which link their formation and maintenance processes to the prevailing hydrodynamic conditions and relative sea-level rise; they, in turn, can be described as active or moribund sand bodies (Kenyon *et al.*, 1981), depending upon their bathymetric setting, in relation to the prevailing hydrodynamic forces. Theories for the origin and maintenance of sandbanks usually fall into two broad categories (Dyer and Huntley, 1999): (a) relict features, created during the post-glacial sea-level rise; and (b) formed as a response to the hydrodynamic and sedimentary regimes, similar to those presently active.

Regarding "tidal" sandbank formation and maintenance, different mechanisms have been proposed: the spiral flow concept (Houbolt, 1968); the bed shear stress stability model (Smith, 1969); the seabed stability model (Huthnance, 1982 a, b); and the "tidal stirring" or "teacup effect" (Pingree, 1978; and Pingree and Maddock, 1979).

The spiral flow, bed shear stress stability and "tidal stirring" concepts are based upon the occurrence of secondary flows, which will produce sand convergence near the bed and towards the bank crest. The stability model applies a coupled hydrodynamic and morphodynamic system, whilst the standing edge waves considers long-period wave motion.

Houbolt (1968) observed changes in current speed across successive parallel sand ridges in the North Sea. This investigator observed a decrease in current speed towards the crest of the bank, followed by an increase towards the swales. To balance the difference in the velocity field, Houbolt (*op cit.*) suggested the presence of a secondary circulation system characterised by two counter-rotating helical flows. These helical flows would lead to near-bed currents directed towards the bank crest. The presence of secondary flows around sandbanks has been observed elsewhere (Heathershaw and Hammond, 1980); however, the spiral flow concept can not explain the initial formation of the sandbank, instead it can describe a maintenance process.

The shear stress stability model proposed by Smith (1969) extends a theory that was developed originally for the formation of sandwaves. The theory is based upon a "phase lag" between shear stress and topography, i.e. for a current flowing across a bedform, maximum shear stress will occur upstream from the bedform crest, leading to erosion and, consequently followed by deposition downstream of this maximum stress zone. This theory might be relevant to the formation and migration of sandwaves (Hulscher, 1996), but it is inappropriate for application to sandbanks.

The "tidal stirring" concept proposed by Pingree (1978) refers only to the formation of headland-associated banks (Type 3), as flow passing headlands will create tidal eddies. The author demonstrates that these residual eddies will generate secondary flows; these, in turn, will converge near the bed and, consequently, lead to the accumulation of sand. This concept is reviewed in more detail later (Section 2.3.1).

The stability model proposed by Huthnance (1982a, b) is based upon the stability of a coupled morphodynamic model (including depth-averaged currents, bedload transport and bed slope), to perturbations in the seabed elevation. This concept has been widely used, developed and applied elsewhere (de Vriend, 1990; Hulscher *et al.*, 1993; Trowbridge, 1995; Hulscher, 1996; Calvete *et al.*, 2001; and Hulscher and van den Brink, 2001), especially to explain the formation and maintenance processes of open shelf linear sandbanks. The stability model assumes: (a) an initial perturbation on the seabed; and (b) that the currents are flowing at an oblique angle towards this perturbation.

The growth of a sandbank, inclined to the mean flow, can be explained by the veering of the current vector towards the bank crest, resulting in sand transport towards the crest (Fig.2.11).

The veering of the current occurs due to acceleration of the across-bank flow component, as the flow approaches the bank obliquely. In terms of continuity, the along-bank flow component has to decrease, leading to the current veering. In a reversal tidal current regime, these dynamical conditions lead to the convergence of sediment transport towards the bank crest. In the absence of any wave activity and infinite sand supply, the model predicts growth of the bank, up to the sea surface.

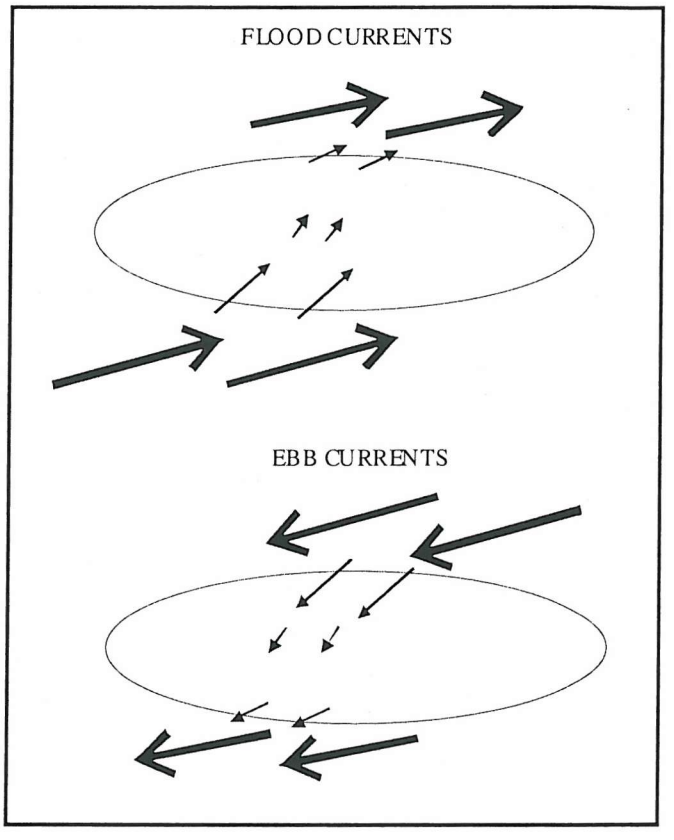

Figure 2.11 Mechanism of sandbank formation proposed by Huthnance (1982). The model predicts the veering of the current vector towards the bank crest, due to bottom friction; this results in sand transport towards the crest.

Huthance's model predicts also that if a velocity asymmetry in the tidal current is present, the model would predict the sandbank to have an asymmetric profile with the steeper side pointing towards the direction of net sand transport, as suggested previously by Kenyon *et al.*(1981).

The flow pattern around a sandbank can be described also in terms of vorticity generation and advection (Zimmermann; 1981; and Robinson, 1983). As the flow approaches the bank, from deeper to shallower waters, a bottom frictional torque is induced; consequently, vorticy is generated. If, for example, a bank in the northern hemisphere is orientated anti-clockwise with respect to the direction of the mean tidal flow, clockwise vorticity is generated as the currents

flow towards the bank crest and anticlockwise vorticty is formed as the flow leaves the bank crest (Fig. 2.12). This pattern occurs during ebb and flood phases of the tide. Huthnance's model for sandbank formation can explain either formation, growth or maintenance processes.

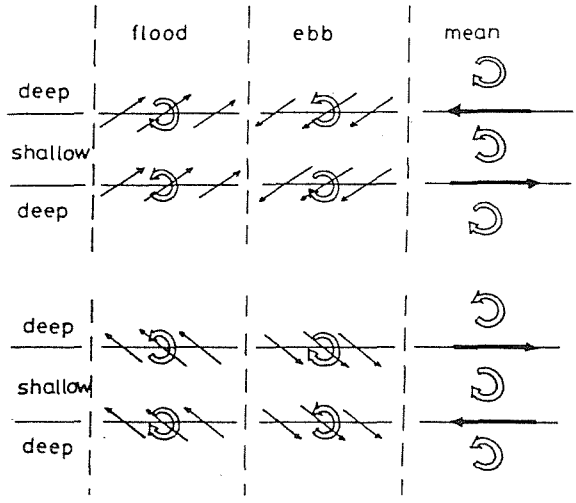

Figure 2.12 Different patterns of vorticity generation, within tidal flow over a sandbank (Robinson, 1983)

However, the importance of waves towards the maintenance of a sandbank, particularly under storm conditions, cannot be underestimated. Several researchers have highlighted the importance of storm waves in the evolution and migration of sedimentary deposits in general, and especially sandbanks (Ferentinos and Collins, 1980; Houthuy *et al.*, 1994; Berne *et al.*, 1994; and Tessier *et al.*, 1999). Under storm condition the crest of the bank is reworked by the action of waves, which act as catalysts by lowering (or just controlling) the height of the sandbank. Moreover, these high energy events are associated also with a significant increase in bed shear stress, which results in a higher mobility of the seabed; consequently, higher rates of sand transport (Pattiaratchi and Collins, 1988).

The evolution of a sandbank can be assessed also in terms of its stratigraphy, or internal structure. The seismic records of the Well Bank and Smith's Knoll (Norfolk Banks, North Sea), presented by Houbolt (1968), were the first (known to the author) recognition of sandbank structure; these showed relatively gentle (5°) and inclined reflectors, lying parallel to the steepest flank of the bank. Houbolt (*op. cit.*) observed also that the Well Bank rests upon a flat surface, supporting the concept of an hydrodynamically-controlled formation.

Based upon their stratigraphic evolution, three different types of sandbanks were recognised (Berne *et al.*, 1994 and Berne *et al.*, 1998) and considered as a continuum (Fig.2.13); these are described below.

(a) The "Houbolt sand accumulation model", or sandbanks resting on a (transgressive) flat surface and related to a convergent pattern of sediment transport (e.g. Well Bank (Houbolt, 1968); Kwintebank in the Southern North Sea (De Moor, 1989); and the "moribund" East Bank in the North Sea (Davis and Balson, 1992);

(b) Sandbanks presenting a "core" of older deposits. In this case, the sandbank facies (as described by Houbolt (*op cit.*)) is restricted to the upper seismic units. The shape of this type of bank is associated with erosional processes and the reworking of underlying deposits (or lower stratigraphic units). Examples of this type of bank are: the Brown Ridge and the Zeeland Group in the North Sea (Houbolt, 1968; D'Olier, 1981; and Laban and Schuttenhelm, 1981), tidal sand ridges in the East China Sea (Yang and Sun, 1988) and the Middlekerke Bank in the southern North Sea (Berne *et al.*, 1994)). Snedden and Dalrymple (1999) associate this "sedimentary core" to the initial perturbation on the seabed assumed by Huthnance (1982) stability model.

(c) Sandbanks considered as an end member unit. The moribund banks in the Celtic Sea best represent this type of Bank (Kaiser-I-Hind Bank, Celtic Sea (Berne *et al.*; 1998)). The formation of these sandbanks reflects a reshaping of pre-existing deposits, rather than a response to a bank-growth process. The banks (or ridges) have been sculpted from former lowstand deposits, or early transgressive deposits.

For the present study, the most suitable model to explain the formation of the sandbanks around headlands is the "tidal stirring" concept. This concept is reviewed here, in relation to sediment transport and deposition processes. Nevertheless, the spiral flow concept, the bed shear stress stability and the seabed stability model should also be considered, principally, as maintenance processes.

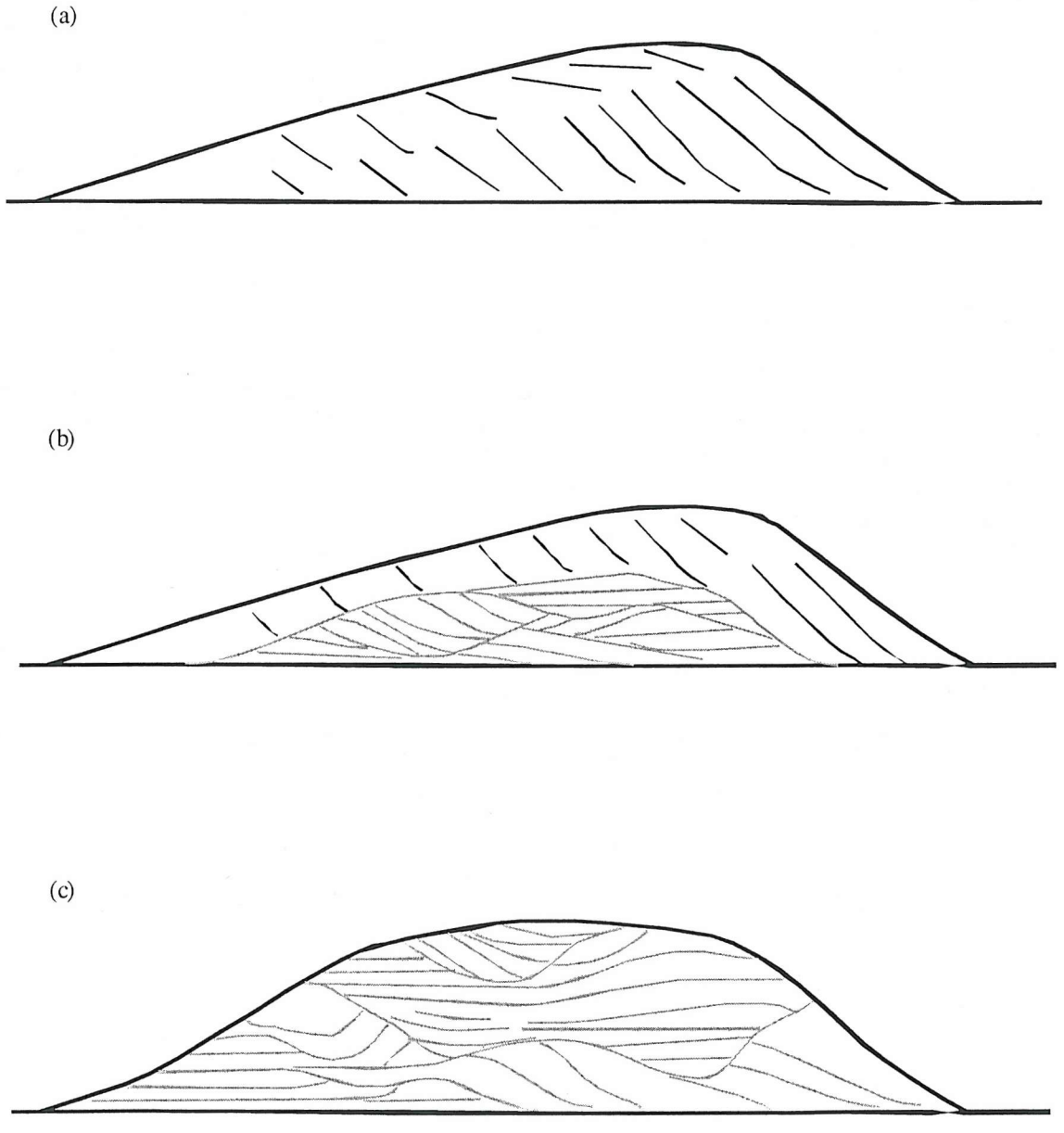

Figure 2.13 Schematic representation of three different types of sandbanks based upon their internal structure: (a) Houbolt sand accumulation; (d) sandbanks with a sedimentary "core" (see text); and (c) sandbanks as end member units. (Note: grey lines represent seismic facies that are not related to sandbanks facies).

2.3 Headland-Associated Sandbanks

2.3.1 Tidal Flow Around Headlands

The physics of tidal flow around headlands is described here, in terms of: vorticity generation; the development of tidal eddies; and the occurrence of secondary circulation. However, initially, a brief introduction to residual currents is presented.

Residual Currents

Residual flows can be generated by asymmetries in the tidal flow, wind stresses on the sea surface and lateral density gradients (Robinson, 1983). The formation of tidal residual circulation is associated with oscillatory tidal current asymmetry. Zimmerman (1981) has pointed out that the formation of residual tidal circulation can be explained as a transfer of vorticity, from the tidal oscillating current field to the mean current field. For shallow water areas, this investigator showed that irregular bottom topography and coastal geometry are necessary conditions to produce a spatial variation in the tidal stress and, as a consequence, generate vorticity.

Tidal residual currents are obtained by considering the mean flow over the tidal cycle. In shallow waters, where the vertical structure of the flow can be usually ignored (neglecting baroclinic motions), the tidal flow can be treated in two dimensions or as a depth-averaged velocity. The Eulerian instantaneous depth-averaged velocity, at a location x, is given by

$$\overline{U} = \frac{1}{h+\zeta}\int_{-h}^{\zeta} U_h(z)dz \tag{2.37}$$

where h is the mean water depth, ζ is the tidal elevation and $U_h(z)$ is the local horizontal component of velocity, at height z (above the bed). The Eulerian residual current, at the same position, can be calculated over a specific period (t), using

$$\overline{U}_{res} = \frac{1}{t}\int_{0}^{0+t}\left(\frac{1}{h+\zeta}\int_{-h}^{\zeta} U_h(z)dz\right)dt \tag{2.38}$$

The presence of residual currents over a specific coastal area indicates that the current velocity is asymmetric about the mean; hence, if the current velocity is asymmetric, this area

will be characterised by a flood or ebb current dominated pattern. This pattern implies that a net sediment transport patterns can be observed (Fry and Aubrey, 1990).

Tidally/Headland-Induced Eddies

The interaction between coastal headlands and oscillating tidal currents results in the formation of tidal eddies. When a tidal flow passes a headland, a bottom frictional torque is induced, by increased velocity near the headland producing vorticity. Vorticity is advected, subsequently, into the flow leaving the headland; this creates a tidal eddy system on the downstream side, during the flood and ebb phases of the tide (Pingree and Maddock, 1979; Robinson, 1983; Zimmerman, 1981; Geyer and Signell, 1990) (Fig.2.14).

The process of eddy formation can be explained in terms of the depth-averaged vertical component of vorticity (Pingree, 1978; Zimmerman, 1981; Robinson, 1983; Signell and Geyer, 1991). Consequently, a brief introduction to the vorticity equation is presented, based upon the work of Signell and Geyer (1991).

Assuming that the water is of constant density, the depth-averaged momentum (2.39) and continuity (2.40) equations can be expressed as

$$\underset{1}{\frac{\partial \overline{U}}{\partial t}} + \underset{2}{\overline{U}.\nabla\overline{U}} + \underset{3}{f(\hat{k}\times\overline{U})} = \underset{4}{-g\nabla\zeta} - \underset{5}{\frac{C_D}{h+\zeta}\overline{U}\,|\,\overline{U}\,|} + \underset{6}{\upsilon(\nabla^2\overline{U})} \qquad (2.39)$$

$$\frac{\partial \zeta}{\partial t} + \nabla\left[\overline{U}(h+\zeta)\right] = 0 \qquad (2.40)$$

where U is the depth-averaged velocity vector (u, v), ∇ is the gradient operator, f is the Coriolis parameter, k is the local vertical unit vector, C_D is the depth-averaged drag coefficient and υ is the horizontal eddy viscosity. In the momentum equation (2.39), the time variation of the horizontal velocity vector (*1*) is the result of acceleration related to: (a) the advection of momentum (*2*); (b) the effect of planetary vorticity (*3*); (c) the slope of the sea surface (*4*); (d) bottom friction (*5*); and (e) transfer of horizontal momentum, by mixing (*6*).

The depth-averaged vorticity can be calculated then by taking the curl of the momentum equation and substituting the mass equation for divergence. The horizontal eddy viscosity is assumed to be constant and η is the total water depth ($h+\zeta$)

$$\frac{\partial \omega}{\partial t} + \overline{U}.\nabla\omega = \frac{\omega + f}{\eta}\left(\frac{\partial \zeta}{\partial t} + \overline{U}.\nabla\eta\right) - \left[\nabla \times \left(\frac{C_D \mid \overline{U} \mid \overline{U}}{\eta}\right)\right].\hat{k} + \upsilon\nabla^2\omega \qquad (2.41)$$

where ω is the vertical component of vorticity given by

$$\omega = \frac{\partial v}{\partial x} - \frac{\partial u}{\partial y} \qquad (2.42)$$

The left-hand side of the vorticity equation represents the local rate-of-change and advection of vorticity following a parcel of fluid with fixed mass. The three right-hand side components of the equation represent the processes that cause the vorticity of the parcel to change: (a) vorticity generated by vertical variations in the water column (stretching or squashing); (b) bottom friction, which can be divided further into slope torque, speed torque and dissipation (see Signell and Geyer (1991) for more details); and (c) diffusion of vorticity, due to horizontal mixing processes.

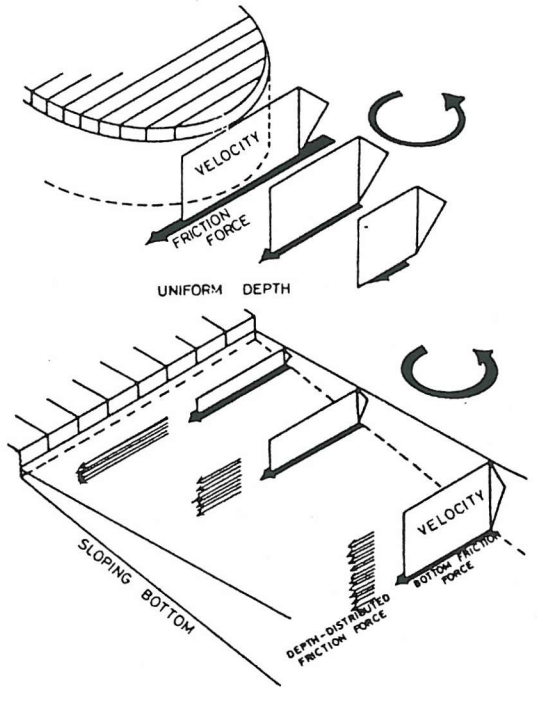

Figure 2.14 Schematic diagram showing vorticity generation due to differential friction, as a function of velocity shear and lateral depth gradients (Robinson, 1983).

The understanding of tidal eddy dynamics is relevant to sediment dynamics, on the basis of their influence on the transport of sediments and fluid dispersion. The formation of eddies has been investigated by several authors, using distinct techniques, including: field observation, numerical modelling, and remote sensing (Tee, 1976; Pingree, 1978; Robinson, 1981; Wolanski *et al.*, 1984, Pattiaratchi *et al.*, 1986; and Signell and Geyer, 1991).

Most of the research undertaken concerning the formation of these eddies investigates the tidally-induced residual eddies (Tee, 1976; Pingree, 1978; Robinson, 1981; and others). However, a different insight, focusing upon the formation and evolution of transient eddies around headlands, is provided by Wolanski *et al.* (1984) and Signell and Geyer (1991). During the tidal cycle, eddies change in their strength, location and limits. Transient (or instantaneous) eddies control the direction of sand transport; hence, they are more appropriate to describe bedload transport, than residual circulation.

Applying an analytical boundary layer model and a depth-averaged hydrodynamic model, Signell and Geyer (1991) have investigated the formation and evolution of eddies, within the flow around headlands. These authors have pointed out that eddy formation and evolution can be described in terms of vorticity production, advection and dissipation. Likewise, that flow separation provides the mechanism for advecting vorticity away from the tip of the headland, into the interior of the flow.

Transient eddy formation and evolution has been demonstrated to be dependent upon three length-scale parameters: (a) the width (b) and length (a) scale of the headland (α (b/a) provides the sharpness parameter, which is related to the importance of the advective terms); (b) $Re_f = h/C_D a$ (h is water depth; C_D is the depth-averaged drag coefficient), which is a non-dimensional quantity, defined as an equivalent Reynolds number based upon bottom friction instead of viscosity (this represents the importance of advection, relative to bottom friction); and (c) a parameter expressing the importance of advection over the local acceleration, represented by the Keulegan-Carpenter number, $K_C = U_o / \sigma a$ (U_o and σ are, respectively, the magnitude and frequency of the tidal flow). Considering that the three aforementioned length scales have the same magnitude, flow separation will occur and eddies will be formed and dissipated, before the subsequent phase of the tide.

Secondary Flows

Another important consideration, relating to tidal flows around headlands, is the occurrence of secondary flows. Secondary flow is the flow in the plane normal to the direction of the mean current and is generated due to the flow curvature (eddies). Pingree (1978) showed that the secondary flow, generated by eddies, provoke convergence towards the centre of the eddy near the bed, and divergence at the surface. The sense depends upon the relative influence of the planetary vorticity (Coriolis), centrifugal (inertial) and pressure gradient forces. This mechanism was referred to as the "tidal stirring" of the seas.

Considering the situation that inertial forces predominate over the Coriolis effect, flow convergence near the bed will occur in both clockwise and anticlockwise eddies. However, if the Coriolis effect is more important than the inertial forces, it is more likely that convergence will occur only where "tidal stirring" and Earth's rotation are in the same sense; this, in the northern hemisphere, occurs within anticlockwise eddies.

The balance between inertial and Coriolis forces is defined by the Rossby number, Ro:

$$Ro = \frac{U}{fR} \tag{2.43}$$

Where U is the speed of the flow, f is the Coriolis force (1×10^{-4} s^{-1}) and R is the radius of the flow curvature.

If Ro>1, inertial forces are more significant; thus, both clockwise and anticlockwise patterns will produce convergence near the bed. On the other hand, Ro<1 defines a significant Coriolis effect, and near-bed convergence takes place only in anticlockwise eddies within the northern hemisphere. Further within the text, the application of the "tidal stirring" concept to the formation of sandbanks will be discussed (Section 2.3.2).

The significance of secondary flows can be examined also in relation to the flow curvature (Dyer and Huntley, 1999); this can be expressed as the ratio between the centrifugal inertial force and the friction force,

$$\frac{h}{RC_D} \tag{2.44}$$

where h is the water depth and C_D is the drag friction coefficient.

Using field measurements obtained from an Acoustic Doppler Current Profiler (ADCP), Geyer and Signell (1990) and Geyer (1993), have confirmed the presence of secondary flows, induced by flow curvature around headlands. Geyer (1993) has shown that the magnitude of the secondary flows varies from 5 to 15% of the primary flow. In earlier investigations, Heathershaw and Hammond (1980) provided indications of secondary flows, in the vicinity of large sandbanks.

2.3.2 Formation and Maintenance

The occurrence of single or isolated sandbanks located in the lee side of coastal irregularities or islands has been observed globally, but mainly on the shelf around the British Isles, such as for example: the Skerries Bank (Start Point, English Channel); the Stanley and North West Banks (Lundy Island, Bristol Channel); the Devil's Ridge, Tripods and Bastram Shoals (Lleyn Peninsula, Cardigan Bay); the Helwick, Scarweather and Nash Sands (Bristol Channel); the Shambles and Portland Banks (Portland Bill, English Channel); and the King Williams, Ballacash, Bahama and Wart Banks (Isle of Man, Irish Sea). The occurrence of headland-associated sandbanks is observed also around the Channel Islands (Great Bank and du Chateau Bank, Jersey), on the coast of France (Corbiere Bank, St. Malo) and on the Irish coast (Burford and Arklow Banks). In the Southern Hemisphere, one particular example is the Levillain Sands, located in Shark Bay, Western Australia. Figure 2.15 presents some of the examples of headland-associated sandbanks (abstracted from Admiralty Charts), as outlined above.

The formation of headland-associated sandbanks has been related to the development of tidal eddies. The most widely accepted theory is the "tidal stirring" concept (or teacup effect) proposed by Pingree (1978). The "tidal stirring" concept explains the formation of sandbanks in the centre of residual eddies, generated by coastal irregularities (e.g. headlands (Tee, 1976; Pingree, 1978; Ferentinos and Collins, 1980)). These eddies generate secondary flows that converge towards the centre of the eddy at the seabed and, by continuity, diverge at the surface. This pattern is controlled by the balance between the pressure gradient, inertial forces and planetary vorticity. A low pressure region at the centre of the eddy leads to a flow convergence at the seabed; this, consequently, gives rise to sand accumulation.

(a)

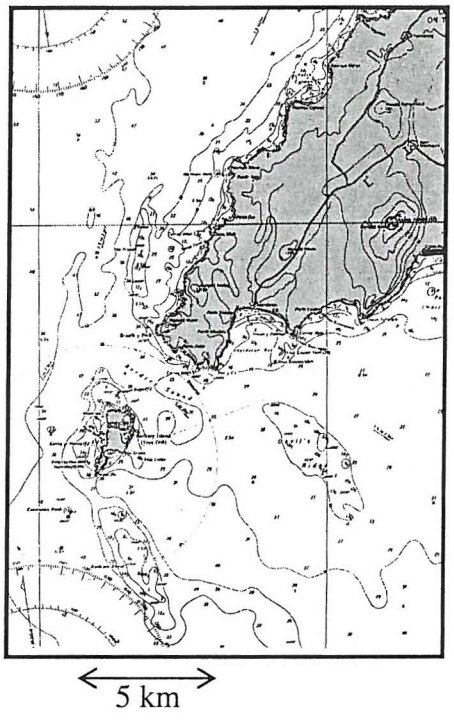
5 km

(b)

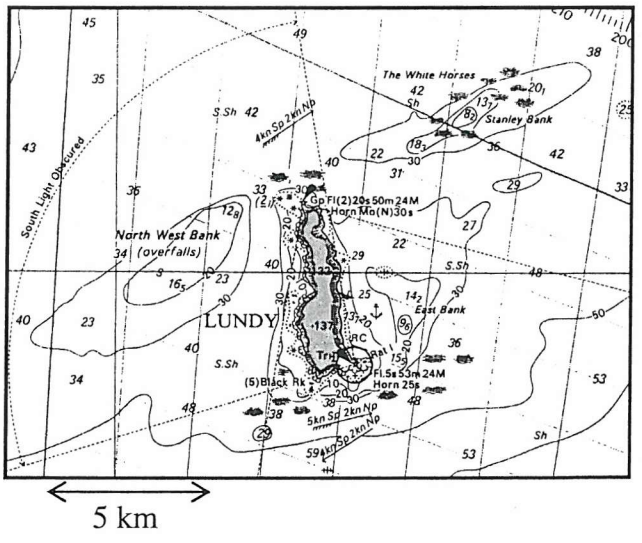
LUNDY
The White Horses
Stanley Bank
North West Bank
(overfalls)
East Bank
South Light Obscured
Gp Fl(2)20s 50m 24M
Horn Mo(N)30s
Fl.5s 53m 24M
Horn 25s
(5)Black Rk
5 km

(c)

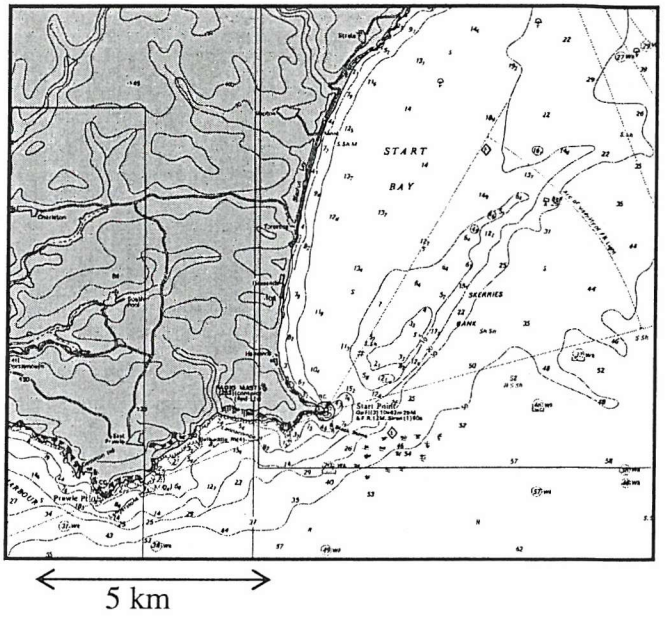

(d)

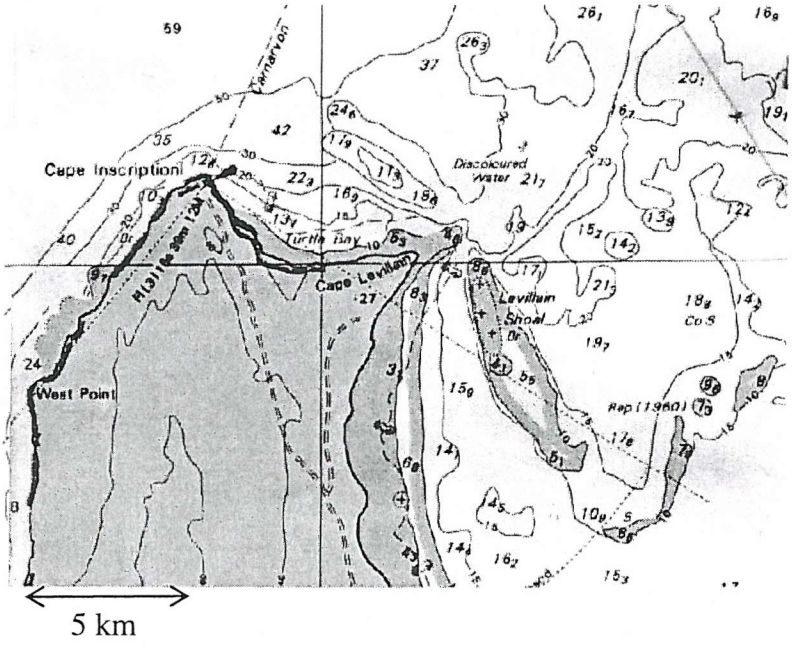

Figure 2.15 Examples of headland-associated banks (abstracted from Admiralty Charts): (a) Leyn Peninsula, northwest Wales; (b) Lundy Island, Bristol Channel; (c) Start Point, English Channel (south England); and (d) Levillain Cape, Shark Bay, western Australia.

On the basis of the output from a depth-averaged hydrodynamic model applied to the inner (continental) shelf around Portland Bill, Pingree (1978) showed that the Shambles Bank is associated with the centre of an anticlockwise residual eddy, located on the eastern side of the headland (Fig.2.16). Despite the formation of an equivalent (clockwise) residual eddy on the western side, a somewhat smaller sandbank (Portland Bank) is observed.

Considering that inertial forces predominate over the Coriolis effect (planetary vorticity), flow convergence near the bed will occur in clockwise and anticlockwise eddies. However, if the Coriolis effect is more important than the inertial forces, it is more likely that convergence will occur only where "tidal stirring" and Earth's rotation are in the same sense (Pingree, 1978); this occurs within anticlockwise eddies in the northern hemisphere. This explanation was used by this same investigator, to explain the formation of asymmetric sandbanks around Portland Bill.

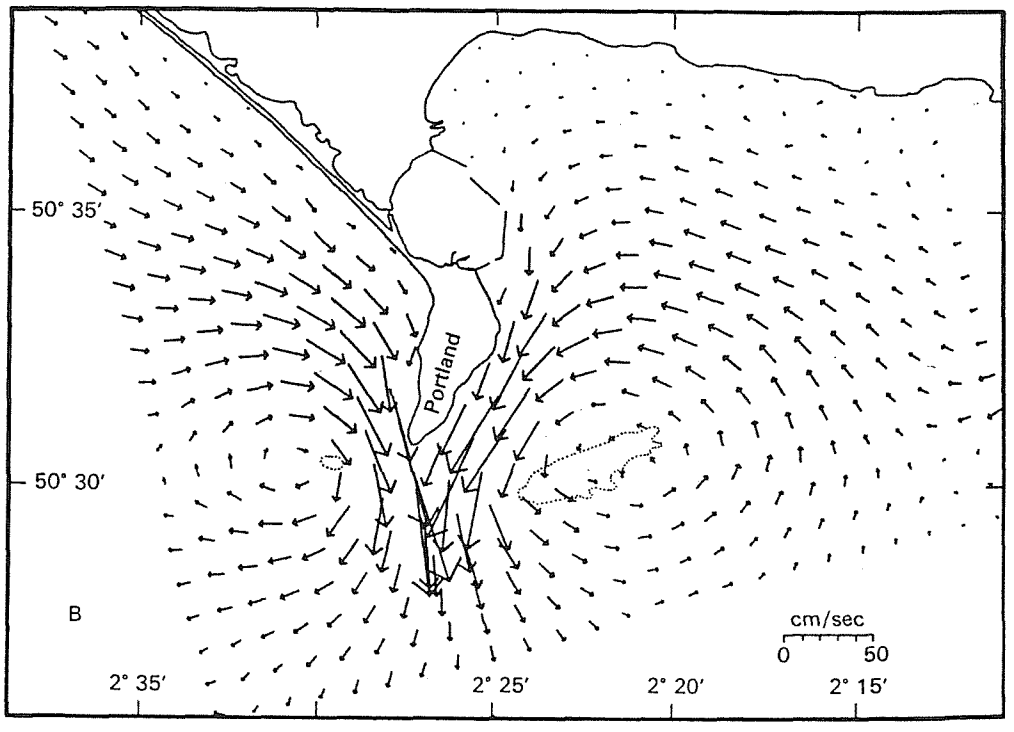

Figure 2.16 Tidally-induced (depth-averaged) residual eddies around Portland Bill (Pingree, 1978).

Pingree (1978) and Pingree and Maddock (1979) extended this physical concept, to explain the formation of symmetric or asymmetric sandbanks in the vicinity of headlands elsewhere. These authors validated this concept by calculating the Rossby number for two different areas, where symmetric (Lundy Island, Bristol Channel) and asymmetric (Isle of Portland, English Channel) sandbanks are observed. For Lundy Island, Ro=5, which may represent sand accumulation on the centre of both eddies. However, for the Isle of Portland, Ro=1; under these conditions, clockwise flows are not associated with pressure gradient forces, resulting in the absence of any tendency towards bank formation.

The determination of the Rossby number around the Isle of Portland appears, however, to be subject to some debate. Subsequent to the earlier investigators, Pattiarachi *et al.* (1986) found Ro= 2-2.7, on the basis of satellite images. An estimation undertaken as part of the present study, using predicted tidal currents from numerical model, derived Ro as 2.3. The discrepancies appear to be related to the value applied to the radius of the flow curvature (R), which can be taken as the length of the headland, for simplicity (Pingree, 1978). Pingree assumed R=10 km, whilst the actual length of the headland (Isle of Portland) is about 6 km.

In order to examine the formation of sandbanks, on the basis of the "tidal stirring" concept, Signell and Harris (2000) used a 3D sediment transport model. A "Gaussian headland" was utilised with the three significant length-scale parameters (see above, Signell and Geyer, 1991) being of about the same magnitude. Long-term suspended and bedload simulations were used.

The final results of this particular investigation predicted fairly symmetric sandbank development around the headland; this demonstrates that, for the case studied, the Coriolis effect could be neglected. For a calculated relative vorticity of about $3f$, different rates of sandbank formation would be expected in response to anticlockwise and clockwise eddies; however, no such tendency was observed. Moreover, the highest rates of deposition and erosion occurred during periods of maximum flood and ebb flows. Gradients in the shear stress and downstream transport of suspended sediments should be controlling the formation of sandbanks. However, wave action must be considered, as well as sediment length-scale parameters (Signell and Harris, 2000).

The significance of the effects of coastal irregularities, on sedimentation processes, was also pointed out earlier by Ferentinos and Collins (1980), examining mud and sand deposits associated with tidally-induced eddies in Swansea Bay (Wales/UK). These authors, based upon the studies of Sugimoto (1975), considered that (topographical) eddies formed downstream from headlands and abrupt coastal discontinuities are the result of flow separation; this is due, in turn, to the combined effect of an adverse pressure gradient and the viscosity acting against inertia. The development of sedimentary deposits, related to topographical eddies, depends upon the type of sediment available.

Chapter 3

Environmental Setting of the Study Area

3.1 The Dorset Coast

The study area is located offshore of the coast of Dorset, between St. Alban's Head and Lyme Regis (English Channel) (Fig. 3.1). The Dorset coastline, between St Alban's Head and Lyme Regis, is an outstanding natural attraction for tourism and recreation. Consisting of Chesil Beach, the Isle of Portland, the Weymouth and Purbeck Coasts, the coastline is associated with large morphological changes in its landscape. The coast ranges from a transgressive shingle barrier (to the west), to a protruding headland and a retreating rocky coast (to the east).

The stratigraphy of the Dorset coast is characterised, basically, by sedimentary rhythmic sequences, clay-sand-limestones, representing transgressive or regressive sequences. In terms of tectonic movements, the Mesozoic rocks have been faulted and folded gently by two major events: (a) the first occurred in the middle Cretaceous (pre-Albian), which is the date of major unconformity within the Mesozoic sequence; and (b) the early and mid-Tertiary events, which are associated with the most prominent structures- the Frome Syncline and the Purbeck Monocline (House, 1993; Donovan and Stride, 1961). The major folding structures are east-west trending.

As a result of the structural patterns, distinct stratigraphic units are observed along the coast; this leads to a wide variety of coastal landforms.

The Purbeck coastline, between St. Alban's Head and Weymouth, is a retreating rocky coast; it consists of Upper Jurassic and Cretaceous rock strata. The rock outcrops are marked by a succession of mudstones, sandstones, limestones and the Cretaceous Chalk formation.

From St. Alban's Head to Redcliff Point, the coastline has a east-west orientation. The differential erosion properties of the rocks lead to the development of a great diversity of coastal features, including sea arches (Durdle Door), stacks, caves (Stair Hole), and the Kimmeridge Ledges and high Chalk cliffs.

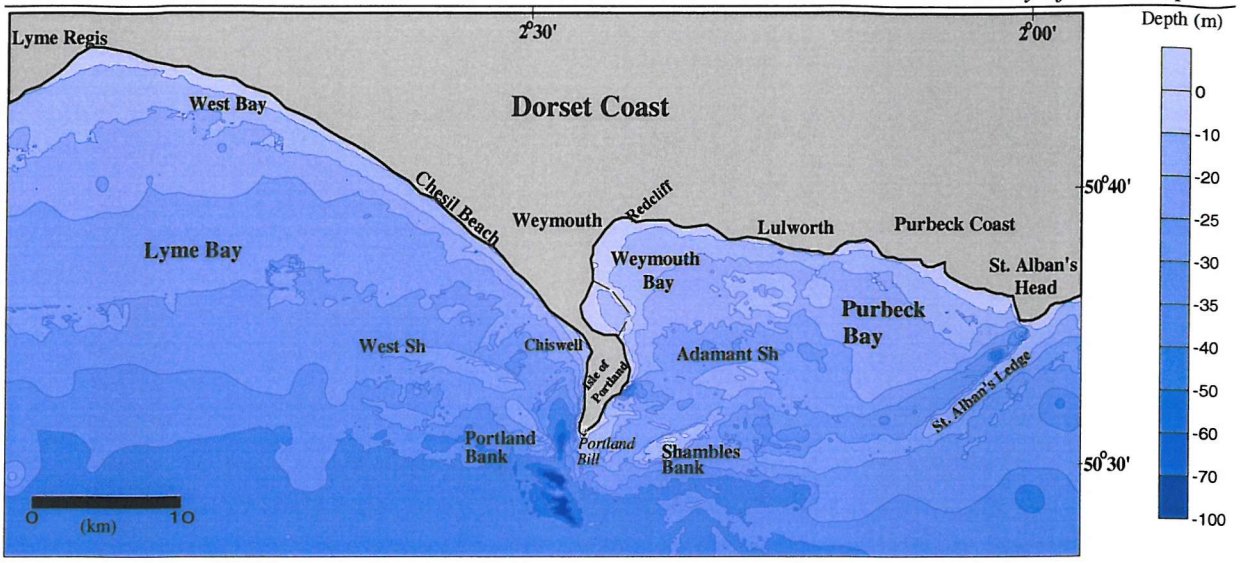

Figure 3.1 Location of the inner continental shelf under investigation. Depth contours are in metres and referred to Chart Datum (Lowest Astronomical Tide).

In Weymouth Bay, the coast assumes a northeast - southwest trending direction and the dominant coastal feature is the Isle of Portland, extending to the south. The geology of Portland consists, basically, of Upper Jurassic rocks dipping southward; an exception is for a Pleistocene deposit of a "raised beach", dated at 125000 and 210000 B.P. (House, 1983), which lies at the southern end of the Isle. The coast of the Isle consists entirely of rocky cliffs, with Portland being a peninsula joined to the mainland by a shingle barrier (Chesil Beach).

The West Dorset coastal geology is characterised by a Holocene transgressive shingle barrier/lagoon system (Chesil Beach/The Fleet) and by high eroding cliffs, comprising Jurassic rocks. The coastal outcrops of West Dorset are world famous due to their Jurassic lithological sections, as well as the resulting landforms and classic landslide sequences (House, 1993; Allison, 1992; Bray, 1997).

Extending about 28 km westward from the Isle of Portland to West Bay, Chesil Beach is a shingle storm barrier rising to over 15m above mean sea-level; for some 13km, this is backed by the Fleet Lagoon (Carr, 1969). Carr and Blackley (1973) have stated that the beach shows a progressively increasing ridge height and pebble size from west to east, exhibiting longshore pebble grading.

Chesil Beach is a finite product of the Holocene transgression, that exhibits reworking and onshore migration with continuing sea-level rise (Carr and Blackley, 1974). Bray (1997) has

identified the occurrence of periodic input of additional shingle to the beach, resulted from cliff erosion.

Westward from Chesil Beach, to Lyme Regis, the coastline is characterised by small beaches; these are delimited by headlands and are backed by high eroding cliffs. The cliff geology consists, basically, of Jurassic rocks (the Lower Jurassic marine sequences, Lias).

According to Bray (1992), although cliff retreat is highly variable, both spatially and temporally, a long-term retreat rate for the coast between Lyme Regis and West Bay is of the order of 0.3 to 0.5m year^{-1}. The same author, in 1997, states that clay is the dominant sediment (78%) yielded by cliff erosion, with significant quantities of sand (17%); in contrast, there are only very small proportions of limestone (3%) and chert and flint gravels (2%).

Compiling information from diverse sources, Bray *et al* (1995) proposed the definition of littoral cells for the central southern English coast, based upon coastal sediment budgets and transport (Fig. 3.2). Concerning the study area, the authors suggest two cells: (a) West Dorset, with an eastward littoral drift along Chesil Beach; and (b) the Purbeck Coast, with a littoral drift not yet established clearly. These cells are delimited by the Isle of Portland.

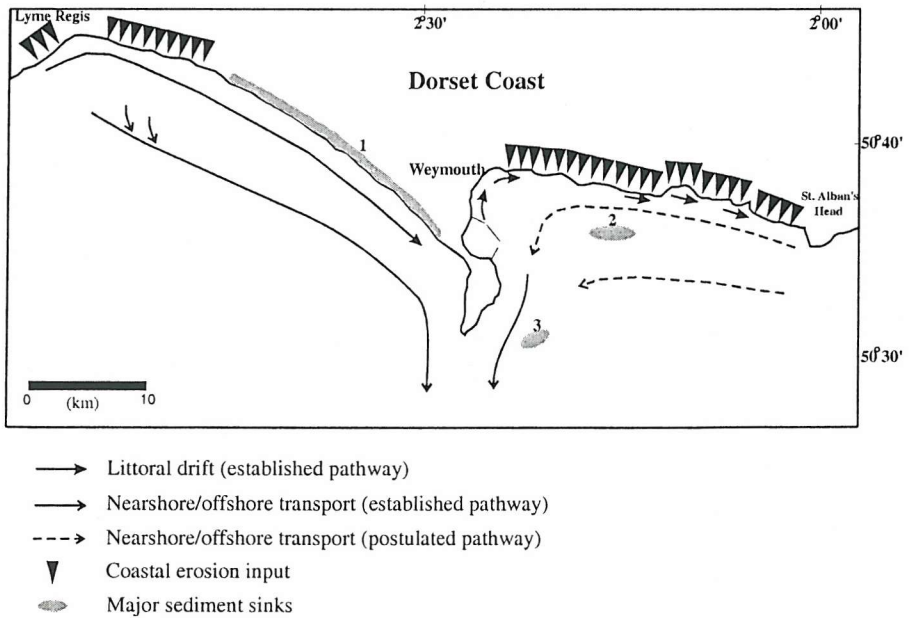

Figure 3.2 Littoral cells defined for the area under investigation (modified from Bray *et al*, 1995). According to these investigators, the major sediment sink areas are: Chesil Beach (1); Lulworth Banks (2); and Shambles Bank (3).

3.2 Regional Hydrodynamics

The combined effects of tide, waves and wind control the water movement within the inner part of the continental shelf, determining the pattern of sediment movement and the seabed mobility.

3.2.1 Winds

The prevailing winds over the area under investigation are from the west and southwest, with wind speeds of around 3.5 m s^{-1} exceeded over 75 % of the time (based upon 17 years (1974 to 1992) of data, collected from a station at Portland Bill). The strongest winds are from the southwest and can reach up to 17 m s^{-1} (with 0.1 % of the year exceedance).

3.2.2 Tides

The Dorset inner continental shelf is subject to the semi-diurnal, west to east, passage of the English Channel tidal wave. The amplitude of the tidal wave decreases eastward, from about 4m on mean springs at Lyme Regis, to about 2 m at Lulworth. From Lyme Regis to Lulworth, the passage of the tidal wave takes about 30 min.

Tidal flow over the area is characterised by strong currents flowing at the tip of Portland Bill, together with the development of tidal eddies on both sides of the headland. In general, tidal current speed tends to increase towards Portland Bill. Mean spring peak speeds, near the water surface, range from 0.40 m s^{-1} up to higher values reaching 3.60 m s^{-1}, in the vicinity of Portland.

The development of eddies around Portland Bill is well documented and have been studied extensively (Pingree, 1978; Maddock and Pingree, 1978; and Pingree and Maddock, 1979). These authors have used a depth-averaged hydrodynamic model to understand the development of the tidal eddies over the region. Pingree (*op cit.*), describes the formation of clockwise and anti-clockwise residual eddy flows around Portland Bill (see Fig. 2.16). The latter would lead to the concentration of sediments and the formation of a sandbank, The Shambles.

3.2.3 Waves

In terms of wave action, Lyme Bay occupies one of the most exposed areas along the southern English coastline. The dominant wave approach is from southwest, which coincides with the maximum fetch; this extends into the northeast Atlantic (Bray, 1997). Hardcastle and King (1972) describe maximum wave heights reaching 9m during very severe storms. Several severe storm waves have been reported, especially at Chiswell, at the eastern end of Chesil Beach (West, 2001). To the east of Portland Bill, Purbeck and Weymouth are more sheltered areas; extreme wave heights could reach 6 to 7m, according to the predictive wave model run by Hydraulics Research (1998). However, Draper (1991) has shown that the significant wave height exceeds 2.5m only 10% of the year.

According to Grochowski and Collins (1994), if the seabed sediment mean grain size is considered, the seabed is disturbed by waves 20% of the time to the east of Portland Bill (around the Shambles) and 5% in Lyme Bay. For sand-sized sediments, the seabed is affected by waves for 20% of the time, along the entire inner continental shelf adjacent to Purbeck and Lyme Regis and 10% of the time, adjacent to Chesil Beach.

3.3 Continental Shelf Geological/Geomorphological Setting

3.3.1 Morphology and Sedimentary Facies Distribution

The part of the continental shelf under investigation is located within the English Channel. The Channel is characterised by an erosive seabed surface, formed during periods of sea-level transgression and regression, during the Quaternary (Curry, 1989; Stride, 1991; and Hamblin *et al*, 1992). The last post-glacial sea-level rise (Flandrian, about 15,000 B.P.) produced a thin and discontinuous veneer of gravel to gravelly sand deposits (lag deposits), over bedrock and channel-fill sediments. Modern sand facies occur throughout the Channel floor and are characterised, mainly, by sand sheets (associated with sandwaves, sand ribbons, rippled sand patches) and, locally, sandbanks (Johnson *et al.*, 1982). The distribution of these features is controlled by the prevailing hydrodynamic conditions and is explained in terms of a bedload parting zone (Stride *et al.*, 1972; Pingree and Griffiths, 1979; and Larsonneur *et al.*, 1982).

The inner shelf under investigation could be described in terms of two embayments separated by the Isle of Portland: Lyme Bay and "Purbeck Bay" (Fig. 3.1). Within either of the

embayments, the seafloor morphology appears to be associated strongly with the: (a) solid geology (structures and bedrock outcrops); and (b) interaction between tidal currents and the headland (Isle of Portland). In general, in water depths of between 20 m and 50 m, the seafloor is characterised by low gradients, associated with banks, shoals and rock ridges. However, close to the coastline, the slope steepens considerably, mainly around the Isle of Portland and along Chesil Beach.

Between St Alban's Head and the Isle of Portland, the rock ridges are formed by resistant sedimentary rocks, with these being widespread throughout the area. The ridges rarely exceed 5 m in height and are formed mainly of Corallian Beds (Lulworth Bank) and Portland Stone (St Alban's Ledge) (Kenyon, 1994).

The bathymetry around the Isle of Portland is somewhat different, when compared with the entire inner continental shelf. To the west of Portland, an elongated deep water area occurs, parallel to the coast; this can reach, at a maximum, 100 m in depth. In terms of sedimentary deposits, the continental shelf around the Isle of Portland is characterised by the presence of sandbanks and sand shoals (Fig. 3.1). To the east of the Isle of Portland, the Shambles Bank is the most prominent sedimentary feature throughout the region. The sandbank has 20m in height and 5km in length.

In terms of sediment distribution, the seabed consists of a discontinuous veneer of coarse lag deposits, associated with mobile sand sheets and bedrock outcrops (Fig. 3.3). The regional sediment thickness is considered to be less than 1 m for the most of the area (BGS, 1983 a). Exceptions are the sandbank and shoal areas.

Sediments within Lyme Bay consist basically of gravel to gravelly sands and sand sheets, with bedrock outcrops widespread throughout the area (BGS, 1983 a; Kenyon, 1994; and Nunny, 1995). To the east of Portland Bill, the inner shelf sediments consist of gravel and sand deposits, with depositional areas such as the Shambles Bank (sandbank), the Adamant Shoal and the fine sand sheet off Weymouth. Similar to Lyme Bay, bedrock outcrops are widespread throughout the area, mainly around Portland Bill and close to the shore.

The regional bedload sediment transport pathways along the Dorset inner continental shelf can be inferred from the regional models for the English Channel (Stride *et al*, 1972; Johnson *et al*, 1982; and Grochowski *et al*, 1993), as being predominantly westward from a divergent

zone (bedload parting zone) located in the central part of the channel (Isle of Wight-Contentin).

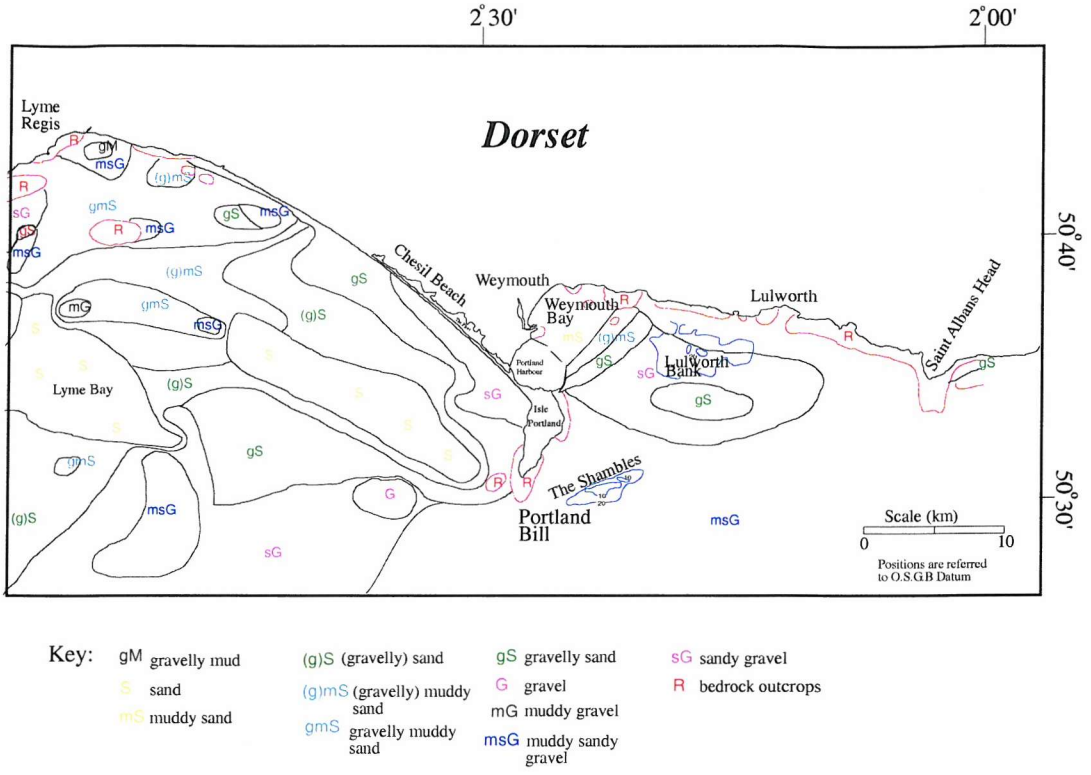

Figure 3.3 Map of the regional seabed sediment distribution, based upon BGS (1983 a). Sediment classification is based upon Folk (1974).

3.3.2 Solid Geology

The offshore solid geology is considered here, in relation to its influence on the seabed morphology. The rocks outcropping on the seafloor are predominantly Jurassic in age (Donovan and Stride, 1961; and BGS, 1983 b). An exception is the Early Cretaceous rocks, occurring to the southeast of Portland Bill and associated with the Shambles Syncline (Fig. 3.4).

The offshore area between the Isle of Portland and St Alban's Head, presents a greater structural control when compared to Lyme Bay. According to Donovan and Stride (1961), the rocks are structurally-controlled by the Purbeck and Weymouth Anticline, with an east-west trend; likewise, by the Shambles Syncline, to the southeast of Portland Bill and with a northwest-southeast trend. The faulting pattern is, generally, north-south trending.

Kimmeridge Clay is predominant over all of the Purbeck Bay. The Corallian Beds are present in the centre of the Bay associated, presumably, with the Lulworth Banks. St Alban's Ledge is

capped by Portland Stone, which forms a rock ridge, "closing" the embayment at Portland Bill.

The offshore area of Lyme Bay is not associated with the structural complexity observed to the east of Portland Bill. From the Isle of Portland to Lyme Regis, the solid geology is characterised by Jurassic sequences. Off Chesil Beach, rock ridges are observed; these lie almost perpendicular to the coast. These outcrops are associated with layers of (more resistant) limestones, within the Kimmeridge Clay sequence.

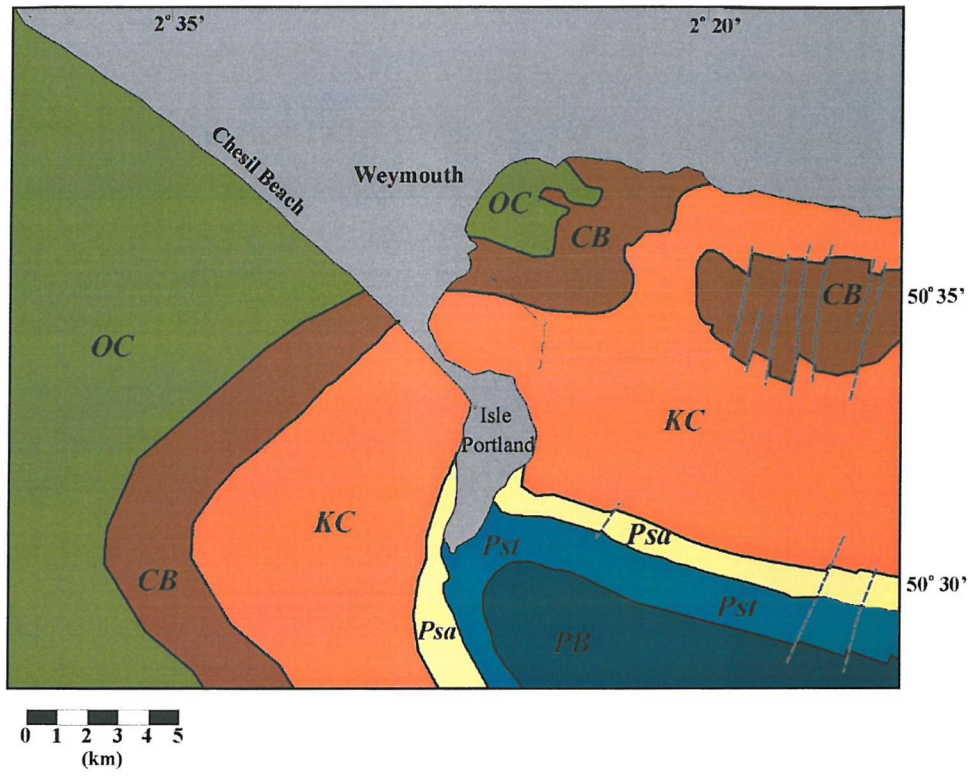

Figure 3.4 Offshore solid geology map (Donovan and Stride, 1961). Key: OC – Oxford Clay, KC – Kimmeridge Clay, CB – Corallian Beds, Pst – Portland Stone, Psa – Portland Sands and PB – Purbeck Beds.

Chapter 4

Bastos, A.C., Collins, M.B. and Kenyon, N.H. Water and sediment movement around a coastal headland: Portland Bill, southern UK. Submitted to Ocean Dynamics Special Publication of the Physics of Estuarine and Coastal Seas Conference (PECS 2002), in October 2002.

Authors	Initiative	Data Processing and Analysis	Interpretation	Manuscript Preparation
Bastos	100%	100%	85%	85%
Collins		-	10%	10%
Kenyon		-	5%	5%

Chapter 4

Water and Sediment Movement around a Coastal Headland: Portland Bill, Southern UK

Abstract

Numerical simulations of tidal flow and sand transport around a coastal headland (Portland Bill, southern UK) were undertaken to investigate patterns of sand transport, during the development of tidally-induced transient eddies. Results obtained from a 2-D finite element hydrodynamic model (TELEMAC-2D) were combined with a sediment transport model (SEDTRANS), to simulate the sand transport processes around the headland.

Simulation of the tidal flow around Portland Bill has shown the formation and evolution of tidally-induced transient eddies, around the headland. During the evolution of these transient eddies, no current-induced bedload (transport) eddy is formed for either sides of the headland. Net bedload sand transport, around a coastal headland, is related to instantaneous gradients in bedload transport rates, during flood and ebb flows, rather than the average flow. Thus, the use of residual (water) circulation to describe patterns of sediment movement as bedload, is considered an inappropriate approach.

Sedimentary processes around coastal headlands are defined by the presence of a scour zone at the tip of the headland (maximum transport rates) and by the occurrence of two distinct zones of sand transport: (a) an *inner zone*, showing sand transport towards the headland, following an increase in gradient in the sand transport rates; and (b) an *outer zone*, showing sand transport away from the headland, following a decrease in gradient in the transport rates. The boundary between these two zones defines a bedload convergence zone.

In the case study presented here, the distinct characteristics of the coastal and seabed morphology around the Isle of Portland (i.e., headland shape and the bathymetry) indicates that these parameters can be influencing tidal (flow) and sediment dispersion around the headland. Such an interpretation has broader implications and applications to headland-associated sandbanks, elsewhere.

Reference: *Bastos, A.C., Collins, M.B. and Kenyon, N.H. Water and sediment movement around a coastal headland: Portland Bill, southern UK. Accepted in Ocean Dynamics Special Publication of the Physics of Estuarine and Coastal Seas Conference (PECS 2002), in January 2003. Reviewers Chris Sherwood, C. Kuhrt and T. Seifert.*

4.1 Introduction

The influence of islands and coastal irregularities (headlands and capes) on the dynamics of tidal flows (magnitude and trajectory) has been recognised and discussed elsewhere, extensively, by different authors, in terms of the development of eddies (Pingree, 1978; Pingree and Maddock, 1979; Robinson, 1983; Wolanski *et al.*, 1984; Pattiaratchi *et al.*, 1986; Geyer and Signell, 1990; Signell and Geyer, 1991 and Davies *et al.*, 1995).

The principal interest in studying the formation of such eddies is explained by their relevance in trapping dissolved pollutants, nutrients, suspended sediment and other components, driven by the tidal flows. The recognition and understanding of these tidal flow patterns is very important, for example, in enabling decisions to be taken concerning locations of sewage outfalls, or for seabed dredging activities, as the eddies can influence the pattern of local and regional sediment transport and deposition. Most of the research undertaken in relation to the formation of eddies has been concerned with the investigation of tidally-induced residual eddies (Tee, 1976; Pingree, 1978; Robinson, 1983; and others). However, a somewhat different insight, focusing upon the formation and evolution of transient eddies around headlands has been provided by Imasato (1983), Wolanski *et al.* (1984) and Signell and Geyer (1991).

The formation and evolution of tidal eddies have been described in terms of vorticity production, advection and dissipation (Imasato, 1983; and Signell and Geyer, 1991). When a tidal flow passes a headland, increased velocities near the tip of the headland induce a bottom frictional torque. Consequently, vorticity is generated and, then, advected away into the flow leaving the headland, creating an eddy system on the downstream side of the headland, during both flood and ebb phases of the tidal cycle. Subsequently, these eddies are dissipated by bottom friction. The evolution and "lifetime" of transient eddies is considered to be related strongly to the time-dependence of vorticity, injected into the interior at the point of flow separation and its dissipation (Imasato, 1983 and Signell and Geyer, 1991).

The significance of eddies on the associated sedimentary processes has been described by different authors, in terms of sandbank formation and/or the facies and bedform distribution around headlands (Pingree, 1978; Ferentinos and Collins, 1980; Signell and Harris, 2000; and

Bastos *et al.*, 2002). However, an investigation into the effects of transient eddies, on the instantaneous patterns of sediment transport, is still a matter of discussion.

Using numerical simulation for processes taking place within the natural environment, this investigation examines sand transport processes around a coastal headland (Isle of Portland, Dorset Coast, southern UK, Fig. 4.1) and the response of this process in relation to the formation and evolution of tidal eddies. The study was undertaken using a 2-D finite element hydrodynamic model (TELEMAC), combined with a sediment transport model (SEDTRANS). The principal objective is to study the potential patterns of sand movement (as bedload) and seabed mobility, induced during the development of (tidally-induced) headland-associated eddies and to examine the comparability of the final results on net bedload sand transport (over a spring tidal cycle), with the tidally-induced residual circulation, in terms of sandbank formation and sedimentary facies distributions.

4.2 Study Site

The inner continental shelf area under investigation is located off the Dorset Coast, southern UK. The shelf is subject to semi-diurnal tides, with an amplitude of 2.4 m at Portland Harbour, during spring tides. Over the region, the tidal currents tend to increase offshore and towards Portland Bill, where (spring) peak currents, near the water surface, can reach up to 3.60 ms^{-1}. During the tidal cycle, tidal eddies develop on both sides of Portland Bill (Maddock and Pingree, 1978).

The inner shelf is characterised by two embayments, separated by the Isle of Portland: Lyme Bay and Purbeck Bay (Fig. 4.1). The seabed morphology presents positive and negative relief features, sandbanks and sand shoals. In terms of sediment distribution, a complex pattern of coarse lag deposits and bedrock outcrops, associated with patches of mobile sands (with D_{50} ranging from 0.18 mm to 1.6 mm) is observed. The variation in grain size composition is associated with the few areas of sand accumulation, which can be recognised over the inner shelf; these include the Shambles and Portland Banks and the Adamant and West Shoals (Fig. 4.1). The banks, located just to the southeast and southwest of the tip of the headland, are composed of very coarse bioclastic sands (D_{50} = 0.9 - 1.6 mm; (settling velocity) w_s = 9.5 - 8.45 cm s^{-1}; carbonate content > 75%); whilst the Adamant Shoals (to the east of Portland) is composed of medium to coarse sands (D_{50} = 0.5 – 0.8 mm , w_s = 6 – 8 cm s^{-1}) and the West Shoals (to the west of Portland) is composed of fine to medium sand (D_{50} = 0.2 – 0.5 mm; w_s = 2 - 5 cm s^{-1}).

4.3 Methods

Hydrodynamic Model

The tidal current information used in the present study was derived from an existing depth-averaged, finite element hydrodynamic model set up and calibrated for the area between St. Alban's Head and Lyme Regis (TELEMAC-2D, developed by Laboratoire National d'Hydraulique of Electricite de France and HR Wallingford). The model is formulated on shallow-water equations that describe the conservation of water mass and momentum. For full details about the TELEMAC, see Hervouet (1991).

The model uses an irregular grid of triangular elements, which allows areas of special interest, e.g. coastal regions and headlands, to be examined in more detail. Figure 4.2 shows the grid points of the tidal flow model.

Results from TELEMAC were provided to the authors, by HR Wallingford, in the form of original TELEMAC output files. These files corresponded to the tidal signature only for two tidal cycles (of 25 hours, with a 15 min time-steps), during spring and neap tides. The original files were processed using a post-processing and interpretation package (RUBENS, provided also by HR Wallingford). Post-processing work involved calculations of vorticity (for each grid point, at each time-step over the tidal cycle), residual currents (by averaging the depth-averaged current, at each point of the grid over a tidal cycle) and the maximum and mean current speeds, at each grid point over a tidal cycle. After processing the original file, the current and water level data were exported as ASCII files and formatted as input data to SEDTRANS. The transient characteristic of the flow is presented here, at every hour over a tidal cycle, during spring tides only.

The development of eddies around Portland Bill has been well documented and studied (Pingree, 1978; Maddock and Pingree, 1978; and Pingree and Maddock, 1979). These authors have used a depth-averaged hydrodynamic model to understand the development of tidal eddies in the Portland region; likewise, to provide information on coastal discharge and sandbank formation. For the present study, the Maddock and Pingree (*op. cit.*) model results were compared with the results obtained from the TELEMAC model. Nevertheless, comparison between the outputs of the two different models showed very good agreement,

principally in terms of eddy development (Note: to facilitate comparison to the Maddock and Pingree (1978) description, the tidal cycle will be described in relation to High Water at Devonport (Devon, 150 kilometres to the west of the area). The beginning of the tidal cycle is considered to be 6 hours before High Water (HW), at Devonport).

Sediment Transport Model (SEDTRANS)

The numerical simulation, to examine the sand transport around Portland Bill, was undertaken by combining the results obtained from TELEMAC model, with the sediment transport model developed by the Geological Survey of Canada, SEDTRANS92 (Li and Amos, 1995). SEDTRANS is an ANSI standard FORTRAN-77 numerical model; it calculates bottom shear stress (for currents alone, or combined wave and current flows) and sediment transport rates for a given input data of water depth, current speed, wave period and height, bed roughness and grain size.

For the present study, the simulations were carried out assuming a uniform grain size distribution over the inner continental shelf; this is due to the complex patterns of sediment distribution (including the presence of coarse lag deposits and bedrock outcrops). Three types of seabed were investigated: a coarse sand bed (D_{50} = 1 mm); a medium sand bed (D_{50} = 0.5 mm); and a fine sand bed (D_{50} = 0.25 mm). The results for instantaneous sand transport, over a tidal cycle, are presented here for the medium sand bed only; those obtained for coarse and fine sand beds are discussed later, in terms of net bedload transport. Net bedload sand transport is defined as the resultant or residual transport rates over a tidal cycle. The bed roughness (z_0) was assumed to be uniform over the area, which was considered as a rippled sand bed (z_0 = 0.6 cm; Soulsby, 1983). On the basis of all the assumptions made for the seabed, the sand transport predicted here is considered to be the "potential" sand transport, over a tidal cycle. The threshold for the initiation of sand movement (critical shear velocity, u_*) was calculated by SEDTRANS, applying Yalin's method (Yalin, 1977). The predicted values (1mm, u_{*crit} = 2.16 cm s^{-1}; 0.5 mm, u_{*crit} = 1.70 cm s^{-1}; 0.25, u_{*crit} = 1.37 cm s^{-1}) plot within the envelop of threshold values, as reviewed elsewhere (Miller *et al.*, 1977; and Paphitis, 2001).

Depth-averaged current data were derived as input, from the results obtained from TELEMAC. Bed shear stress and sediment transport rates were calculated using SEDTRANS, at each point of the original grid (on a triangular element mesh) imported from TELEMAC.

Near-bed currents (at 1m above the seabed) were calculated using SEDTRANS, assuming a logarithmic velocity profile law. The bed shear stress, under currents alone, was calculated by applying a quadratic friction law; this utilised a friction factor (f_c=0.006), based upon the field experiments of Sternberg (1972).

$$\tau_b = 0.5\rho f_c u_{100}^2 \tag{4.1}$$

Where, τ_b is the bed shear stress, ρ water density and u_{100} is the current speed, at 1 m above the seabed.

Potential bedload transport rates were predicted/calculated, using the algorithm proposed by Gadd *et al.* (1978), for currents alone:

$$q_s = \left(\beta / \rho_s\right)(u_{100} - u_{cr})^3 \tag{4.2}$$

Where q_s is the bedload transport rate, β is an empirical coefficient (1.73 x 10^{-3}), ρ_s is sediment density, and u_{cr} is the critical velocity, for the initiation of bedload transport.

The reason for applying this particular algorithm is based upon the results presented by Grochowski *et al.* (1993). This algorithm produced the best results, in terms of predicting sand transport rates for the English Channel, when compared to radioactive tracer measurements experiments undertaken along the French coastline (Dewez *et al.*, 1989).

4.4 Results

The results obtained by comparing the tidal flow with the potential bedload transport, over a tidal cycle, have revealed patterns of sediment movement during the formation and evolution of transient eddies. In addition, net bedload transport could be compared with residual water circulation around coastal headlands. The results are presented here in terms of: (a) depth-averaged current vectors; (b) potential bedload (medium) sand transport vectors; and (c) contour maps of the vorticity distribution.

Water and Sediment Movement, at Hourly Intervals

At the beginning of the tidal cycle, the currents are flowing westward (ebb currents), with maximum depth-averaged speeds reaching 2.0 - 2.5 m s^{-1} close to the tip of the headland. The ebb currents tend to flow parallel to the Purbeck coastline, then veer gently towards the south, to follow the headland coastline and the bathymetric contours. At the tip of the headland, the currents turn abruptly towards the north; offshore, they tend to show a very gentle veering, towards the northwest or no veering. The vorticity field shows maximum negative values (-25 x10^{-4} s^{-1}), just off the tip of the headland (Fig. 4.3a). In terms of sediment movement, sand is being transported westward over Purbeck Bay. A gradient, in increasing transport rates, is observed from the Adamant Shoal (0.005 kg m^{-1} s^{-1}) towards the tip of the headland (2 kg m^{-1} s^{-1}). No sand transport is predicted over Weymouth Bay and Lyme Bay.

One hour later (5h before HW), the current velocities have reached their maximum off the tip of the headland (3.0 m s^{-1}). The flow has started to separate, forming a clockwise eddy just along the western boundary of the headland. The high negative vorticity has now extended across the tip boundary, into the western side of the headland (Fig. 4.3b). Gradients in sand transport rates are now observed, on both sides of the headland. On the eastern side, a gradient in increasing transport rates is still observed between the Adamant Shoal (0.1 kg m^{-1} s^{-1}) and the tip of the headland (5 kg m^{-1} s^{-1}). It should be noted that sand transport is still not predicted for Weymouth Bay. At the tip of the headland, there is a significant veering in the sand transport direction (towards NW) and a decrease in the sand transport rates. No transport is predicted in the inner area along the western boundary of the headland, where a clockwise eddy is being formed by the tidal flow. A gradient in decreasing transport rates is observed between the Portland Bank (1 kg m^{-1} s^{-1}) and the West Shoal (0.005 kg m^{-1} s^{-1}).

Locally, the bottom friction generated by the Shambles Bank (Fig. 4.1), on the eastern side of the headland, has enhanced also the generation of vorticity. As the bank is aligned obliquely and clockwise to the flow, an anti-clockwise vorticity (positive) is generated, as the flow moves on to the sandbank. Clockwise vorticity (negative) is observed as the flow leaves the sandbank. This process is entirely in accordance with the concepts proposed elsewhere, by Zimmerman (1981) and Robinson (1983). A detailed examination of the bedload transport over the Shambles Bank reveals that sand transport vectors veer slightly towards the south (or towards the crest), when approaching the bank in a southwestern direction; when leaving the bank, the transport vectors veer again towards southwest.

Ebb currents are still flowing strongly, at four hours before HW (2.5 – 3.0 m s^{-1}, at the tip of the headland). The transient characteristic of the eddy pattern is observed, as it starts moving westward and is becoming detached from the headland. A southward flow (0.75 m s^{-1}) is formed, parallel to western coast of the headland (Fig. 4.3c). The maximum vorticity field (-25 x10^{-4} s^{-1}) has now moved a little offshore from the headland; at the centre of the eddy, the vorticity is -12 x10^{-4} s^{-1}. Gradients in increasing and decreasing transport rates are still observed on the eastern (0.1 – 5 kg m^{-1} s^{-1}) and western (1 – 0.05 kg m^{-1} s^{-1}) sides, respectively. On the western side, a more significant veering in the transport vectors can be observed, as they leave the tip of the headland (Note: far offshore from the headland, the vectors do not present significant veering); however, no sand transport is predicted within the eddy pattern. A sand transport shadow zone is formed along the western inshore area, close to the headland and off Chesil beach. On the Shambles Bank, the positive and negative vorticity fields, described previously, are still occurring; likewise, veering of the sand transport vectors.

During the middle part of the half-cycle (3 hours before HW), the currents are still flowing westward. The eddy has now moved farther downstream and vorticity at its centre is around -10 x10^{-4} s^{-1}. The southward flow along the western coast of the headland has reached a speed of 1.0 m s^{-1} (Fig. 4.3d). Maximum depth-averaged currents are now observed offshore from the tip of the headland (2.0 - 2.5 m s^{-1}). Overall, sand transport rates have decreased on both sides; an exception being a narrow area of the inner shelf, along the western coast of the headland, where transport has increased (0.0025 kg m^{-1} s^{-1}) because of the reversal of the flow, associated with the eddy formation. At 2 hours before HW, the tidal currents are significantly weaker (maximum speed 1.0 – 1.5 m s^{-1}, offshore from the tip), but are still flowing westward. A large-scale eddy has now developed along the western side of the

headland; at its centre, the vorticity magnitude is -8 $x10^{-4}$ s^{-1} (Fig. 4.3e). The southward flow, parallel to the western coast of Portland, has increased to speeds of up to 1.0 m s^{-1}. Sand transport is restricted basically to the areas close to the tip of the headland (including the Shambles and Portland Banks), offshore regions and along the western coast of the headland (0.005 kg m^{-1} s^{-1}). No transport is predicted over the West and Adamant Shoals.

At 1 hour before HW, the eastern side of Portland is associated with slack water; on the western side, a remaining large-scale eddy is still observed, farther downstream (Fig. 4.3f). The vorticity at the centre of the eddy is still high (-8 $x10^{-4}$ s^{-1}). The strongest currents (1.0 – 1.5 m s^{-1}) are found near to the tip of the headland; however, they are associated with flow parallel to the western coast of the headland. Sand transport is restricted to the inshore region, along the western coast of the headland and at its tip. The transport vectors show sand movement towards the south (along the western side of the headland, of 0.0025 kg m^{-1} s^{-1}) and veering to the east at the tip of the headland (0.1 kg m^{-1} s^{-1}). For the other areas, no transport is predicted.

One hour later, at HW, the flood currents start flowing, with a maximum speed (2.0-2.5 ms^{-1}) at the tip of Portland (Fig. 4.3g). The flood currents tend to flow parallel to the Chesil Beach coastline; they then turn sharply towards the south, to follow the headland coastline. At the tip of the headland, the currents again veer abruptly, towards the north. The vorticity field now shows maximum positive values (25 $x10^{-4}$ s^{-1}) at the tip, whilst the vorticity associated with the previous clockwise eddy has decreased to -5 $x10^{-4}$ s^{-1} (Fig. 4.3g). The eddy formed during the previous phase of the tide has now been dissipated totally, by bottom friction. Sand transport is predicted to the west of the headland and to restricted areas to the east. A gradient of increasing sand transport rates is observed between the West Shoal (0.0005 kg m^{-1} s^{-1}) and Portland Bill (2 kg m^{-1} s^{-1}). On the western side, sand transport is towards the southeast. Leaving the tip of the headland, the transport rates decrease considerably and the vectors veer towards the north and northeast.

At 1 hour after HW, the current velocities have increased (2.5-3.0 m s^{-1}) and the flow has started to separate, forming an anti-clockwise eddy along the eastern boundary of the headland (Fig. 4.3h). The vorticity has extended downstream across the boundary. Sand transport rates have increased greatly. Likewise, the same pattern of increasing (towards the headland) and decreasing (away from the headland) gradients, in the transport rates, are

observed. No sand transport is predicted along the eastern coast of the headland, where an anti-clockwise eddy is observed.

At two hours after HW, the flood currents have reached their maximum (3.5 m s^{-1}) at the tip of the headland. The anti-clockwise eddy has moved eastward, being now detached from the headland. Along the eastern boundary of the headland, the currents have turned southward, forming a flow parallel to the headland coast (Fig. 4.3i). At the centre of the eddy, the vorticity is around 10 x10^{-4} s^{-1}. The vorticity field is now characterised by two distinct centres; at the centre of the eddy and a second one, associated with interaction between the flow and the Shambles Bank (5 x10^{-4} s^{-1}). Sand transport is predicted for almost the entire area, with exceptions being Weymouth Bay and the inner area along the eastern coast of the headland, where an anti-clockwise eddy is being formed by the tidal flow. A gradient in increased transport rates is observed between the West Shoal (0.025 kg m^{-1} s^{-1}) and Portland Bill (5 kg m^{-1} s^{-1}). High rates of sand transport are predicted along the southern flank of the Shambles Bank (1 kg m^{-1} s^{-1}); at the Adamant Shoal, the predicted rates are around 0.005 kg m^{-1} s^{-1}. On the western side, sand transport vectors are still towards the southeast; at the tip of Portland Bill, the vectors start veering gently towards the north and northeast.

During the middle part of the second half of the tidal cycle (3 hours after HW), flood currents are flowing, with a maximum speed of around 2.5 m s^{-1}. On the eastern side of the headland, an anti-clockwise eddy is still observed, and, although it is increasing in size, it has not moved significantly from its previous position (Fig. 4.3j). The vorticity at its centre is 8 x10^{-4} s^{-1}. Sand transport is still predicted for the western side. However, on the eastern side, transport rates have decreased considerably and sand movement is no longer predicted between the Adamant Shoal and the Purbeck coastline.

At 4 hours after HW, the flood currents are much weaker (1.5 - 2.0 m s^{-1}) along the tip; however, a large anti-clockwise eddy has now moved farther downstream and has developed in size (Fig. 4.3k). The vorticity at the centre of the eddy has decreased (7 x10^{-4} s^{-1}), but the two centres are still observed. Sand transport rates have decreased considerably, over the entire area. On the eastern side, sand movement is predicted only at the tip of the headland, offshore from the Shambles Banks (southward) and parallel to the eastern coast of the headland. Transport vectors now indicate an eastward sand transport. There is no sand transport associated with the large eddy formed during this phase of the tide. On the western

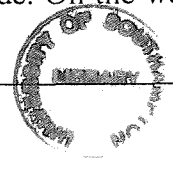

side, a gradient of increasing transport rates is still observed, between the West Shoal (0.0005 kg m^{-1} s^{-1}) and Portland Bill (0.5 kg m^{-1} s^{-1}).

Close to the end of the tidal cycle (5 hours after HW), slack water occurs on the western side. On the eastern side, a very large anti-clockwise eddy is now observed over the Shambles Bank (with vorticity at its centre, of around 3 x10^{-4} s^{-1}) (Fig. 4.3l). Sand transport is predicted only along the eastern coast of the headland, with vectors indicating southward transport. For the remainder of the area, no transport was predicted at the end of the tidal cycle.

At 6 hours after HW (end of the 12.4 hours tidal cycle), a complete reverse of the tidal flow is observed. Ebb currents are flowing westward, with maximum depth-averaged speeds reaching 1.5 – 1.8 m s^{-1} close to the tip of the headland. The eddy on the eastern has dissipated completely. The vorticity field shows maximum negative values (-25 x10^{-4} s^{-1}), just off the tip of the headland (Fig. 4.3m). Sand transport is westward over Purbeck Bay. A gradient, in increasing transport rates, is observed from the Adamant Shoal (0.002 kg m^{-1} s^{-1}) towards the tip of the headland (1 kg m^{-1} s^{-1}). No sand transport is predicted over Weymouth Bay and Lyme Bay.

4.5 Discussion

Simulation of the tidal flow around Portland Bill has illustrated the formation and evolution of tidally-induced transient eddies, around the headland. It was observed that, during the tidal cycle, these eddies change in their position and magnitude (Fig. 4.4).

By simulating the potential bedload sand transport around a coastal headland, the non-linear property of sediment transport is taken into consideration; this is, instead of the (simple) analysis of water residual circulation, representing patterns of sediment transport. Because sand transport rates are calculated here based upon the excess shear stress, i.e. a critical threshold value must be reached before sediment initiates movement, instantaneous sand transport patterns do not follow (necessarily) the same transient pattern as that of the tidal flow. Herein, this concept is observed clearly around Portland Bill, during the formation and evolution of tidally-induced eddies. Analysis of the hourly time-steps during the tidal cycle, has revealed that during the evolution of the tidally-induced transient eddies, no current-induced bedload (transport) eddy is formed for either of the sand beds. Hence, because the transient flow does not reflect, completely, the bedload sand transport, the residual circulation does not indicate the pattern of net sand transport and deposition.

The residual circulation over the study area is characterised by the presence of two residual eddies, on both sides of the headland, as described previously by Pingree (1978) (Fig. 4.5a). The physical significance of tidally-induced residual eddies has been questioned by Imasato (1983). This author has argued that Eulerian tidally-induced residual currents are the result of averaging a transient phenomenon; as such, it is merely a mathematical representation, having no physical meaning. The nature of tidal flows around headlands is dependent upon the relationship between three length-scale parameters (Signell and Geyer, 1991): tidal excursion, headland length scale and the bottom friction. In the case of Portland Bill, the bottom friction scale is comparable to that of the tidal excursion; both are approximately the same magnitude as that of the headland length-scale. This similarly means that an eddy is formed during each half of the tidal cycle; it is dissipated before the development of another eddy, during the subsequent half (tidal) cycle (refer to Case 1, in Signell and Geyer, 1991).

The simulation of instantaneous sand transport over the tidal cycle has revealed that most of the bedload transport processes occurred during the period of maximum flood and ebb flows, when gradients in the bed shear stress and transport rates are also at maximum.

The significance of this pattern, in relation to the development of an understanding of sand dispersal around the headland, relies upon the fact that these instantaneous gradients (in transport rates) occur upstream and downstream from the headland, during the same half of the (tidal) cycle. Nevertheless, considering that currents, shear stress and bedload transport rates are at maximum at the tip of the headland, over the entire tidal cycle, a reverse in the gradient of transport rates is observed as the flow passes the headland. In general, the coastal headland induces acceleration in the tidal flow towards the headland, which is followed by an increase in the bed shear stress and bedload transport rates. At the tip of the headland, a local region of maximum bed shear stress occurs; this is characteristic of a scour zone (Harris *et al.*, 1995), or an area of erosion. As the tidal flow passes the headland, a decrease in the gradient of the transport rates is observed.

The same pattern of resultant bedload transport direction was observed for fine, medium and coarse sands (Fig. 4.5b). However, the net transport rates differ due to the calculated excess bed shear stress, which depends upon the threshold (or critical shear velocity) associated with of sediment movement. The net bedload (sand) transport direction is characterised by two distinct zones of potential sand transport, around coastal headlands: the inner and outer sand-mobile zones (Bastos *et al.*, 2002) (Fig. 4.6).

The inner sand transport zone is characterised by resultant sand transport towards the tip of the headland (i.e. southward on both sides of the headland); this is followed by a downstream increase in gradient in the transport rates. Ebb and flood currents are constrained by the coastal geometry; they flow parallel to the coastline, then veer towards the south (with increased velocities), to follow the headland coastline. This zone is associated with sand transport, enhanced by the maximum ebb and flood currents; these flow parallel to the coastline, on the eastern and western sides, respectively.

The outer sand transport zone is situated offshore from the tip of the headland; it is defined by sand transport away from the headland, with a downstream decrease in gradient in the transport rates. At the tip of the headland, the currents reach their maximum speed and a bottom frictional torque is induced, producing vorticity. When the flow leaves the tip of the

headland, vorticity is advected away into the flow, which starts veering towards the north. Because of these increased speeds at the tip of the headland, the currents leaving the headland are very strong and the bedload transport rates are high. This process forms the outer sand transport zone, which is characterised by a veering in the sand transport vectors, towards the north.

The boundary between the inner and outer zones defines a zone of bedload convergence; consequently, this can be recognised on both sides of the headland and coincides with the presence of sandbanks (Fig. 4.6). At the tip of the headland, a zone of maximum erosion occurs. Thus, the net sediment transport around a coastal headland reflects the instantaneous gradients in the bedload transport rates, during the flood and ebb flows (phases of the tidal cycle), rather than the average flow conditions.

The formation of sandbanks around coastal headlands has been related to the residual tidal flow patterns around coastal headlands, i.e. sandbanks occur in the centre of residual eddies (Pingree, 1978). However, as discussed previously, in terms of bedload (sediment) transport, the length-scale of the excess bed shear stress has to be taken into consideration.

According to Signell and Harris (2000), the headland length-scale controls the scale of the shear stress variability. Thus, if the shear stress is comparable to the tidal excursion and bottom friction scales, the bedload-generated bank will coincide with the presence of the residual eddy. However, the results obtained for the western side of Portland Bill contradict this particular concept. Net bedload transport does not follow the pattern of the residual currents; neither does the presence of the Portland Bank coincide with the centre of the clockwise residual eddy (Fig. 4.7a). For the area under investigation, the occurrence of the sandbanks is related to the formation of a bedload convergence zone, on either sides of the headland. Thus, if the length-scale parameters are of about the same magnitude, it might be expected that sandbanks would be observed in the centre of the residual eddies; however, this is true only for the eastern side of Portland Bill. Therefore, other parameters must be influencing the nature of the flow and sediment transport around the headland.

An aspect which has not been considered previously, in modelling studies of tidal flows and sandbank formation around headlands, is the asymmetry of the important geomorphological components, i.e. the headland and coastline geometry and the irregular bathymetry. Because it was not the objective of this investigation to develop a numerical model to study the

relationship between these parameters, with changes in flow patterns and sandbank formation, this particular subject area can only be addressed qualitatively in this particular situation.

In the case study presented here, the distinct characteristics of the coastal and seabed morphology around the Isle of Portland (i.e., headland shape and the bathymetry) indicates that these parameters can be influencing tidal (flow) and sediment dispersion around the headland. A detailed analysis of the results for net bedload transport (for all of the sand beds) shows that the net transport rates are not distributed symmetrically around the headland tip, as would be expected for a situation were the length-scales are approximately the same magnitude. It is clear from Figure 4.5b that the narrow linear deep area (Portland Deep, which reaches up to 100 m in depth, see Fig. 4.1), to the west of the headland tip, has a significant influence on the regional distribution of the net transport rates. Higher net transport rates are concentrated to the east of the headland tip, whilst a significant decrease in the net rates is immediately observed along the Portland Deep; these followed by a subsequent increase in the net transport rates (to westward). This deep zone, immediately downstream of the headland tip, acts as a physical boundary that decreases the sediment transport rates. The same pattern is observed for each of the three sand beds considered.

Furthermore, the occurrence of a suite of bedforms and sedimentary facies, as described by Bastos *et al.* (2002) reinforce the results obtained here, i.e. that the residual circulation is not appropriate to be used as a net sediment transport indicator. The sand transport pathways indicated by the asymmetry of large and very large sandwaves corroborates the prediction of net bedload transport, as well as the occurrence of sandbanks associated with the bedload convergent zones.

4.6 Conclusion

Using a numerical simulation for a real (natural) environment, this investigation has examined the water circulation and sediment transport processes around a coastal headland (Isle of Portland, southern UK) and the response of this process in relation to the formation and evolution of tidal eddies. The main conclusions derived from the investigation are outlined bellow.

(a) The numerical simulation has revealed that, during the evolution of the tidally-induced transient eddies, no current-induced bedload eddy is formed, for either of the sand beds; hence, the instantaneous bedload sand transport patterns do not follow (necessarily) the same transient pattern as that of the tidal flow.

(b) Net bedload sand transport, around a coastal headland, reflects instantaneous gradients in bedload transport rates during the flood and ebb flows, rather than the average flow. Thus, the use of residual (water) circulation, to describe patterns of sediment movement as bedload, is considered as inappropriate.

(c) Sediment transport and erosion around coastal headlands is defined by the presence of a scour zone, or erosive area, at the tip of the headland (maximum transport rates) and by the occurrence of two distinct zones of sand transport: (a) an *inner zone*, showing sand transport towards the headland, following an increase in gradient in the sand transport rates; and (b) an *outer zone*, showing sand transport away from the headland, following a decrease in gradient in the transport rates.

(d) Local characteristics and irregularities in coastal and seabed morphology, around the headland, should be considered as a parameter for modelling the tidal and sand dispersal around headlands. Despite the same magnitude of the different length-scale parameters (such as tidal excursion, headland-scale and bottom friction), net sand transport rates do not follow the pattern of residual circulation over the study area; neither could the concept of sandbanks occurring in the centre of residual eddies be verified. For the present study, the occurrence of headland-associated sandbanks is related to the bedload convergence zones observed on both sides of the headland.

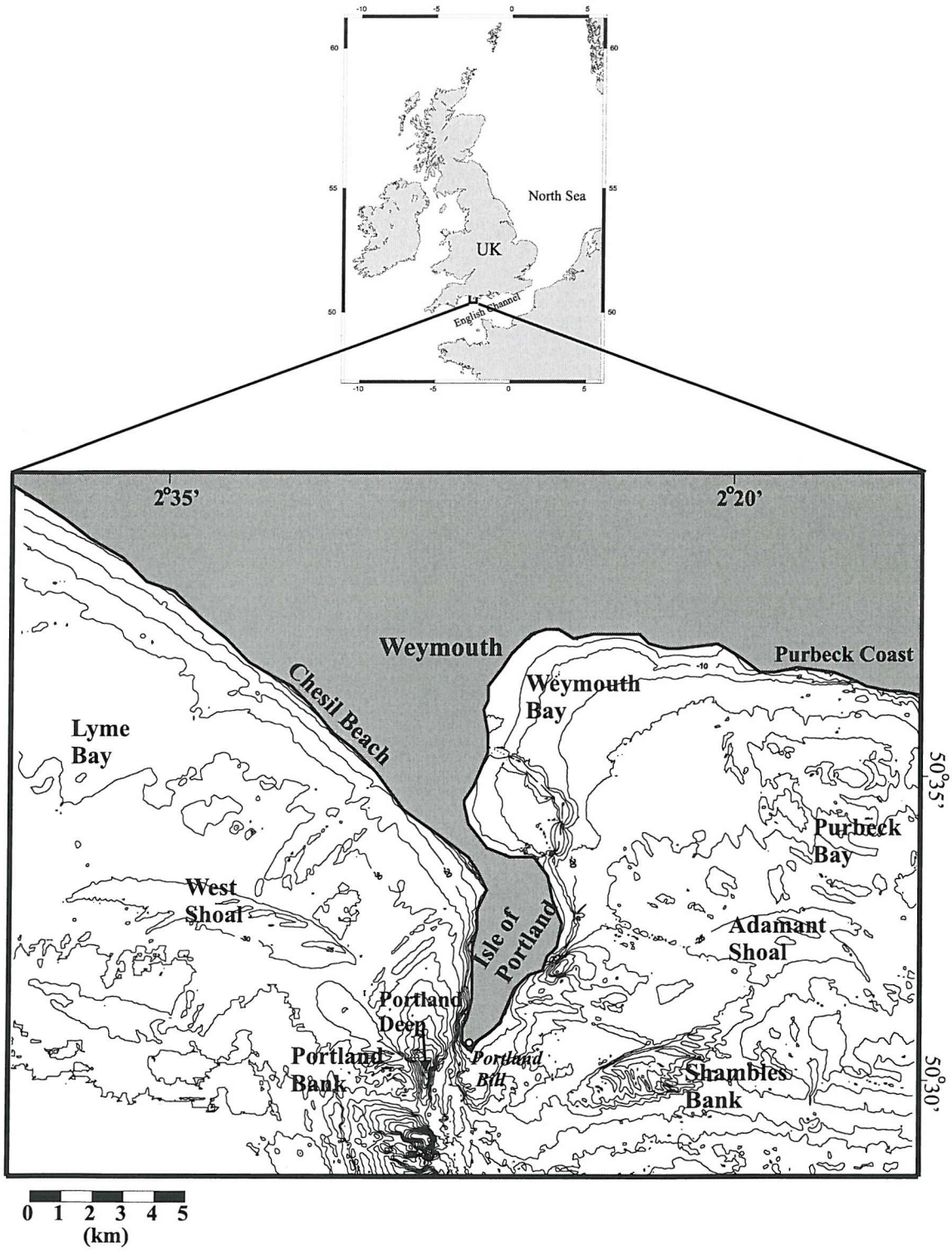

Figure 4.1 Location of the area under investigation showing the regional setting of Portland Bill and the bathymetry over the study area. The detailed bathymetric map is based upon UK Hydrographic Office Fair Sheets. The contour interval is in metres, reduced to Chart Datum.

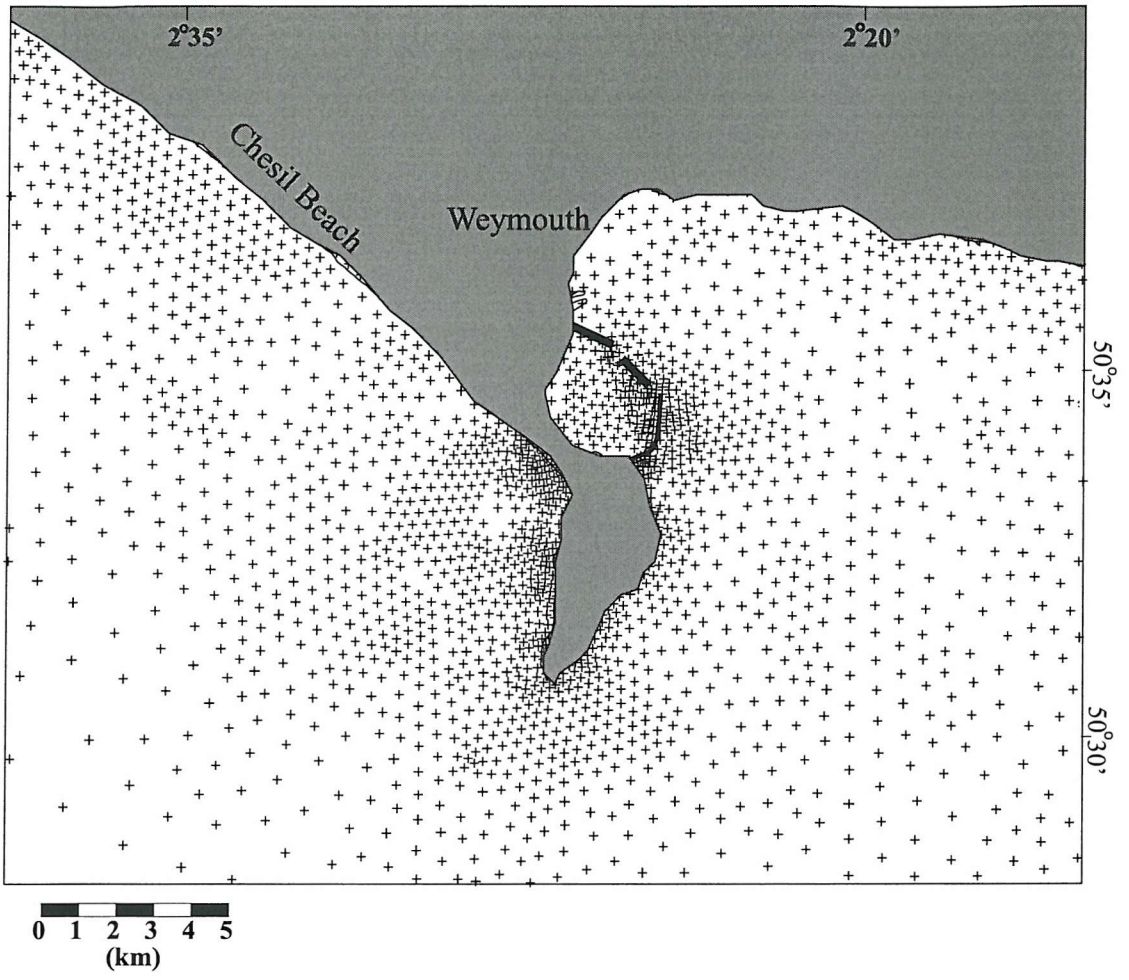

Figure 4.2 Original finite element grid of the hydrodynamic model (TELEMAC-2D).

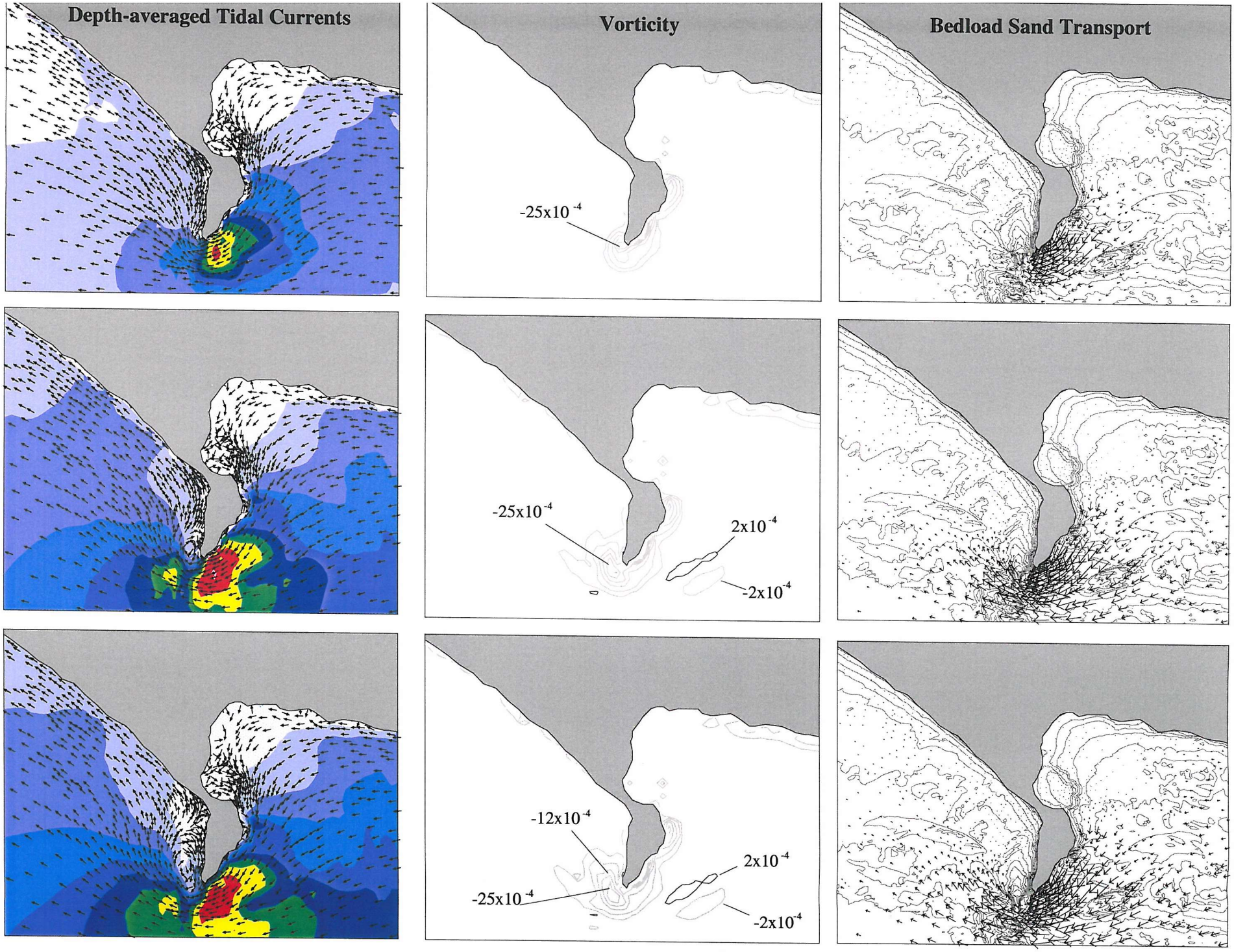
Depth-averaged Tidal Currents
Vorticity
Bedload Sand Transport
(a)
(b)
(c)
-25x10 -4
-25x10 -4
2x10 -4
-2x10 -4
-12x10 -4
-25x10 -4
2x10 -4
-2x10 -4

Figure 3

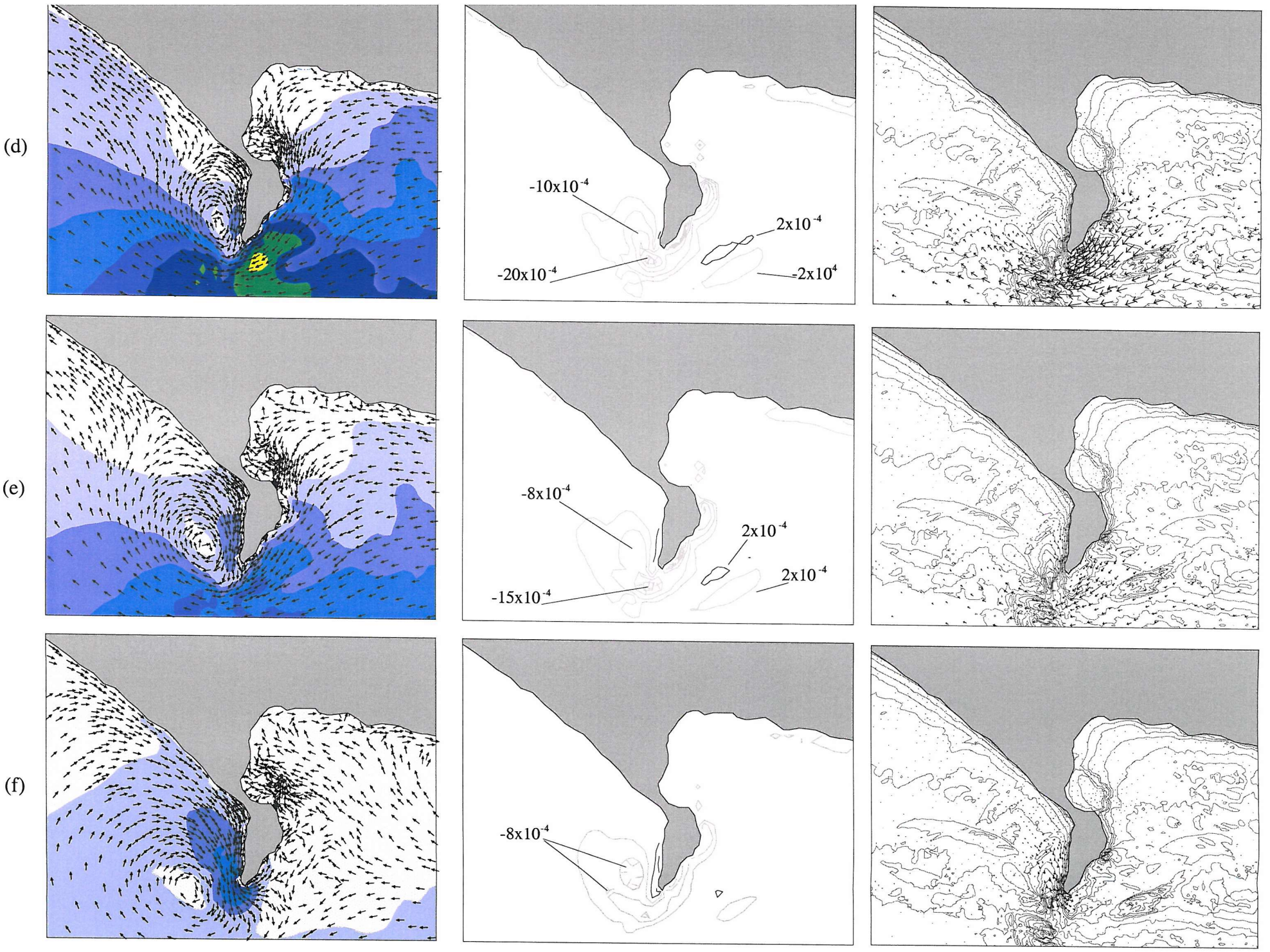
(d)
-10x10^{-4}
2x10^{-4}
-20x10^{-4}
-2x10^{4}
(e)
-8x10^{-4}
2x10^{-4}
2x10^{-4}
-15x10^{-4}
(f)
-8x10^{-4}

Figure 3

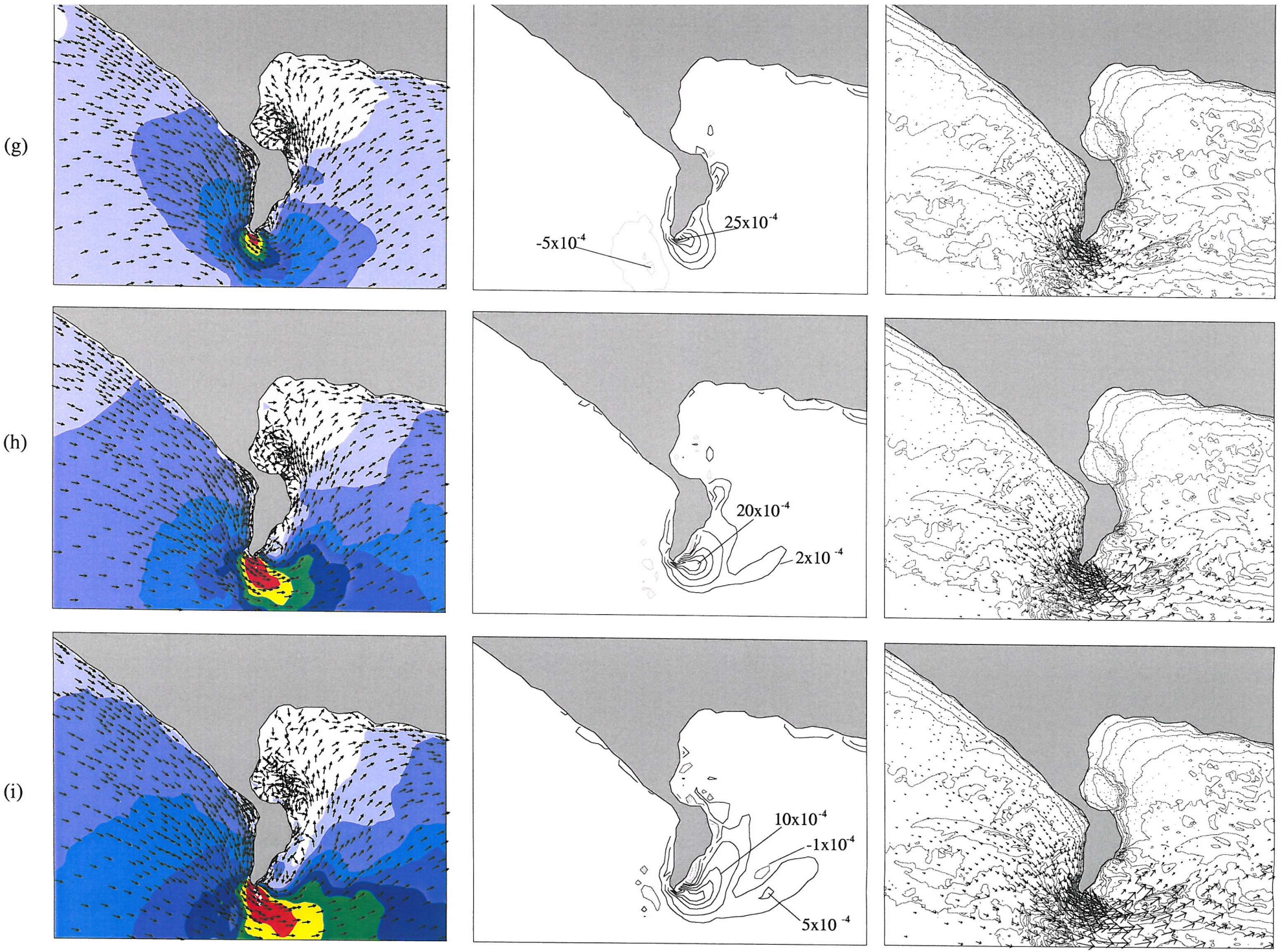

Figure 3

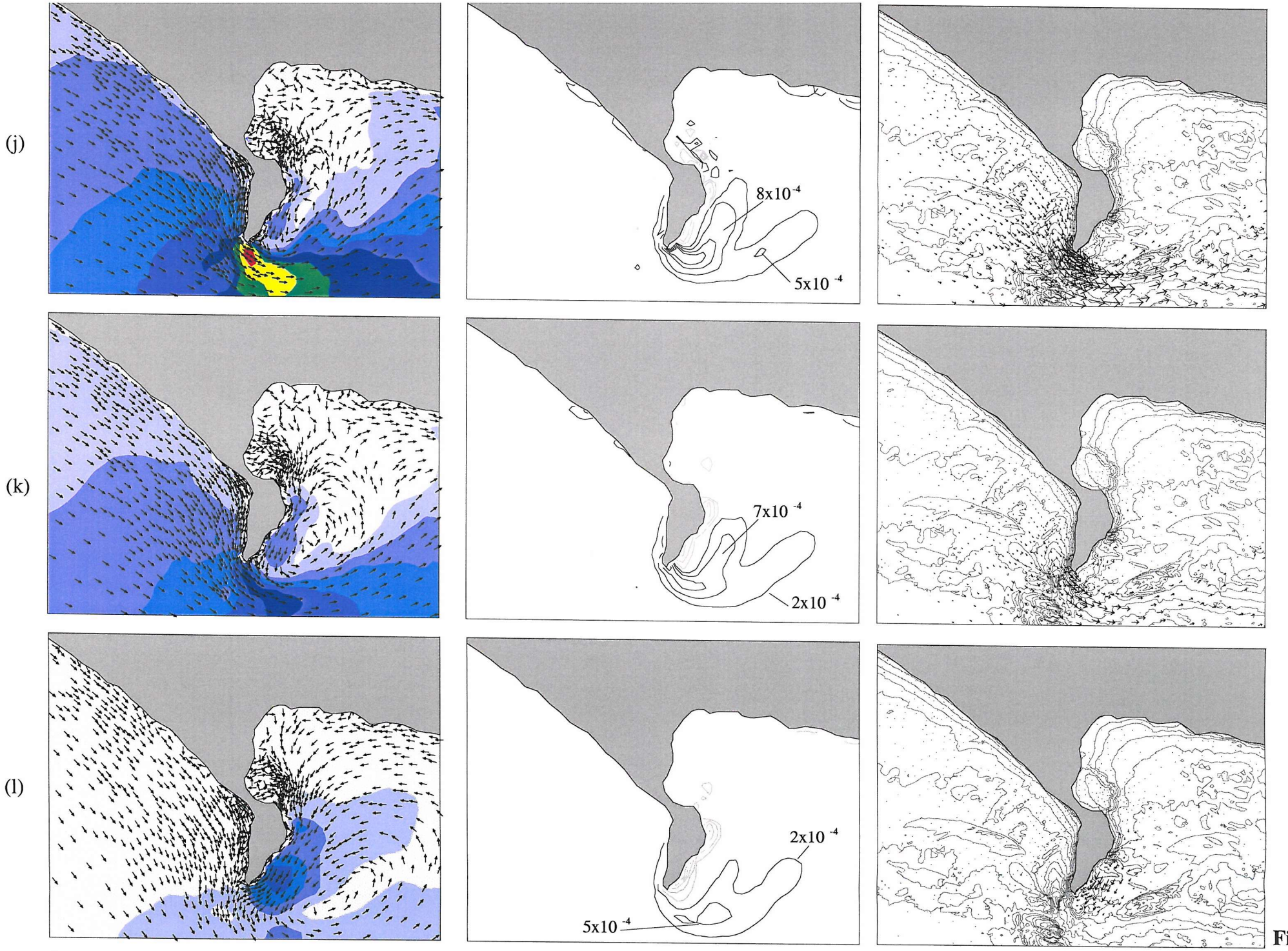

Figure 3

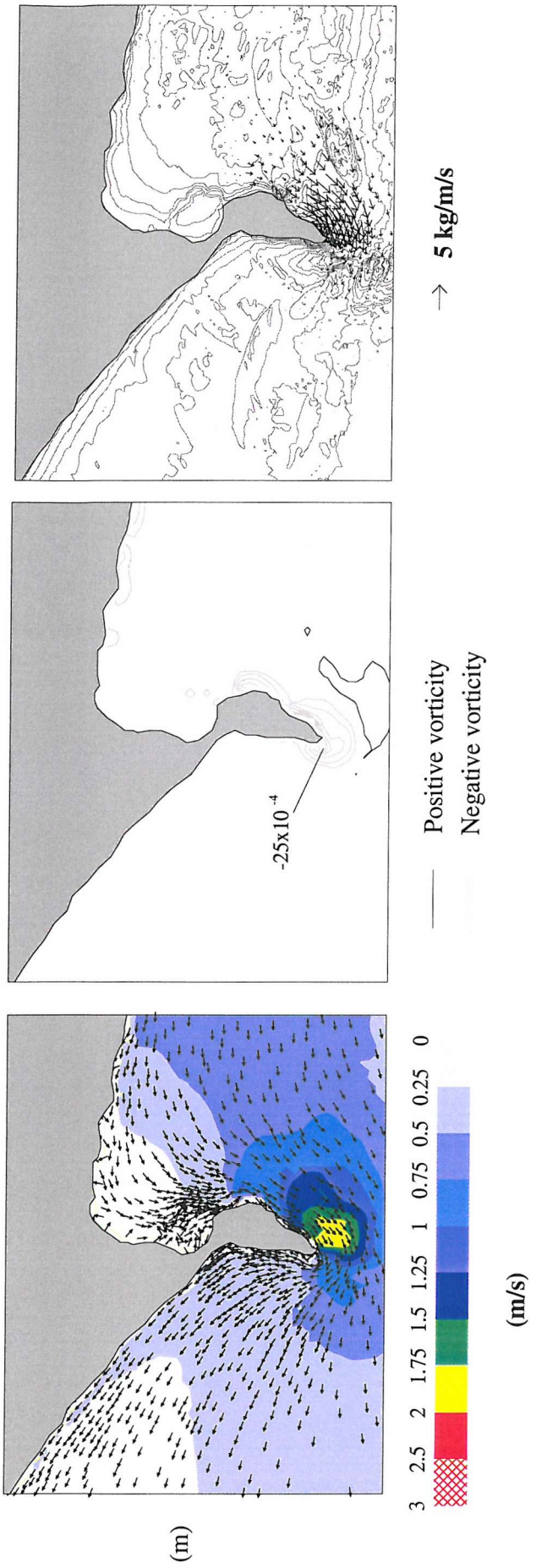

Figure 4.3 Time-series of tidal currents, vorticity and bedload (medium-grained sand) transport over a (spring) tidal cycle.

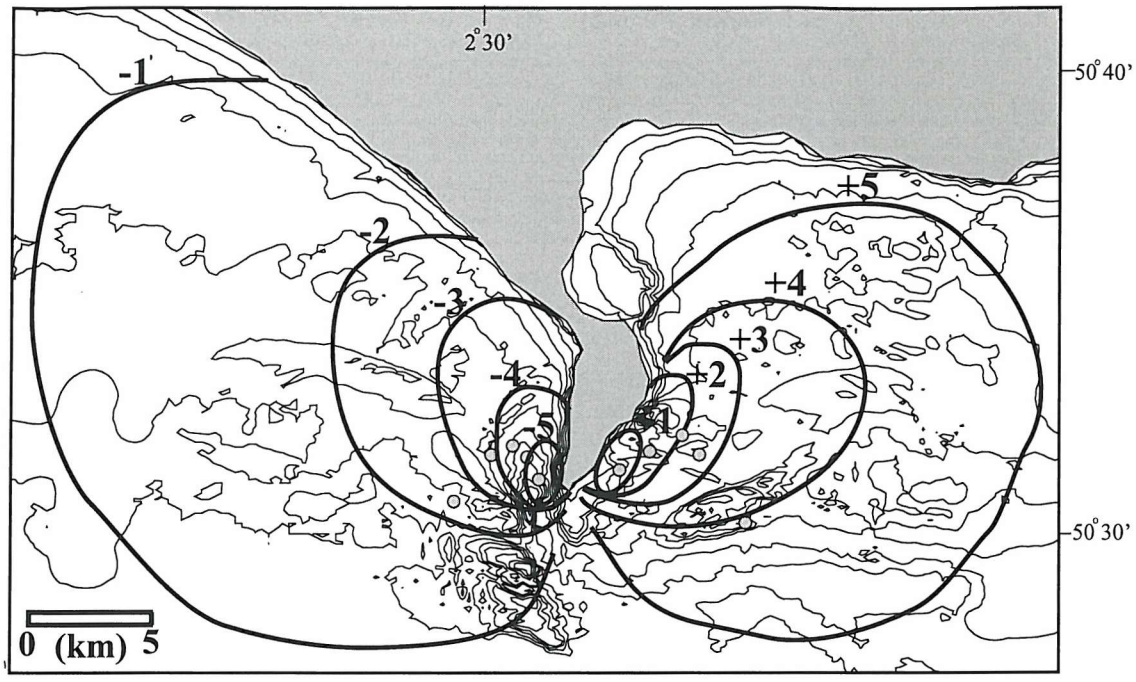

Figure 4.4 Evolution of the tidally-induced transient eddies during the (spring) tidal cycle. Black lines represent the outer limit of the eddies and the grey dots represent the centre of the eddies at different phases of the tide (Note: the different phases of the tide are presented in hourly time-steps in relation to HW in Devonport).

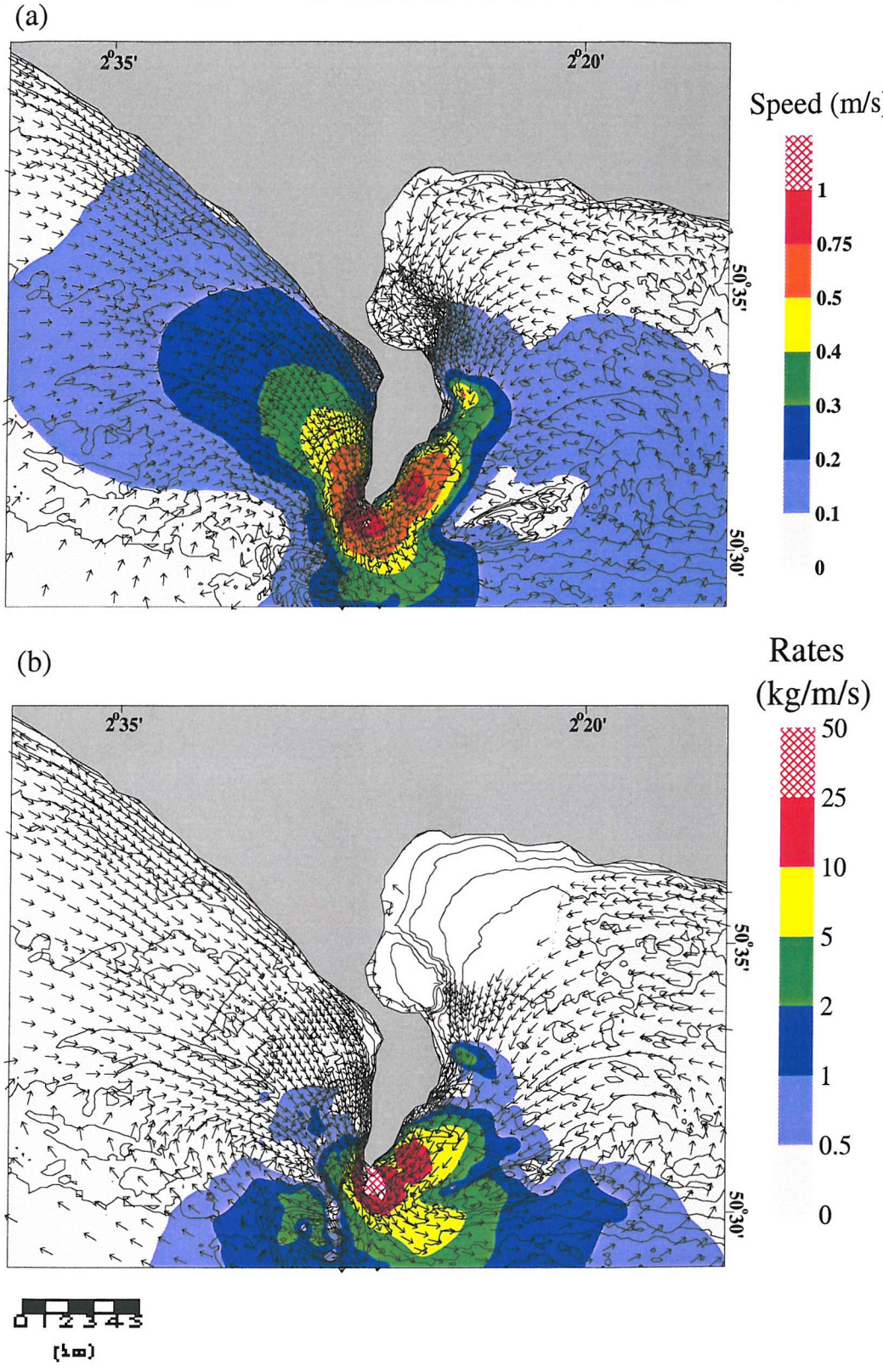

Figure 4.5 (a) Vectors and magnitude of depth-averaged residual currents abstracted from the hydrodynamic model TELEMAC-2D (residual currents were derived by averaging the depth-averaged current, at each point of the grid over a tidal cycle); (b) Vectors and rates of net bedload (medium-grained sand) transport, calculated using SEDTRANS (see text).

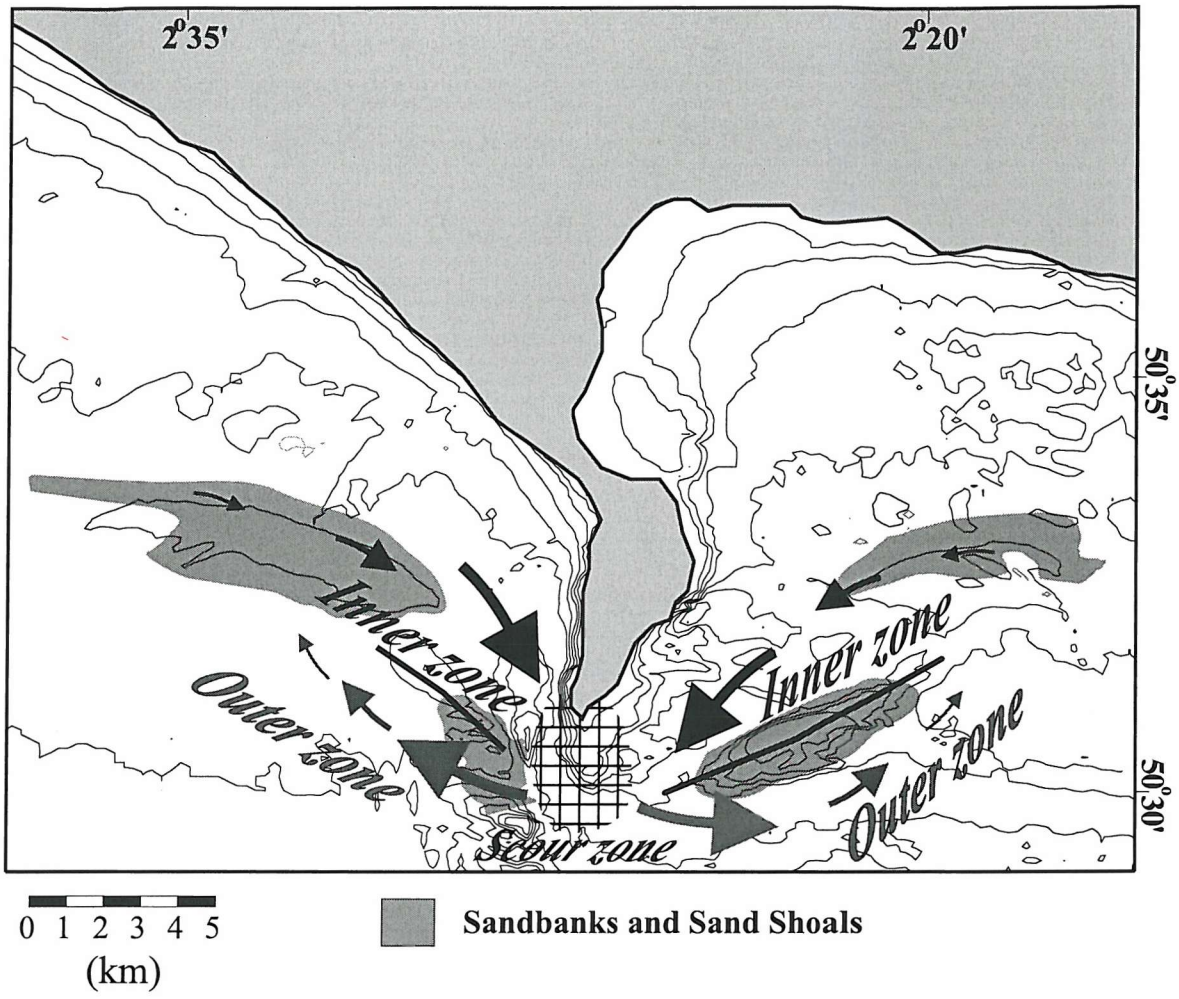

Figure 4.6 Conceptual model of net bedload transport pattern around Portland Bill. Sand transport is characterised by an inner sand mobile zone (black arrow) and an outer sand mobile zone (grey arrow). The scale of the larger arrows represents the direction of increased gradients in bedload transport rates (see Figure 5b). The boundary between those zones represents a sand convergence zone (black line). At the tip of the headland, a zone of maximum erosion occurs (scour zone).

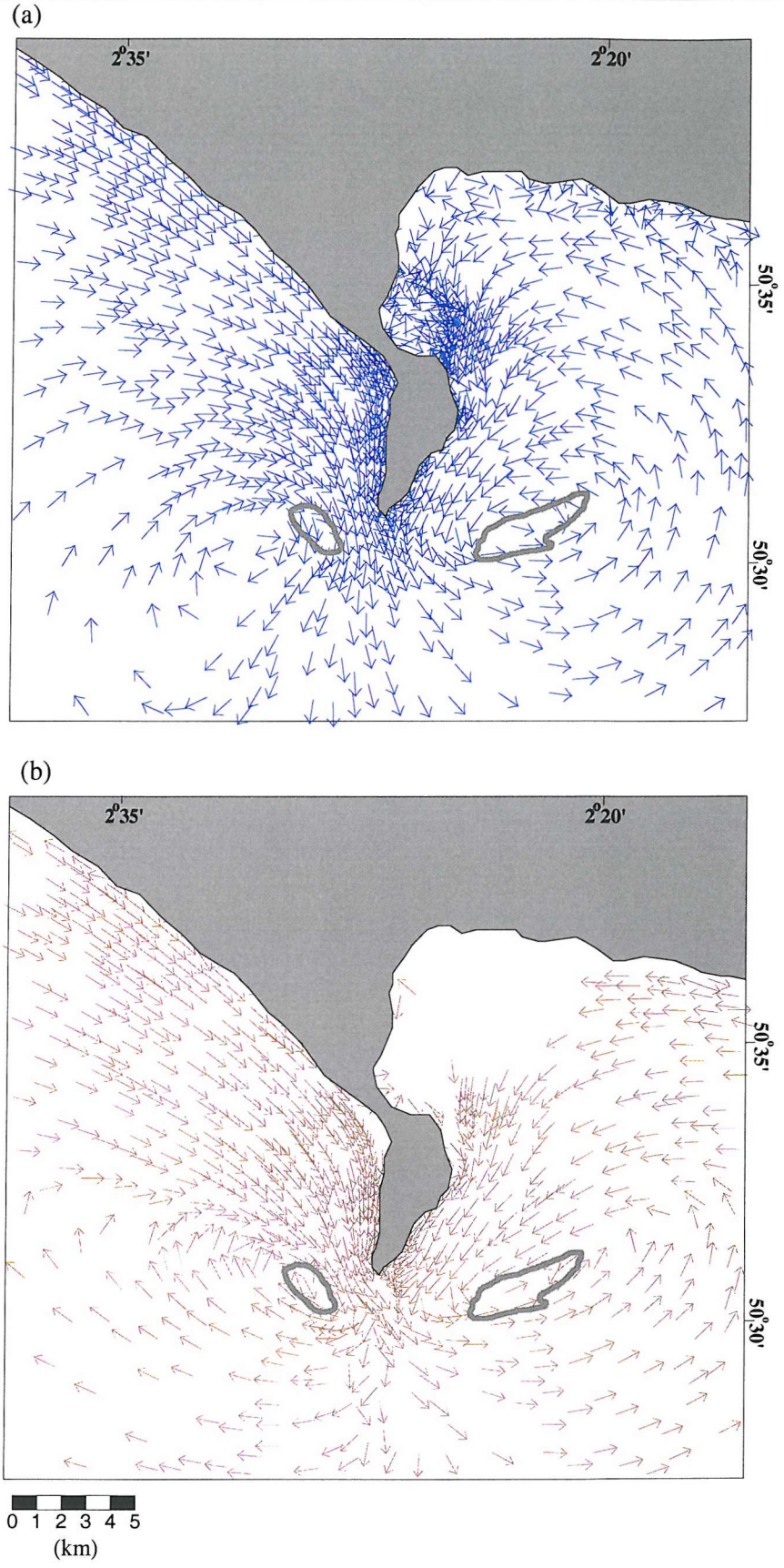

Figure 4.7 (a) Depth-averaged residual current vectors, showing the residual eddies and their relation to the Shambles and Portland Banks; (b) Net bedload transport vectors, showing the occurrence of the bedload convergent zones and their relation to the sandbanks. Arrows are not to scale, in terms of magnitude

Chapter 5

Bastos, A.C.; Paphitis, D., and Collins, M.B. Short-term dynamics and maintenance processes of headland-associated sandbanks: Shambles Bank, English Channel, UK. Submitted to Estuarine, Coastal and Shelf Science in October 2002.

Authors	Initiative	Data Collection and Analysis	Interpretation	Manuscript Preparation
Bastos	100%	100%	70%	70%
Paphitis	-	-	20%	20%
Collins	-	-	10%	10%

Chapter 5

Short-Term Dynamics and Maintenance Processes, of Headland-Associated Sandbanks: Shambles Bank, English Channel, UK

Abstract

The short-term (over a spring tidal cycle) dynamics of a headland-associated sandbank (Shambles Bank, English Channel) are investigated, by means of field measurements (synchronous data, using an Acoustic Doppler Current Profiler (ADCP) and repeated side-scan sonar imagery) and hydrodynamic and sediment transport models. The dynamics of the bank are described in terms of along- and cross-bank velocity components, sand transport pathways and bedform asymmetries.

The results showed the occurrence of a net bedload convergent zone along the crest of the bank as a result of anti-clockwise veering of sediment transport towards the crest. This transport pattern is the results of two distinct tidally-related processes acting over the sandbank, during each phase of the tidal cycle. Overall, the maintenance process is argued to be the consequence of the dynamic interplay between: (a) the formation and different stages of a transient tidal eddy that drives bedload movement, during the flood phase of the tide; and (b) the bottom-friction induced by the presence of the sandbank that governs the bedload transport dynamics, during the ebb phase of the tidal cycle.

Reference: *Bastos, A.C.; Paphitis, D., and Collins, M.B. Short-term dynamics and maintenance processes of headland-associated sandbanks: Shambles Bank, English Channel, UK. Submitted to Estuarine, Coastal and Shelf Science in October 2002.*

5.1 Background

Sandbanks are present on tidally- and wave-dominated continental shelves and within coastal and estuarine environments; they are, generally, the result of abundant sediment availability and strong currents capable of inducing bedload movement (Off, 1963). The formation of a sandbank is associated with the accumulation of sand; this, in fact, is a response to regional sediment transport patterns and gradients in the transport rates. Sand accumulation is likely to occur due to bedload convergence, or a decrease in the bed shear stress along the transport pathway (Dyer and Huntley, 1999). Once formed, sandbanks develop and are being maintained through the continued (dynamic) interaction with the hydrodynamics; these processes can be rather different from the process of formation (Pattiaratchi and Collins, 1987). Different types of banks have been described elsewhere, in relation to their morphology and regional setting (e.g. Off, 1963; Caston, 1972; Swift, 1975; Kenyon *et al.*, 1981; Belderson *et al.*, 1982; Pattiaratchi and Collins, 1987; Berne *et al.*, 1994; and Bastos *et al.*, 2002). Likewise, different mechanisms have been proposed with regards to their maintenance (e.g. Houbolt, 1968; Smith, 1969; Caston, 1972; Pingree, 1978; Huthnance, 1982 a,b; Pattiaratchi and Collins, 1987; Hulscher, 1996; Signell and Harris, 2000; and Calvete *et al.*, 2001).

Off (1963) described rhythmic linear sand bodies caused by currents, based upon world-wide occurrences. Swift (1975) distinguished two different types of sandbanks, based upon Off's description: estuarine or embayment ridges (parallel to the axis of the embayment or estuary) and ridges, off capes and promontories (coast-parallel, tending to be elongated normal to the shore). A third type was described by Swift (1975) as occurring on shelf edges. Pattiaratchi and Collins (1987) described seven different categories of sandbanks, based upon the orientation of the adjacent coastline and to the direction of the prevailing currents. Subsequently, in an extensive review on sandbank classification, Dyer and Huntley (1999) suggested a generic classification based upon sandbank origin and development. These investigators pointed out the necessity to distinguish between the regional context of banks, in terms of their geological origin, and the localised and short-term hydrodynamic processes acting towards its development and maintenance. Three different types of sandbanks were proposed: open shelf ridges (Type 1); estuary mouth banks (Type 2, ridges and tidal deltas); and headland-associated banks (Type 3, banner banks and alternating ridges).

In relation to the maintenance of sandbanks, different theories have been proposed: the spiral flow concept (Houbolt, 1968); the bed shear stress stability model (Smith, 1969); the seabed stability model (Huthnance, 1982a,b); response to standing edge waves (Dolan *et al.*, 1979); and the "tidal stirring" concept (Pingree, 1978). Each of the theories can be applied to the different types of sandbanks. Huthnance (1982a,b) explained the formation of sandbanks as being the result of instabilities on the seabed, in response to interaction between the seabed topography, tidal currents and sediment transport. The stability model (followed, subsequently, by other authors such as: de Vriend, 1990; Hulscher *et al.*, 1993; Trowbridge, 1995; Hulscher, 1996; Calvete *et al.*, 2001; and Hulscher and van den Brink, 2001) explains the growth of a sandbank, lying obliquely to the tidal current direction, by describing the pattern of cross- and along-bank components of the flow; this can be described also in terms of vorticity (see Zimmerman, 1981; Robinson, 1983). As the tidal flow approaches the bank, the along-bank component decreases, due to an increased bottom-friction which, in turn, increases (by continuity) the cross-bank component towards the crest of the bank (the flow veers, as it moves onto the bank); in effect, decreasing the sand transport gradient directed towards the crest. Subsequently, with the reverse of the tidal currents, a convergent sand transport pattern occurs towards the crest of the bank. This concept is supported by the observed morphology of linear sandbanks elsewhere (e.g. Caston, 1972; Kenyon et al, 1981; Belderson et al, 1982; Lanckneus and de Moor, 1995).

The formation of headland-associated sandbanks (Type 3, according to Dyer and Huntley (1999)), could be explained by the convergence of secondary flows associated with residual eddies (the "tidal stirring" concept, introduced by Pingree (1978)) and/or the convergence of sand transport induced by transient eddies (Signell and Harris, 2000; Bastos *et al.*, 2002). The "tidal stirring" concept explains the formation of sandbanks in the centre of residual eddies, generated by coastal irregularities (e.g. headlands (Tee, 1976; Pingree, 1978; Ferentinos and Collins, 1980)). These eddies generate secondary flows, that converge towards the centre of the eddy at the seabed and, by continuity, diverge at the surface. This pattern is controlled by the balance between the pressure gradient, inertial forces and planetary vorticity. A low pressure region at the centre of the eddy leads to a flow convergence at the seabed; this, consequently, gives rise to sand accumulation. However, major limitations to the application of this concept are: (a) that secondary flows represent only around 5-15% of the overall flow; and (b) residual flows can be an order of magnitude lower than the instantaneous flow patterns (Heathershaw and Hamond, 1980; Geyer, 1993). These observations can be important in terms of sediment transport, in cases where the critical shear stress required for

the initiation of sediment movement is not reached (Dyer and Huntley, 1999; Bastos *et al.*, 2002).

The present study examines the short-term (ebb-flood spring tidal cycle) hydrodynamics and sediment dynamics, associated with the tidally-related maintenance processes, of the Shambles Bank (English Channel, see Fig. 5.1). Current measurements (with an Acoustic Doppler Current Profiler (ADCP)) and geophysical data (obtained synchronously) are used; these are combined with a hydrodynamic and sand transport models. This investigation hypothesizes that the bedload sediment transport, responsible for the maintenance of the bank, cannot be explained adequately by simply using one of the aforementioned theories. The dynamic interplay between two different tidally-related processes, operating during each (flood/ebb) phase of the tidal cycle seems to better explain the maintenance process, such as: (a) the development of (headland-associated) transient eddies during the flood phase; (b) bottom-friction induced by the presence of the bank during the ebb phase of the tidal cycle.

5.2 Environmental Setting

The Shambles Bank (Fig. 5.1) is an elliptically-shaped bank lying on top of a flat bedrock erosional surface (Bastos *et al.*, 2002), with a maximum height of 22m above the surrounding seabed; it is about 5km long and 2km wide. The bank is aligned in a NE-SW direction, sub-parallel to the eastern coast of the Isle of Portland; it shows a strongly asymmetric profile, being steeper towards the coast (NW). The bank is characterised by the occurrence of very large sandwaves (wavelength of 300m and maximum crest heights of 7m), with medium and smaller size sandwaves superimposed upon the flanks (stoss side) and/or along the troughs. These small- and medium-sized sandwaves form usually an oblique angle, with the major sandwave crest. A convergent zone of sand transport is indicated by the asymmetry of these large sandwaves, observed along the bank. Flood-dominated asymmetric profiles (pointing towards the NE) are observed along the southwestern flank, whereas the northeastern flank is characterised by the presence of ebb-dominated asymmetric profiles (pointing towards the SW). In terms of sediment composition, the Shambles Bank is characterised, predominantly, by bioclastic material (70% to 80%, by weight) ranging from coarse sand (D_{50} = 0.9mm) to sandy-gravel size (D_{50} = 2.4mm); cohesionless quartz grains represent the remainder of samples. The carbonate content was identified (on the basis of qualitative analysis) as shell fragments of the mussel *Mytilus edulis* (ρ_s = 2.72g cm^{-3}). The spatial distribution of the mean grain size was found to decrease, towards the southwestern end of the bank.

5.3 Methods

5.3.1 Field Survey

A fieldwork programme was designed to provide synchronous information on the prevailing hydrodynamics and the associated seabed response, throughout a complete tidal cycle (13 hours, during the peak of spring tides, in July 2001) across the Shambles Bank (Fig. 5.1). The survey was undertaken under mild meteorological conditions, with wind speeds below 3m s^{-1}; this resulted in relatively weak wave climate, superimposed upon the prevailing tidal currents. The experiment consisted of repeated 3.75km long transverse transects over the bank (each completed within a 30min period), using a ship-mounted ADCP (600Hz, with a vertical resolution of 2m and depth range of 47m) and a high-resolution side-scan sonar (GeoAcoustic, 500kHz). Navigational data were acquired using a Differential Geographical Positioning System (DGPS), precise to within ±1m.

The first of the velocity measurements acquired by the ADCP was about 1m below the transducer (herein referred to as 'surface currents'), whereas the deepest measurement was about 1.5m above the seabed (herein referred to as 'near-bed currents'). The instrument transmitted averaged data, to an on-board PC, once every 5s; these were processed and averaged, to a horizontal sampling interval of 50m (or a time interval of 20s for a boat speed of 2.5m s^{-1}). Given the main orientation of the sandbank (major axis orientated at 70°-250° and the survey transect 340°-160°) the data were transformed into along-bank (parallel, x-component positive to the NE) and cross-bank (perpendicular, y-component positive to the NW) velocity components.

Seabed imagery was acquired, in parallel to the ADCP current data, using side-scan sonar (50m range on either side); these transects formed a time-series and were analysed individually. The data were used to investigate changes (orientation and asymmetry) in the small-scale bedforms (small to medium sandwaves, according to Ashley *et al.*, 1990). A specific area along the bank crest (about 250m long) was selected, to represent the observed bedform changes (Fig. 5.1). The mean water depth at the selected site was 10m, with an associated mean grain size of 1.1mm (75% carbonate content).

5.3.2 Numerical Modelling

Hydrodynamic Model

Tidal flow patterns were characterised over the study area using the results derived from a depth-averaged hydrodynamic model (TELEMAC-2D) set up and calibrated for flow characteristics over the area between the Isle of Wight and Lyme Bay. TELEMAC-2D is a finite element model, based upon shallow-water equations that describe the conservation of water mass and momentum (Hervouet, 1991). The model uses an irregular grid of triangular elements, allowing areas of special interest (e.g. sandbanks) to be examined in greater detail. Output files containing tidal current and water-level data (for spring and neap tides) were processed (over the whole tidal cycle and for every grid point), in relation to vorticity (calculated at each time-step), residual currents (calculated by averaging the depth-averaged current) and the maximum and mean current velocities. The ADCP measurements were used to examine the operational validity of the model over the Shambles Bank. The results obtained (Fig. 5.2) have indicated a good correlation between the depth-averaged velocities (magnitude and direction) derived by the ADCP measurements and those computed by the model.

Sediment Transport Model

Bedload transport was computed using a sediment transport model (SEDTRANS), which calculates bottom shear stresses (under currents alone and combined flows) and sediment transport rates for a given input data set of: water depth; current speed and direction; wave height and period; bed roughness; and grain size (for further details see Li and Amos, 1995). For the present study, the 'potential' bedload transport rates were calculated using the algorithm proposed by Gadd *et al.* (1978). This selection was based upon the results obtained by Grochowski *et al.* (1993). According to these investigators, the algorithm proposed by Gadd *et al.* (1978) showed the best results, in terms of predicting bedload transport rates within the English Channel, when compared to results obtained using radioactive tracers along the French coastline (Dewez *et al.*, 1989). Transport simulations were carried out using the mean grain size (D_{50}) distribution, established over the study area. Critical shear velocities (calculated using Yalin, 1977), required to induce transport, were found to be in reasonable agreement with the results obtained in laboratory experiments, for bioclastic sands (Paphitis *et al.*, 2002). Along the survey transect, the measured (ADCP) velocities were used for the computation of bedload transport; for the remainder of the study area, the computed (hydrodynamic model) velocities were used.

5.4.1 Hydrodynamics

The results obtained from the ADCP measurements show distinct current patterns over the Shambles Bank, associated with the ebb and flood phases of the tidal cycle. The patterns relate to the spatial distribution of the along- and cross-bank flow components. The depth-averaged velocities computed by the hydrodynamic model are plotted in the background, together with the ADCP results (Figures 5.3, 5.4, 5.5 and 5.6), to establish a more complete picture of the prevailing hydrodynamics over the study area.

During the flood phase (about 3 hours after slack water), the currents are flowing towards the E-NE; they are affected by the presence of the headland (Fig. 5.3). Along the bank (Fig. 5.3a), strong currents occur generally offshore (~2.00m s^{-1}) of the southern flank; these reduce significantly as the flow approaches the bank crest (down to ~0.30m s^{-1}). The observed reduction in the along-bank component is followed by an increase in the cross-bank velocity component (from 0.20m s^{-1} to 1.00m s^{-1}) (Fig. 5.3b). Flow acceleration is observed, locally, at the crest of the large bedforms. Overall, water circulation during the flood induces an anti-clockwise veering of the tidal currents, towards the bank crest; this is associated with the development of a tidal (transient) eddy (clearly visible between the bank and the headland). Tidal current veering is observed throughout the entire water column; however, it is more pronounced in the near-bed currents, than in the surface currents (Fig. 5.3c). As the flow leaves the bank crest over its northern flank, a continuous and significant decrease in the along-bank velocity component is followed by a small decrease in the cross-bank component, to coincide with an overall reduction in the current speed.

In Fig. 5.4, the time-step at which the centre of the eddy was detected along the survey transect (about 6 hours into the flood phase, close to slack water) is presented. The along-bank velocity component shows a general reduction, down to 1.25m s^{-1} offshore (on the southern flank of the bank) and 0.20m s^{-1} at the crest (Fig. 5.4a), together with a reversal in the direction (westward flow) observed towards the northern flank. The cross-bank velocity component decreases (down to zero) as the (northward) flow approaches the southern flank of the bank from offshore (Fig. 5.4b); here it reverses to a southward flow. The observed changes in the current direction are influenced, primarily, by the development of the transient

eddy, whose presence is supported by the measured and computed velocity pattern over the area (Fig. 5.4c).

With the tidal reversal, the ebbing currents flow towards the SW (generally, with a direction of 230°), following the coastline contour. The time-step within the tidal cycle, at which the ebb flow is at its maximum (about 3 hour after slack water), is shown in Figure 5.5. Along the survey transect, a decrease in the overall flow is observed towards the bank crest, as the contours tend to follow the topography. The current speeds reach up to 1.65m s^{-1} (inshore) to the north, 0.90m s^{-1} at the bank crest and 1.60m s^{-1} (offshore) to the south (Fig. 5.5a). The cross-bank velocity component shows a slight increase towards the crest, as the flow approaches the bank obliquely from the N-NE (Fig. 5.5b). However, as the flow leaves the bank along the southern flank, the decrease in the cross-bank component is followed by a significant increase in the along-bank velocity component (Fig. 5.5a). The presence of the bank induces an anti-clockwise veering of the tidal currents, towards the crest, as the flow approaches the bank obliquely from the NE. Similarly, a clockwise veering is induced as the flow leaves the crest of the bank, at the southern flank (Fig. 5.5c). This pattern is observed throughout the entire water column; however, because of bottom-friction, the veering is more pronounced in the near-bed currents (Fig. 5.5c).

5.4.2 Bedload Sediment Transport

The derived bedload transport rates, computed using the methodology described previously, are shown in Figure 5.6. During the flood phase of the tide, sand transport was predicted to be significantly high (2.20kg m^{-1} s^{-1} at maximum flood currents), towards the E-NE, just offshore from the southern flank of the bank. Towards the bank crest, a decrease in the transport rates was predicted, ranging between 0.07kg m^{-1} s^{-1} to 0.80kg m^{-1} s^{-1}; this is followed by a slight anti-clockwise veering in the sand transport direction (Fig. 5.6a). The steady decrease in the flow (as it leaves the bank) over the northern flank (observed previously, see Fig. 5.3) is followed by a significant reduction in the sand transport rates. When the core of the transient eddy was positioned over the survey transect (close to slack water, see Fig. 5.4), no sand movement is predicted along the bank crest. There is only a very low transport rate predicted towards the SW, at the northern end of the transect (0.009kg m^{-1} s^{-1}) (Fig. 5.6b). Higher rates are predicted towards the NE, just offshore of the southern flank of the bank (of up to 0.25kg m^{-1} s^{-1}). During the above two time-steps (Figs 6a and 6b) the flow pattern and, in turn, the

bedload transport rates are influenced by the presence of the headland and the different stages of the transient eddy. The flood-associated bedload sediment transport is characterised by an anti-clockwise veering towards the crest, from the southern flank; this is followed by a decrease in the transport rates at the crest.

In contrast to the flood phase of the tidal cycle, the ebbing flows induce a significant level of sediment movement throughout the entire system, with a notable reduction towards the crest of the bank. At maximum ebb currents (Fig. 5.5), the rates vary from 0.25kg m^{-1} s^{-1} (along the crest) to 0.92kg m^{-1} s^{-1} (at the northern flank). The sediment movement is associated with an anti-clockwise veering (towards the crest), of the transport path pathway (Fig. 5.6c). Along the crest, the rates were observed to reduce within the troughs of the larger bedforms. Along the southern flank, where the flow leaves the bank, the sand transport rates are increased significantly (reaching 0.85kg m^{-1} s^{-1}); this is followed by a clockwise veering of the transport pathway. The bedload sediment transport, associated with the ebb phase of the tide, is characterised by an anti-clockwise veering towards the crest from the northern flank; this is followed by a decrease in the predicted transport rates, at the crest.

Bedload transport computations were not undertaken under the influence of superimposed waves, given their absence at the time of the survey. However, waves can contribute towards the maintenance of sandbank, particularly under storm conditions. Several researchers have highlighted the importance of storm waves in the evolution and migration of sedimentary deposits (Ferentinos and Collins, 1980; Houthuy *et al.*, 1994; Berne *et al.*, 1994; Tessier *et al.*, 1999). Under storm conditions, the crest of the bank is reworked by wave action, which controls the height of the sandbank.

5.4.3 Bedform Dynamics

The seabed imagery time-series has revealed reversal in the asymmetry of the small sandwaves (SSW), lying along the bank crest; these have an average wavelength of 3m and an average height of 0.65m. Bedform reversal was observed on the basis of the backscatter response of the profiles (whereby low tonality is related to low backscatter). The SSW crestlines over the selected area, were found to lie at a SE-NW orientation (100°-280°); this placed them obliquely to the transect direction, at a 60° angle. The seabed at the time of maximum flood currents (1.35m s^{-1} depth-averaged, see Fig. 5.3) is shown in Figure 5.7a; the

lee (steep) side of the sandwaves faced N-NE (10° from N). Such flood-dominated asymmetry was observed for another 3 hours, following the maximum currents. With reversal in the tidal flow and the beginning of the ebb half-cycle, the side-scan sonar records show a pattern associated with ripple *cat-back* formations (van Veen, 1935; Berne *et al.*, 1993); this is indicative of the initial erosion of the SSW crests (Fig. 5.7b). At maximum ebb currents (1.50m s^{-1} depth-averaged, see Fig. 5.5), the lee side of the sandwaves was found to be orientated towards the S-SW (190° from N) (Fig. 5.7c). Towards the end of the tidal cycle, the ripple *cat-back* formations are again observed on the side-scan sonar record; they correspond with flow reversal from ebb- to flood-dominated currents.

5.4.4 Bedload Transport and Bedform Dynamics

The time-series bedload transport rates, predicted using near-bed (ADCP) currents and a mean grain size of 1.1mm, are plotted in Figure 5.8, together with bedload transport direction, as inferred from the bedform asymmetries, at the selected location (Fig. 5.1) along the survey transect. During the flood phase of the tide, bedload transport is reduced gradually to become insignificant 2hrs before reversal of the tide. Over this period, the bedforms are flood-dominated, revealing a transport pathway towards the N-NE (10° from N). Within the first hour after the initiation of the tidal reversal, when bedload transport begins to increase, *cat-back* formations (near-bed currents ~0.9m s^{-1} and transport rates ~0.18kg m^{-1} s^{-1}) are observed; these coincide with the bedforms attempting to adjust to the changing hydrodynamic conditions. By the time the ebbing currents (near-bed ~1m s^{-1}) and bedload transport rates (0.32kg m^{-1} s^{-1}) reach their maximum, the sandwaves have adjusted to the prevailing conditions and are completely reversed (indicating a transport pathway towards the S-SW, about 190° from the N). With the ebb phase of the tide drawing to an end (after about 6hrs), transport rates are reduced. At the point of reversal, with subsequent acceleration of the flood currents, the *cat-back* formations were again detected; this was followed once again, by a reversal in the bedform asymmetry.

5.5 Discussion

The present investigation has examined the short-term dynamics of a sandbank (the Shambles Bank), in terms of water circulation, bedform mobility, and bedload transport rates and pathways; these are summarised in a conceptual model (Fig. 5.9). The results indicate that two distinct tidally-related sandbank maintenance processes act, sequentially, throughout the tidal cycle. Hence, the tidally-related sedimentary processes are influenced by: (a) the formation of headland-associated (Portland Bill) transient eddies during the flood phase of the tidal cycle; and (b) bottom-friction, induced by the presence of the sandbank during the ebb phase of the tidal cycle. Distinct patterns of sediment transport were identified during the tidal cycle, in relation to the hydrodynamically-associated sandbank processes (as described above). Because of the non-linearity of sediment transport, to the prevailing flow conditions, instantaneous sand transport patterns do not necessarily follow the same transient pattern as that of the tidal flow.

During the flood phase of the tide (Fig. 5.9a), a zone of flow separation occurs at the tip of the headland, with the strongest currents flowing towards the east. In relation to the main axis of the Shambles Bank, orientated in a NE-SW direction (70°-250°), an anticlockwise veering of the flood currents is produced; this is created, mainly, by vorticity being advected away into the flow, as it passes the headland (Fig. 5.3). Hence, it appears that, during the flood, the centrifugal forces induced by the flow curvature (due to the presence of the headland) are, relatively, more significant in terms of bank maintenance processes than the bottom-friction induced by the presence of the Shambles Bank. Throughout the development of the transient eddies (during the flood tide, see Fig. 5.9a), sand transport is observed along the southern flank and towards the crest of the bank (Fig. 5.6a and 5.6b); this reduces significantly along the northern flank, due to flow deceleration. During later stages of the flood tide, as the centre of the transient eddy migrates towards the bank, the transport rates reduce gradually; however, the transport pathway remains the same (as indicated by the bedform asymmetries).

The presence of secondary flows in the plane normal to the mean current field, as indicated by the veering of the current direction with depth, was observed directly in the ADCP measurements and reached speeds of up to 0.20 m s^{-1} (10% of the maximum surface currents). These currents are comparable with those observed (5 to 15% of the streamwise flow) by Geyer (1993) around Gay Head (Massachusetts, USA) and those predicted (about 10% of the

peak currents) by Heathershaw and Hammond (1980) for the Scarweather Sands (Bristol Channel, UK). Secondary flows are generated by the flow curvature; they interact with the primary flow and can influence significantly its structure and affect the horizontal and vertical water-mass transport around a coastal headland (Geyer, 1993). In terms of sediment transport processes around a sandbank, the presence of such currents have been related to *helical cells* that would act as a mechanism to transport and concentrate sand along the crest of the banks (Houbolt, 1968; Heathershaw and Hammond, 1980). However, considering that the magnitude of such currents is only about 10% of the maximum primary flow, their capacity in transporting sediments appears to be minimal; hence, secondary flows may have an indirect influence (related to the current veering) in sand transport processes around sandbanks.

The ebb currents (Fig. 5.9b) are flowing towards the SW, approaching the northern flank of the bank obliquely at an angle of 10° to 15°; these set up an anticlockwise veering towards the crest, followed by acceleration in the cross-bank velocity component (Fig. 5.5). As the flow leaves the sandbank, a clockwise veering of the currents occurs; this is followed by an increase in the along-bank component. Thus, the observed water circulation pattern, during the ebb phase of the tidal cycle, highlights the influence of bottom-friction induced by the presence of the sandbank; this is supportive of the stability model of Huthnance (1982b). The flow pattern results in an anticlockwise sand transport veering, towards the crest. The main difference, on the ebb, to the pattern observed during the flood tide is the clockwise veering of sand transport, followed by an increase in transport rates, along the southern flank (as the ebbing flow leaves the sandbank) (Fig. 5.6c). The presence of secondary flows, as indicated by the veering in the tidal currents, was again observed in the ADCP data.

The predicted bedload transport rates and directions, throughout the complete tidal cycle, indicate that the crest of the bank acts as a bedload convergence zone. This has resulted from an anticlockwise veering of the sand transport towards the crest, followed by a decrease in transport rates. This pattern has been observed elsewhere, on the basis of geomorphological evidences and *in situ* measurements, by various authors (Houbolt, 1969; Caston, 1972; Kenyon *et al.*, 1981; Pattiaratchi and Collins, 1987; Lanckenaus and de Moor, 1995; Collins *et al.*, 1995; Williams *et al.*, 2000). Such an interpretation differs conceptually from the residual circulation results; it includes the non-linear dependence of sand transport. Pingree (1978) has suggested that the formation and maintenance of headland-associated sandbanks can be the result of near-bed flow convergence and surface flow divergence, established with a residual eddy. However, such a concept may be applicable only to the description of water

circulation, rather than sediment movement, given that residual currents are an order of magnitude less than the instantaneous flow; for such (low) currents, sand transport is not predicted (Dyer and Huntley, 1999; Bastos *et al.*, 2002). Nonetheless, the occurrence of a sand convergence zone can be considered, in specific cases (see Signell and Harris, 2000), to represent the sediment dynamic expression of a residual eddy.

In terms of the morphology of the Shambles Bank, a geophysical investigation has revealed the occurrence and distribution of very-large asymmetric sandwaves (Bastos *et al.*, 2002); these show convergent sand transport towards the bank crest, corroborating the predicted net sediment transport patterns. However, the presence of superimposed small and medium sandwaves, forming usually an oblique angle (with crest directions at about 280°-100°) with the main bank axis and with the very-large sandwave crests (Fig. 5.7), indicates the veering of sand transport paths towards the bank crest. This provides evidence of the significance of the cross-bank velocity (transport) component. Such a pattern has been observed also on Type 1 sandbanks (or linear sand ridges) in the North Sea (Houlbolt, 1968; Kenyon *et al.*, 1981; McCave and Langhorne, 1982; and Lanckneus and de Moor, 1995). The seabed time-series obtained over the Shambles Bank has revealed the complete reversal of small sandwaves, during the ebb-flood cycle (on spring tides), with an intermitting period (indicating the beginning of the reversal process) characterised by *cat-back* formations. The short-term reversal of small to medium sandwaves, over sandbanks and shoals, has been described elsewhere (Hawkins and Sebbage, 1972; Boersma and Terwindt, 1981; Terwindt and Brouwer, 1986). Moreover, the reversal of large sandwaves over sandbanks has also been observed, however, in a medium- to long-term temporal scale (Berne *et al.*, 1993; and Lanckneus and de Moor, 1995). Hence, small and medium sandwaves can provide a good indication of short-term dynamic sediment transport processes over a sandbank.

In the case of headland-associated sandbanks, Pattiaratchi and Collins (1987) suggested previously that the maintenance process for the Scarweather Sands (Bristol Channel, U.K) was the result of a combination of different possible mechanisms: the "tidal stirring" concept (Pingree, 1978); bottom-friction, induced by the sandbank (stability model, Huthnance, 1982); and the presence of helicoidal (secondary) flows (the spiral flow concept; Houlbolt, 1968 and Heathershaw and Hammond, 1980). For the Shambles Bank, the field observations described here confirm, similarly, the occurrence of different mechanisms acting over the sandbank, at different stages of the tide. The associated bedload transport investigations have indicated that transient tidal eddy formation is the dominant process over the flood phase of the tide.

Bottom-friction, induced by the presence of the sandbank, appears to explain better the maintenance process during the ebb phase of the cycle. Although the presence of helicoidal (secondary) flows was observed, their contribution to bedload transport is uncertain, as the magnitude of the vertical circulation of the flow was only some 10% of the surface peak tidal currents.

5.6 Conclusions

Although the derived residual sand transport pattern is similar to those described elsewhere (Caston, 1972, Kenyon *et al.*, 1981; Belderson *et al.*, 1982; Pattiaratchi and Collins, 1987, Lanckneus and de Moor, 1995; Collins *et al.*, 1995; and Williams *et al.*, 2001), processes differ between the flood and ebb phases of the tidal cycle. For the Shambles Bank, sand transport is controlled by the formation of transient tidal eddies, during the flood phase of the tide. At this time, sand transport is directed through its southern flank, towards the bank; this is in response to flow rotation, imposed by the vorticity generated at the tip of the headland and advected into the downstream flow. During the ebb phase of the tide, sand transport is directed again towards the bank crest; however, this time, bottom-friction induced by the presence of the bank forces veering in the sand transport vector, towards the bank crest. Finally, although the study has shown that sand transport is controlled by different tidally-related mechanisms, the overall net sand transport circulation pattern is related to: (a) deceleration in the along-bank component; and (b) an increase in the cross-bank component (with a general decrease in flow, over the bank). This process was observed during both phases of the tidal cycle; as such it can provide a mechanism for the veering of sand transport, towards the bank crest, together with the deposition of sedimentary material.

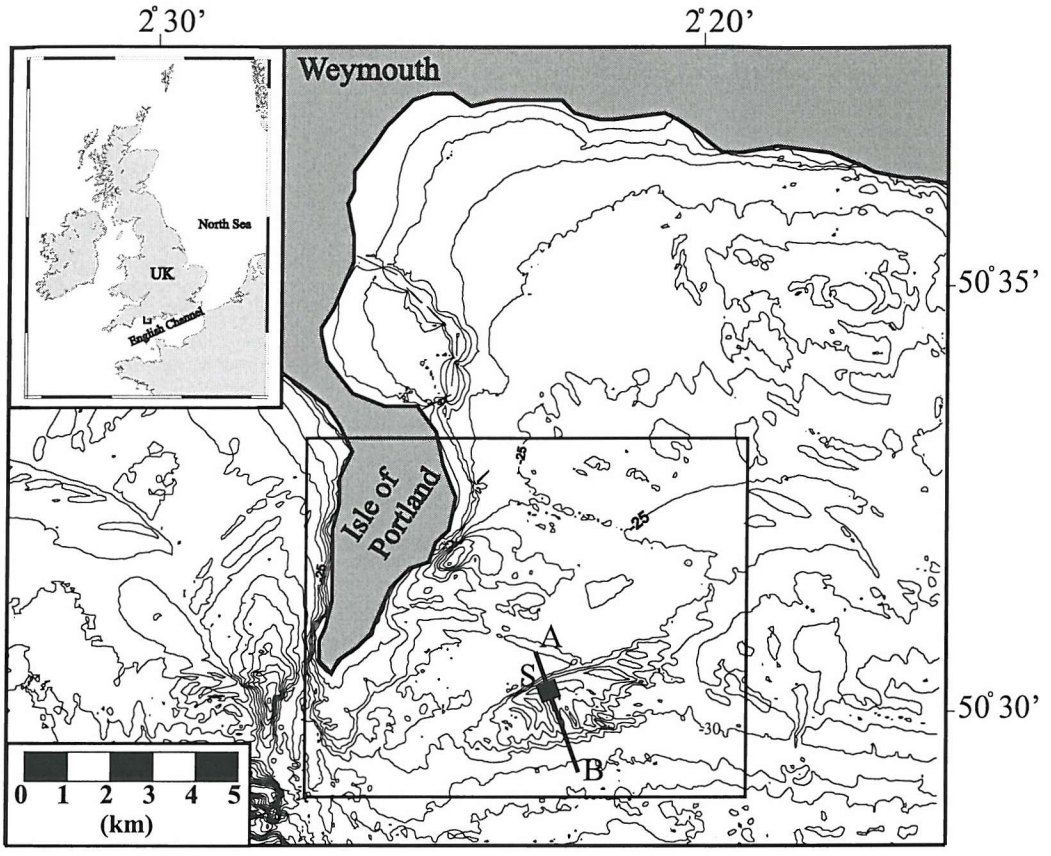

Figure 5.1 Regional setting of the Shambles Bank along the southern coast of the U.K. Bathymetry in metres (relative to Chart Datum). Line A-B is the survey transect and the box marks the selected side-scan sonar survey area.

(a)

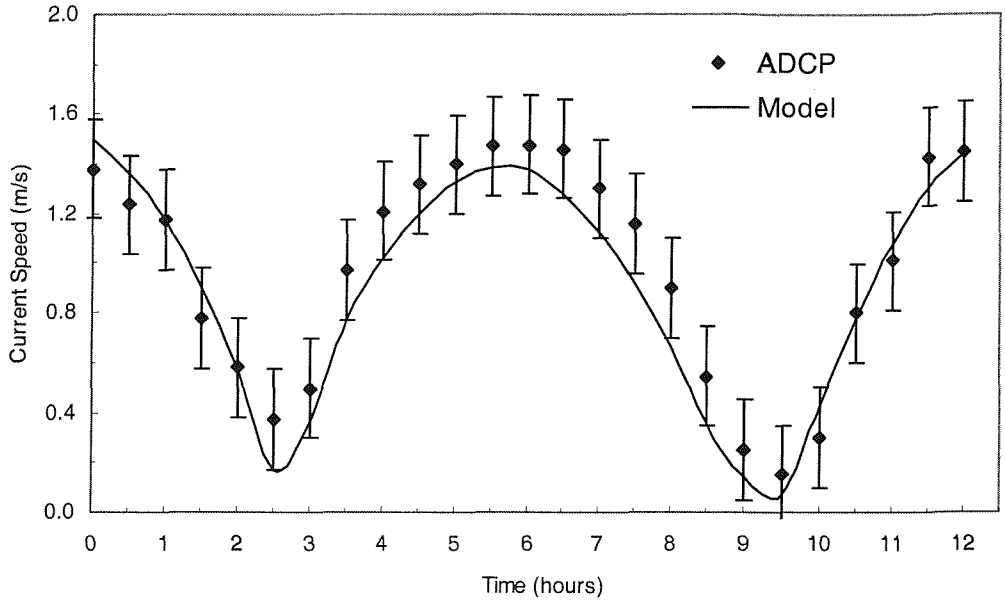

(b)

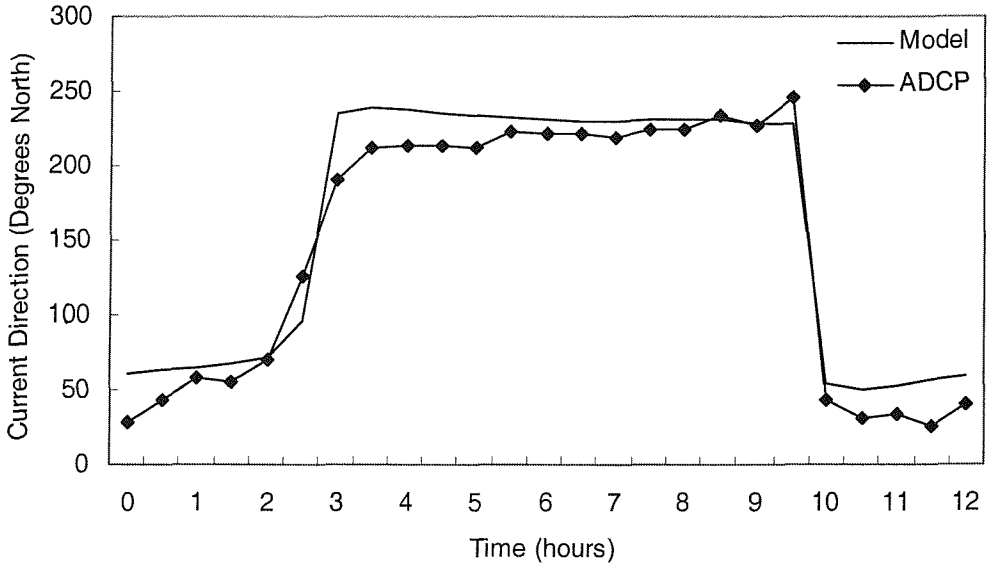

Figure 5.2 Operational validation of the hydrodynamic model, using the ADCP measurements, at a point along the crest of the Shambles Bank: (a) tidal current depth-averaged velocities; (b) tidal current direction.

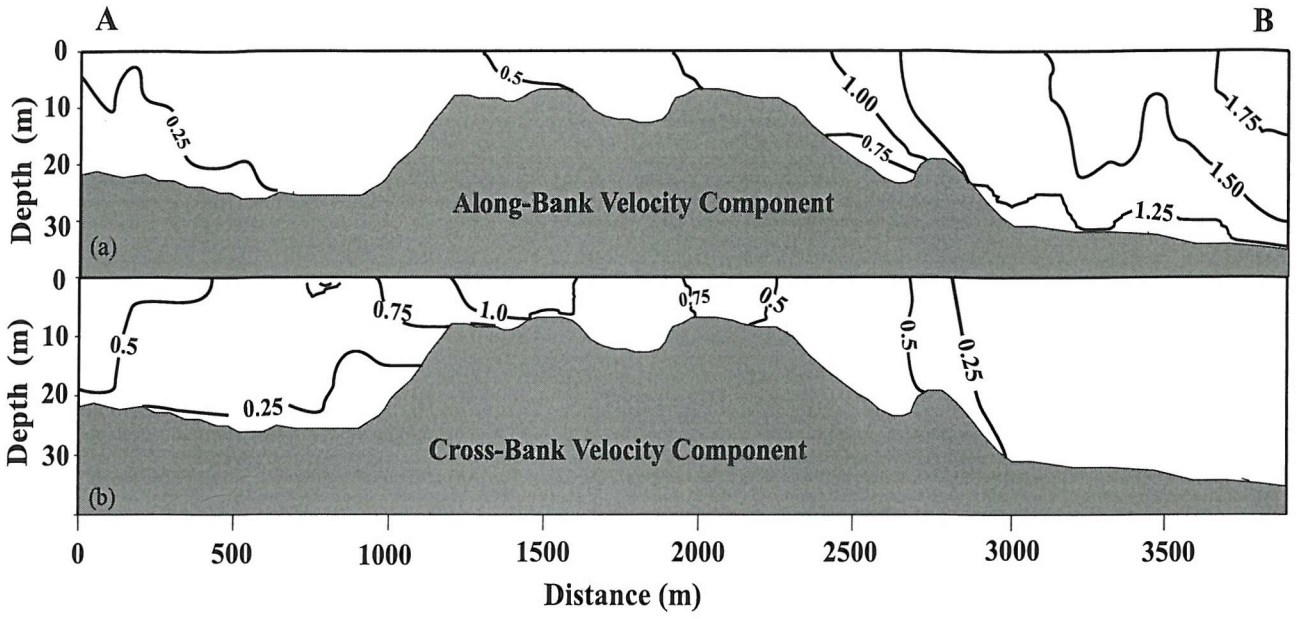

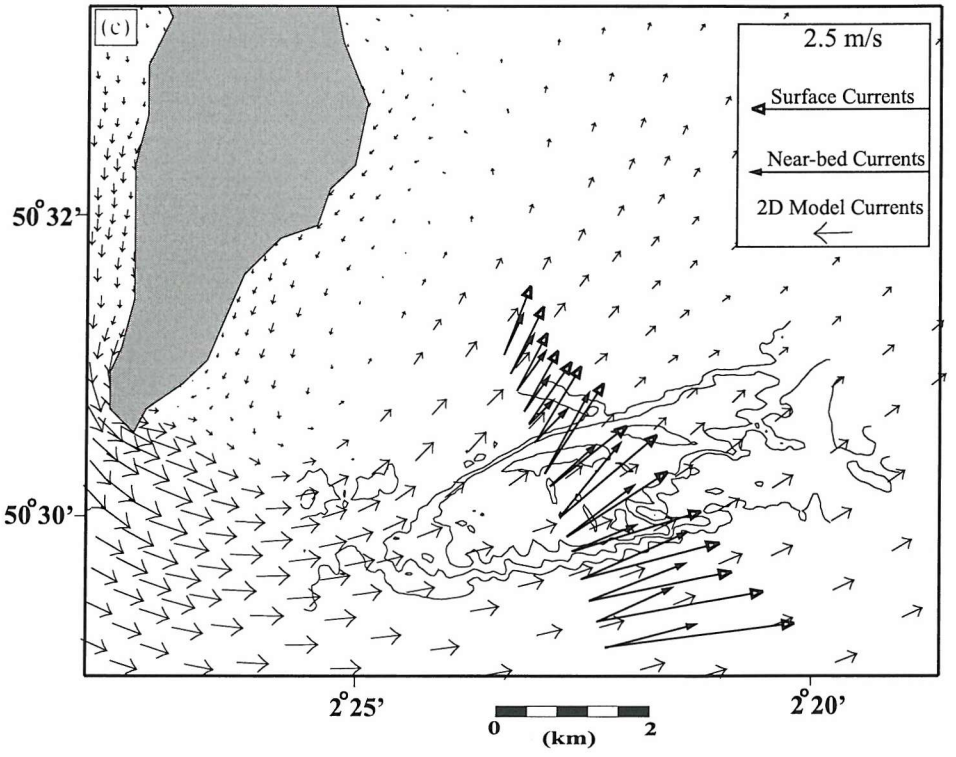

Figure 5.3 Flow pattern obtained from the ADCP results, during the maximum flood currents: (a) the along-bank current component (ms^{-1}; positive x-axis toward the NE); (b) cross-bank current component (ms^{-1}; positive y-axis toward the NW); and (c) surface (open arrows) and near-bed (black arrows) tidal current vectors, together with the depth-averaged velocities, as computed by the numerical model. Note: scale differences between the ADCP arrows and the numerical model arrows.

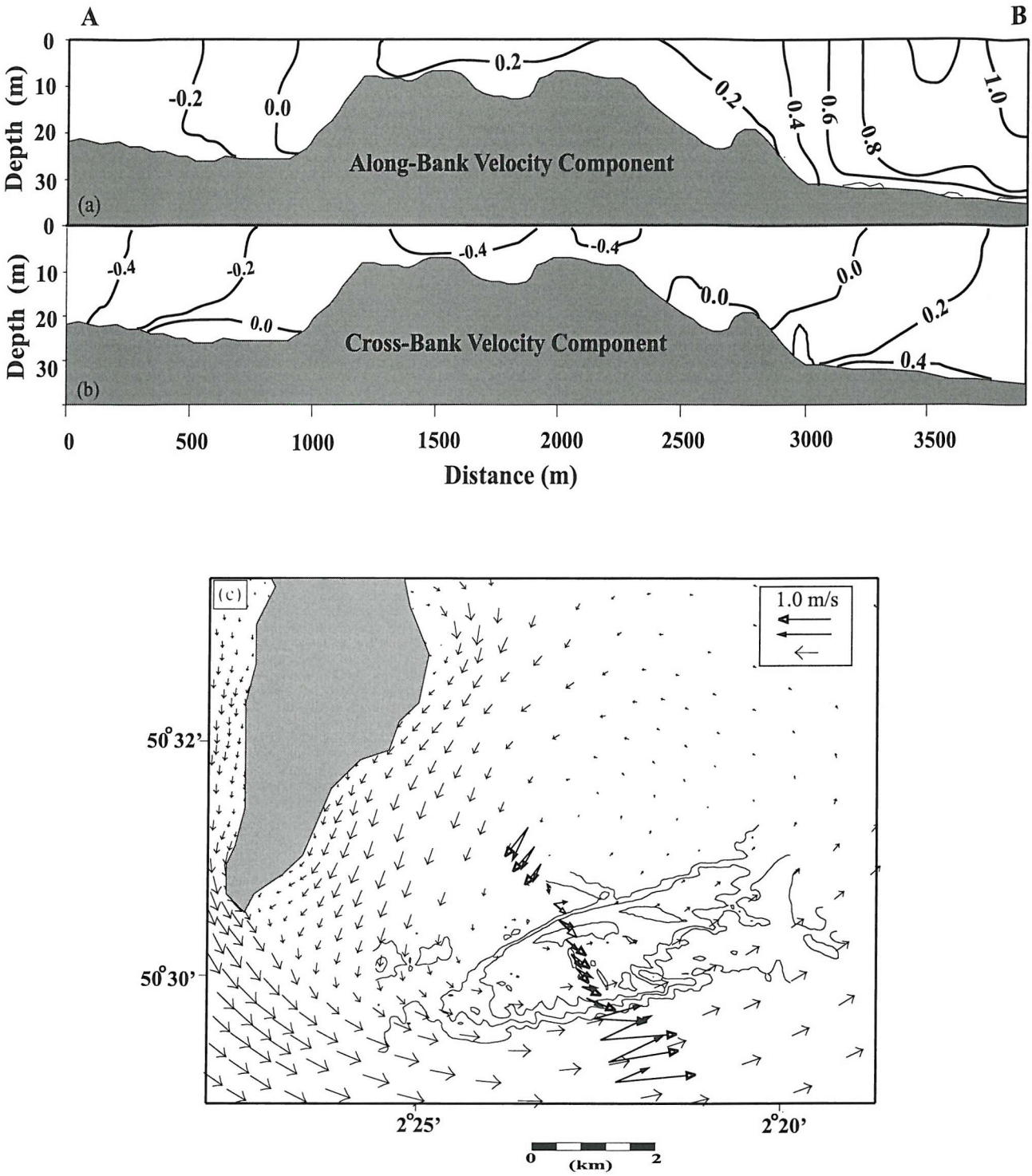

Figure 5.4 Flow pattern obtained from the ADCP results, during the time-step at which the centre of the transient eddy lies over the Shambles Bank: (a) along-bank current component (ms^{-1}; positive x-axis toward the NE); (b) cross-bank velocity current (ms^{-1}; positive y-axis toward the NW); and (c) surface (black arrows) and near-bed (grey arrows) tidal current vectors, together with the depth-averaged velocities, as computed by the numerical model. Note: scale differences between the ADCP arrows and the numerical model arrows.

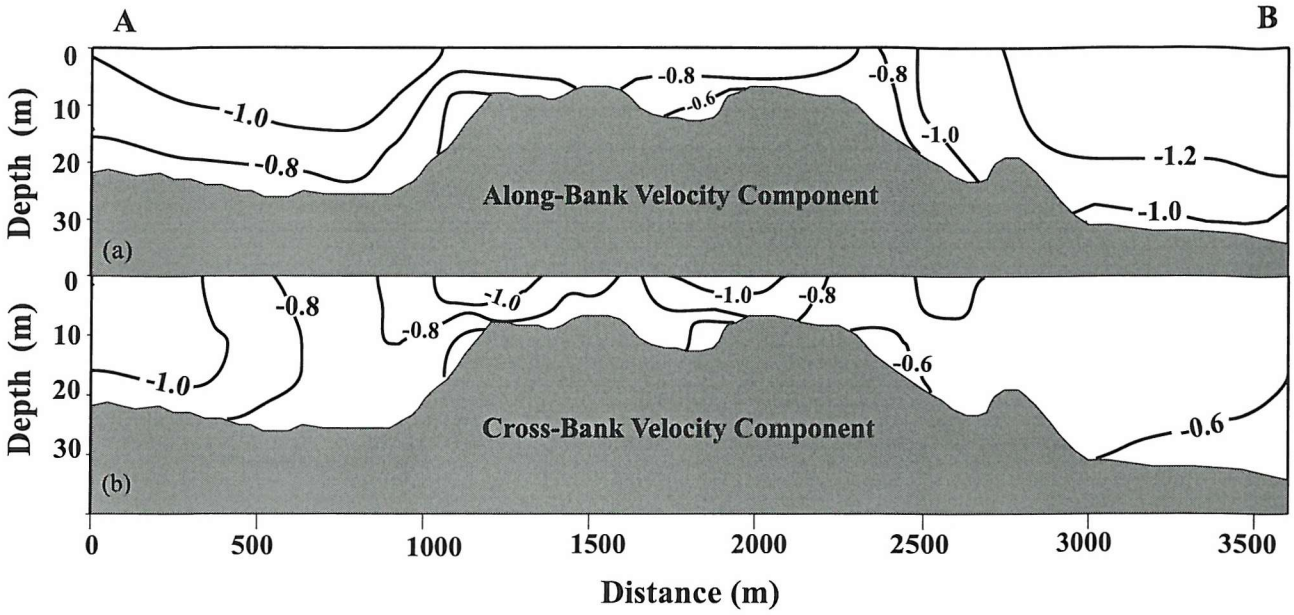

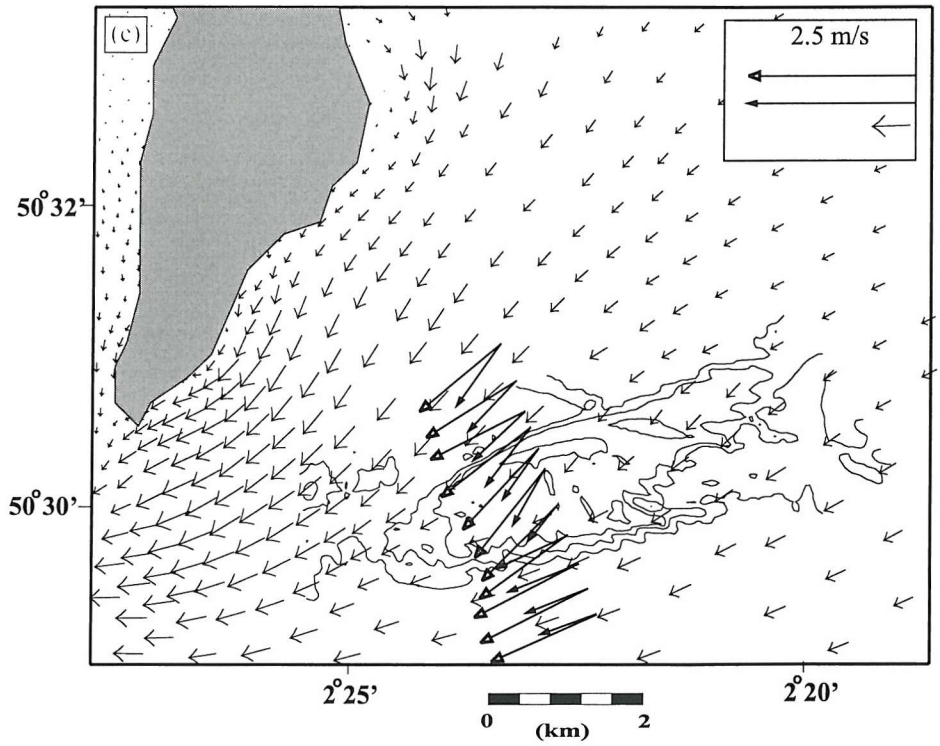

Figure 5.5 Flow pattern obtained from the ADCP results, during the maximum ebb currents: (a) along-bank current component (ms^{-1}; positive x-axis toward the NE); (b) cross-bank velocity current (ms^{-1}; positive y-axis toward the NW); and (c) surface (black arrows) and near-bed (grey arrows) tidal current vectors, together with the depth-averaged velocities, as computed by the numerical model. Note: scale differences between the ADCP arrows and the numerical model arrows.

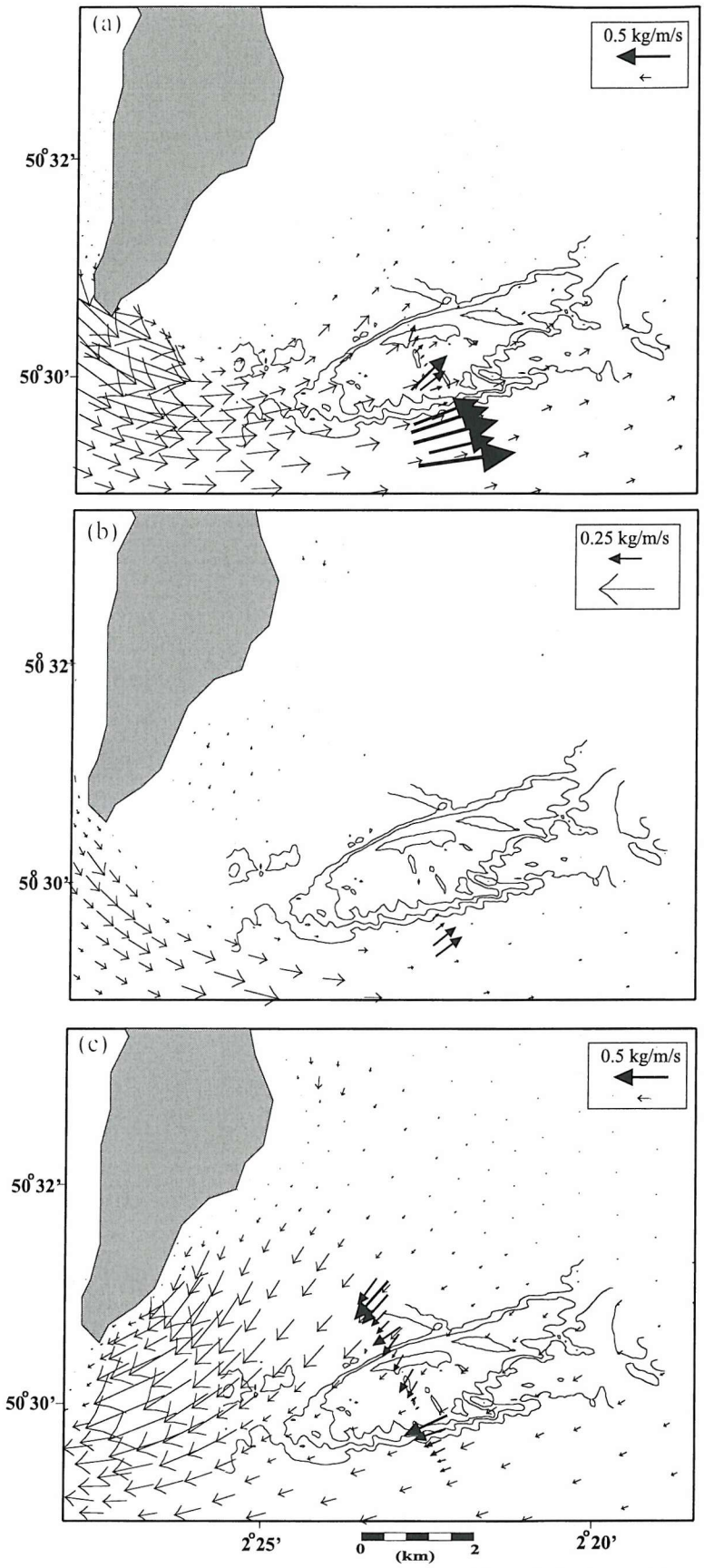

Figure 5.6 Instantaneous bedload (sand) transport vectors predicted during: (a) maximum flood (Fig. 3); (b) a transient eddy over the bank (Fig. 4); and (c) maximum ebb (Fig. 5). The ADCP results were used for the survey transect whereas, for the remainder of the area, the model results were utilised. Note: scale differences between the arrows showing the rates calculated using ADCP and numerical model results.

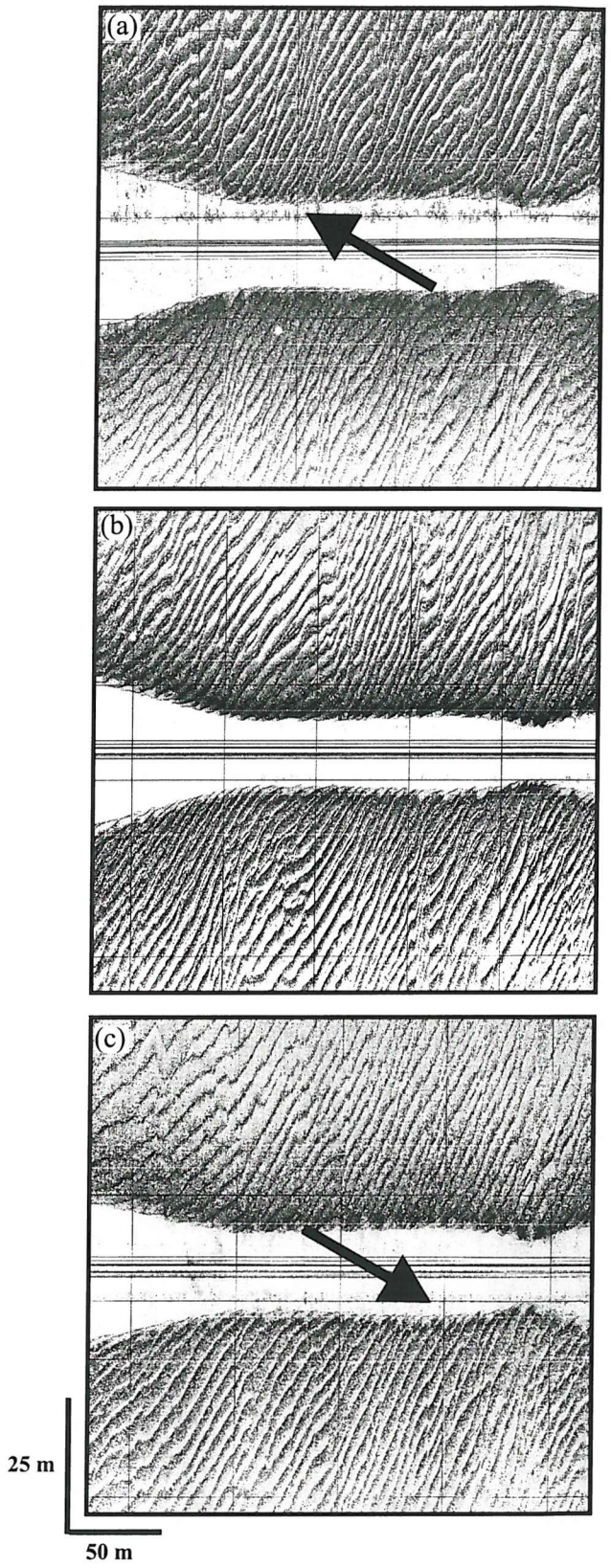

Figure 5.7 Side-scan sonar images (for location, see Fig. 1) showing (light tone, associated with low backscatter): (a) small sandwaves, with flood-dominated asymmetry (indicated by the black arrow); (b) small sandwave *cat-back* formation, indicating erosion of the crest (during reversal); and (c) small sandwaves, with ebb-dominated asymmetry (indicated by the black arrow).

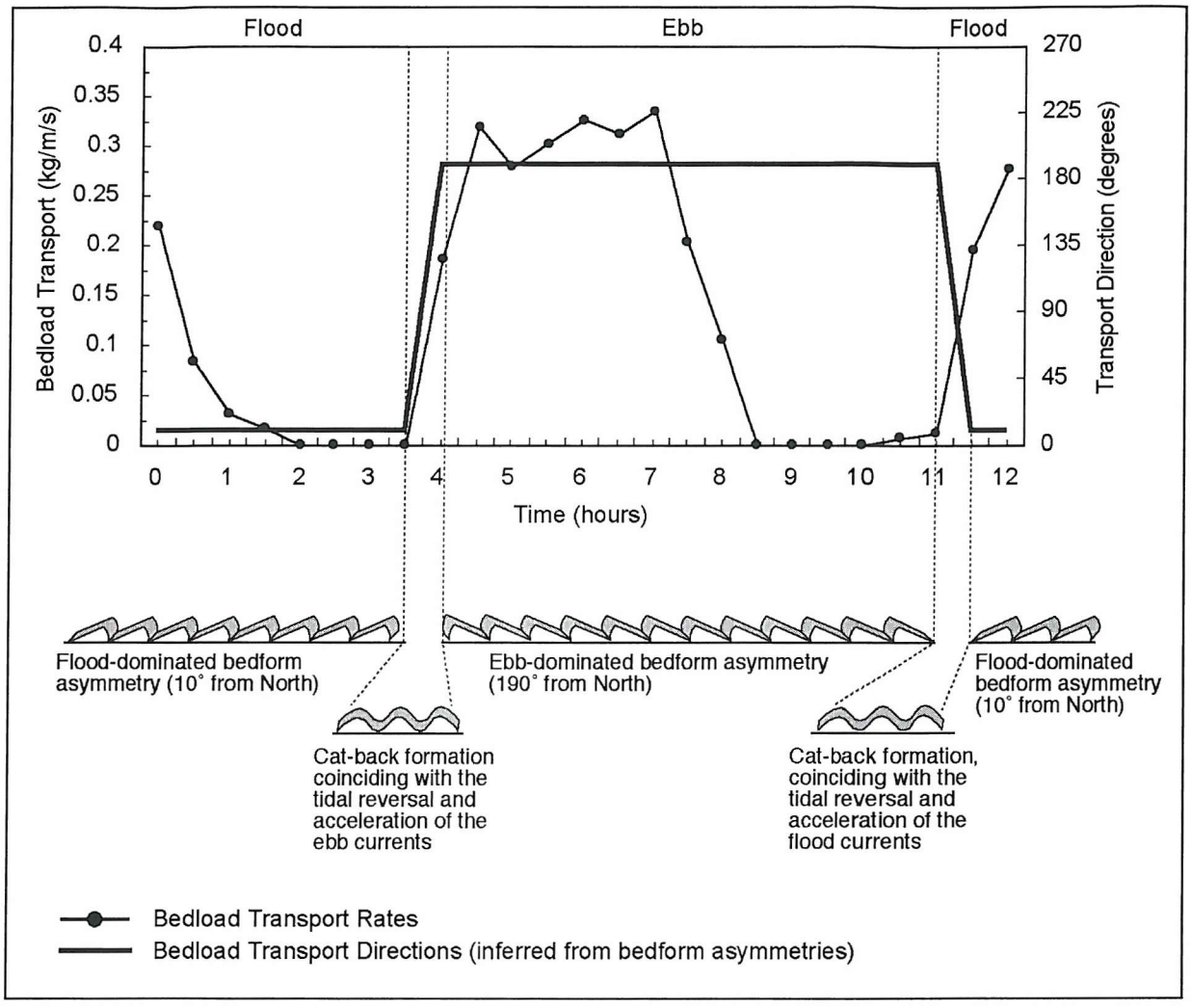

Figure 5.8 (a) Time-series of predicted bedload transport rates and directions calculated for the selected site associated with the sandwave reversal (Fig. 7; for location see Fig. 1). The transport rates were calculated using the near-bed currents measured by the ADCP, with a mean grain size of 1.1mm. The bedload transport direction, as inferred by the bedform asymmetries, is also plotted. The observed bedform asymmetries representing the different stages of the tidal cycle are schematic represented at the bottom of the Figure.

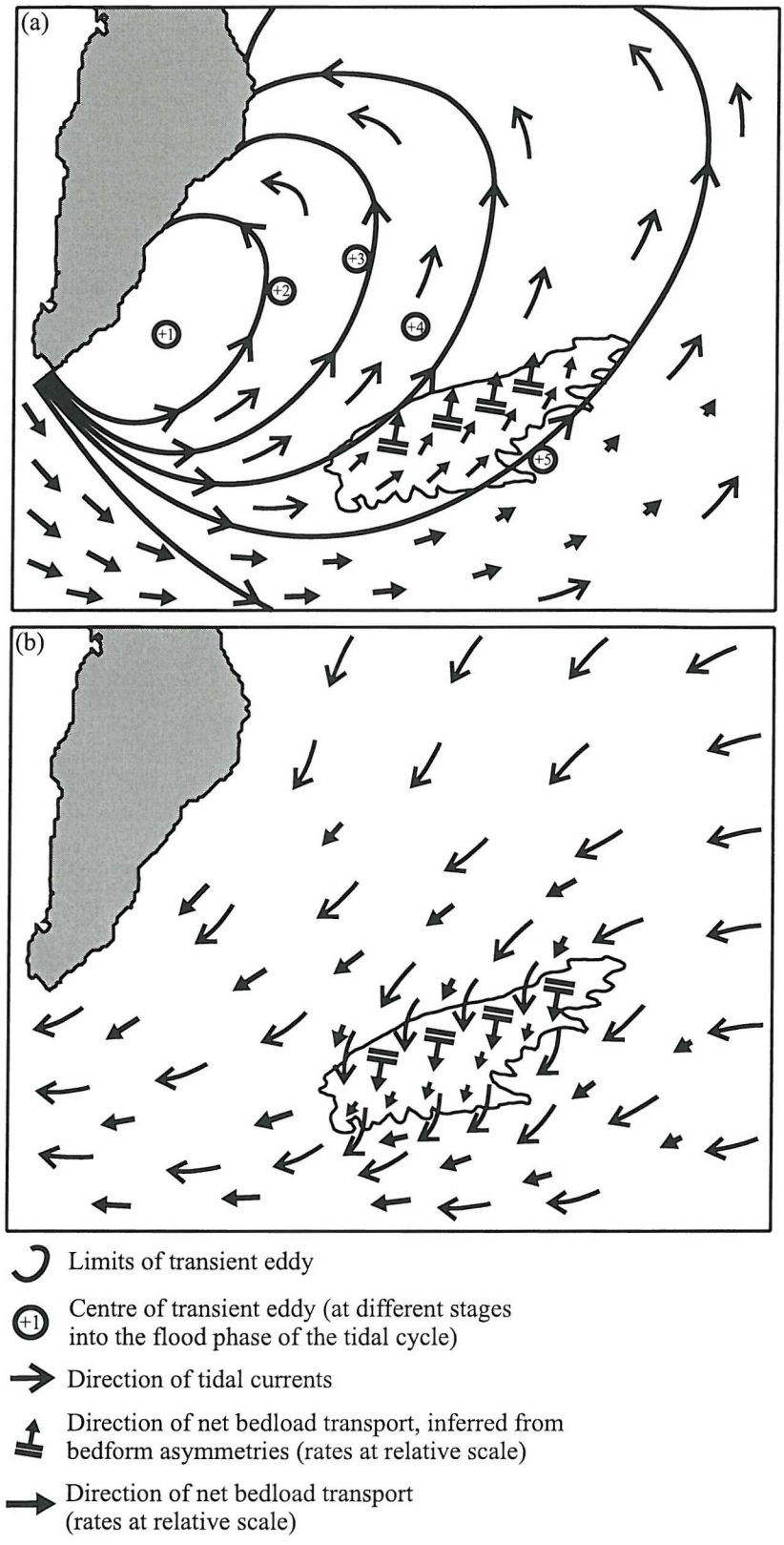

Figure 5.9 A conceptual model of the tidally-related maintenance processes, acting on a headland-associated sandbank: (a) the development of transient eddies, during the flood phase of the tidal cycle; and (b) the effect of bottom friction induced by the presence of the sandbank, during the ebb phase of the tidal cycle.

Chapter 6

Bastos, A.C. and Collins, M.B., 2002. Seabed mobility and sand transport pathways along the Dorset inner continental shelf (southern UK). This Chapter forms part of a Technical Report, presented to the Standing Conference on Problems Associated with the Coastline (SCOPAC) in August 2002.

Authors	Initiative of the Study	Data Collection and Analysis	Interpretation	Manuscript Preparation
Bastos	70%	100%	90%	90%
Collins	30%	-	10%	10%

Chapter 6

Seabed Mobility and Sand Transport Pathways along the Dorset Inner Continental Shelf (Southern UK)

Abstract

The scientific results of an investigation into seabed mobility and sediment transport pathways along the inner continental shelf adjacent to the Dorset Coast, between St. Alban's Head and Lyme Regis, are described. The objective of the present research was to investigate patterns of sediment transport under different energy conditions; likewise to predict the seabed sediment mobility over the inner continental shelf.

The research has applied a range of different scientific approaches, such as: (a) a review of all the available information on regional seabed morphology, sediment/bedform distribution and current and wave measurements; (b) field data collection, including seafloor mapping (using side-scan sonar and seabed sampling) and *in-situ* hydrodynamic measurements (using an Acustic Doppler Current Profiler); and (c) the application of (hydrodynamic and sediment transport) numerical models, to simulate and predict seabed mobility and sediment transport pathways, under different prevailing hydrodynamic (tidal and wave) regimes.

In general, the results have revealed that the inner continental shelf around Portland is characterised by very strong tidal currents and an erosive seabed, associated with specific areas of sediment accumulation. Such areas are observed on either sides of Portland Bill and the deposits are described as: the Adamant Shoal; the sand/gravel East Flat and Shambles Bank, to the east; and the West Shoal, the sand/gravel West Flat and Portland Bank, to the west.

The potential for seabed mobility has been assessed. The results show, overall, that the seabed around the headland is extremely mobile. The sandbanks are mobile for more than 75% of the time, whilst the shoals are mobile for more than 50% of the time (considering all the simulations, under currents alone and a combination of wave and currents). Net sand transport is clearly towards the headland and, because (instantaneous) tidal eddies are developed during the tidal cycle, sand convergent zones are formed along both sides of the headland; these coincide with the occurrence of the Portland and Shambles Banks. In terms of wave action, only storm waves (H=2.0 m and Tz=10 s) can disturb significantly the seabed over the area, i.e. storm waves can potentially disturb a medium-grained sand bed, in water depths greater than 35m. By combining different scientific results, an explanatory (conceptual) model of the sediment transport processes around Portland Bill is produced.

Reference: *Bastos, A.C. and Collins, M.B., 2002. Seabed mobility and sand transport pathways along the Dorset inner continental shelf (southern UK). This Chapter forms part of a Technical Report, presented to the Standing Conference on Problems Associated with the Coastline (SCOPAC) in August 2002.*

6.1 Introduction

The nearshore seabed is of considerable importance for coastal engineers/scientists and Authorities; principally, those interested in shoreline management plans and seabed resources. The use of coastal areas for recreation, tourism, port/shipping and industrial activities has increased significantly during the past decades, raising the value of any land or property located close to the coast. At the same time, due to rigorous legislation on the exploitation of land-won aggregates in the EU Member States (Bell, 2000), marine aggregates have become a strategic mineral resource; these are used not only for beach replenishment, but also for the construction industry, in general. Therefore, in order to balance the necessity to protect the shoreline and to exploit the seabed, without threatening the integrity of the natural coastline, a scientific understanding of the marine, coastal and terrestrial processes acting over the area is required. Indeed, predicting and quantifying continental shelf sediment transport, together with the frequency of seabed mobility, have become an important consideration for coastal managers and engineers.

A framework to investigate sediment transport and seabed mobility along the inner continental shelf adjacent to the Dorset Coast, between St. Alban's Head and Lyme Regis (Fig. 6.1), was established and the final results are presented here. During the first phase of the investigation, all the available information on seabed morphology, sediment/bedform distribution, current and wave measurements were collected and analysed. The objective of this initial analysis was to provide a regional characterisation of the inner shelf under investigation. On the basis of a regional overview of the inner shelf, decisions were made then regarding the selection of specific areas of interest (according to the objectives of the research) and the need to collect additional field data. Hence, an area around Portland Bill was selected for investigation, based upon the occurrence of significant sedimentary deposits, such as sand shoals and sandbanks. This area is described, from now on, as the study area or the shelf around Portland Bill (Fig. 6.1). The framework established to investigate the seabed mobility around Portland Bill relies upon: (a) field observation or seafloor mapping, to characterise the seabed geomorphology and sedimentology; (b) *in-situ* measurements, to determine the prevailing hydrodynamic processes; and (c) the application of numerical models, to simulate and predict the seabed mobility and sediment transport pathways, under different prevailing hydrodynamic (tidal and wave) regimes.

The objectives of the present study are: (a) to predict the seabed mobility over the inner continental shelf; and (b) to investigate patterns of sediment transport under different energy conditions. The research is particularly relevant in terms of sediment dynamic processes, as the inner shelf under investigation is characterised by an erosive seabed, associated with specific areas of sand accumulation. Therefore, understanding the hydrodynamics and sediment transport, associated with these shelf sand deposits, is a fundamental requirement for the management of the adjacent coastal environment.

6.2 Methods

6.2.1 Desk-top Study : Analysis of Existing Data

In order to review the sedimentary processes around Portland Bill, seabed morphology, sediment and bedform distribution, current and wave measurements were considered in a desk-top study. All the available information was digitised and combined, using the AutoCad software; this was used as a Geographical Information System (GIS) in order to present visually the different parameters and interpret their interrelationships.

Mapping of the seabed morphology and sediment distribution

Bathymetric charts and fair (bathymetric) sheets were obtained from the UK Hydrographic Office (UKHO), to provide a detailed seabed morphology of the sand deposits along the study area. The final bathymetric chart produced is based upon in excess of a hundred thousand sounding points; this has permitted a grid resolution of some 50m (Fig. 6.2).

Sediment and bedform distribution were characterised from existing maps of the seafloor, based upon side-scan sonar data held at the UKHO (Nunny, 1995; Kenyon, 1994) and bottom samples (available from the British Geological Survey, (BGS)). Grain size analyses of sediment samples were provided by the BGS and Ambios Consultants (Nunny, 1994). The offshore sediment samples are restricted to the Lyme Bay area.

Hydrodynamics

Existing current meter data over the area are concentrated within the Lyme Bay area (A, C, D, E, F, G, H in Figure 6.1). To the east of Portland, only a single measurement station is available; this is located some distance offshore of St. Alban's Head (I). Current meter data for locations A, C, D and I were provided by the British Oceanographic Data Centre (BODC), whilst observations at locations E, F, G and H were made available by Ambios Consultants and the Wessex Water Authority. Because all of the stations do not lie within the specific area of interest, these data were not used in the final sand transport calculations.

Analysis of the wave climate (wave height and period) has been applied to characterise the prevailing wave conditions and determine the associated near-bed wave-induced orbital velocities and shear stresses. The objective of this part of the investigation is to predict wave activity on the seabed. Wave data are available in Lyme Bay (LB and CB, see Figure 6.1) and

close to the Shambles Bank (SL, analysis of which was published by Draper (1977)); these were used to characterise the wave climate over the area (Fig. 6.1). All the existing wave data were provided by the British Oceanographic Data Centre (BODC). Analysis of the wave data was undertaken through a scatter diagram of significant wave height (Hs) and zero-crossing period (Tz), together with the Hs and Tz distributions, in relation to the wave direction. The persistence diagram for wave conditions, as proposed by Draper (1977), was used to characterise a storm wave with 10% exceedance over a one year period.

6.2.2 Data Acquisition

Based upon the results obtained from the desk-top study, the need for additional data acquisition was evaluated and a fieldwork campaign was planned. The objective of this field campaign was to provide complementary data, to fulfil existing gaps related to sediment-bedform distribution, sediment thickness and hydrodynamic measurements. The survey was designed to obtain detailed information on the sand deposits around Portland Bill. The results obtained from the fieldwork were digitised and coupled to AutoCad (see above).

Sedimentological and Geophysical Surveys

Acoustic and seabed sampling surveys were designed, overall, to provide coverage of the sand deposits. Hence, two separate fieldwork campaigns were undertaken, to investigate seabed morphology, sediment and bedforms distribution (Fig. 6.3). The first acoustic survey was undertaken in June 2000, using a Widescan system (100 kHz); this consisted of 100 km of side-scan sonar track. Seabed sediment sampling was undertaken also, during this survey. Eighty grab samples of the seabed were collected, using a Day grab. A second acoustic survey was carried out in June 2001, using a GeoAcoustic Side-Scan Sonar (500kHz). A total of 150 km of side-scan were collected, incorporating the two smaller coastal areas: Weymouth Bay and off Chesil Beach (West Bay). A GPS Trimble system was used for navigation positioning during both surveys, providing approximately ±5m accuracy.

Sediment samples were analysed through the use of sieving and settling tower techniques, to obtain sieve diameters and settling velocities, respectively. Interpretation of the side-scan sonar records was based upon different backscatter patterns (to map the different seabed facies) and morphological features. Transverse bedforms (sandwaves) were described using the classification proposed by Ashley *et al.* (1990). The classification is based upon sandwave wavelength (L) and height (H): very large (L>100m, H>5m); large (L-10-100m, H-0.75-5m);

medium (L-5-10m, H-0.4-0.75m); and small (L-0.6-5m, H-0.075-0.4m). However, the term sandwave was considered more applicable here, instead of subaqueous dune as proposed by Ashley *et al.* (1990).

Hydrodynamics and Sediment Dynamics Data – in-situ Measurements

Hydrodynamic measurements were undertaken along a transverse transect over the Shambles, using an Acoustic Doppler Current Profiler (ADCP) (Fig. 6.3). The measurements were collected throughout a complete tidal cycle in July 2001 (of about 13 hours, during the peak of the spring tides). The transect was completed every 30 min.; this means that, within a one hour period, two current velocity values were obtained at each sampled position along the track. For the present purposes of the present Report, the ADCP data were used only to validate the results (tidal currents) obtained with the hydrodynamic model.

6.2.3 Numerical Simulation

Seabed mobility and sand transport simulations were undertaken, for different hydrodynamic conditions: under tidal flows only; under wave action only; and under the combined action of currents and waves.

Hydrodynamic Model

Tidal flow patterns were characterised over the study area using results derived from a hydrodynamic model, the TELEMAC-2D. TELEMAC-2D was developed originally by Laboratoire National d'Hydraulique, Electricite de France and is distributed and applied by HR Wallingford. It is a depth-averaged, finite element model, formulated on shallow-water equations that describe the conservation of water mass and momentum (Hervouet, 1991).

The results used in this investigation are derived from an existing hydrodynamic model, that was set up and calibrated for the area between St. Alban's Head and Lyme Regis (Note: The original model covers a more extensive area, between the Isle of Wight and Lyme Bay). The model uses an irregular grid of triangular elements, which allows areas of special interest, e.g. coastal areas and headlands, to be examined in more detail. Figure 6.4 shows the model grid points.

ADCP measurements were used to validate the model. Figure 6.5 shows a comparison between measured data and the TELEMAC output data, for a location over the crest of the

Shambles Bank. The validation plot shows a very good agreement between measured and predicted tidal currents (speed and direction); the estimated error between measured and predicted current speed is less than 10%.

Output files containing the modelled tidal current and water level data (for spring and neap tides) were provided, to the authors, by HR Wallingford. The output files were processed using the RUBENS package (provided also by HR Wallingford). Post-processing work involved the calculation of residual currents (calculated by averaging the depth-averaged current, at each point of the grid, over a tidal cycle) and the maximum and mean current speeds at each grid point, over a tidal cycle. After processing the original file, the current and water level data were exported as ASCII files and formatted as input data to the sediment transport model. Tidal flows are described here for a tidal cycle, during spring tides.

Wave Refraction Model

The wave climate for the area was established by analysing the existing wave data, as described previously (see above). In order to predict the distribution of wave height over the area, a wave refraction model (RCPWAVE, U.S. Army Corps of Engineers; Ebersole *et al.*, 1986) was applied. RCPWAVE is a short-wave numerical model, used to predict linear plane wave propagation over an open coast region of arbitrary bathymetry; it is a module within the CEDAS (Coastal Engineering Design and Analysis System) numerical model package. Input data for the wave refraction model consists of: Hs, Tz, angle of approach and the bathymetric grid. The bathymetric grid was created using the grid generator in CEDAS. Waves are generated offshore (deep water waves), along the boundary line of the grid; hence, the model simulates the wave propagation and refraction due to bathymetric changes, coastal contours or artificial structures.

Simulations were undertaken for three different wave conditions: (a) SW - significant waves approaching from SW (Hs=0.8m, Tz=4.5s, DIR= 220°N); (b) SE - significant waves approaching from ESE (Hs=0.7m, T=4.5s, DIR=115°N); and (c) Storm - storm waves approaching from SW, with an exceedance of 10% over a year (Hs=2.0m, Tz=10s, DIR=220°N). These were defined based upon the analysis of the existing data.

The output from the RCPWAVE model consists of wave height, period and (refracted) wave directional distributions. In order to examine the seabed mobility under wave action, the bottom orbital velocity, induced by the waves on the seabed, was calculated; to calculate this,

the procedure described by Soulsby (1997, p.72 and 73) was used. The wave orbital velocity (U_w), near the bed (for monochromatic waves), is given by:

$$U_w = \frac{\pi H}{T \sinh(kh)} \tag{6.1}$$

where sinh is the hyperbolic sine, $k=2\pi/L$ is the wave number and L is the wavelength. After obtaining the bottom orbital velocity, the threshold of sand motion (U_{wcr}), under waves, was determined by applying the equations proposed by Komar and Miller (1984):

for d < 0.5 mm

$$U_{wcr} = [0.118 g(s-1)]^{2/3} D^{1/3} T^{1/3} \tag{6.2}$$

and for d > 0.5 mm

$$U_{wcr} = [1.09 g(s-1)]^{4/7} D^{3/7} T^{1/7} \tag{6.3}$$

where, g is the acceleration due to gravity (9.81 m s^{-2}), s is the ratio of grain and water densities, D is the grain-size and T is the wave period. The final results obtained are shown in terms of areas where the bottom orbital velocity lies above the determined threshold, i.e. areas of potential seabed mobility, under wave action.

Sediment Transport Model

The use of sediment transport models is an important and useful tool to characterise patterns of sand movement, especially over large areas of the continental shelf. However, their application should be undertaken with caution: a final evaluation and interpretation should be undertaken, before assuming that the results are correct. Problems in modelling sand transport arise due to the difficulty and uncertainty in understanding and measuring all the relevant processes involved in transporting sediments; likewise, to incorporate the spatial and temporal changes in the bed and sediment characteristics, during the process. Nevertheless, calibration of sand transport rates is still inaccurate and results obtained from the different proposed algorithms have shown a great deal of variance (Heathershaw, 1981; Pattiaratchi and Collins, 1988; Soulsby, 1997).

A continental shelf sediment transport model developed by the Geological Survey of Canada (GSC), Atlantic Geoscience Centre (SEDTRANS92, Li and Amos (1995)) was used in the

present study, to simulate sand transport over the area. The model has been calibrated extensively and applied by the GSC (Amos *et al.*, 1988; Amos *et al.*, 1995; Li *et al.*, 1997). It provides solutions for the calculation of bed shear stress under the action of currents alone and combined wave and current activity, using either the Grant and Madsen (1986) or Smith (1977) boundary layer models. The model computes sediment transport rates using one of seven different algorithms. SEDTRANS was provided, to the authors, by the Geological Survey of Canada.

The input parameters for SEDTRANS are: water depth (m); current speed (m s^{-1}); current direction; height of the current measurement above seabed (m); significant wave height (m); wave period (sec); wave direction ; sediment grain size (m); and bed roughness height (m)

The simulations were undertaken assuming a uniform grain size distribution over the inner shelf; this was due to the complex patterns of sediment distribution (including coarse lag deposits and bedrock outcrops). Three types of sandy beds were considered: a coarse sand bed (D_{50} = 1 mm); a medium sand bed (D_{50} = 0.5 mm); and a fine sand bed (D_{50} = 0.25 mm). The bed roughness (z_0) was assumed to be uniform over the area, as a rippled sand bed (z_0 = 0.6 cm; Soulsby, 1983). Form drag, due to the presence of large bedforms, was not considered. The critical threshold for sand movement (critical shear velocity, u_*) was calculated, using SEDTRANS, by applying the Yalin method (Yalin, 1977).The predicted values (for bedload: 1mm - u_* =2.16 cm s^{-1}; 0.5 mm - u_* = 1.70 cm s^{-1}; and 0.25 - u_* = 1.37 cm s^{-1}; for suspended load: 1mm - u_* =11.70 cm s^{-1}; 0.5 mm - u_* = 5.63 cm s^{-1}; and 0.25 - u_* = 2.27 cm s^{-1}) plot within the envelope of threshold values reviewed elsewhere (Miller *et al.*, 1977; Paphitis, 2001). In relation to all the assumptions made concerning the seabed, the transport rate predicted here is considered to be that of "potential sand transport", over a spring tidal cycle.

The original grid from TELEMAC (triangular element mesh), with water depth and depth-averaged current data, were used as input data to SEDTRANS. Sediment grain size and bed roughness parameters were added at each point of the grid. SEDTRANS calculated the bed shear stress and sediment transport, at each point of the original grid.

The bed shear stress under currents alone was calculated by applying a quadratic friction law, using the friction factor (f_c=0.006), based upon the field experiments of Sternberg (1972).

$$\tau_b = 0.5\rho f_c U_{100}^2 \qquad (6.4)$$

where, τ_b is the bed shear stress, ρ water density and U_{100} is the current speed 1 m above the seabed. In order to apply the quadratic friction law, SEDTRANS first calculates the near-bed currents (1m above seabed, u_{100}), by assuming a logarithmic velocity profile law.

Potential bedload transport rates were predicted/calculated, using the algorithm proposed by Gadd *et al.* (1978), for currents alone:

$$q_s = \left(\beta / \rho_s\right)\left(U_{100} - U_{cr}\right)^3 \tag{6.5}$$

where q_s is the bedload transport rate, β is an empirical coefficient (taken as 1.73×10^{-3}), ρ_s is sediment density, and U_{cr} is the critical velocity for the initiation of bedload transport.

This particular algorithm was selected for use in the present study, based upon the results obtained by Grochowski *et al.* (1993). These investigators identified that the algorithm proposed by Gadd *et al.* (1978) provided the best results, in terms of predicting sand transport rates for the English Channel, when compared to radioactive tracer dispersion experiments undertaken along the French coastline (Dewez *et al.*, 1989).

Sediment transport rates were predicted also under the influence of combined flows (waves + currents). The simulation was undertaken using the most significant wave condition over the area (Hs=0.8, Tz=4.5s, Dir=220°N). Results obtained for the wave and direction distributions, from RCPWAVE, were combined with the spring tidal currents derived from TELEMAC. The data points were re-gridded and used as input files into SEDTRANS. The three sand seabeds were simulated, as described previously.

In order to calculate the bottom friction factor and the bed shear stress under combined wave and currents, the boundary layer model developed by Grant and Madsen (1986) was applied. This model considers the non-linear interaction of wave and currents and assumes a time-invariant eddy viscosity function. Calculations of sand transport rates were undertaken, using the total-load Bagnold (1963) algorithm:

$$q = K\tau_{cw}\frac{U}{(\rho_s - \rho)g} \tag{6.6}$$

where K is the coefficient of proportionality (Sternberg, 1972), τ_{cw} is the combined wave-current shear stress and U is the mean current velocity.

Bagnold's (1963) concept assumes that, if the surface wave power is expended onto the seabed, the sediments will be mobilised and swept away by unidirectional currents. Hence, the presence of wave-induced orbital velocities on the seabed should increase the sediment transport rate.

Another concept of seabed mobility, not considering the direction of sand transport, was applied also during the present study. The results presented here, as seabed mobility, are related to the percentage of time that the predicted shear stresses is above the critical threshold values for sediment motion, i.e. the percentage of time that sand is moving as bedload, or suspended load. This concept is very useful in providing a clear observation of the influence of waves on mobilising the seabed. Comparative results are presented here, showing the potential mobility of the seabed (as bedload and suspended load), under the action of tidal currents alone and combined wave-current interaction.

The results obtained from the simulation of the sediment transport model were interpreted, together with the field observation and measurement data set. The "predicted" sediment transport pathways were compared with the geomorphological and sedimentological characteristics of the sedimentary deposits (including bedforms, grain size distribution and internal structure), for comparison with the model simulations.

6.3 Results

The seabed mobility and sand transport pathway results are presented here in a methodological format, to emphasise the different scientific approaches that can be considered to evaluate the mobility of seabed sediments and their transport patterns. Three hydrodynamic conditions are considered: tidal currents (during a spring tidal cycle), waves and combined action of tidal currents and waves. The seabed mobility is considered, firstly, in terms of the percentage of time that sediments are mobile, i.e. above the critical threshold value. Subsequently, the sand transport pathways are analysed, based upon distinct parameters, such as: tidal circulation and shear stress; bedform asymmetry and sand distribution; and sediment transport models.

6.3.1 - Seabed Mobility, based upon Numerical Simulation

Sand (seabed) mobility has been investigated here, over the inner continental shelf, for conditions of: currents alone; wave action; and combined current/waves. Seabed mobility is presented as the percentage of the time over which sand (fine, medium and coarse sand beds) is mobile, i.e. shear velocities above threshold, as bedload and suspended load, during a spring tidal cycle.

For bedload transport under currents alone, the sand mobility increases towards the headland, as expected (Figs. 6.6, 6.7, 6.8). Similar gradients in fine, medium and coarse sand mobility occur along both sides of the headland, terminating in 100% mobility at the tip of the headland (Figs.6.6a, 6.7a, and 6.8a). No sand transport is predicted inside Weymouth Bay and off Lyme Regis.

In terms of the seabed mobility over the sand deposits, the Adamant-West Shoals are mobile, at least, for 50-75% the time (medium and coarse sands) and up to 90% for a fine sand bed. The Shambles-Portland Banks are mobile for 75-90% of time, considering coarse sands; they are up to 100% of the time, for a fine sand bed.

In terms of suspended load, fine-grained sands are predicted to be transported over an extensive area of the inner continental shelf (Fig. 6.6b). Medium-grained sands are transported effectively in suspension only in areas around the tip of the headland, including the Shambles and Portland Banks. Coarse-grained sands are predicted to be in suspension for

less than 5% of the time in a restricted area just off the tip of the headland (Figs. 6.7b and 6.8b).

Wave Analysis and Refraction Simulation

Existing wave data, acquired for Lyme Bay and close to the Shambles Bank, were used to represent the wave climate for the area. Analysis of the results obtained from a directional waverider buoy (from July 1992 to July 1994), located in the centre of Lyme Bay (LB, Fig. 6.1), reveals a most frequently occurring significant wave height (Hs) of 0.8m and a zero-crossing wave period (Tz) of 4.5s (Fig. 6.9a). Waves approaching from the southwest quadrant are predominant over 65% of the time, whilst SE waves occur over some 15% of the time (Fig. 6.9b).

The only data available to the east of the Isle of Portland correspond to a wave recorder deployed at the Shambles Light Vessel (SL, for location see Figure 6.1), acquired in 1968. Analysis of this data set was published by Draper (1977), showing a Hs of 0.7 m and a mean period (T) of 6 s. Using these data, Draper (1977) demonstrated that the significant wave height exceeds 2.0 m over this area, for only 10% of the year.

Wave action over the area is presented here using the results obtained from simulations generated by the wave refraction model. Based upon the existing wave data, three different wave conditions were tested (SW, ESE and Storm (see Methods)) using the present bathymetry (water depths, referred to the LAT).

The distribution of wave height over the inner continental shelf under investigation is shown in Figures 6.10, 6.11 and 6.12. For the SW wave case, the wave height distribution does not show any significant variation over the shelf, apart from the "shadow zone" created by the Isle of Portland, together with a slight increase (of about 0.2 m) in wave height over the Shambles Bank (Fig. 6.10). The wave height over Lyme Bay and Purbeck Bay is about 0.79 m; over the Shambles Bank, waves can reach up to 1m in height. The Weymouth Bay area is sheltered by the presence of the Isle of Portland. The wave heights over these areas decrease to values of below 0.5 m; in Weymouth Bay wave height was no more than 0.2 m.

Waves approaching from ESE occur over less than 15% of the time; however, ESE waves can influence significantly the seabed and the coastline over Weymouth Bay. The results obtained from simulating the propagation of ESE waves (Hs = 0.7 m, Tz = 4.5 s) show that waves can

reach Weymouth Bay with heights of 0.65 to 0.7 m (Fig. 6.11). The wave height over Purbeck Bay is around 0.75 m, showing no significant increase over the Shambles Bank (0.8 m). Once again, the Isle of Portland acts as a natural shelter for the incoming waves. The Chesil Beach area is associated with waves of very low height (0.2m).

The "storm" wave simulation has revealed the influence of the Shambles Bank, on refracting the incoming waves. The simulation demonstrates that storm waves have a greater impact along the coast of Lyme Bay (for Chesil Beach, Hs = 2.5 m), compared with the Purbeck west coast (Hs = 1 to 1.5 m) (Fig. 6.12). Nearshore sandbanks can modify the wave pattern, by refracting and/or diffracting the direction of wave propagation. In a sense, sandbanks protect the coastline by dissipating the wave energy. However, depending upon the characteristics of the incoming waves, sandbanks can also refract the waves; this can generate an energy convergent zone along the coast. Therefore, despite the Shambles Bank acting as a natural barrier for the incoming swell waves, by dissipating wave energy, it also creates a narrow wave energy convergence zone along the coast of Purbeck (Fig. 6.12).

In terms of wave height distribution over the inner shelf, the higher waves occur over Lyme Bay (Hs = 1.8m). To the east of the Isle of Portland, higher waves occur over the Shambles Bank (Hs = 1.8 to 2.1 m) and along the narrow refracted zone to landward of the Shambles Bank. In general, the inner shelf area, sheltered by the Shambles, are associated with heights of up to 1 to 1.2 m; in Weymouth Bay, wave heights are around 0.5 m.

The wave activity on the seabed was simulated for three different wave conditions: (a) SW waves, SE waves and a Storm wave (see Methods). The results are presented in terms of potential areas where waves affecting the seabed can mobilise sand-sized sediments (fine-, medium- and coarse-grained sands).

Under the action of significant SW waves, only the shallow water areas along the coastline, together with the Shambles Bank (fine sands only), are potentially mobile (Fig. 6.13). SE waves can affect some areas over Purbeck Bay, but no potential mobility is predicted over Lyme and Weymouth Bays (Fig. 6.14). Potentially, storm waves can disturb fine- and medium-grained sand beds, over an extensive area of the shelf, including water depths up to 45 and 35 m, respectively (Fig.6.15). Coarse sands can be mobilised in response to storm waves, in shallow areas along the coastline and over the Shambles Bank. Therefore, in terms

of wave activity on the seabed, storm waves can mobilise significantly sand beds, over the inner shelf.

In terms of the combined action of tidal currents and waves, the presence of waves enhances the bed shear stress and, consequently, the potential for sand mobility over the inner shelf. For a fine sand bed, the shelf around Portland Bill (including the sand deposits) is predicted to be mobile over more than 90% of the time; furthermore, with the superimposed presence of waves, fine sands are predicted to be mobile within Weymouth Bay, for more than 50% of the time (Fig. 6.6c). A significant increase in the level of mobility is also observed in medium-grained sand beds, especially over the sand deposits and within Weymouth Bay. The Shoals are predicted to be mobile over more than 75% of the time, whilst, for the Banks, it was more than 90% of the time (Fig. 6.7c). In Weymouth Bay, medium sands are predicted to be transported as bedload, over 5-25% of the time.

In the case of a coarse sand bed, a significant increase in seabed mobility is observed, once again, over the entire inner continental shelf. Coarse sands are predicted to be mobile for more than 90% of the time, over the Shambles Bank and between 75-90%, over Portland Bank (Fig. 6.8c). Over the Adamant Shoal, coarse sands are mobile for 75-90% of the time whilst over the West Shoal, the mobility ranges over 50-90% of the time. A significant increase in the mobility of coarse sands is observed along Chesil Beach.

The effect of combined flows was not proved to be significant, to increase the percentage of time sand would be transported in suspension, apart from the fine sand bed (Figs. 6.6d, 6.7d, and 6.8d). Generally, for medium and coarse sand beds, only areas that had shown already a potential for sediment suspension under currents alone, presented a slight increase in the percentage of time over which the bed was mobile. In contrast, a significant increase in the percentage of time that the fine sands can be transported in suspension is observed over the entire shelf, especially along the coast off Lyme Bay (off Chesil Beach).

6.3.2 Net Sand Transport, based upon Tidal Circulation and Shear Stress (derived from the numerical hydrodynamic model)

On the basis that the movement of sediments is controlled by the prevailing hydrodynamic conditions, the residual tidal circulation pattern, or the direction of the peak currents, can be used as indicators of the direction of sand transport over tidally-dominated areas (Pingree and Griffiths, 1979; Johnson *et al.*, 1982). The residual water circulation in relation to the inner

continental shelf around Portland Bill reveals the presence of eddies on both sides of the headland (Fig. 6.16a); this would indicate that sand accumulates in the centre of these eddies. However, some caution should be applied when adopting this interpretation, because sand is not necessarily being transport by the tidal flow throughout all of the time (see above), especially as bedload transport; this is because a threshold level must be reached for the sediment to commence movement. Conversely, for fine to very fine sediments (silt and/or clay), transported as suspended load, the use of residual (water) circulation is a more reasonable approach (Ferentinos and Collins, 1980; Johnson *et al.*, 1982).

Another manner in which the flow characteristics can be adopted, in order to predict sand transport pathways, is to assume that the resultant sand transport will follow the peak current asymmetry direction (used extensively by Stride and co-workers; see Stride *et al.*, 1982). Johnson *et al.* (1982) explain the concept that peak current direction indicates the net sand transport, using the tidal current ellipse and the speed asymmetry between the flood and ebb currents.

The tidal current ellipse is defined by four parameters (two amplitudes and two phases) abstracted from the tidal harmonic constituents. Basically, this approach means that the current vector is described in terms of its direction and speed, at a particular location and time, i.e. that the ellipse represents direction and speed variations throughout the tidal cycle. Therefore, considering a rectilinear tidal flow, the semi-major axis of the ellipse (elongation) indicates the direction of the flow; as a consequence, the orientation of the effective sediment transport. The direction of sand transport can be abstracted, then using the speed asymmetry of the peak (ebb-flood) currents.

The asymmetry of the peak current is defined, in this case, by the different peak current speeds during ebb and flood phases of the tidal cycle. Considering that sand transport rates are related to the current speed minus a threshold current speed, cubed and multiplied by a constant, the net bedload sand transport follows the direction of the strongest peak current (Johnson *et al.*, 1982). These authors suggest also that, in a case of unequal ebb and flood duration, even if the shorter duration current has a higher peak speed, it can determine the net transport of sand. Therefore, the net bedload sand transport is in the direction of the strongest flow, not necessarily in the direction of the residual flow, as would be expected in response to a non-linear relationship.

The direction and magnitude of the peak tidal currents are shown in Figure 6.16b. Note that the difference between residual circulation and peak currents can be identified, when comparing Figures 6.16a and 6.16b. On the basis of the peak current direction, the results would indicate the occurrence of two sediment convergent zones, associated with the Shambles and the Portland Banks. Moreover, sediment could be transferred to both sides, at the tip of the headland, i.e. instead of being transported offshore, as shown in the residual (tidal current) pattern. A significant contrast in the predictions of the direction of sand transport would occur, over the Adamant Shoal. Peak currents indicate transport towards the tip of the headland (SW), whilst residual circulation indicates transport towards the coast of the Isle of Portland (NW).

In terms of the bed shear stress, the same concept as used for tidal currents can be applied. Maximum bed shear stress patterns can be used, as an indication of sand transport pathways. The distribution of maximum shear velocities reveals a pattern similar to that shown by the peak tidal current vectors, i.e. the formation of two convergent zones, on both sides of the headland (Fig. 6.17a). However, in utilising the shear stress calculations to identify patterns of sediment movement, the effect of waves combined with tidal currents can also be simulated. Despite this increase in the shear velocity, no significant changes in the direction of the shear stress vectors were observed (Fig. 6.17b).

6.3.3 Net Sand Transport, based upon Bedform Asymmetry and Sand Distribution

In terms of facies distribution, the seabed consists, predominantly, of a discontinuous veneer of coarse lag deposits and bedrock outcrops, associated with areas of mobile sands. Figure 6.18 presents a regional map of the facies distribution. Seven distinct sedimentary facies were identified over the study shelf, based upon bathymetric charts, side-scan sonar data and seabed samples: (a) bedrock outcrop; (b) bedrock, with patches of sediment; (c) lag deposits (gravel); (d) homogeneous sandy gravel facies; (e) fine sand sheet; (f) onshore sand patches; and (g) sandbanks and sand shoals.

A few areas of sand accumulation were recognised over this particular area of the inner shelf, such as the Shambles and Portland Banks and the Adamant and West Shoals (Fig. 6.2). Sandy areas occur also within the inner regions of Weymouth Bay, which are covered by a fine sand sheet; likewise, for the central areas of Lyme Bay, where a thin fine sand sheet occurs (Fig. 6.18). Sand patches are also observed off Chesil Beach.

The sedimentology of the deposits can be described in terms of their grain size characteristics, such as: mean sieve diameter (D_{50}); sorting (σ); and mean (sand) settling velocity (w_s). In principle, the three parameters show good spatial agreement, i.e., sand-sized deposits are related to well-sorted sands, whilst the coarse and fine sands (D_{50}) are related to higher and lower w_s, respectively. Figure 6.19 shows the distribution of the parameters described above, including the sand content.

In general, a similar bedform distribution occurs on both sides of the headland: medium and large sandwaves on the shoals; and very large sandwaves (superimposed with medium and small sandwaves) on the banks (Fig. 6.20).

The asymmetry of transverse bedforms has been used widely for the determination of the net sand transport (Belderson and Stride, 1966; Kenyon and Stride, 1970; Johnson *et al.*, 1982, McCave and Langhorne, 1982; Lanckneus and de Moor, 1995, and others). The use of transverse bedforms, as an indicator of the direction of sand transport, is based upon the asymmetric profile of the transverse bedforms, with the steeper side showing the direction of sand transport and bedform migration. However, once again, some degree of caution should be applied and some limitations should be considered, in relation to this concept. These conditions have been described elsewhere (Lanckneus *et al.*, 2001), as: (a) that the bedform should be active, i.e. the asymmetry should be defined by the prevailing hydrodynamic conditions; (b) the bedform asymmetry should represent long-term equilibrium, i.e. its asymmetry should not reverse during a tidal cycle; and (c) the bedform lee face (or the steep slope) should be a depositional surface. These conditions are imposed because of reversal in the asymmetry of the bedforms (especially small and medium sandwaves) has been described elsewhere (Hawkins and Sebbage, 1972; Terwindt *et al.*, 1986; Berne *et al*, 1993; Lanckneus and De Moor, 1995). For the analysis applied here, only large and very large sandwaves are considered (see Methods, for sandwave classification).

The occurrence of large and very large sandwaves is restricted to the sandbanks and sand shoals (Fig. 6.20). The asymmetry of these features reveals a general pattern of sand transport, towards the tip of the headland, and a local sand convergent pattern over the sandbanks.

In terms of modern processes, the Adamant and West shoals could be described as *sand streams*, characterised by a sequence of medium to large sandwaves (wavelength of 150-200

m and height of about 2m); these are associated, generally, with an asymmetric profile, directed towards the tip of the headland. A veering on the sandwave crest direction occurs on both of the shoals, following the morphological shape of the features and the adjacent coastal geometry. Along the Adamant Shoal, for example, at its northeastern end, medium to large sandwaves have an almost north-south (340°-160°) crest direction; at its southwestern end, the direction is approximately northwest-southeast (310°-135°) (Fig. 6.21). This pattern is in total agreement with the ebb tidal current patterns (strongest currents), as predicted by a hydrodynamic model (see above) for this area. Similarly, a veering of the sandwave crests is present on the West Shoal.

Overall, the sandbanks are characterised by large and very large asymmetric sandwaves; these show a convergent sand transport pattern, towards the crest of the banks (Fig. 6.21). Very large sandwaves on the Shambles Bank have a wavelength of around 300m, with heights ranging from 5 to 7 m; on the Portland Bank, the sandwave wavelength is about 250 m, with heights of about 4 to 6 m.

Due to the restricted occurrence of sand over the shelf, the pattern of facies distribution can be used also as an indicator of sand transport pathways. The occurrence of sand shoals and sandbanks, around the headland, provides a strong indication that sand is being transported towards the headland, especially when considering the geometry of these deposits. The facies sequence is described as: fine sand sheet; sand shoals or sandwave fields (Adamant and West Shoals); sand/gravel Flats (East and West Flats); coarse-grained sandbanks (Shambles and Portland Banks); and a non-depositional zone (bedrock), or zone of maximum bottom stress (maximum currents). This facies sequence is associated with an increase in the prevailing current speed, from the fine sand sheet towards the zone of the maximum current speed

6.3.4 Net Sand Transport, based upon the results of the Sediment Transport Model

The net bedload (sand) transport, under currents alone, has been calculated for three sand beds, as described previously. A similar pattern of resultant bedload transport direction was observed, for the fine-, medium- and coarse-grained sand beds (Fig. 6.22).

The resultant sand transport direction is characterised by a zone of bedload convergence, which, subsequently, can be recognised on both sides of the headland and coincides with the presence of the Shambles and Portland Banks. At the tip of the headland, a zone of maximum

transport rates occurs. This zone is characterised by bedrock outcrops (Fig. 6.23) and is being interpreted as a "non-depositional" area, or a zone of maximum erosion; it has been related to the "scour zone" described by Harris *et al.* (1995) and the "bedload parting zone" concept described by Stride *et al.* (1982).

In terms of the tidal flow, the net sand transport direction can be estimated also on the basis of the direction of maximum transport rates over the tidal cycle (see above). Maximum transport rates for the medium-grained sand bed are shown in Figure 6.24a. The bedload convergent zones are observed, once again, on both sides of the headland; these are associated with the occurrence of sandbanks.

Net sand transport rates were derived also for combined flow conditions, using the SW wave conditions. In this case, the algorithm of Gadd *et al.* (1978) was not an appropriate approach to incorporate the wave action; therefore, the equation proposed by Bagnold (1963) was used to calculate the total load transport, under combined flows. Net total load sand transport rates are shown in Figure 6.25, for a medium-grained sand bed.

Net sand transport under currents and waves has shown a similar pattern, as recognised previously under the "currents alone" conditions. An increase in the net transport rates is observed around the tip of the headland. The sand convergent zones occur over the sandbanks, in association to the formation of the inner and outer sand-mobile zones. A plot of maximum total load transport rates show also similar patterns of sand transport, around the headland (Fig. 6.24b)

Sediment transport models can generate, as described previously, inaccurate results; consequently, their application must be considered with some caution. However, the results obtained from the SEDTRANS (numerical model) were considered to be satisfactory, in terms of describing the potential sand transport patterns over the inner shelf study area. However, the errors derived from the calculation of transport rates could not be assessed; this was due to the difficulty in calibrating the transport rates, i.e. in the absence of *in-situ* measurements (bedload traps, fluorescent tracers, etc).

6.4 Concluding Remarks

A seabed mobility study has been undertaken to characterise the sedimentary geological conditions and the sand transport pathways over the inner continental shelf around the Isle of Portland, Dorset. This study has applied a range of scientific approaches: (a) seabed mapping, including that of the sediment and bedform spatial distribution; (b) hydrodynamic measurements; and (c) numerical modelling, including the utilisation of an hydrodynamic model, a wave transformation model and a sediment transport model. The objective of the application of various methods, to investigate the seabed mobility over an area, is to increase the level of accuracy and confidence in establishing the (net and instantaneous) sand transport pathways; this can be achieved by comparing the different results obtained, then combining them in a final synthesis map (see Fig. 6.26).

The potential for seabed mobility has been assessed here by applying numerical modelling techniques; this has allowed the prediction of the percentage of time a (sand) seabed is mobile, under the action of currents, waves and the combined action of currents and waves. The results have shown, overall, that the seabed around the headland is extremely mobile. The sandbanks are mobile for more than 75% of the time, whilst the shoals are mobile for more than 50% of the time (considering all the simulations, under currents alone and a combination of wave and currents). In terms of wave action, only storm waves can disturb significantly the seabed over the area; such waves can potentially disturb a medium-grained sand bed, in water depths up to 35m.

Sand transport pathways have been characterised based upon different approaches: tidal circulation and shear stress distribution; bedform asymmetry and sand distribution; and the output obtained from a sediment transport model. The results revealed very good agreement in terms of the net sand transport over the deposits; likewise, the occurrence of a zone of maximum erosion at the tip of the headland.

The derived directions of net sand transport were equivalent, when comparing: transverse bedform asymmetry (restricted to the sand deposits); peak tidal current directions; maximum bed shear stress directions; net sand transport; and maximum sand transport derived from SEDTRANS. The occurrence of convergent zones over the sandbanks was observed, in addition, in all of the approaches cited above.

In terms of the "level of confidence", to be adopted in relation to the results obtained for the direction of net sand transport, areas associated with the deposits have a higher confidence level than the surrounding areas; this is because, over the deposits, the results derived from SEDTRANS and TELEMAC were validated in relation to the bedform asymmetries.

The presence of a zone of maximum erosion, at the tip of the headland, is considered also as one of "high confidence". This zone has been confirmed by the occurrence of bedrock outcrops over that area (the area is depleted of sediments, as revealed by side-scan sonar and seismic surveys); this coincides with zones of maximum shear stress and sand transport rates.

In summary, the inner continental shelf is swept by very strong currents, inducing a high mobility of the seabed. Net sand transport is clearly towards the headland and, because tidal eddies are developed during the tidal cycle, bedload convergent zones are formed along both sides of the headland; these coincide with the occurrence of the sandbanks.

Wave activity over the study area is more pronounced along the coastline; however, the superimposed presence of waves can enhance the sand transport rates. Storm waves can have a considerable influence over the area, by disturbing almost the entire shelf seabed. The occurrence of sand patches, associated with gravel waves off Chesil Beach, reveals that a wave-dominated zone exists along the coastline of Lyme Bay. In contrast, very fine-grained sand and mud deposits over Weymouth Bay are indicative of a low energy environment, which is corroborated by the seabed mobility simulations. However, the simulations have revealed also that the seabed over Weymouth Bay can be remobilised, under the combined action of waves and currents. This interpretation indicates that, although Weymouth Bay is sheltered from the direct action of southwestern storm waves, a small increase in wave height or the action of south and southeast waves can enhance the sand transport rates within the Bay.

Finally, the coastal system cannot be considered as a "closed" beach/surf zone coupled-system. The inner continental shelf (water depth < 50m), adjacent to the coast, is dynamically, morphologically and sedimentologically contiguous with the beach and the surf zone (Wright, 1995). Hence, dynamic interaction (driven by waves, current and wind/wave-induced currents), between the coastline and the inner continental shelf, plays a very important role in the morphological evolution of the coastal system; this relates to short-, medium- and long-

term time-scales (De Vriend, 1990; Cowel and Thom, 1994; Wright, 1995; MacDonald and O'Connor, 1996; and Whitehouse, 2001). Thus, the results presented here are relevant to those dealing with coastal management. Understanding the regional seabed sediment mobility and the characteristics of the inner continental shelf deposits is a fundamental requirement for coastal managers and engineers; this is on the basis of the balance that needs to be reached, between conservation and socio-economic development of the coastal zone.

The presence of sandbanks and sand shoals can have a significant influence on (regional) coastal sediment transport pathways and rates, as described elsewhere (Brampton *et al.*, 1998; Whitehouse, 2001; Lanckneus *et al.*, 2001). The presence of a sandbank on the inner shelf can alter significantly the hydrodynamic patterns (Pattiaratchi and Collins, 1987; Williams *et al.*, 2000; and Whitehouse, 2001), influencing directly the physical processes along the coastline; it can create localised tidal currents and alter the wave propagation (by acting as a natural coastal defence) (MacDonald and O'Connor, 1996; and Maa and Hobbs, 1998). Consequently, the sandbank morphology can be modified by the local hydrodynamic conditions, especially during storm surges (Ferentinos and Collins, 1980; Houthouys *et al.*, 1994); this causes a morphological response along the coast.

On the basis of the results presented here, the occurrence of the symmetric deposits on either sides of the headland suggests the presence of four "sand accumulation centres" around Portland Bill (West Shoal, Adamant Shoal, Portland Bank, and Shambles Bank). This pattern could be relevant in terms of shelf/coast sediment exchange, because it suggests that: (a) the formation (or accumulation) of these deposits is strongly related to the tidally-related processes; and (b) waves have a more dispersive and destructional influence (Ferentinos and Collins, 1980), principally over the Shambles Bank. The results have shown also that the Shambles Bank has a major influence on the local hydrodynamics, i.e. the Bank alters the tidal flow patterns and refracts the incoming waves. Moreover, the results have indicated that the Shambles Bank is associated, potentially, with high rates of seabed mobility and sand transport; this indicates that the presence of the Bank plays an important role on the local hydrodynamics and sand transport patterns – offshore, or associated with the adjacent coastline.

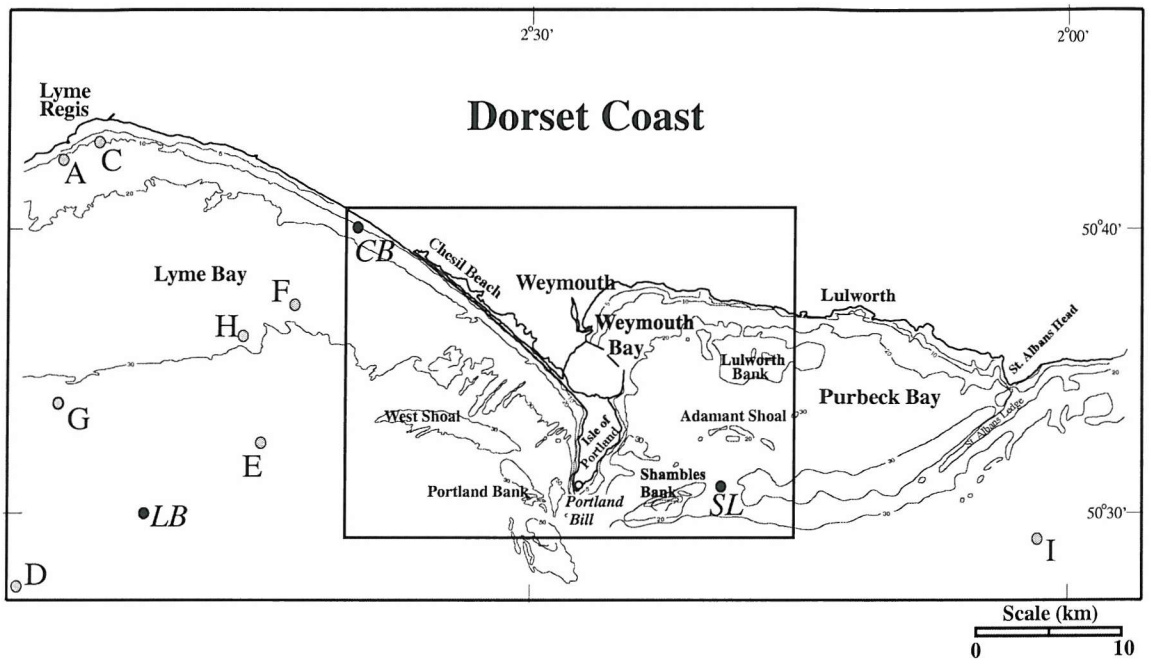

Figure 6.1 Regional setting of the area under investigation. Location of existing current meter (○) and wave (●) data.

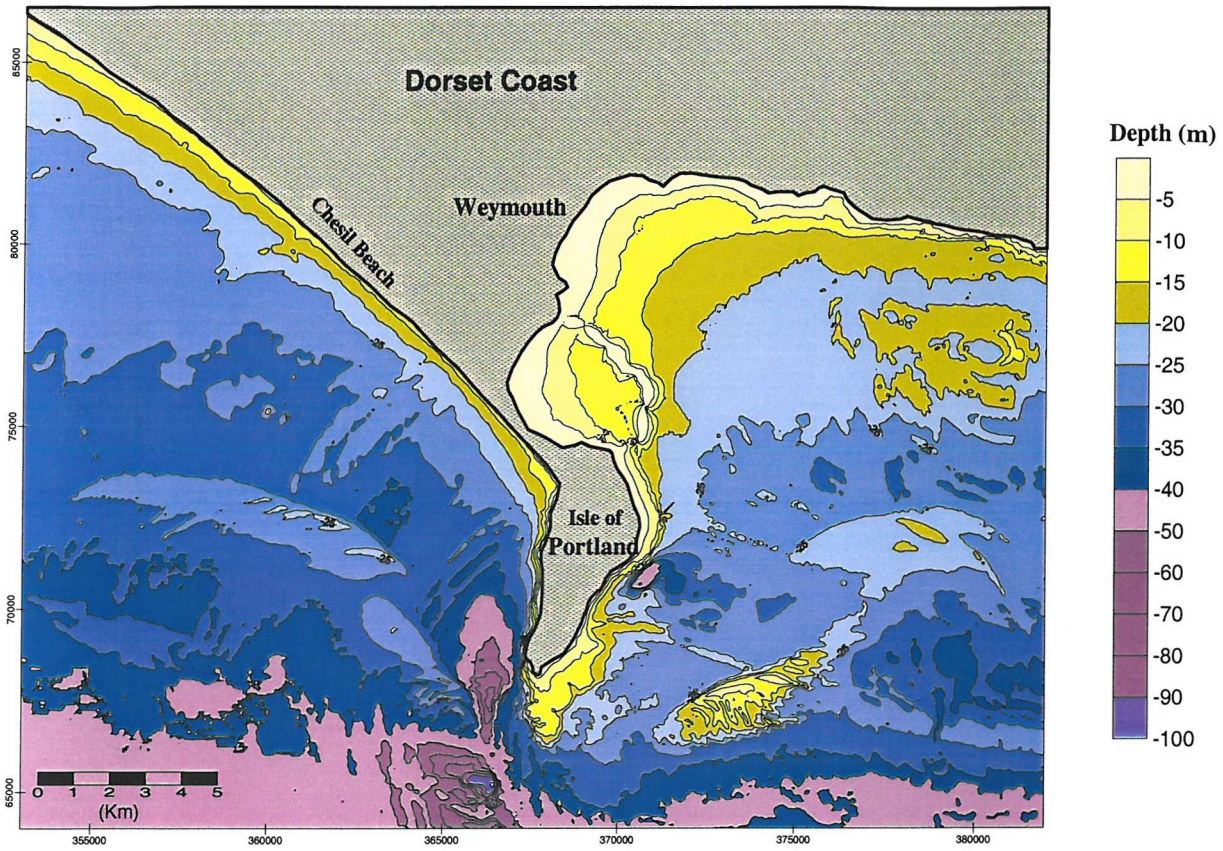

Figure 6.2 Bathymetric map of the inner continental shelf around Portland Bill. Depth contours in metres, referred to Chart Datum (Lowest Astronomical Tide, LAT).

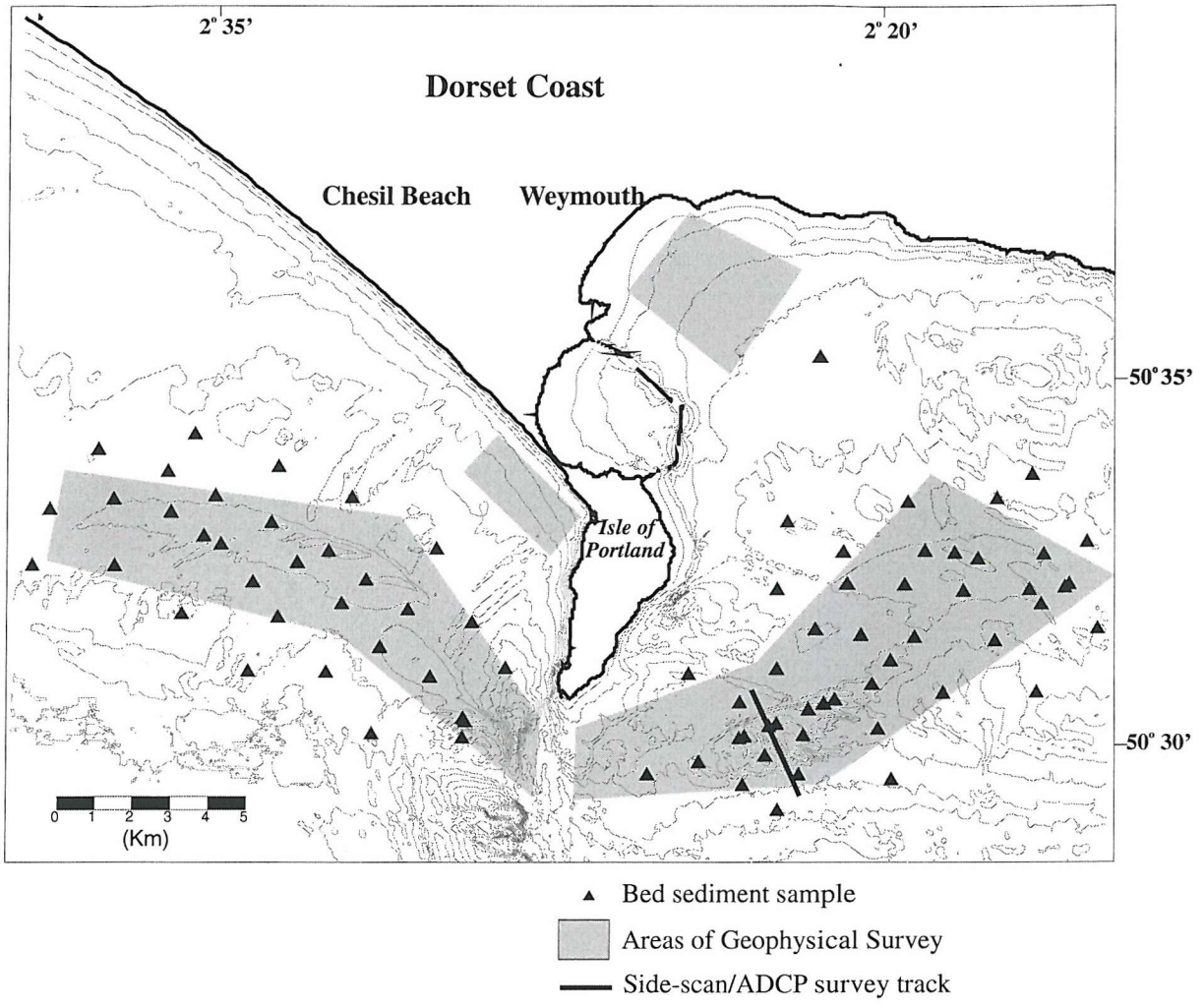

Figure 6.3 Location of seabed sediment samples collected, geophysical surveys and ADCP transect undertaken.

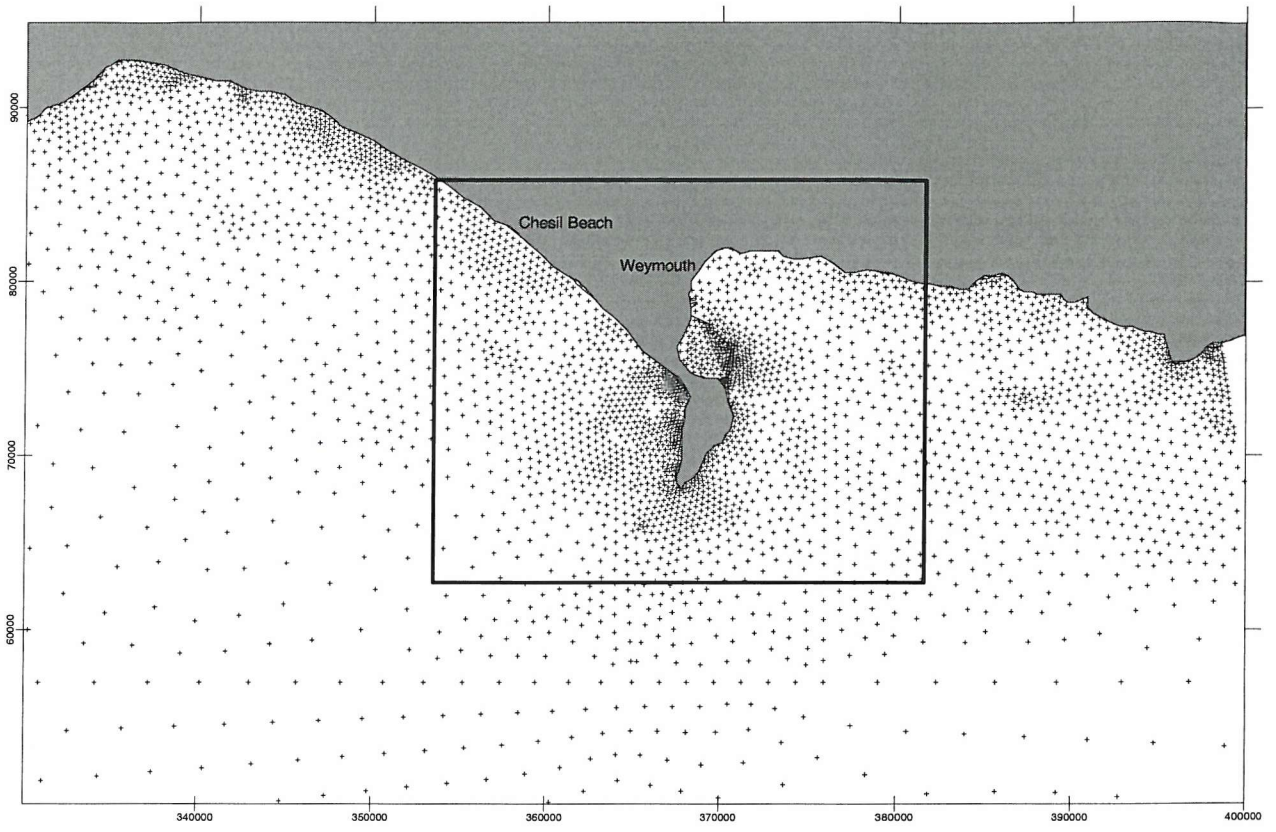

Figure 6.4 Original finite element grid abstracted from TELEMAC-2D. Coordinates are referred to National Grid, in metres.

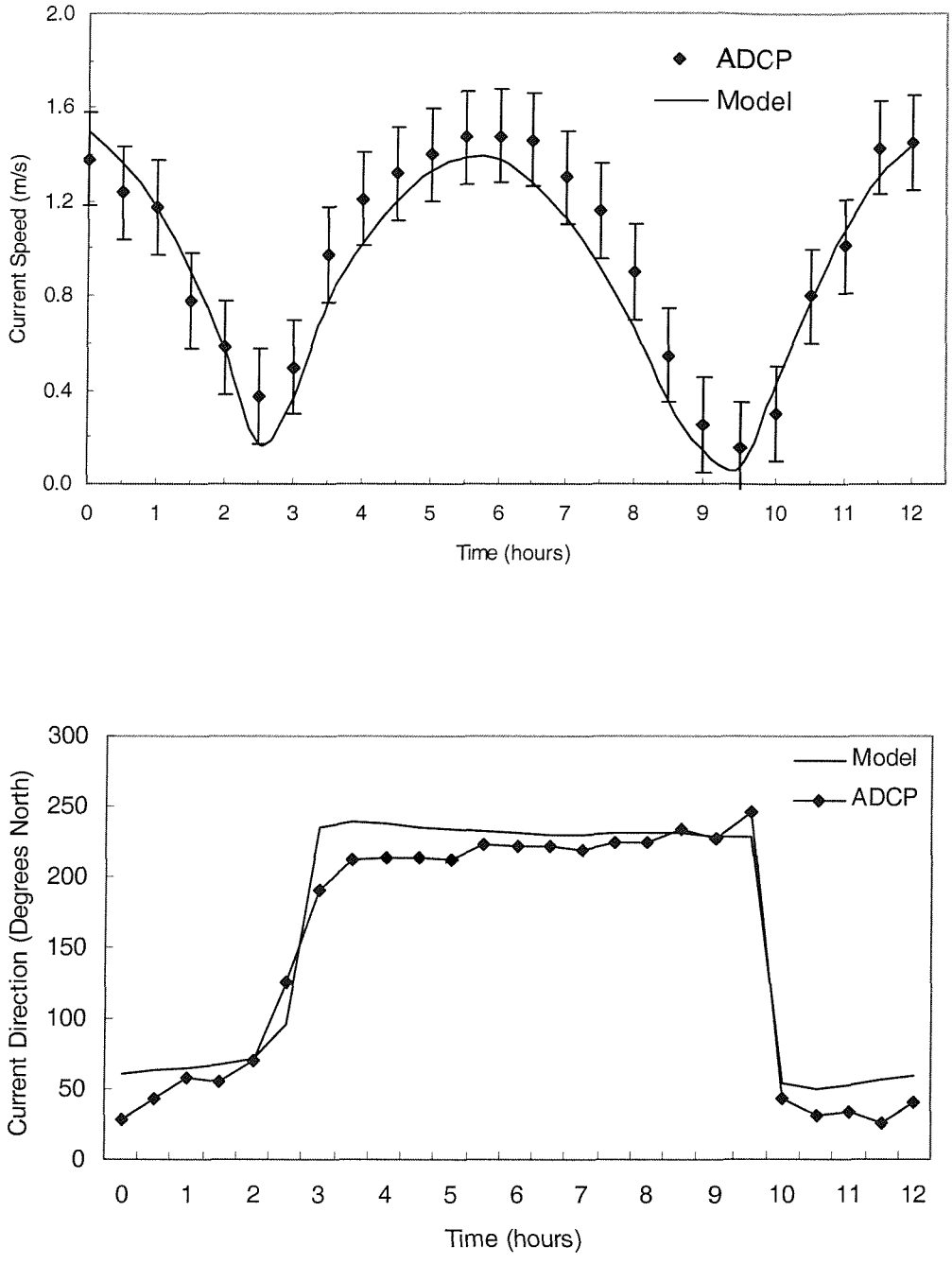

Figure 6.5 Validation of the hydrodynamic model for the area, using measured current speed and direction data obtained with the ADCP. This plot is referred to a location along the crest of the Shambles Bank.

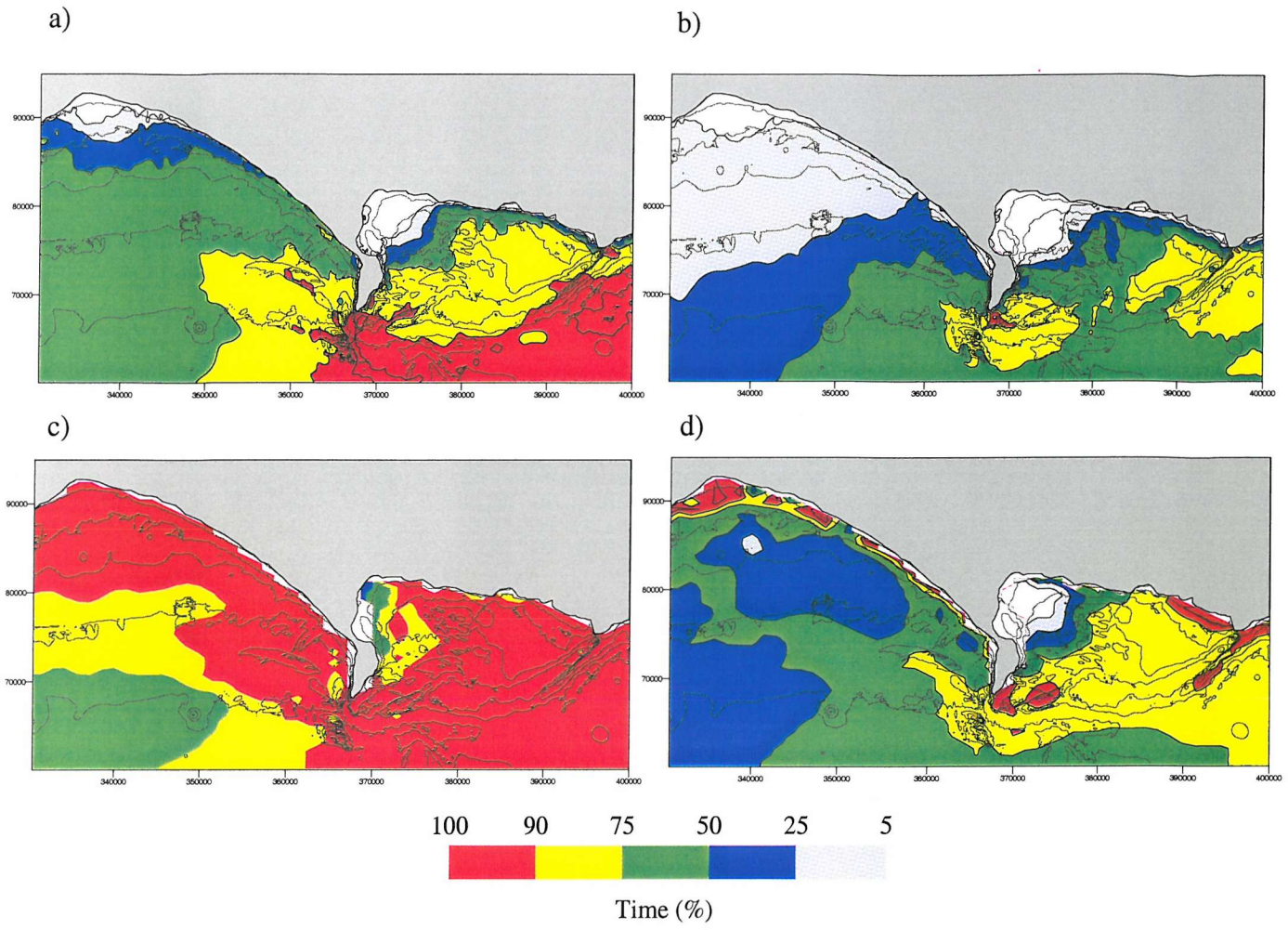

Figure 6.6 Seabed mobility simulation for fine-grained sands (D_{50} = 0.25 mm): (a) bedload mobility under currents alone; (b) suspended load transport, under currents alone; (c) bedload mobility, under combined wave and currents (SW Wave: Hs=0.8 m; Tz= 4.5 s; Dir= 220°); and (d) suspended load transport, under combined wave and currents.

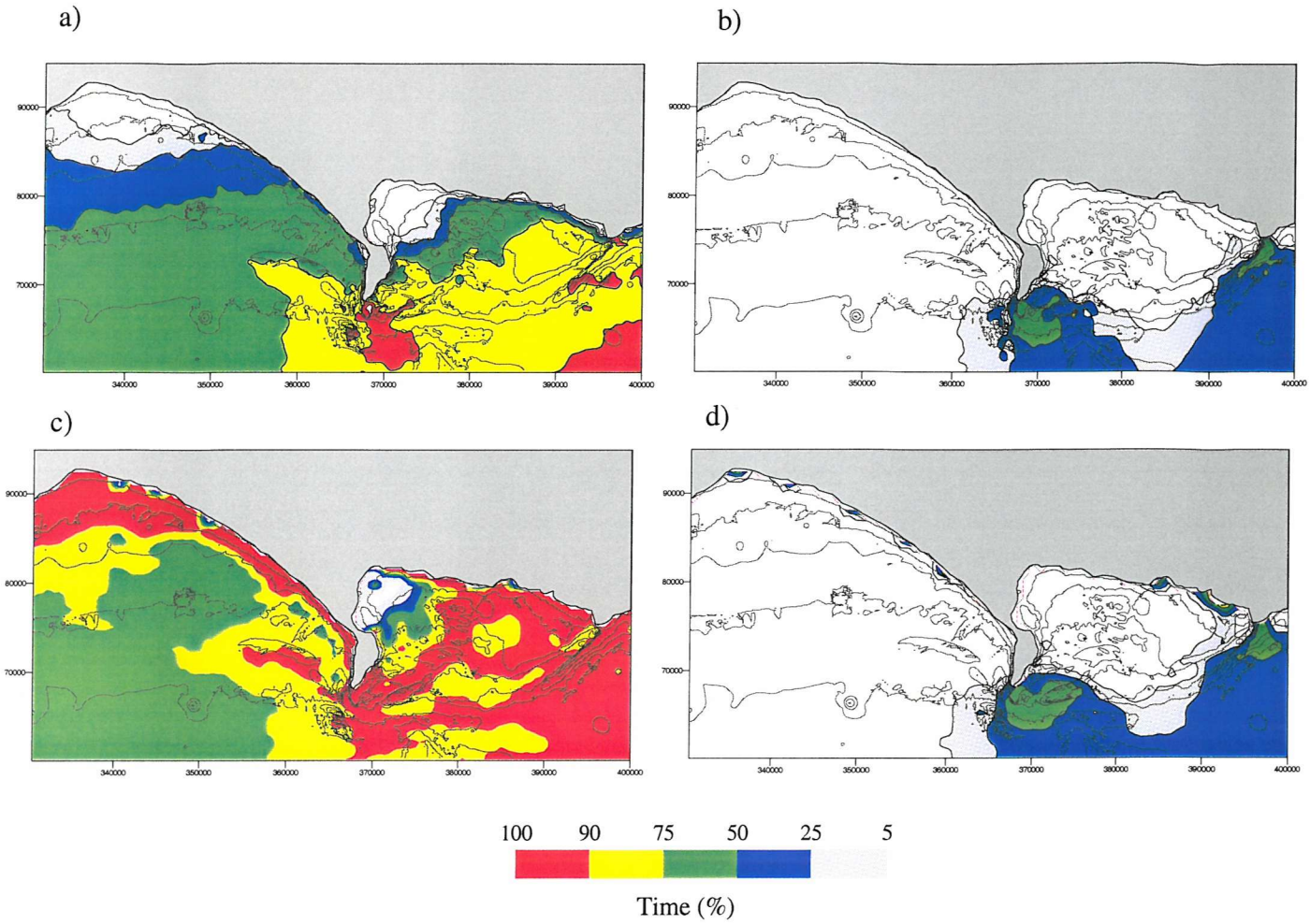

Figure 6.7 Seabed mobility simulation for medium-grained sands (D_{50} = 0.50 mm): (a) bedload mobility under currents alone; (b) suspended load transport, under currents alone; (c) bedload mobility, under combined wave and currents (SW Wave: Hs=0.8 m; Tz= 4.5 s; Dir= 220°); and (d) suspended load transport, under combined wave and currents.

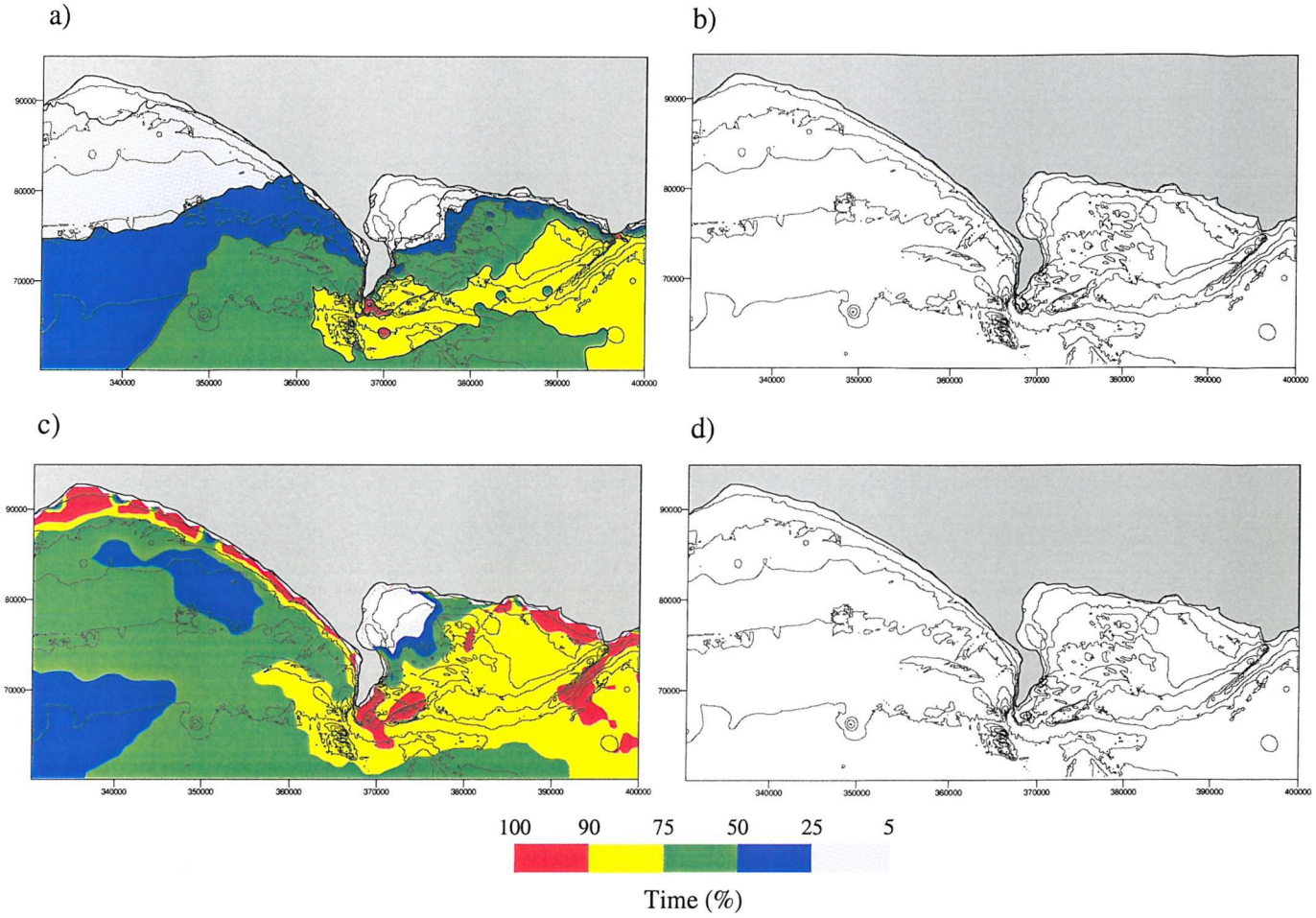

Figure 6.8 Seabed mobility simulation for coarse-grained sands (D_{50} = 1.00 mm): (a) bedload mobility under currents alone; (b) suspended load transport, under currents alone; (c) bedload mobility, under combined wave and currents (SW Wave: Hs=0.8 m; Tz= 4.5 s; Dir= 220°); and (d) suspended load transport, under combined wave and currents.

a)

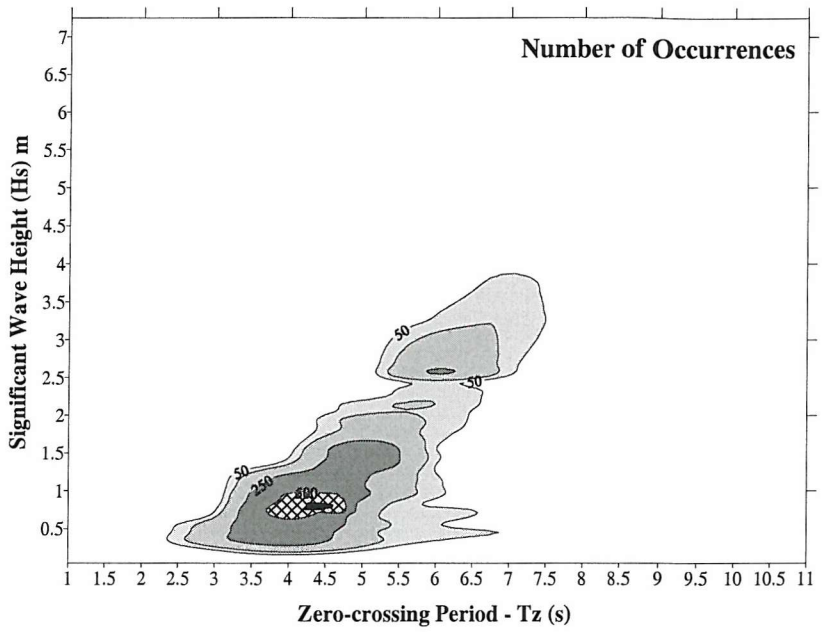

b)

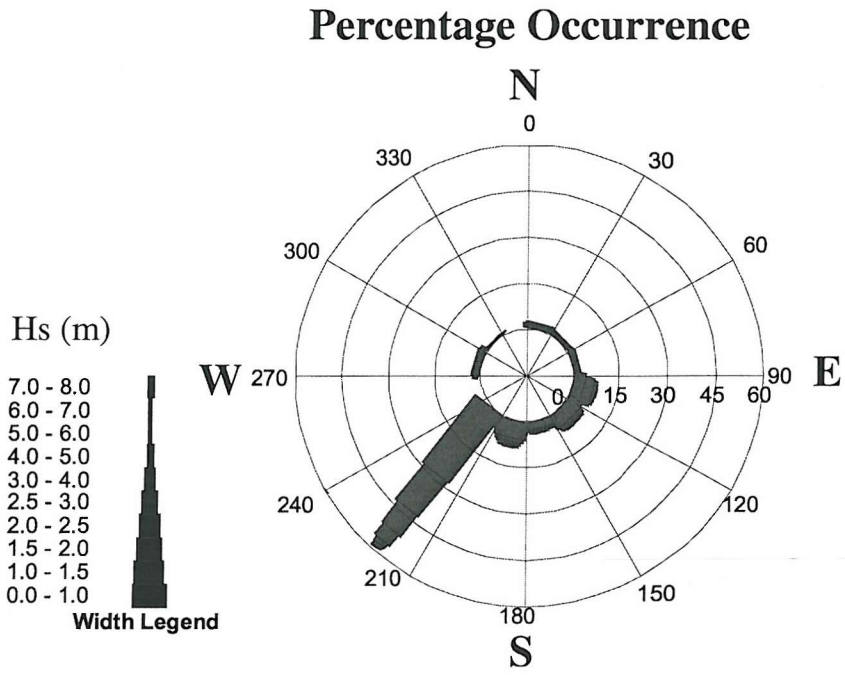

Figure. 6.9 Wave data from Lyme Bay (LB, for location see Figure 6.1): (a) scatter diagram of Hs and Tz, in terms of number of occurrences (for the period between 1992-1994); (b) wave rose diagram, showing the predominant direction of the waves in relation to their Hs.

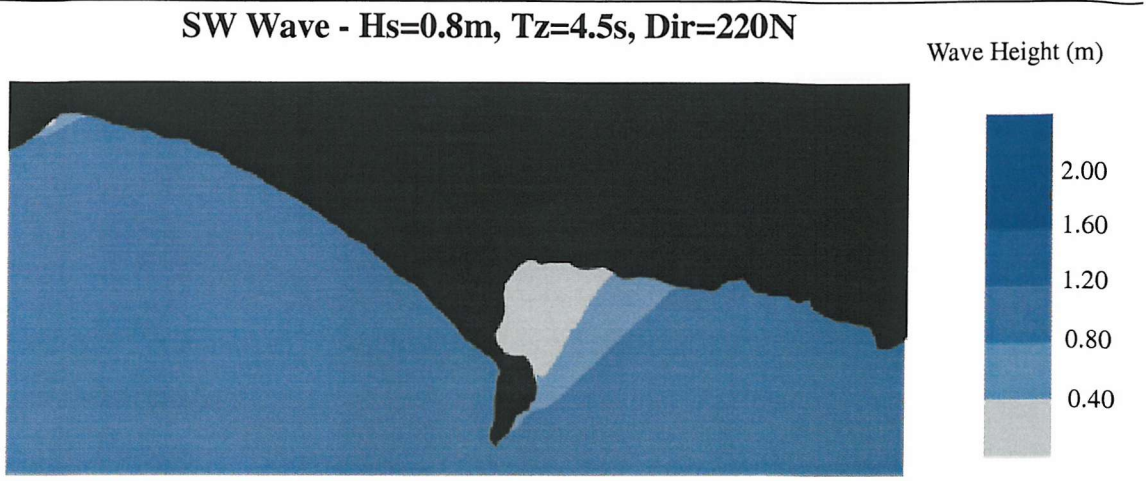

Figure 6.10 Wave height distribution over the inner continental shelf, calculated using the RCPWAVE model. Results obtained from the simulation using SW waves.

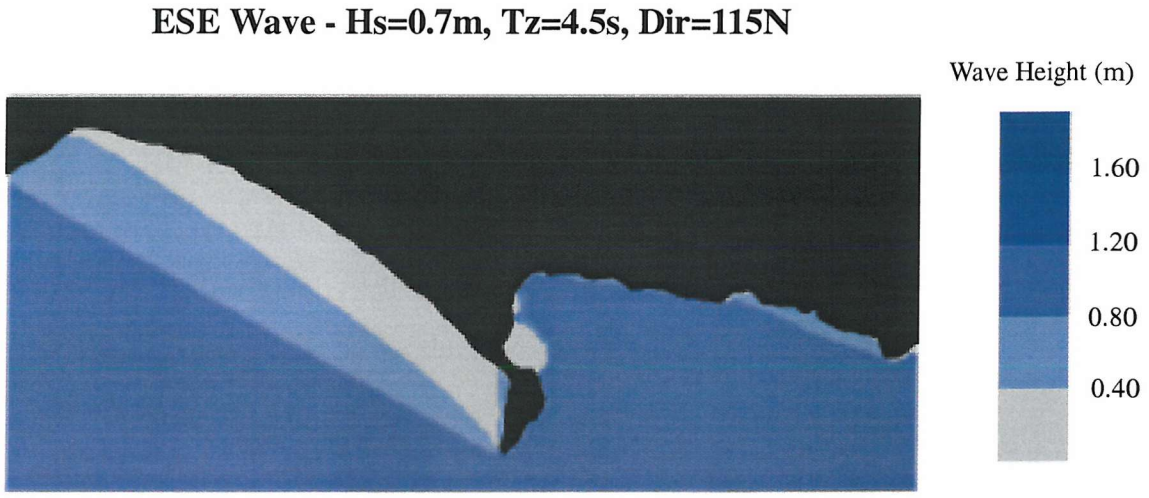

Figure 6.11 Wave height distribution over the inner continental shelf, calculated using the RCPWAVE model. Results obtained from the simulation using ESE waves.

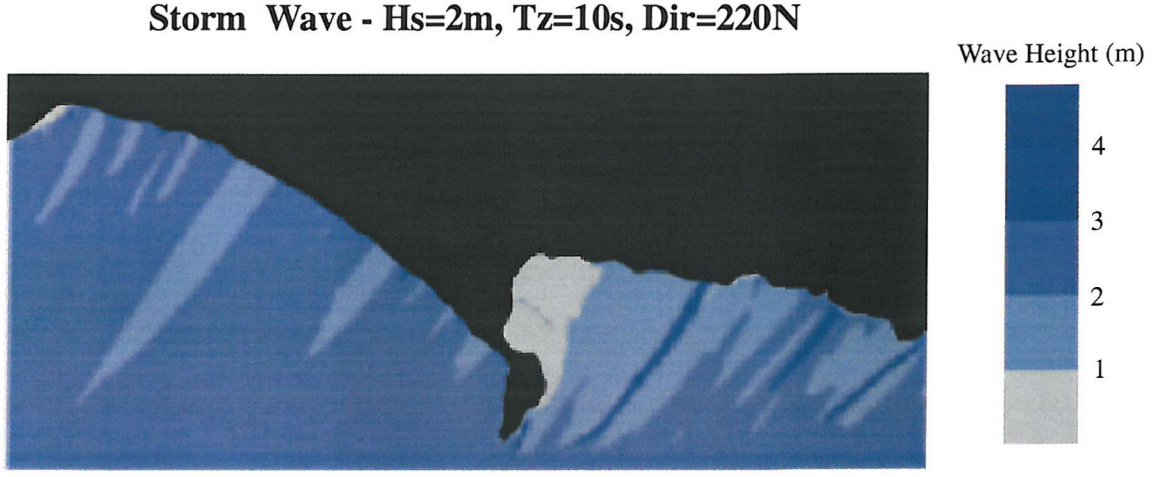

Figure 6.12 Wave height distribution over the inner continental shelf, calculated using the RCPWAVE model. Results obtained from the simulation using "Storm" waves.

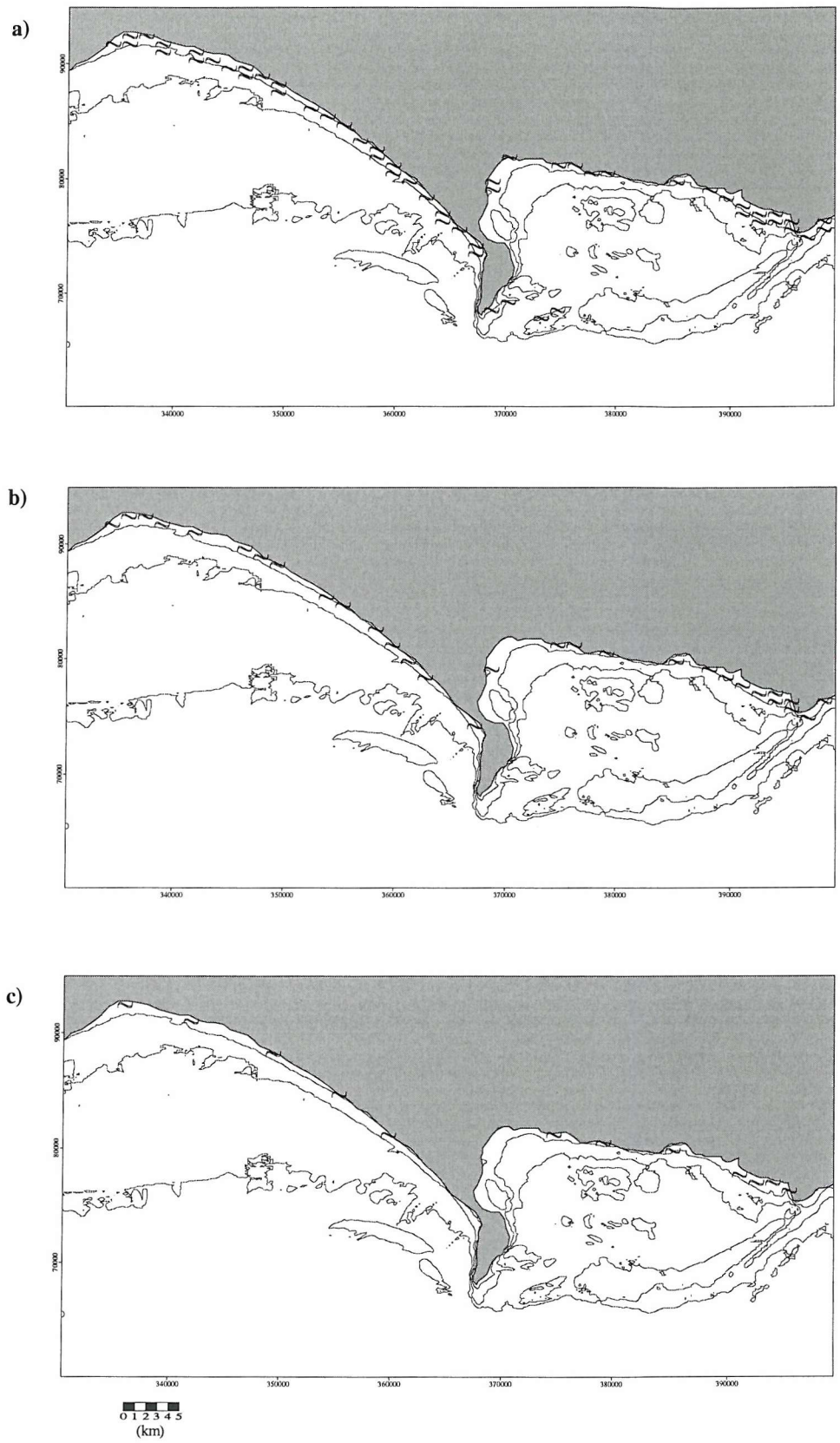

Figure 6.13 Seabed mobility under SW wave action (Hs = 0.8 m, Tz = 4.5 s, Dir = 220°N). The mobility is simulated for: (a) fine-grained sand beds; (b) medium-grained sand beds; and (c) coarse-grained sand beds.

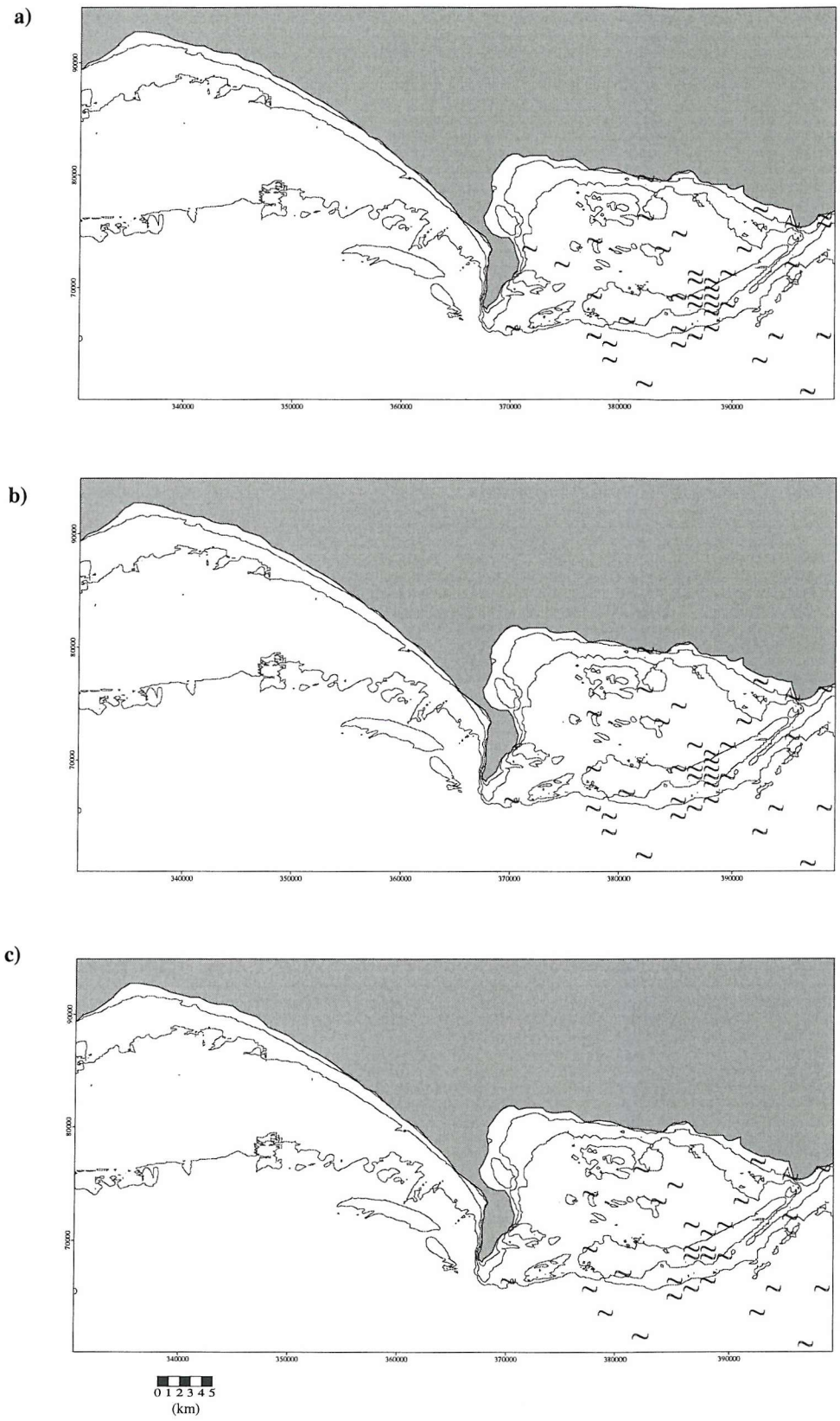

Figure 6.14 Seabed mobility under ESE wave action (Hs = 0.7 m, Tz = 4.5 s, Dir = 115°N). The mobility is simulated for: (a) fine-grained sand beds; (b) medium-grained sand beds; and (c) coarse-grained sand beds.

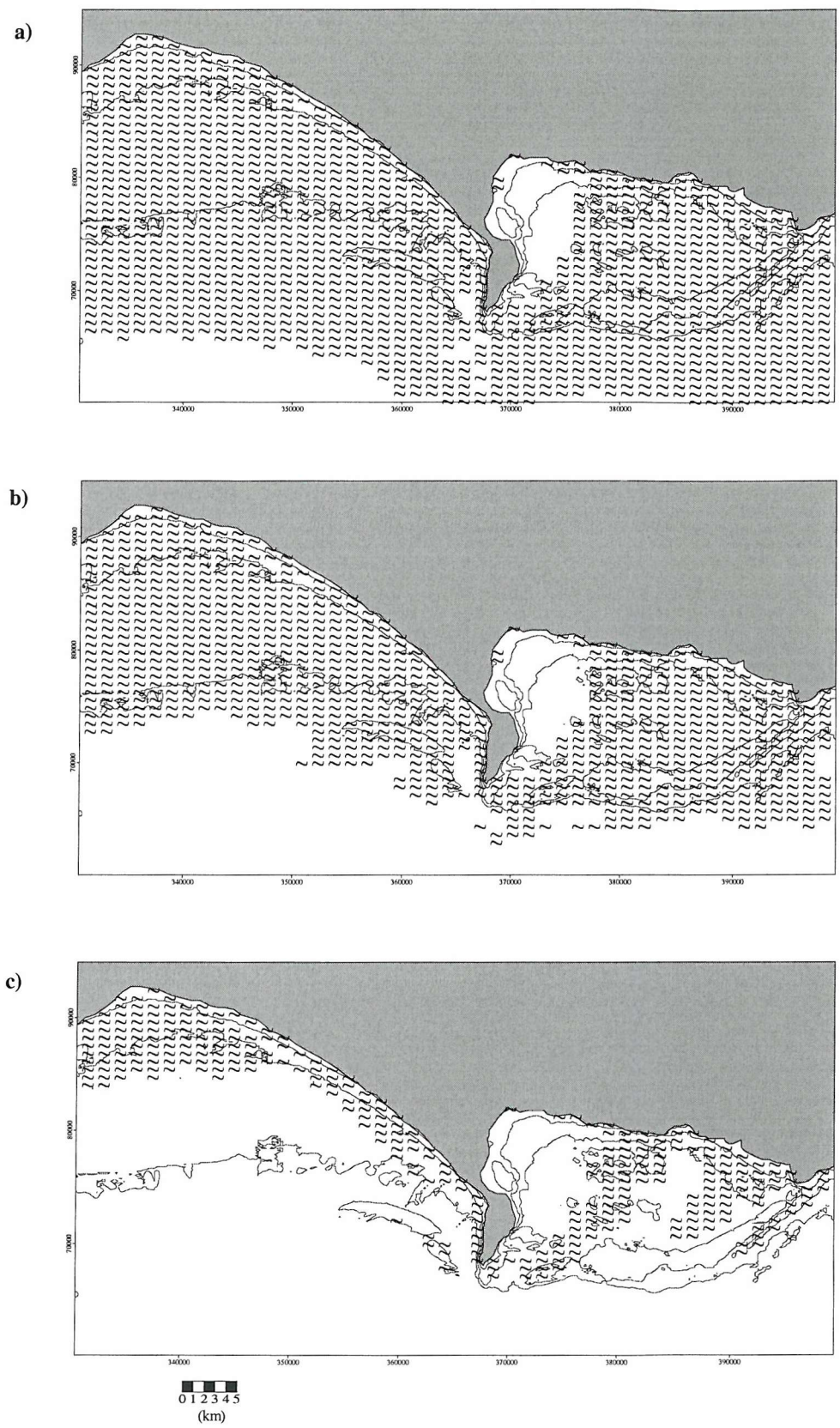

Figure 6.15 Seabed mobility under Storm wave action (Hs = 2.0 m, Tz = 10 s, Dir = 220°N). The mobility is simulated for: (a) fine-grained sand beds; (b) medium-grained sand beds; and (c) coarse-grained sand beds.

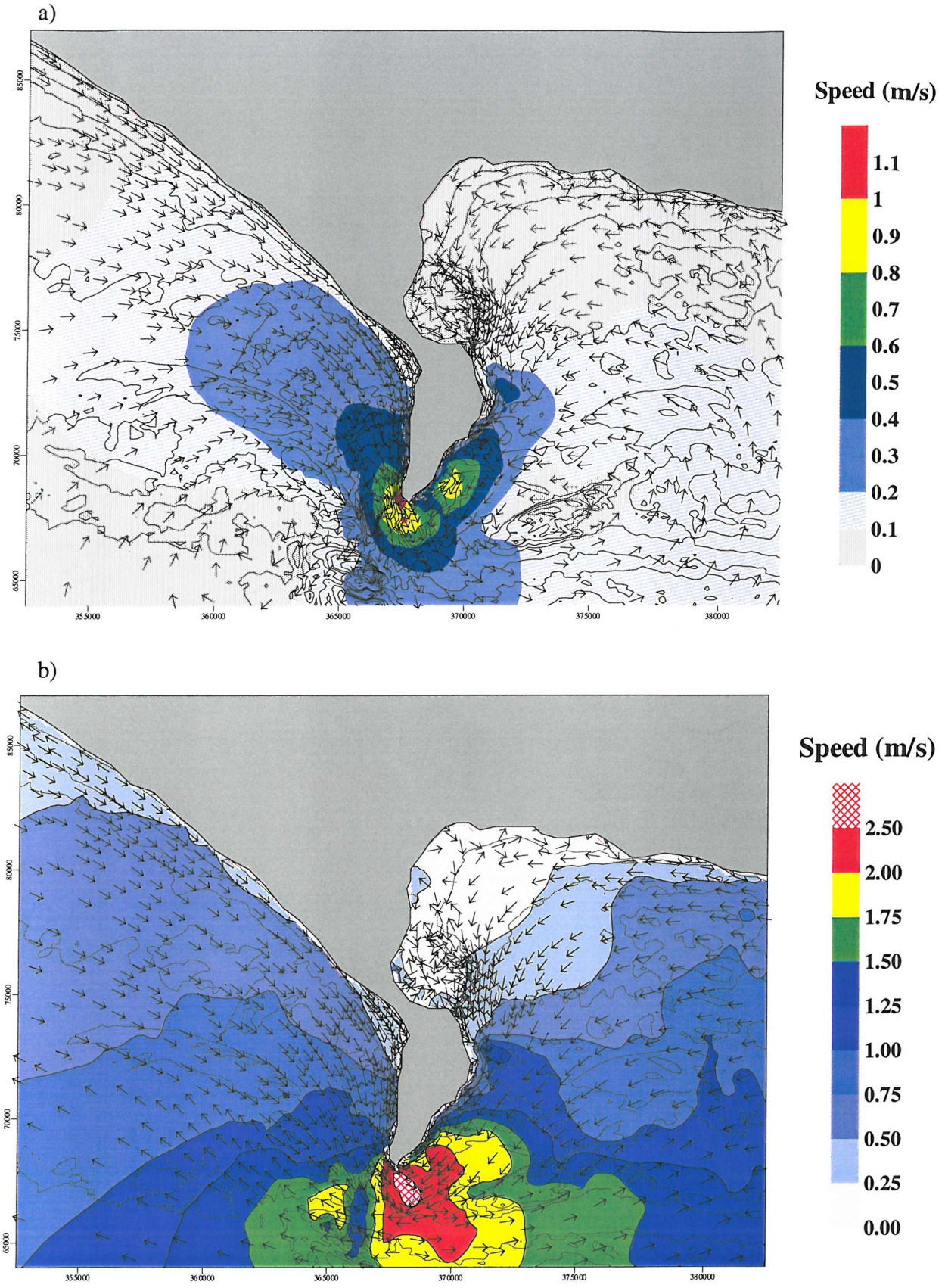

Figure 6.16 (a) Residual depth-averaged currents; (b) maximum depth-averaged currents. (Note: Tidal currents abstracted from the TELEMAC-2D numerical model output).

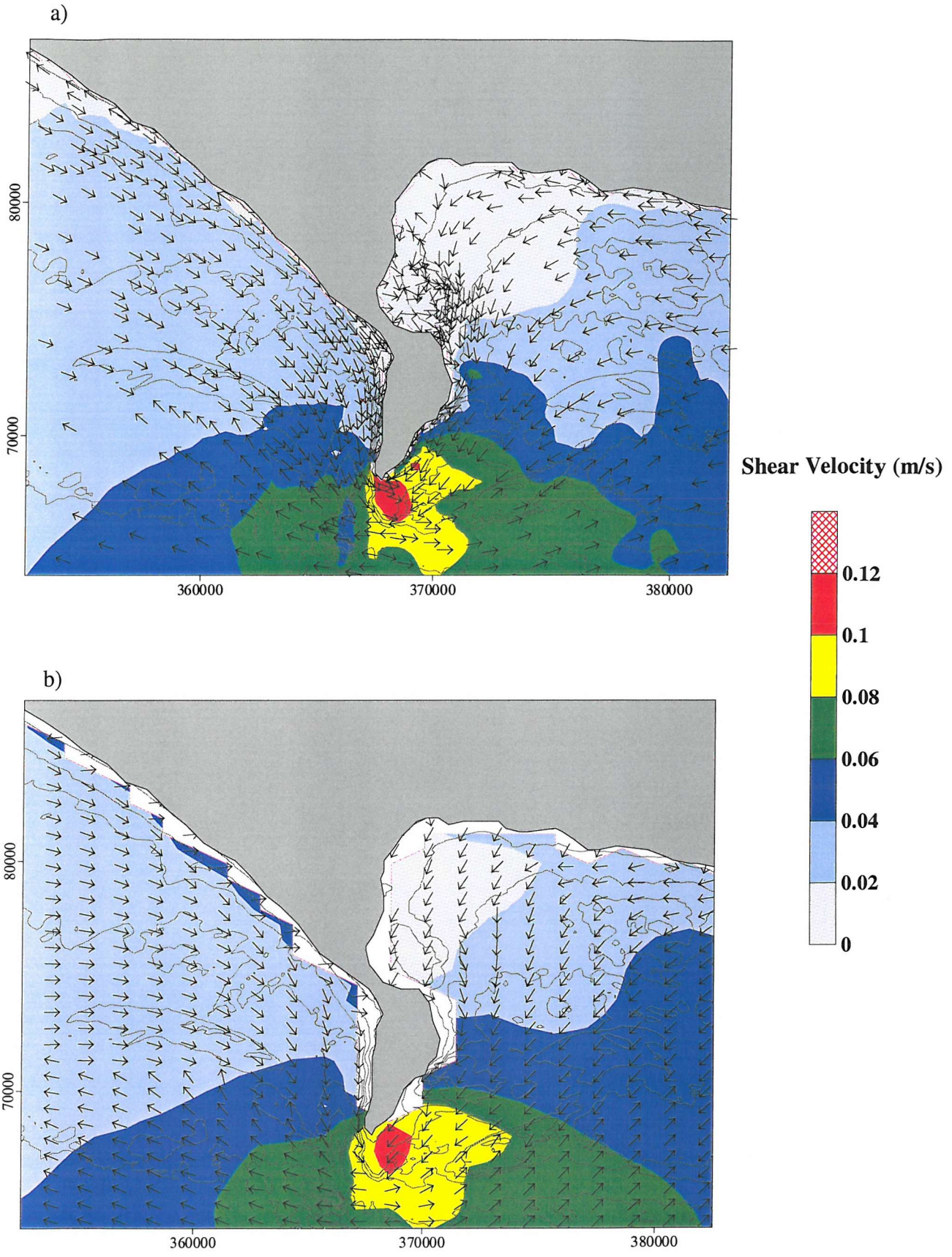

Figure 6.17 Maximum bed shear stress: (a) under currents alone; (b) under combined wave (SW) and currents.

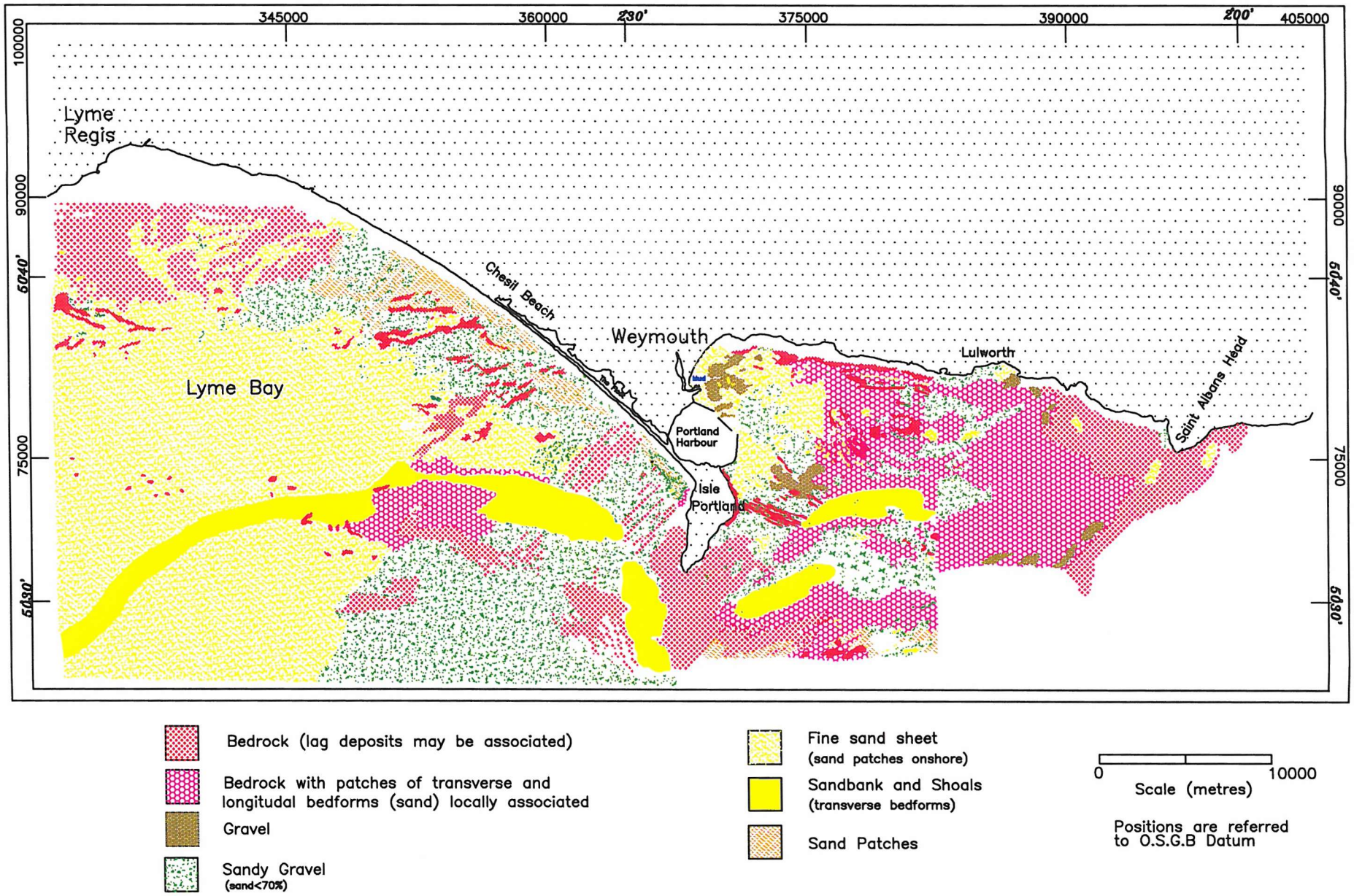

Figure 6.18 Seabed facies distribution map, based upon collected field data and available datasets (Kenyon, 1994; and Nunny, 1995).

a)

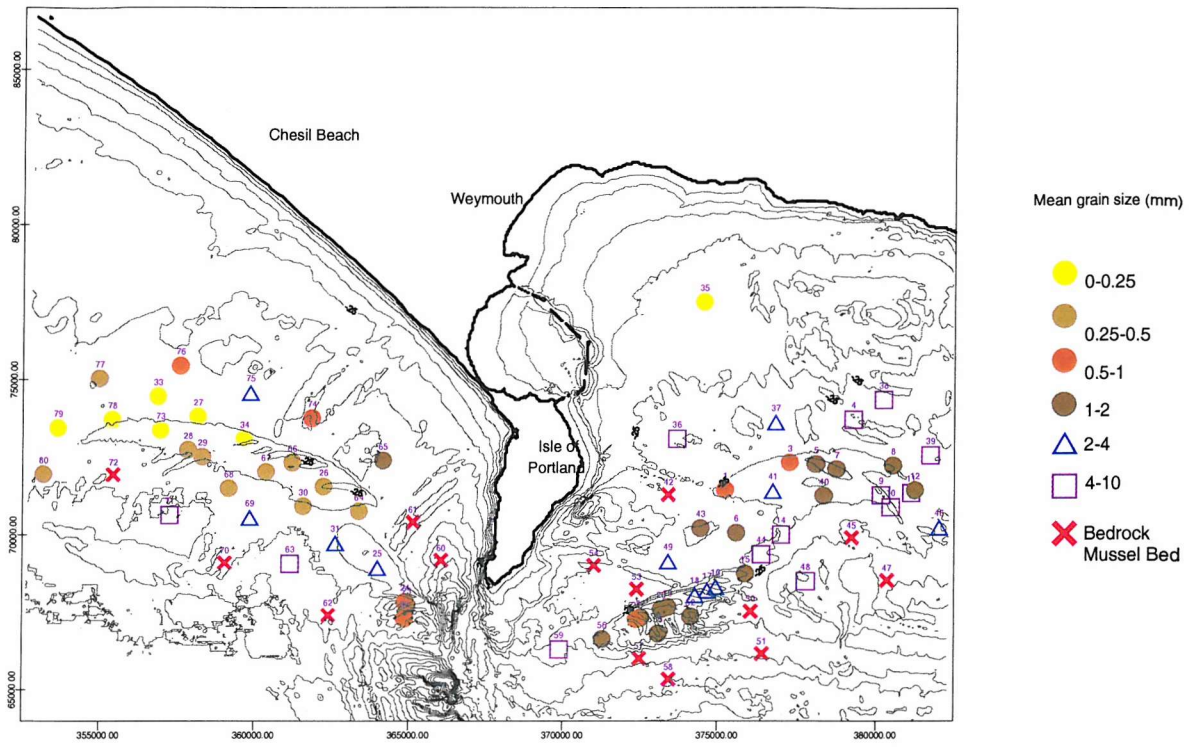
Chesil Beach
Weymouth
Isle of Portland
85000.00
80000.00
75000.00
70000.00
65000.00
355000.00
360000.00
365000.00
370000.00
375000.00
380000.00
Mean grain size (mm)
0-0.25
0.25-0.5
0.5-1
1-2
2-4
4-10
Bedrock
Mussel Bed

b)

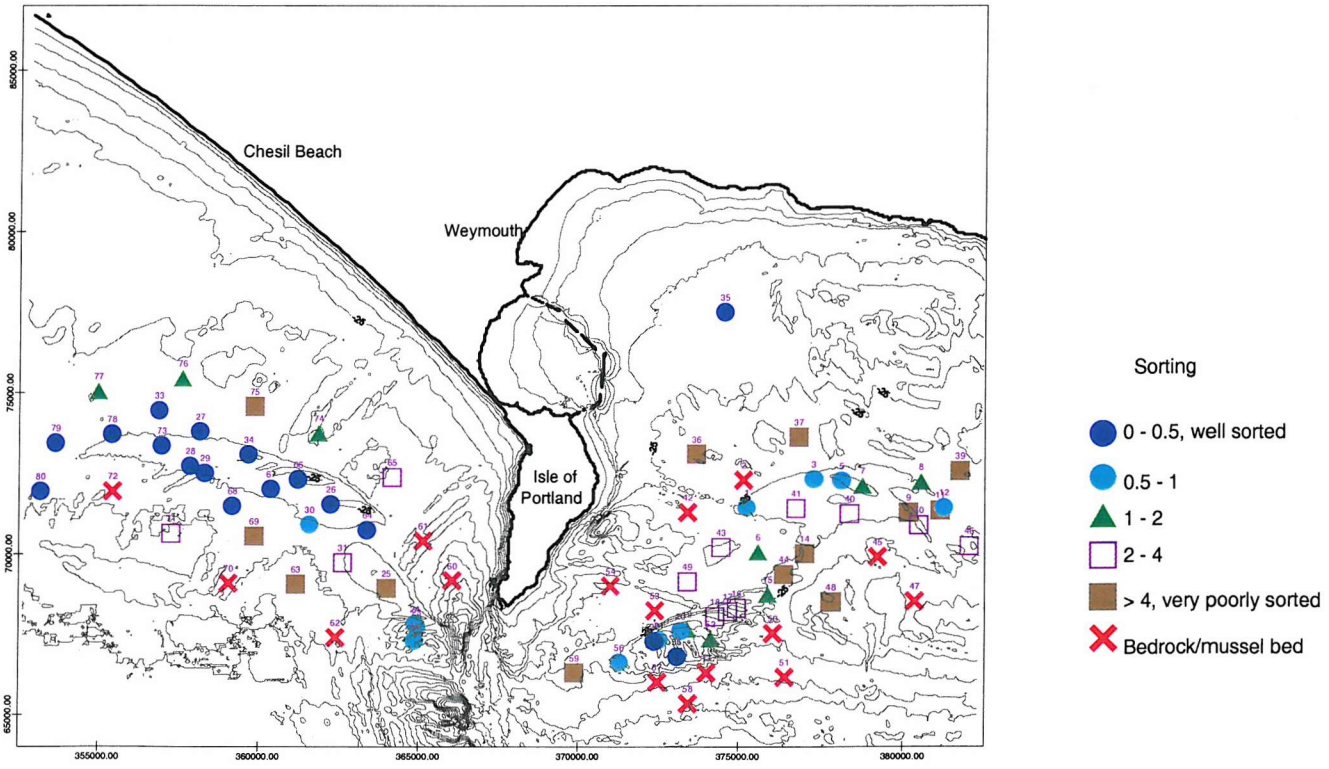
Chesil Beach
Weymouth
Isle of Portland
85000.00
80000.00
75000.00
70000.00
65000.00
355000.00
360000.00
365000.00
370000.00
375000.00
380000.00
Sorting
0 - 0.5, well sorted
0.5 - 1
1 - 2
2 - 4
> 4, very poorly sorted
Bedrock/mussel bed

c)

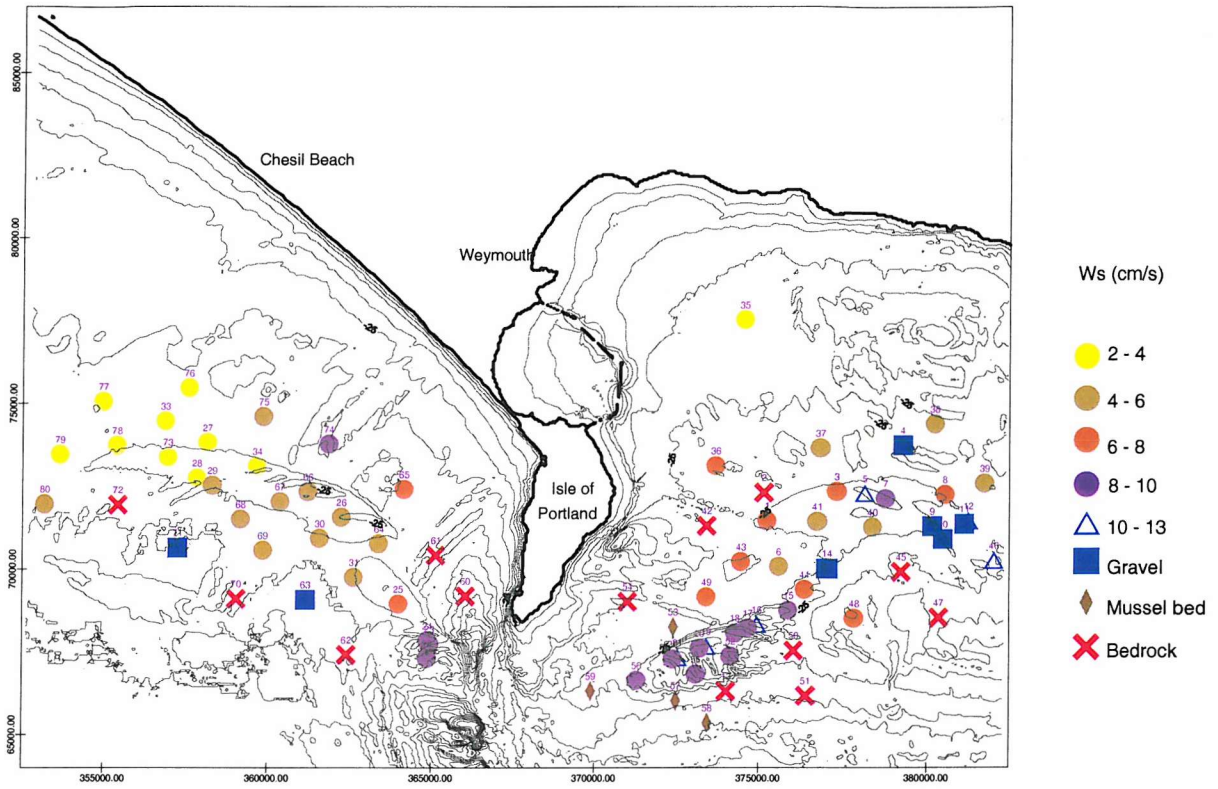

Figure 6.19 Distribution of the grain size parameters and sand content over the study area, based upon: (a) mean sieve diameter (D_{50}, mm); (b) sorting (σ, mm); and (c) mean (sand) settling velocity (w_s, cm s^{-1}).

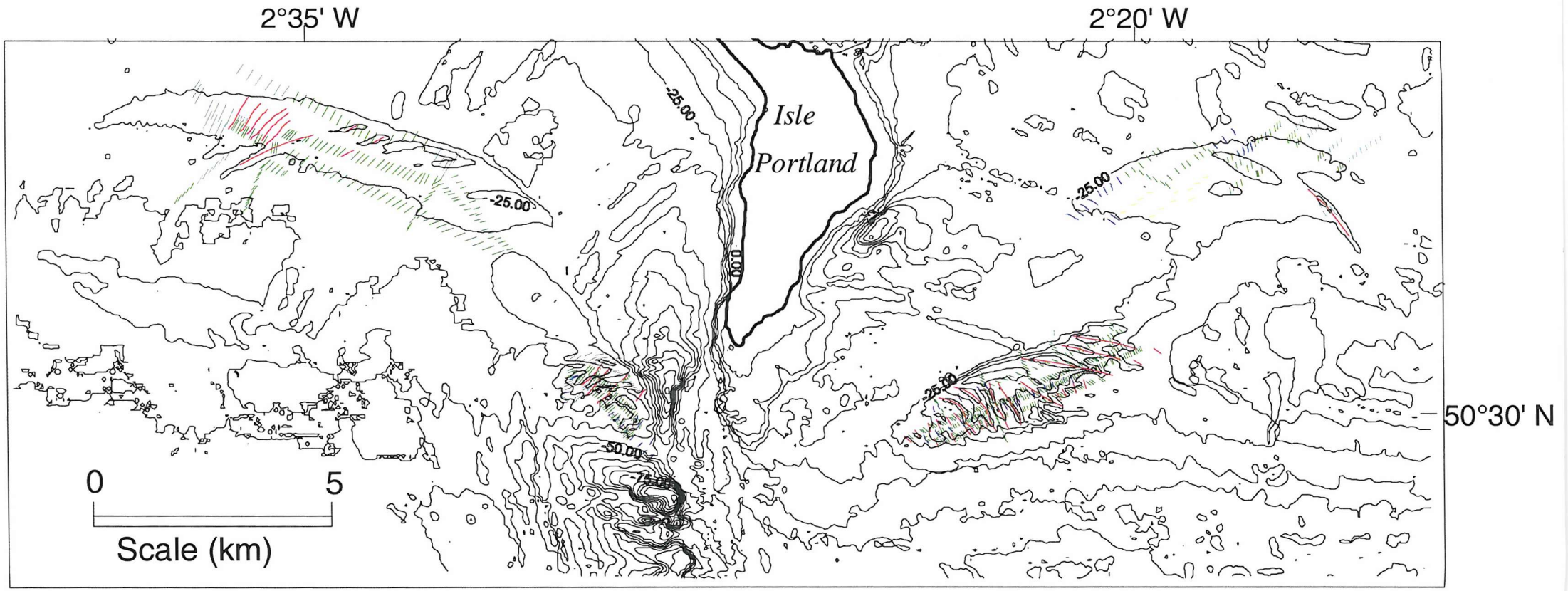

Figure 6.20. Chart showing the bedform distribution over the sedimentary deposits. Key: red line - very large sandwave (H > 4m, L > 100 m); blue line – large sandwave A (1.5<H<5 m, 30<L<100m; cyan line – large sandwave B (0.75<H<1.5 m, 10<L<25 m); green line – medium sandwave (H < 0.75 m, L < 10 m); yellow line – patches of bedforms, overlying bedrock.

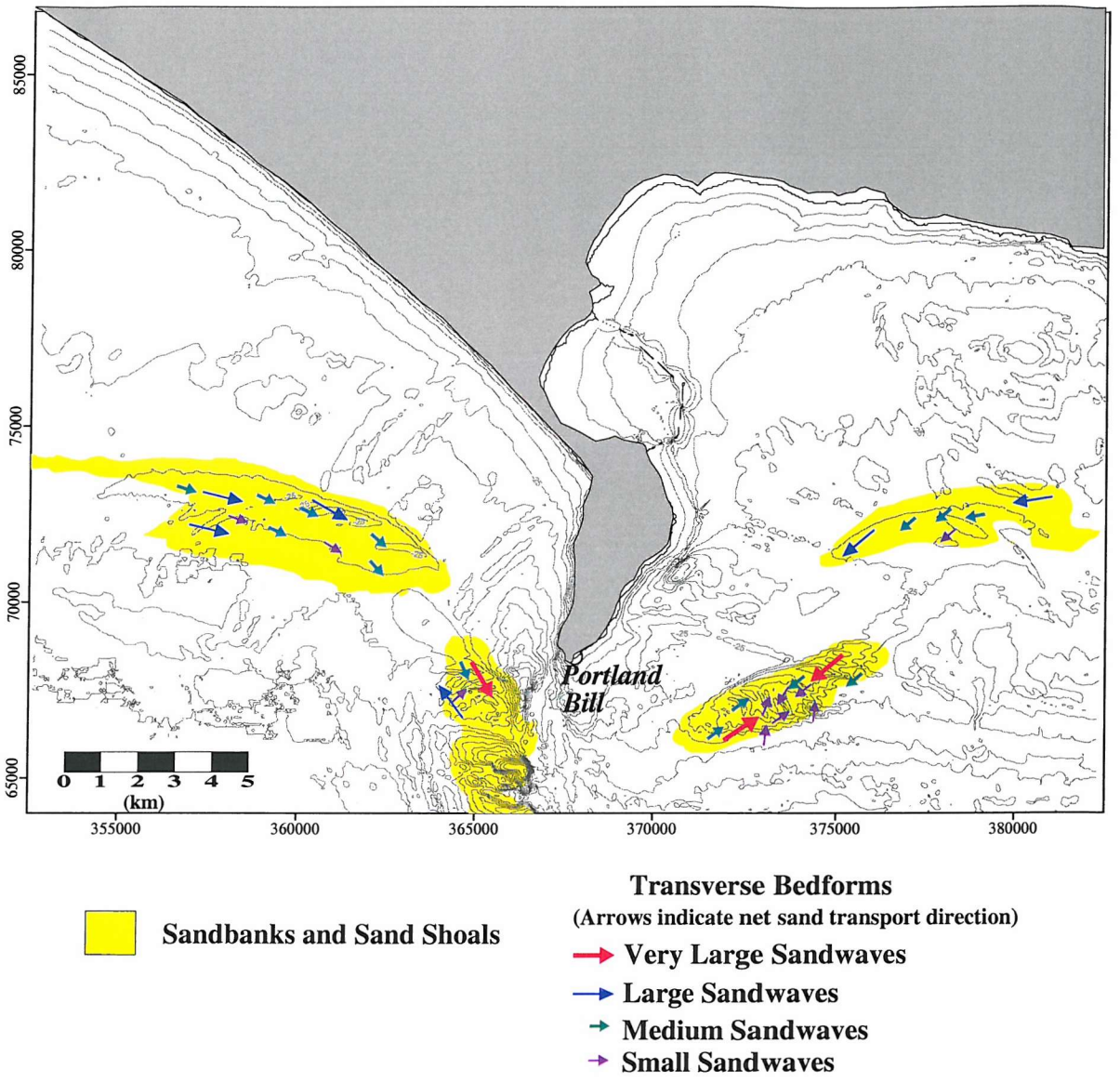

Figure 6.21 Sand transport pathways derived from the asymmetry of large and very-large sandwaves. Sandwave classification is based upon their wavelength (L) and height (H), following Ashley et al. (1990), i.e.: very large (L)100m, H>5m); large (L-10-100m, H-0.75-5m); medium (L-5-10m, H-0.4-0.75m); and small (L-0.6-5m, H-0.075-0.4m).

a)

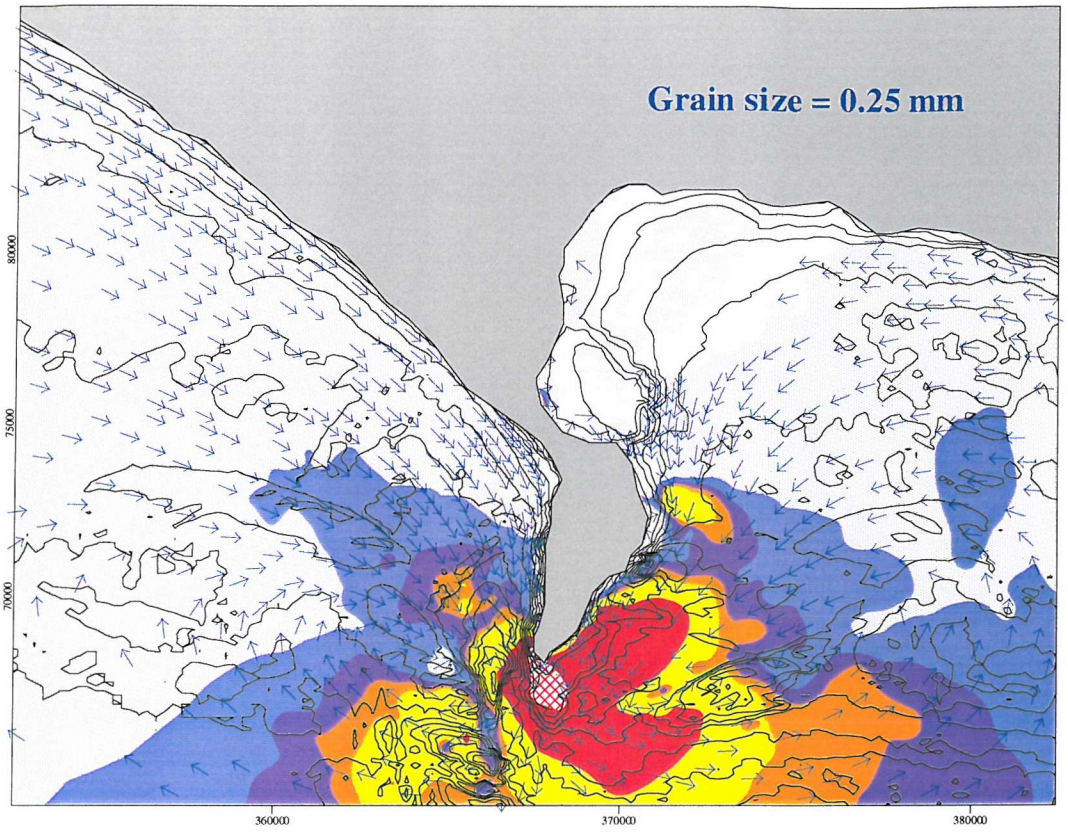
Grain size = 0.25 mm
80000
75000
70000
360000
370000
380000

b)

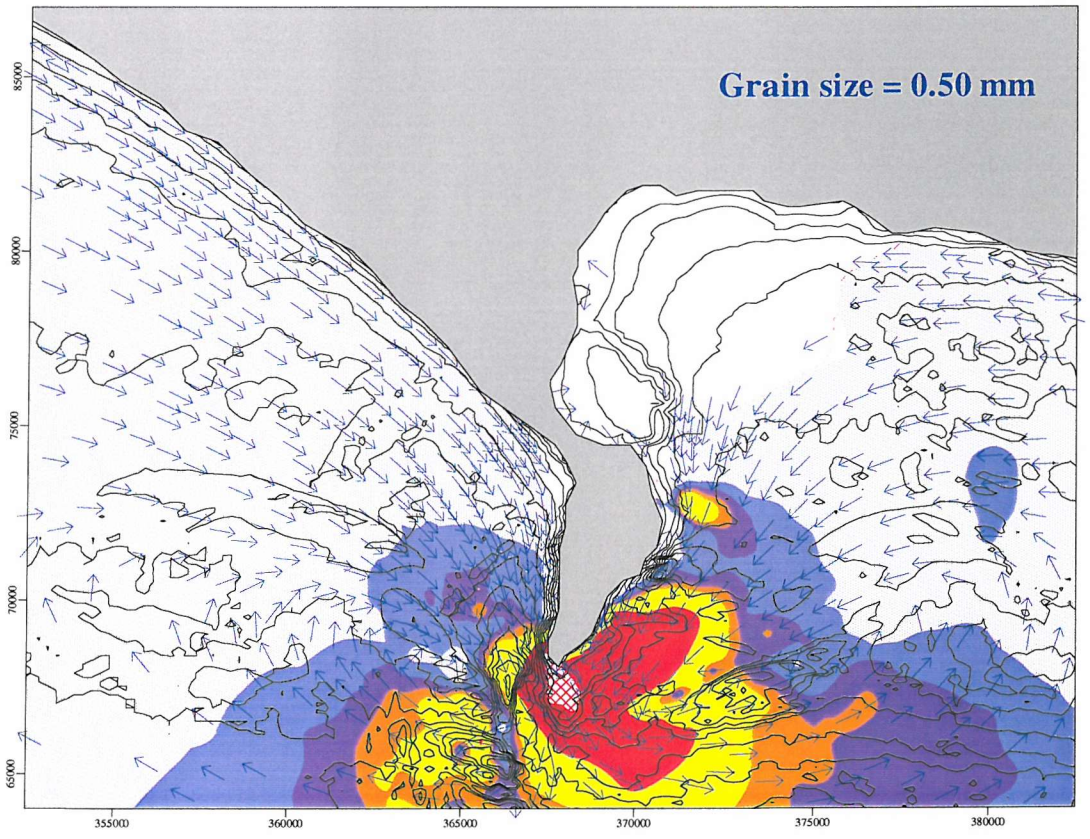
Grain size = 0.50 mm
85000
80000
75000
70000
65000
355000
360000
365000
370000
375000
380000

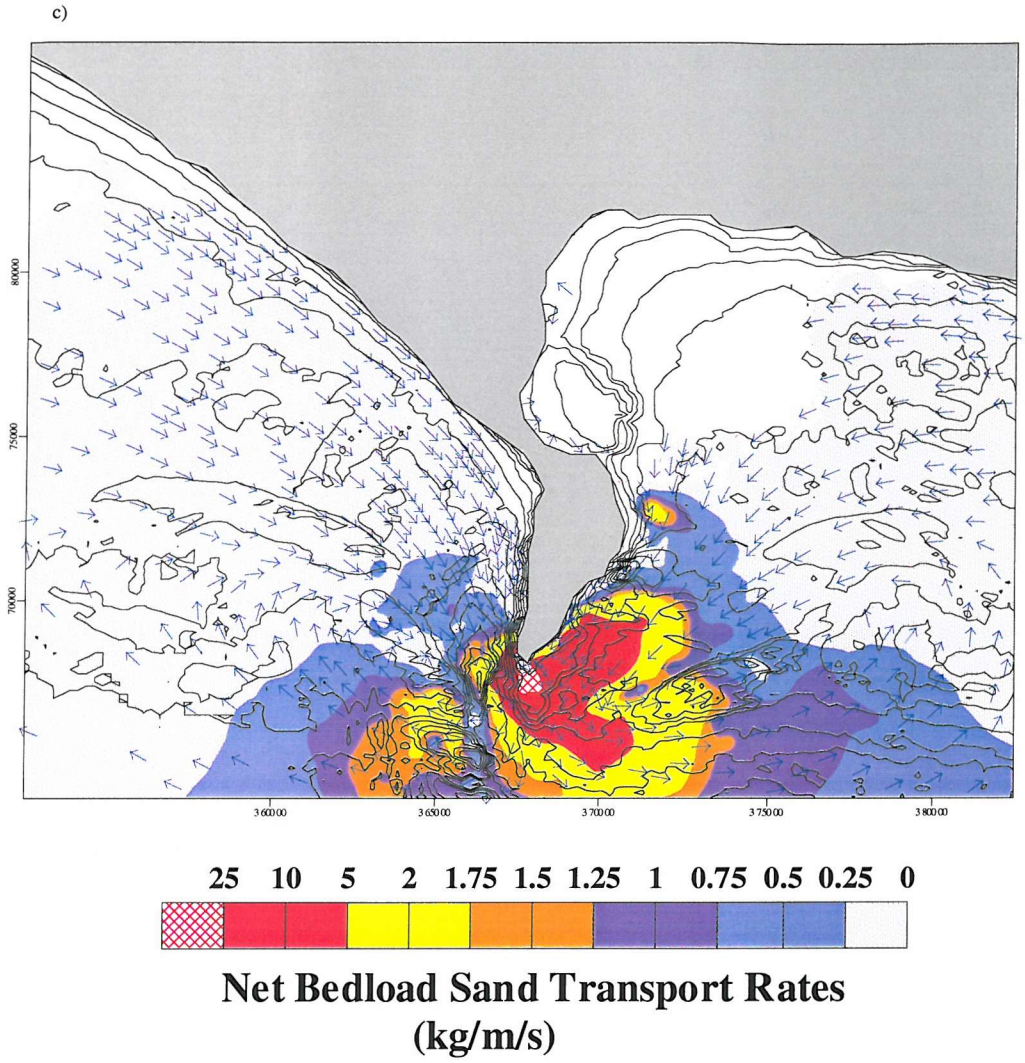

Figure 6.22 Net bedload (sand) transport, calculated for: (a) a fine-grained sand bed; (b) medium-grained sand bed; and (c) coarse-grained sand bed. Transport rates were calculated using the algorithm proposed by Gadd et al. (1978).

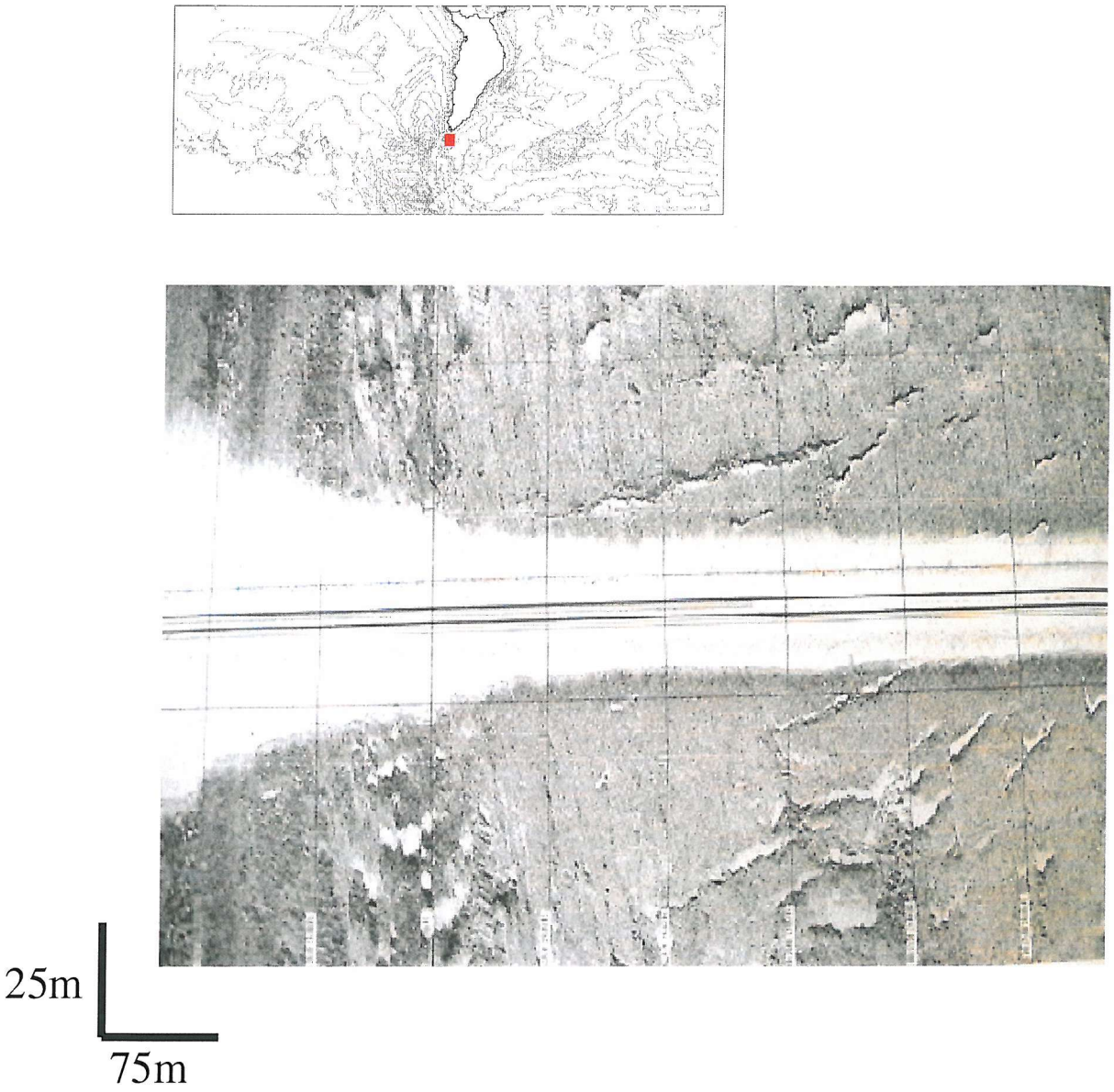

Figure 6.23 Side-scan sonar image, showing bedrock outcrops near the tip of the headland.

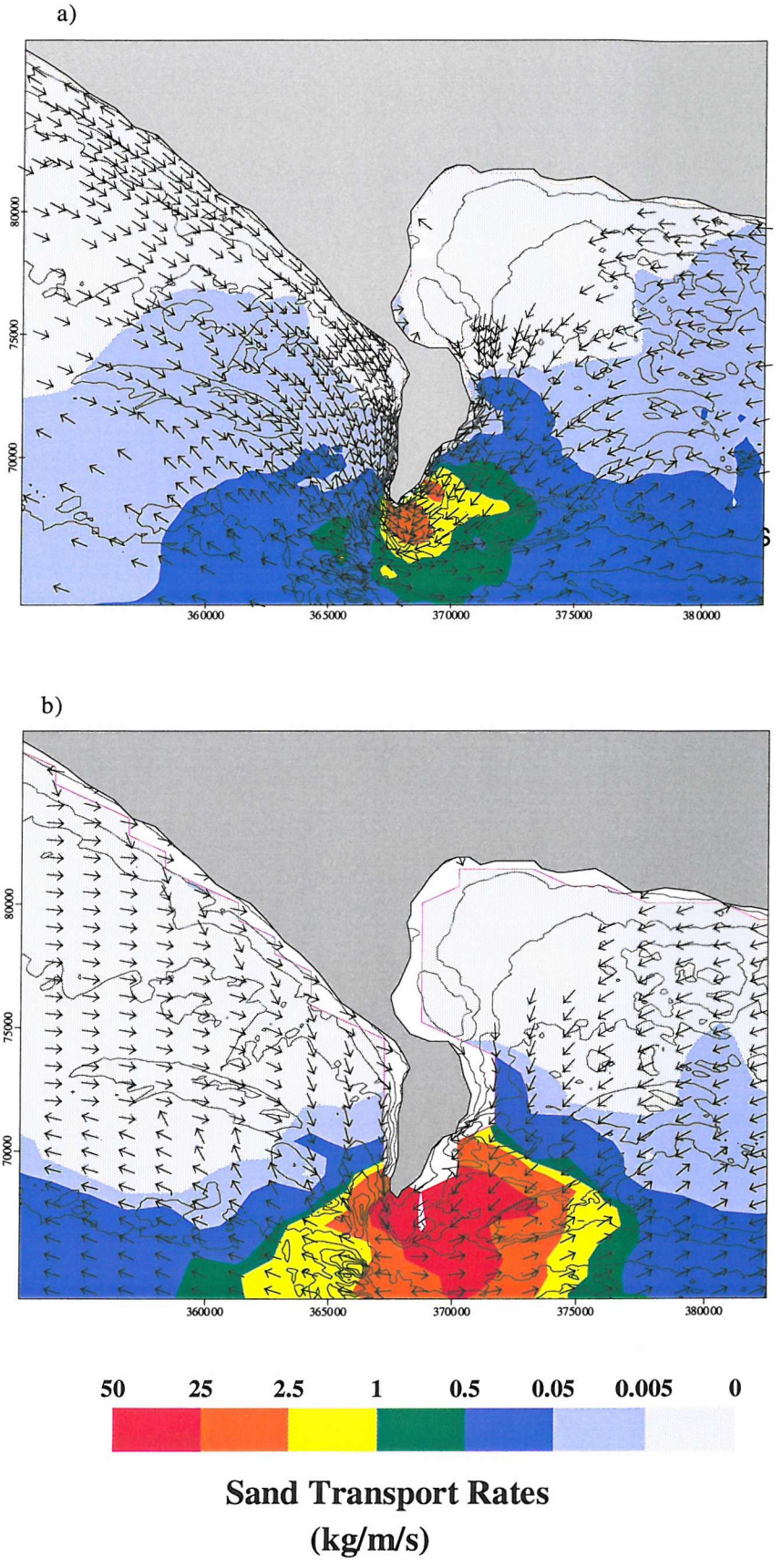

Figure 6.24 Maximum (medium-grained) sand transport rates, throughout a spring (ebb-flood) tidal cycle: (a) bedload transport rates under currents alone (based on the algorithm of Gadd et al., 1978), and (b) total-load rates under combined waves (SW) and currents (based upon the algorithm of Bagnold, 1963).

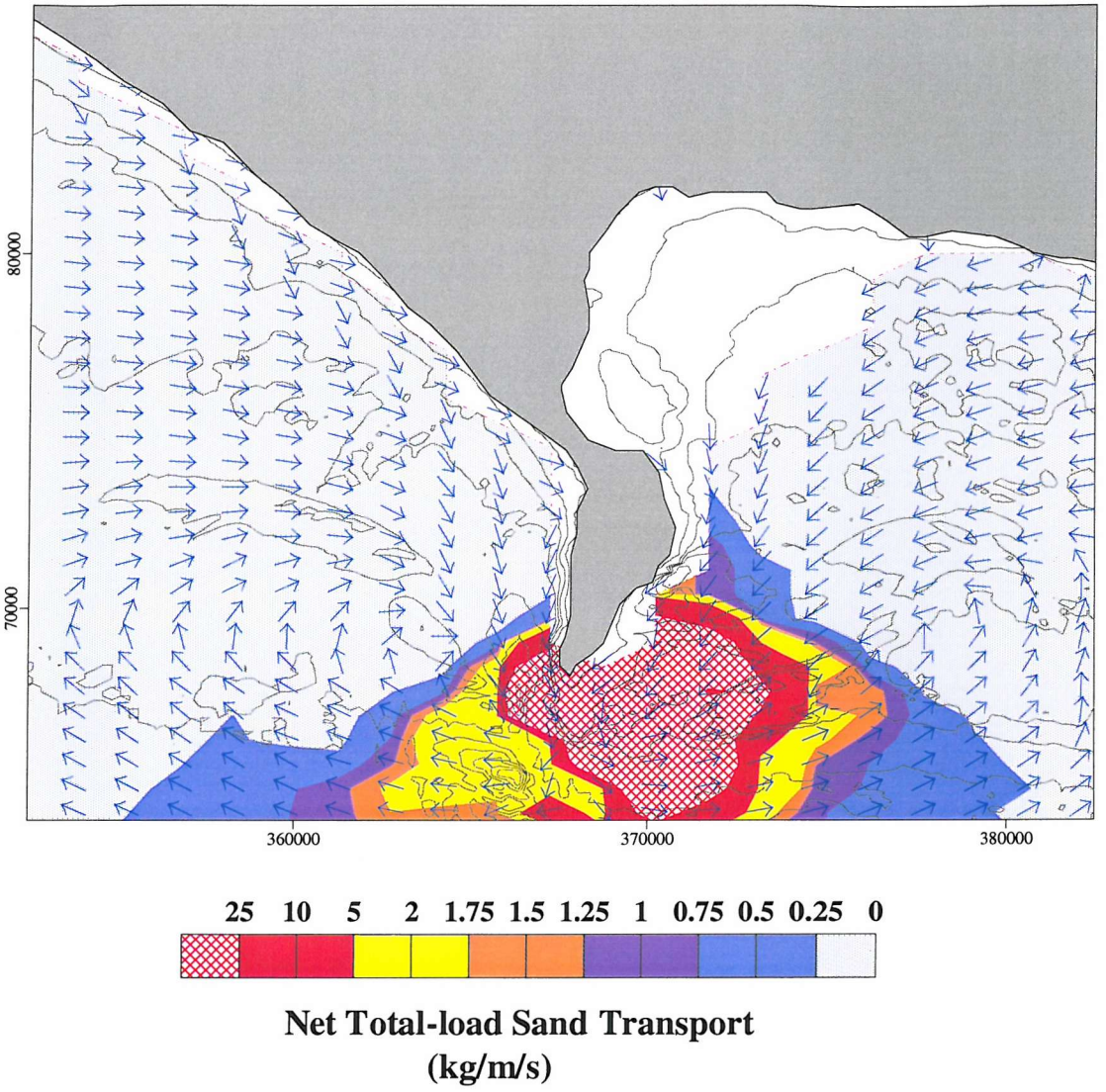

Figure 6.25 Net total-load (medium-grained) sand transport rates, calculated for the combined action of waves (SW) and currents. Total load rates were calculated using the algorithm of Bagnold (1963).

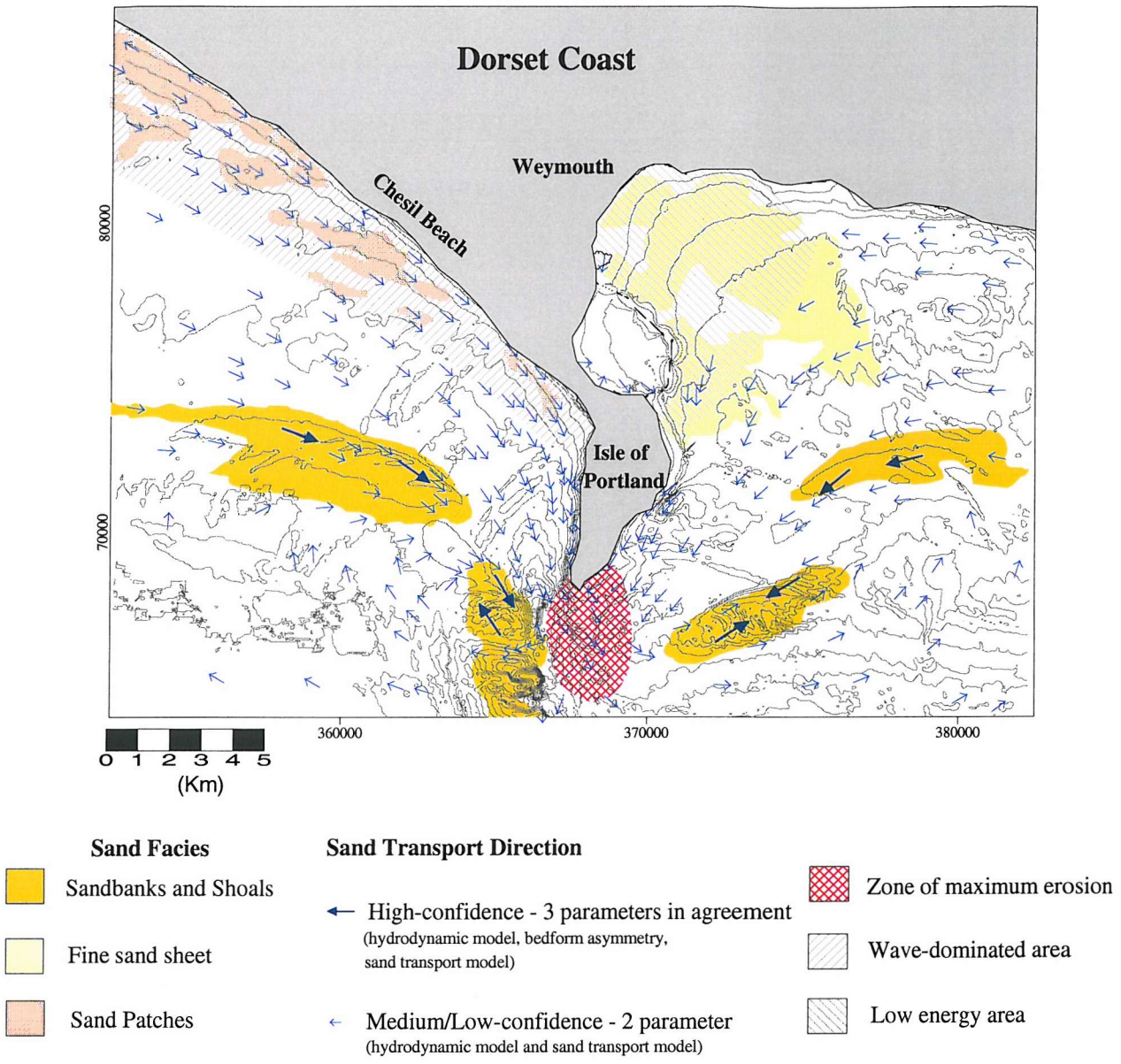

Figure 6.26 Synthesis (conceptual) map, showing an explanatory model of sand transport pathways and the different levels of confidence, based upon the methodology applied in this study (see text).

Chapter 7

Bastos, A.C., Kenyon. N.H. and Collins, M.B., 2002. Sedimentary processes, bedforms and facies, associated with a coastal headland: Portland Bill, southern UK. Marine Geology, *187 (3/4), 235-258.*

Authors	Initiative of the Study	Data Collection and Analysis	Interpretation	Manuscript Preparation
Bastos	70%	100%	70%	80%
Kenyon		(Involded in fieldwork)	15%	10%
Collins	30%	-	15%	10%

Chapter 7

Sedimentary Processes, Bedforms and Facies, Associated with a Coastal Headland: Portland Bill, southern UK

Abstract

This investigation presents new findings on the sedimentary processes and deposits associated with a coastal headland, in a mixed tide-wave setting, using data compilation (bathymetric and sediment distribution maps), collected field data (side-scan sonar and seabed sampling) and sand transport modelling. Sand transport pathways are described: (a) on the basis of coupled-system seabed morphology/sand distribution; and (b) from bed shear stress and (medium-grained) sand transport rate simulations.

The presence of a sequence of sedimentary deposits, associated with a complex suite of bedforms and sedimentary facies within an overall framework of limited sediment supply, represents a gradient in shear stress and sand transport towards the headland. These sequences are observed on both sides of Portland Bill, tending towards a symmetrical distribution.

The sedimentary facies distribution is combined with sand transport rates and maximum bed shear stress distribution, to suggest a conceptual model for sand dispersal and deposit formation around headlands. Sand dispersal can be explained in terms of a headland-associated eddy/bedload convergent zone concept. Maximum bed shear stress is observed at the tip of the headland and is associated with bedrock exposed on the seabed. The sequence of sedimentary deposits, away from the headland, is: sandbanks (Shambles and Portland Banks); sand/gravel flats; sand shoals (Adamant and West Shoals); and rippled sand sheets.

The banks lie in an area of very high bed shear stress ($u_* = 0.08$ m s^{-1}); this is greater than that for other tidal sandbanks, not associated with headlands. Bank formation is the result of the strong convergent (transport) component, enhanced by the development of transient headland-eddies. The sandbanks are to some extent also morphologically-controlled, i.e. the Portland Bank is affected by the deep bathymetry, to the west side of Portland Bill.

The principal characteristic of headland-associated eddy/bedload convergent zones is the development of bed shear stress convergent zones, on both sides of the headland. Two conceptually-distinct regions of sedimentary processes, associated with the coastal headlands, are recognised: (a) an inner zone, with increasing gradients in sand transport and bed shear stress towards the headland; and (b) an outer zone, in which sand transport is away from the headland, associated with a decrease in the bed shear stress. These zones merge into a bed shear stress (sand bedload transport) convergent zone, which enhances the formation of sandbanks around headlands.

Thus, headland-associated sedimentary deposits are a complex system, compared with the occurrence of isolated sandbanks described elsewhere. The identification of a sequence of deposits related to and extending much farther from the headland than previously supposed, demonstrates that the "tidal stirring concept" of headland-associated sandbanks may explain the formation of headland-associated sandbanks; however, it ignores the presence of a suite of sedimentary deposits around such headlands. The conceptual model proposed here provides a sedimentological perspective on the formation and occurrence of headland-associated deposits, including sandbanks.

Reference: *Bastos, A.C., Kenyon. N.H. and Collins, M.B., 2002. Sedimentary processes, bedforms and facies, associated with a coastal headland: Portland Bill, southern UK. Marine Geology, 187 (3/4), 235-258. This paper was submitted in July 2001 and it was accepted in May 2002.Reviewers: Edward Anthony and Serge Berne.*

7.1 Introduction

The interaction between coastal headlands and oscillating rectilinear tidal currents results in the formation of tidal eddies. When a tidal flow passes a headland, a bottom frictional torque is induced by increased velocity near the headland; consequently, vorticity is produced. Subsequently, vorticity is advected away into the flow leaving the headland; this creates a tidal eddy system on the downstream side, during the respective flood and ebb phases of the tide (Pingree and Maddock, 1979; Zimmerman, 1981; Robinson, 1983; Geyer and Signell, 1990).

The understanding of tidal eddy dynamics is relevant to sediment dynamics, because of its influence on the transport of sediments and fluid dispersion. The formation of eddies has been investigated by several authors, using distinct techniques, including field observations, numerical modelling and remote sensing (e.g. Tee, 1976; Pingree, 1978; Robinson, 1981; Wolanski *et al.*, 1984, Pattiaratchi *et al.*, 1986; and Signell and Geyer, 1991).

The effects of headland-associated eddies on sedimentary processes (erosion, transport and deposition) around a coastal headland have been described elsewhere, in terms of the occurrence of sandbanks (Pingree, 1978; Pingree and Maddock, 1979; Ferentinos and Collins, 1980; Dyer and Huntley, 1999 and Signell and Harris, 2000). However, sedimentologists have overlooked the study of these type of sandbanks, whilst the concepts regarding headland-associated sandbank formation are considered under a physical oceanographic perspective. In relation to sandbank formation associated with headlands, the most widely known and accepted theory is the "tidal-stirring concept", as suggested by Pingree (1978). On the basis of the output from a depth-averaged hydrodynamic model applied to the inner (continental) shelf around Portland Bill, Pingree (1978) showed that the Shambles Bank is associated with the centre of an anticlockwise residual eddy, located on the eastern side of the headland (Fig. 7.1). Despite the formation of an equivalent (clockwise) residual eddy on the western side, a somewhat smaller sandbank (Portland Bank) is observed. The presence of asymmetric or symmetric sandbanks around headlands was explained (Pingree, 1978), as a function of the balance between the Coriolis effect (related to the Earth's rotation) and inertial and pressure gradient forces. However, the spatial and temporal gradients in the bed shear stress could produce changes in the distribution of the sedimentary facies. Thus, the transient characteristics of such headland-associated eddies (Signell and Geyer, 1991; Davies *et al.*,

1995) might lead, it could be hypothesised, to the development of a suite of bedforms and sedimentary facies, instead of only isolated sandbanks. Further, a morphodynamic model has been used recently (Signell and Harris, 2000) to demonstrate that the processes responsible for the formation and maintenance of headland-associated sandbanks are due more to instantaneous patterns of shear stress and sediment flux, throughout the tidal cycle, than to tidal residual circulation.

Conceptual models, relating sedimentary facies and bedform distribution to changes in tidal current strength, have been described previously for flow transverse and flow-parallel features (Belderson *et al.*, 1982; Johnson *et al.*, 1982; Harris *et al.*, 1995). Similarly, the concept of bedload-parting zones (Stride, 1963; Belderson and Stride, 1966; Kenyon and Stride, 1970) refers commonly to an eroded basal bed, associated with maximum current speeds from where sediment is winnowed downstream. A depositional sequence of bedforms is generated, following a decrease in the bed shear stress. From such a zone, sand ribbons and scattered dunes are observed, grading into a sandwave field or linear sandbanks (depending upon the availability of sediment) and, finally, to muddy sand sheet deposits. However, bedload partings can be recognised also where erosion is not occurring and currents are not at a maximum; for example, in the very sandy area of the Southern Bight of the North Sea (Johnson *et al.*, 1982).

The significance of bedload-parting zones has been discussed elsewhere by Harris et al (1995). A model for the development of scour zones has been suggested, as a function of sediment supply and maximum bed shear stress. Scour zones are considered to be produced by advective and/or diffusive processes, in association with maximum bed shear stress; they are correlated always with the lag-gravel/bedrock members of a facies succession. Advection processes associated with the parting zones are related to asymmetries in the tidal wave; they do not necessarily correspond to a specific sedimentary facies. These investigators proposed a staged evolutionary model for scour zones: mutually evasive, incipient, partial, and complete. According to the analysis undertaken, a bedload-parting zone is a specific case of a scour zone, i.e. complete. In such a system the distribution of maximum bed shear stress coincides with divergent sediment transport pathways.

In terms of bedforms and their significance in indicating net sand transport over the continental shelf, Belderson *et al.* (1982) developed a model to predict the evolution of a

suite of bedforms, reflecting a decrease in current strength (for high, medium and low levels of sand supply). A generalised model, independent of sediment supply, shows the following sequence, as the current speed decreases along a longitudinal gradient: furrows and gravel waves → sand ribbons → large sand waves → small sand waves → rippled sand sheet and sand patches. In the high sand supply model the development of sandbanks is likely to replace the sand ribbon zone of the medium (sand) supply model.

Hitherto, headland-associated sandbanks have been considered from a hydrodynamic perspective (Pingree, 1978; Ferentinos and Collins, 1980) or, more recently, using morphodynamic modelling (Signell and Harris, 2000). In the present study, sedimentary processes and deposits associated with a coastal headland (Isle of Portland, southern U.K.; Fig. 7.1) are reviewed. New findings on headland-associated deposits are presented on the basis of recently collected morphological, sedimentological and geophysical field datasets. A discussion about these deposits is guided not only with a hydrodynamic or sediment transport perspective, but considering also their distribution, morphological and sedimentological characteristics and associated bedforms. This investigation derives a conceptual model for processes controlling the occurrence of a sequence of deposits and sedimentary facies, associated with coastal headlands. Likewise, the presence of sandbanks is discussed within the geological/sedimentological context of headland-associated sedimentary facies distribution and sand transport pathways.

7.2 Area under Investigation

7.2.1 Hydrodynamics

The Dorset inner continental shelf (< 60m) is subject to the semi-diurnal, west to east, passage of the tidal wave in the English Channel. The amplitude of the tidal wave decreases eastwards, from about 4m on mean spring tides at Lyme Regis, to about 2 m at Lulworth (Fig. 7.1). From Lyme Regis to Lulworth, the passage of the tidal wave takes about 30 min., i.e. the high water difference. The tidal amplitude is reduced significantly to the east of Portland, where the tidal wave becomes asymmetric about mean sea level. Slack water occurs about 2 hours before and 4 hours after high/low water, respectively; the strongest currents flow with a consistent direction over 2-3 hours (Maddock and Pingree, 1978).

In general, over the region, the tidal currents tend to increase offshore and towards Portland Bill. Spring peak near-surface tidal current speeds range from 0.4 m s^{-1}, up to 3.60 m s^{-1} in the vicinity of Portland. Throughout a tidal cycle, the development of tidal eddies is observed, on both sides of Portland Bill (Maddock and Pingree, 1978).

The prevailing winds over the region are from west and southwest with wind speeds of around 3.5 m s^{-1} exceeded over 75 % of the time (based upon 17 years (1974 to 1992) of data collected from a station at Portland Bill). The strongest winds are from the southwest and can reach up to 17 m s^{-1} (with 0.1 % of the year exceedance). Only limited information is available for wind-driven currents for the area under investigation; however, Pingree (1978) attempted to investigate the effects of weather conditions on the formation of residual eddies around Portland Bill. According to this author, wind stress acting on the sea surface affects the formation of the eddies only if the wind speed is > 10 m s^{-1}. Under gale force conditions (with wind speed > 20 m s^{-1}, originating from west-southwest), the wind effect eliminates the residual eddy formation on the western side of Portland Bill.

In terms of wave activity, Lyme Bay occupies one of the most exposed areas along the southern English coastline. The dominant wave approach is from the southwest, which coincides with the maximum fetch extending into the northeastern Atlantic (Bray, 1997). Hardcastle and King (1972) have described maximum wave heights as reaching 9m, during very severe storms. Extreme wave heights could reach 6 to 7 m, according to the predictive

wave model run by HR Wallingford (1998). However, Draper (1991) has shown that the significant wave height exceeds 2.0 m over this area, for only 10% of the year.

Wave data acquired in Lyme Bay (between July/1992 and May/1994) and close to the Shambles Bank (Draper, 1977), can be used to represent the regional wave climate. Analysis of data from a directional waverider buoy, located in the centre of Lyme Bay (LB, Fig. 7.1), reveals a significant wave height (Hs) of 0.8 m and a zero-crossing wave period (Tz) of 7 s. Waves approaching from the southwest (225° N) are predominant over 65% of the time, whilst SE waves occur some 15% of the time. To the east of Portland Bill, data are available from a wave recorder on the Shambles Light Vessel (SL, Fig. 7.1), acquired in 1968. Analysis of this data set (Draper, 1977) showed a Hs of 0.7 m and Tz of 6 s.

7.2.2 Geological/Geomorphological Setting

During the Quaternary, the English Channel experienced a succession of transgressions and regressions in response to climate and sea-level fluctuations, developing a submarine erosive surface (Hamblin et al, 1992). The post-glacial sea-level rise produced a thin and discontinuous veneer of gravel/gravelly sand (lag) deposits overlying bedrock and channel-fill sediments. These lag deposits are overlain, locally, by mobile sands forming sandwaves, sand ribbons, rippled sand patches and sandbanks.

The inner shelf adjacent to the Dorset coast, between Lyme Regis and St. Alban's Head, can be described in terms of two embayments Lyme Bay and Purbeck Bay, separated by the Isle of Portland (Fig. 7.1). The seabed morphology here is characterised by sandbanks and shoals, lag deposits and positive and negative "relief features" formed by bedrock outcrops (Fig. 7.2). The morphology is a result of: the different resistance of the seafloor rocks; interaction between tidal currents (and waves) and the influence of the headland (Isle of Portland); and post-glacial transgression. Two regional morphological compartments can be established throughout the study area, in terms of water depth: (a) Purbeck Bay, where the average water depth is 25 m and low bathymetric gradients are observed near the coast; and (b) Lyme Bay, where the average water depth is 35 m and steep gradients occur offshore of Chesil Beach (Figs. 7.1 and 7.2).

In terms of sediment distribution, the seabed consists, predominantly, of a discontinuous veneer of coarse lag deposits and bedrock outcrops, associated with patches of mobile sands. A few areas of sand accumulation can be recognised over the inner shelf, such as the

Shambles and Portland Banks and the Adamant and West Shoals (Figure 2). Apart from these areas, the sand thickness over the area is less than 0.5 m (BGS, 1983). The associated sediment facies distribution is shown in Figure 7.3.

The solid geology along the inner shelf comprises Upper Jurassic sequences (Donovan and Stride, 1961[a]), represented by: Corallian Beds (sandstones and limestones); Kimmeridge Clay (shales with thin layers of limestone); Portland Beds (sandstones and limestones); and Purbeck Beds (limestones). Middle and Lower Jurassic sequences lie to the west of Lyme Bay.

Due to the occurrence of distinctive rock types (Donovan and Stride, 1961[a]), differential erosion of the seafloor plays a very important role in controlling the Dorset shelf morphology. Seafloor erosion is a function of the relative intensity of the shear stress exerted by a water flow (with sand acting as an abrasive (Donovan and Stride, 1961[b]) and the lithologically-related resisting force (Sunamura, 1993). Thus, because of the distinct erodibility characteristics of the sandstones, limestones and shales, together with the prevailing structural patterns (folds and faults), positive or negative "relief features" are formed; these can be recognised in the bathymetric contours (e.g. the Shambles Ledge and Lulworth Banks) (Fig. 7.2).

Immediately to the west-southwest of Portland Bill, a linear deep lies almost parallel to the shore, and reaches about 100 m in depth at its southern end (Fig. 7.2). This linear deep follows the lithological contact between sandstones (Portland Sands Formation) and shales (Kimmeridge Clay Formation). Outcrops along the northwestern coast of the Isle of Portland show that this lithological contact is responsible for a series of landslides. Therefore, it is considered that the deep is an evolutionary geomorphological feature, resulting from differential erosion of the seabed.

The distribution of sand is restricted, basically, to the region of the shoals and the banks. Exceptions are the inner parts of Weymouth Bay, which are covered by a fine-grained sand sheet; likewise, the central areas of Lyme Bay, where a thin fine sand sheet occurs. Nearshore sand deposits are also observed off Chesil Beach, which consists of pebbles (Carr and Blackley, 1974).

7.3 Methods

7.3.1 Hydrodynamics

The tidal current data used in the present study were derived from an existing hydrodynamic model, covering the area between the Isle of Wight and Lyme Bay (TELEMAC-2D, developed originally by Laboratoire National d'Hydraulique, Electricite de France and distributed and applied by HR Wallingford). TELEMAC-2D is a depth-averaged, finite element model, formulated on shallow-water equations that describe the conservation of water mass and momentum (Hervouet, 1991).

Output files for spring and neap tides were provided, to the authors, by HR Wallingford. Results are referred to the tidal signature only, with no consideration given to wind-driven currents. Post-processing and interpretation were performed through the RUBENS package (provided also by HR Wallingford). RUBENS is an Unix-based software that allows end-users to read a file (model run) created by TELEMAC model, then export it as an ASCII file for other applications. Post-processing work involving the calculations of vorticity and residual, maximum and mean currents was undertaken using RUBENS. Tidal flows are described here for a tidal cycle during spring tides.

Time-series of wave data, including Hs, Tz and wave direction (only for LB, Fig. 7.1), were provided by the British Oceanographic Data Centre (BODC); these were used to characterise the wave pattern over the area. A significant wave condition (the most common occurrence in a scatter diagram of significant wave height and zero-crossing period), defined as Hs=0.8m and Tz=4.5 s, is used to calculate the bed shear stress under the combined action of current and waves. The distribution of wave height over the area was simulated by applying a wave refraction model (RCPWAVE, U.S. Army Corps of Engineers; Ebersole *et al.*, 1986); this utilised the significant wave condition described above, together with the most predominant direction of approach (225°N). RCPWAVE is a short-wave numerical model, used to predict linear plane wave propagation over an open coast region of arbitrary bathymetry.

7.3.2 Seabed Morphology

The seabed morphology was investigated, based upon regional bathymetric charts (Fig. 7.1). The inner continental shelf around the headland was then analysed in more detail (Fig. 7.2). The bathymetry of the study area was mapped by digitising recent Fair Sheets provided by the U.K. Hydrographic Office (Taunton). A (50x50m) grid was generated from the digitised data, resulting in a detailed and contoured bathymetric chart.

Seabed sediment and bedform distribution were characterised, initially, on the basis of an extensive compilation of unpublished data sets (Kenyon (1994), for the east of Portland Bill; Nunny (1995), for the west of Portland Bill); this generated a seabed sediment distribution map for the inner shelf (Fig. 7.3). This pattern was validated then on the basis of fieldwork, consisting of side-scan sonar (surveying a total of 100 km of track) and sediment sampling (with a total of 80 seabed samples) (Fig. 7.4). The survey was undertaken during June and August 2000, from the fishing vessel *Miss Pattie*, using a DGPS Trimble system for positioning (to ± 2 m). The side-scan sonar used was a Widescan system (100 kHz); the data were acquired in analogue and digital formats. Grab samples of the seabed were collected using a Day grab.

The survey was designed overall to provide detailed coverage of the sand deposits, in terms of sediment and bedform distribution. Sediment samples were analysed through the use of sieving and settling tower techniques, to obtain sieve diameters and settling velocities, respectively. To avoid particle shape effects, settling velocity was used here to characterise the deposits. Bedforms were described using the classification proposed by Ashley *et al.* (1990); however, the term sandwave was considered more applicable here, instead of subaqueous dune.

7.3.3 Sediment Dynamics

Inner shelf sediment transport pathways have been investigated, based upon the interpretation of bedform asymmetry, sediment distribution and numerical simulation.

A numerical model, developed by the Geological Survey of Canada, SEDTRANS92 (Li and Amos, 1995), was used for the calculation of: (a) bed shear stress (shear velocity, u_*) under currents alone; (b) bed shear stress under the combined action of currents and waves (for the significant wave condition, see above); and (c) potential medium-grained sand (D_{50} = 0.5

mm) transport rates, in response to currents alone. Near-bed currents (1m above the seabed) were calculated, by assuming a logarithmic velocity profile law. A quadratic friction law was applied to calculate the bed shear stress under currents alone, using the friction factor f_c=0.006, based upon the field experiments of Sternberg (1972). For the calculation of the shear stress under combined flows, the friction factor was calculated using the near-bed combined-flow boundary layer model developed by Grant and Madsen (1979). Bed roughness (z_0) was assumed to be uniform over the area (z_0 = 0.6 cm; Soulsby, 1983). Potential bedload transport rates were predicted/calculated for medium-grained sands (0.5 mm), using the algorithm proposed by Gadd *et al.* (1978), for currents alone. This particular algorithm was selected for use in the present study, based upon the results obtained by Grochowski *et al.* (1993). These investigators found that the algorithm proposed by Gadd *et al.* (1978) provided the best results, in terms of predicting sand transport rates for the English Channel, when compared to radioactive tracer dispersion experiments undertaken along the French coastline (Dewez *et al.*, 1989).

7.4 Results

7.4.1 Shelf Morphology and Sediment Distribution

The presence of sand shoals and sandbanks, providing a symmetrical arrangement of sedimentary deposits around the headland, can be recognised; this is based upon the interpretation of seabed morphology. Further investigation has shown that these deposits are associated also with the sand distribution patterns (Fig. 7.5). The symmetrical deposits are described below, in relation to their position with respect to the headland: (a) sand shoals (the Adamant and West Shoals); (b) sand/gravel flat deposits (intermediate area); and (c) coarse-grained sandbanks (Shambles Bank and Portland Bank) (Fig. 7.2). In general, the edges of these deposits are defined sharply, by morphological changes, rock outcrops and areas consisting of patches of bedforms overlying hardground.

The sedimentological character of the deposits was determined, in terms of their mean sieve diameter (Ds) and mean (sand) settling velocity (w_s) (Table 7.1).

Sand shoals are observed on both sides of the headland: the Adamant Shoal, to the east; and the West Shoal, to the west (Figs. 2 and 5). These shoals are aligned parallel to the coastline, in a concave-southward arcuate form and with their steeper sides towards the coast; in general, they are 5 to 7 m thick, reaching 10m beneath the larger bedforms.

The shoals are similar in terms of their relationship to the regional sand transport pathways; they are formed, essentially, by fields of asymmetric transverse bedforms, usually medium sandwaves (Ashley *et al.*, 1990). In both of the areas, large asymmetric sandwaves (wavelength ~100 m) are present, whilst small and medium sandwaves can be observed on the stoss sides of the larger bedforms (Fig. 7.6).

Despite their morphological similarity, the shoals are contrasting in terms of their associated water depth and sediment grain size. As discussed previously, the shelf to the east of Portland is shallower; this results in the Adamant Shoal lying about 5 m shallower than the West Shoal. In terms of (sand) grain size, the sediments of the West Shoal are finer than those of the Adamant Shoal; this pattern is followed by the settling velocity characteristics

(Table 7.1) For the West Shoal, a clear westward-fining trend is observed; this contrasts with the Adamant Shoal eastward-coarsening tendency. Such patterns reveal that both shoals are associated with a grading in their sand size distribution.

Table 7.1. Grain parameters (D_{50}, w_s), shear stress and sand transport associated with the different sedimentary deposits. Shear stress was calculated using the sediment transport model - SEDTRANS92 (Note: tidal currents used in the calculations were abstracted from the hydrodynamic model, TELEMAC-2D (see text)).

Sand Deposits*	**Water Depth (m)**	**D_{50} (mm)**	**Settling Velocity (w_s cm s^{-1})**	**Mean Velocity (m s^{-1})**		**Maximum Shear Velocity (m s^{-1})**		**Maximum Shear Velocity Direction (°N)**	
				CUR	C+W	CUR	C+W	CUR	C+W
Adamant Shoal	25	0.5	6 - 8	0.02-0.025	0.035-0.04	0.03-0.04	0.05-0.06	233	228
East Flat	30	2 - 10	4 – 6	0.02-0.03	0.035-0.04	0.03-0.06	0.05-0.08	240	230
Shambles Bank	15 - 10	0.8- 1.4	8 – 10	0.04-0.05	0.06-0.09	0.06-0.08	0.08-0.12	59-231	50-225
Portland Shoal	27	0.8 –1.4	8 – 10	0.035-0.045	0.04-0.05	0.06-0.08	0.05-0.09	310-140	305-130
West Flat	30	2 - 4	4 – 8	0.025-0.035	0.03-0.04	0.04-0.07	0.04-0.07	135	125
West Shoal	27	0.18 – 0.5	2 - 6	0.02-0.025	0.025-0.03	0.03-0.04	0.03-0.05	123	115

*for location, see Figure 7.2

Note:

CUR = currents alone

C+W = current + waves (significant wave conditions (see text))

As part of the symmetrical deposits, intermediate areas lie between the shoals and the banks. These areas are classified as sand/gravel flat deposits and can be observed clearly on the bathymetric map (Fig. 7.2); they are characterised by a thin and discontinuous sand veneer, associated with a bioclastic/lithoclastic gravel bed. As a consequence, the sediments are poorly-sorted and the mean grain sizes lie within the (fine) gravel size range (usually, the seabed samples consist of < 50% of sand). These deposits form a flat, homogeneous seabed,

depleted of transverse bedforms (Fig. 7.7). The eastern deposit appears to be coarser than that on the western side of the headland; this is similar to the pattern of the sand shoals.

Although the sand shoals and sand/gravel deposits are similar in their morphology, the sandbanks differ in other ways. The Shambles Bank, to the east of Portland, is an elliptically-shaped bank, asymmetrical (steep) towards the coast, about 20 m in height and 5 km in length (Fig. 7.2). The bank lies in an area of very strong tidal currents (peak currents, at 1 m above the seabed, of 1.4 m s^{-1}); these are stronger than is usual for tidal sandbanks located elsewhere and not associated with headlands, as for example, the Norfolk Banks (0.9 m s^{-1}; Collins *et al.*, 1995) and the Middelkerke Bank (0.75 m s^{-1}; Lanckneus *et al.*, 1994), in the Southern North Sea. The upper layer (30 cm) of the Shambles Bank consists of well-sorted coarse bioclastic sands, with settling velocities ranging from 8 to 10 cm s^{-1}. The bank morphology appears to consist of a complex suite of transverse bedforms, including very large sandwaves (Fig. 7.8). Overall, large and very large asymmetric sandwaves show a convergent sand transport pattern, towards the crest of the bank. Small and medium sandwaves are observed on the stoss side of the large sandwaves, but do not necessarily follow the same inferred direction of movement. The complexity of the bank morphology is associated with the shape and direction of the crests, combined with the occurrence of very large sandwaves, with straight linear crests lying orthogonal to the bank main axis (along its northeastern part).

The Portland Bank, to the west of Portland Bill (Fig. 7.2) is an oval-shaped bank, about 2.5 km in length, 1 km in width and up to 12 m in height, above the surrounding seabed. The bank consists of well-sorted coarse bioclastic sand, with settling velocities ranging from 8 to 10 cm s^{-1}. The crest of the bank is characterised by large asymmetric sandwaves, with associated small and medium sandwaves (Fig. 7.9). A bedform-convergent pattern was not observed clearly along the bank crest, however large ebb-dominated sandwaves were present along the southwestern flank of the bank.

The eastern and southern edges of the Portland Bank are bounded by deeps. The sediment distribution pattern reveals that these deep areas are covered by coarse bioclastic sands. The side-scan sonar data has revealed the occurrence of transverse bedforms, within these deeper water regions.

7.4.2 Sediment Dynamics

Sediment transport pathways over the inner part of the continental shelf are inferred, initially, on the basis of sedimentological and geomorphological evidence. Sand transport pathways towards the headland are indicated by the restricted distribution of sands, forming the sand shoals and sandbanks. Bedform asymmetry corroborates the regionally-convergent pattern, towards the headland (Fig. 7.5).

Net sand transport can be inferred also by the direction of the peak currents (Johnson *et al.*1982). Peak current directions and speeds were abstracted from a hydrodynamic numerical model (TELEMAC). Regionally, a westward (ebb-dominated) transport can be inferred; this coincides with the sand transport model for the English Channel, as proposed by the bedform/sediment distribution (Stride *et al.*, 1982) and numerical model predictions (Grochowski *et al.*, 1993). The influence of the coastal headland on the current is characterised by a significant increase in the speed, towards the tip of the headland; likewise, by enhanced convergent currents, on both sides of the headland. Peak current direction, bedform asymmetry and sand distribution patterns appear to be in reasonable agreement, as indicators of converging net sand transport towards the headland.

Sediment transport is related to the stress exerted on the seabed by the overlying flow. Thus, to predict sand transport pathways, a sediment transport model (SEDTRANS) was used to calculate the bed shear stress and potential sand transport, under tidal currents alone over the area. The bed shear stress is represented here as a function of shear velocity. The plot produced (Fig. 7.10) shows the maximum (bed) shear velocities for current activity.

A gradient in increasing shear velocities is observed, towards the tip of the headland. Following this gradient, the Adamant and West Shoals are located within the same shear velocity range (0.03 to 0.04 m s^{-1}), whilst the Shambles Bank and the Portland Bank are located within a higher (0.06 to 0.08 m s^{-1}) range. The linear deep on the western side of Portland Bill acts as a physical boundary, limiting the 0.08 m s^{-1} shear velocity contours (Fig. 7.10). Thus, the maximum shear velocities are not symmetrically concentrated around the tip of the headland; rather, they are shifted to the eastern side of the linear deep. This observation indicates that the seabed topography controls the local bed shear stress distribution.

Convergence in the direction of the shear velocities is observed on both sides of the headland. These zones of bed shear stress convergence cross, longitudinally, the northern edges of each

of the banks (Shambles and Portland Banks) and the intermediate areas; they end with a gentle turn, just to the south of the Adamant and West Shoals.

Shear velocities calculated for the combined flows (significant wave condition) show an increase in the bed shear stress over Purbeck Bay, in contrast to Lyme Bay. Enhanced shear velocities, in response to waves, were observed over both Purbeck and Lyme Bays. According to the wave refraction model applied, to simulate the propagation of waves over the area, basically no major differences in the wave transformation heights were observed over the inner continental shelf of the region. Exceptions to this generalised pattern are associated with Weymouth Bay (more sheltered) and the Shambles Bank (shallower area).

Although Lyme Bay appears to be more exposed to the Atlantic fetch, it is reasonable to assume that for waves approaching from the southwest (225°N was the direction used in this simulation, because it is the predominant direction) there is no major difference, in terms of wave exposure, between the Shambles Bank/Adamant Shoal area and the Portland Bank/West Shoal (Fig. 7.1). No attempt is made here to discuss the wave variations along the adjacent coastline.

The different responses in the enhanced combined shear velocities relies upon two important parameters: (a) water depth (with Purbeck Bay being shallower than Lyme Bay); and (b) the angle between the currents and the waves (with the higher angles, almost orthogonal, associated with Lyme Bay) (Grant and Madsen, 1979).

Despite the fact that a gradient in the shear velocity is observed towards the tip of the headland, the deposits (sandbanks and shoals) are not related to each other, in terms of the bed shear stress magnitude. For significant wave conditions no distinct changes were observed in the bed shear stress direction. Thus, areas of bed shear stress convergence are observed on both sides of the headland; this pattern is similar to that derived for currents alone.

On the basis of the bed shear stress, a sand transport algorithm has been applied to derived estimates of the potential sediment transport rates over the study area. The simulation of transport rates was undertaken for medium-grained sands (0.5mm). The results are shown in Figure 11, as maximum transport rates over a tidal cycle during spring tides.

There are two similar convergent zones, on both sides of the headland, as discussed for the shear velocities; these separate the inner and outer mobile-sand zones (Fig. 7.12). The zones themselves can be recognised as being associated with sand (bedload) transport, under currents alone and in response to combined flows.

The inner zone is characterised by sand transport towards the headland (i.e. southward), followed by an increasing gradient in transport rates and shear stress. This area is characterised, morphologically, by the Adamant and West Shoals; these are associated with very asymmetric transverse bedforms.

The outer zone is situated to the south of the tip of the Isle; it is defined by sand transport away from the headland, with a decrease in transport rates and bed shear stresses. The Shambles Bank and Portland Bank lie within this area of the inner continental shelf.

Although no (sand transport) simulation was undertaken to predict the patterns of sand movement under storm conditions, it has been identified elsewhere that storm waves can influence the sand transport process by increasing transport rates and altering (sometimes reversing) sand transport direction (Pattiaratchi and Collins, 1988; Green *et al.*, 1995; Williams and Rose, 2001). Moreover, storm waves can play an important role in controlling the evolution and migration of sedimentary deposits, especially sandbanks (Ferentinos and Collins, 1980; Houthuys *et al.*, 1994; Berne *et al.*, 1994; Tessier *et al.*, 1999). The dispersive and destructional influence of storm waves can sweep out small and medium (current-induced) sandwaves along a sandbank crestline and, at the same time, lower the height of the large sandwaves, i.e. controlling the sandbank height.

7.5 Discussion

An investigation, based upon seabed morphology and sedimentology, has revealed the presence of a sequence of sedimentary deposits distributed symmetrically around a coastal headland: sand shoals; sand/gravel flats; and coarse-grained sandbanks. This sequence of deposits is associated with a complex suite of bedforms, representing gradients in bed shear stress and sand transport rates.

The correlation between sand grain settling velocity and local maximum shear velocity (under currents) confirms that the deposits are related to changes in the bed shear stress. A significant correlation between these two parameters is shown in Figure 7.13. The sedimentological response of the deposits (expressed here as the (sand) grain settling velocity, i.e. independent of shape) follows the increase in shear velocity. The sandbanks, for example, consist of the coarsest sands present; they are associated also with the highest shear velocities of all the sedimentary deposits described around the headland. Nevertheless, different sedimentary facies can be recognised within the same representation, by limiting the regions of distinct sand transport/deposition (hydraulic) behaviour. The plot incorporates a lower limit, defining an area that has been interpreted as a critical maximum shear velocity, for sand grains to settle or be swept away.

It should be noted that the limited availability of samples from Region III (the sand/gravel flat area) in Figure 7.13 is, at least in part, related to the fact that the region is characterised by a sand veneer associated with an underlying gravel bed. Conversely, the wide range in the observed settling velocities is related to differences in the sand (bioclastic content) composition.

The facies sequence, in response to an increase in the prevailing current speed, can be described for the study area as: rippled sand sheet (Region I), sand shoals or sandwave fields (Region II – Adamant and West Shoals), sand/gravel flat bed (Region III – East and West Flat intermediate Areas), coarse-grained sandbanks (Region IV - Shambles and Portland Banks) and a non-depositional zone, or zone of maximum bottom stress (Fig. 7.14). The occurrence of a rippled sand sheet is related to a regional decrease in the bed shear stress, away from the headland. This pattern occurs on the western side of Portland Bill, where it is associated with a westward-fining trend in the sediment grain size. However, it is not characteristic of the

eastern side, where an increase in shear stress is observed; this is because of the presence of another small headland to the east (St. Alban's Head, see Fig. 7.1).

On the basis of the above summary, this particular facies sequence model represents the influence of the headland-associated hydrodynamic patterns, on a more general facies/bedform sequence developed over a tidally-dominated inner continental shelf. Attempts to establish a relationship between the sedimentary facies (or bedforms) and the bed shear stress (or current speed) distribution have been proposed elsewhere (Flemming, 1980; Belderson et al, 1982; Belderson, 1986; Vianna *et al.* 1991; and Harris *et al.*, 1995). The observed facies sequence around the headland can be explained in terms of a conceptual model, considering headland-associated eddy/bedload convergent zones. Such a model is related to bedload-parting or scour zones (Stride, 1963; Belderson and Stride, 1966, Kenyon and Stride, 1970; Harris *et al.* 1995), at a scale of the headland. The assumption of such a scale relies upon: (a) the coastal headland (coastal constriction (Johnson *et al.*, 1982)) inducing tidal flow acceleration towards the headland, enhancing a local region of maximum bed shear stress; and (b) the sedimentary facies being restricted to the area of the headland-associated hydrodynamic/sedimentary processes (the inner and outer zones (see, for example, Fig. 7.12)).

Associated with headlands, a scour zone is present at their tip, where a region of maximum bed shear stress and no deposition is observed. The sedimentary facies are distributed along axes, which follow the bed shear stress gradients. Two conceptually-distinct regions of sedimentary processes are recognised: (a) the inner zone, characterised by sand transport towards the headland and related morphologically to the sand shoals; and (b) the outer zone, characterised by sand transport away from the headland and associated morphologically to the sandbanks. However, as the bed shear stress distribution is constrained by the coastal geometry, the arrangement of the sedimentary facies will lie at an angle to the scour zone. Usually, this arrangement will follow the direction of the coastline, or the headland geometry (Fig. 7.14).

The principal characteristic of headland – associated eddy/bedload convergent zones is the development of bed shear stress convergent zones; these result in a sedimentary facies distribution (formation and evolution) representing down-current and up-current decreases in the bed shear stress. Shear stress convergent zones will be directed towards a (sand) bedload convergent zone, which enhances the formation of sandbanks. The occurrence of sandbanks

associated with very strong tidal currents is the result of the strong convergent component of sand transport, enhanced by the local formation of transient headland-associated eddies.

The formation of morphologically-asymmetric sandbanks around Portland Bill (the Shambles Bank and the Portland Bank) has been explained by Pingree (1978), as a function of the balance between planetary vorticity (the Coriolis effect) and the relative vorticity of the residual eddies. The effect of planetary vorticity, as a major cause for asymmetric sandbank formation around headlands, has been discussed elsewhere by Signell and Harris (2000); this is through the application of a three-dimensional morphodynamic model. These investigators identified that transient patterns in the shear stress and sediment flux play a more important role in the bank formation, than the tidally-induced residual circulation.

The results of the present investigation demonstrate that asymmetric banks do not occur in response to the effect of planetary vorticity alone. In this case, the sandbanks appear to be hydrodynamically/morphologically-controlled features. Notably, the Shambles Bank is located within a water depth of 25-30m over the Shambles Ledge (of low gradient, with an approximately flat seabed), which consists of limestones. On the western side of the bank, a deep erosive area, characterised by a linear deep with high gradients, characterises an area suitable hydrodynamically for the development of a sandbank. Thus, both sandbanks can be characterised as hydrodynamically/morphologically-controlled features. Moreover, the occurrence of such sandbanks should be considered within a regional geological/geomorphological context of the headland-associated sedimentary facies distribution.

Finally, a sequence of sedimentary deposits has been characterised here. These related to the headland and extend farther than previously supposed. The occurrence of this sequence can be explained in terms of a conceptual model, which considers the morphological and sedimentological characteristics of headland-associated deposits and the transient characteristics of the tidally-induced and variable bed shear stresses and sand transport rates (headland – associated eddy/bedload convergent zones); this is in contrast to the tidal residual circulation alone (tidal-stirring, Pingree, 1978). The results obtained indicate that the "tidal stirring" concept of headland sandbanks neglects the presence of a suite of sedimentary deposits, around headlands. This concept considers only sandbank formation within the centre of residual eddies, but does not incorporate sand transport processes in relation to the formation and evolution of sedimentary deposits. Rather, the concepts of sediment transport

processes (principally, as bedload) should be considered. Elsewhere, it has been established that sediment transport is a non-linear process (Pingree and Griffiths, 1979; Heathershaw, 1981; Johnson *et al.*, 1982); as such, residual (water) circulation or mean bed shear stress do not represent necessarily the net sediment transport direction. Moreover, residual flows can be an order of magnitude lower than the instantaneous flow patterns, whilst associated secondary flows represent only around 5-15% of the overall flow (Geyer, 1993). Such observations may be important in terms of (sediment) transport, if the magnitude of the flows do not reach the critical shear stress required for the initiation of sediment motion. Hence, processes responsible for the formation and maintenance of the sequence of sedimentary facies, as described previously, are associated with spatial and temporal changes in sand transport rates, over the tidal cycle.

7.6 Conclusion

Sedimentary processes and deposits associated with a coastal headland (Portland Bill, Southern UK) are presented, based upon: seabed morphology and sedimentology; bed shear stress distribution; and the simulation of sediment transport rates. The area under investigation is characterised by a discontinuous veneer of coarse lag deposits and bedrock outcrops; these are associated with patches of mobile sand and specific areas of sand accumulation (Shambles Bank, Portland Bank, Adamant and West Shoals).

The occurrence of headland-associated sandbanks, within a high energy and low sand-supply environment, is the result of the strong convergent component of sand transport around the coastal headland. However, for this specific area, the association of the seabed morphology with the solid geology is a further controlling parameter on sandbank formation and evolution, i.e. the Portland Bank is affected by the deep bathymetry, on the western side of Portland Bill.

The results obtained reveal a symmetric distribution of sedimentary deposits, on both sides of the headland. The deposits are associated with a sequence of sedimentary facies and bedforms, representing a gradient in the bed shear stresses and sand transport rates, towards the headland. A scour zone occurs near to the tip of the headland, where the maximum bed shear stress is observed and bedrock is exposed at the sea floor. Away from the zone of maximum shear stress, a sequence of sedimentary facies can be observed, sequentially, as: sandbanks; sand/gravel flat (coarse-grained flat bed); sand shoals (sandwave field); and rippled sand sheets.

The presence of these symmetric deposits, on both sides of the headland, can be explained in terms of a conceptual model ("headland-associated eddy/bedload convergent zones") for sand dispersal and deposit formation around headlands. This concept is based upon the development of bedload convergent zones separating two distinct regions of sedimentary processes: the inner (net sand transport towards the headland) and outer (net sand transport away from the headland) mobile-sand zones. The occurrence of these zones is related to the development of transient eddies, together with changing patterns in the shear stress and sediment transport rates, during the tidal cycle.

The identification of a sequence of deposits related to and extending much farther from the headland, than supposed previously, demonstrates that the "tidal stirring concept" may provide a satisfactory explanation for the formation of headland-associated sandbanks; however, it ignores the presence of an associated suite of sedimentary deposits. The proposed conceptual model incorporates new observations, regarding the morphology and sedimentology of headland-associated deposits with the prevailing hydrodynamics and sediment dynamics characteristics. Such a model provides a sedimentological perspective on the formation and occurrence of headland-associated deposits including sandbanks.

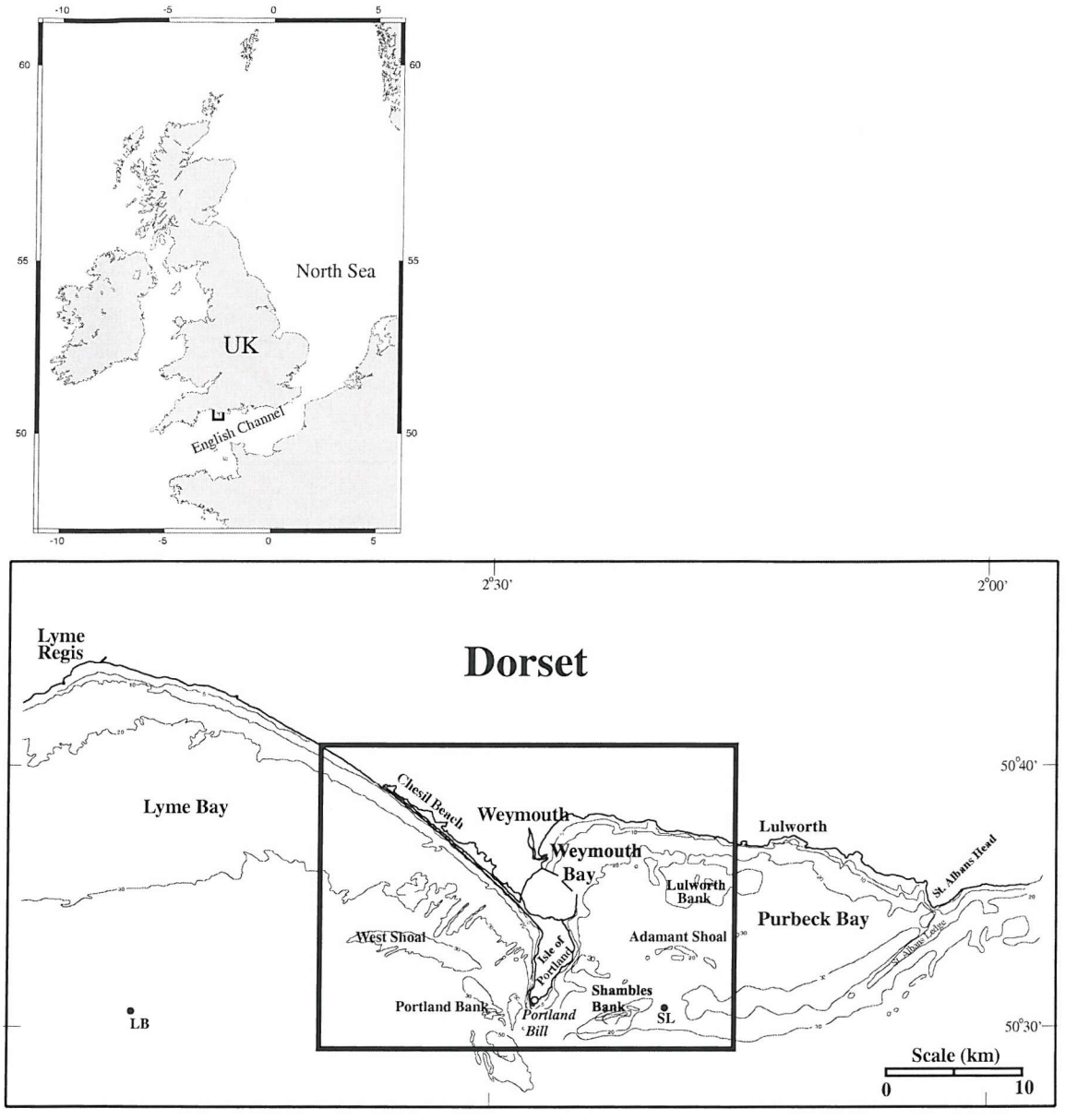

Figure 7.1. Regional setting of Portland Bill and the area under investigation. LB and SL refer to wave data stations (see text).

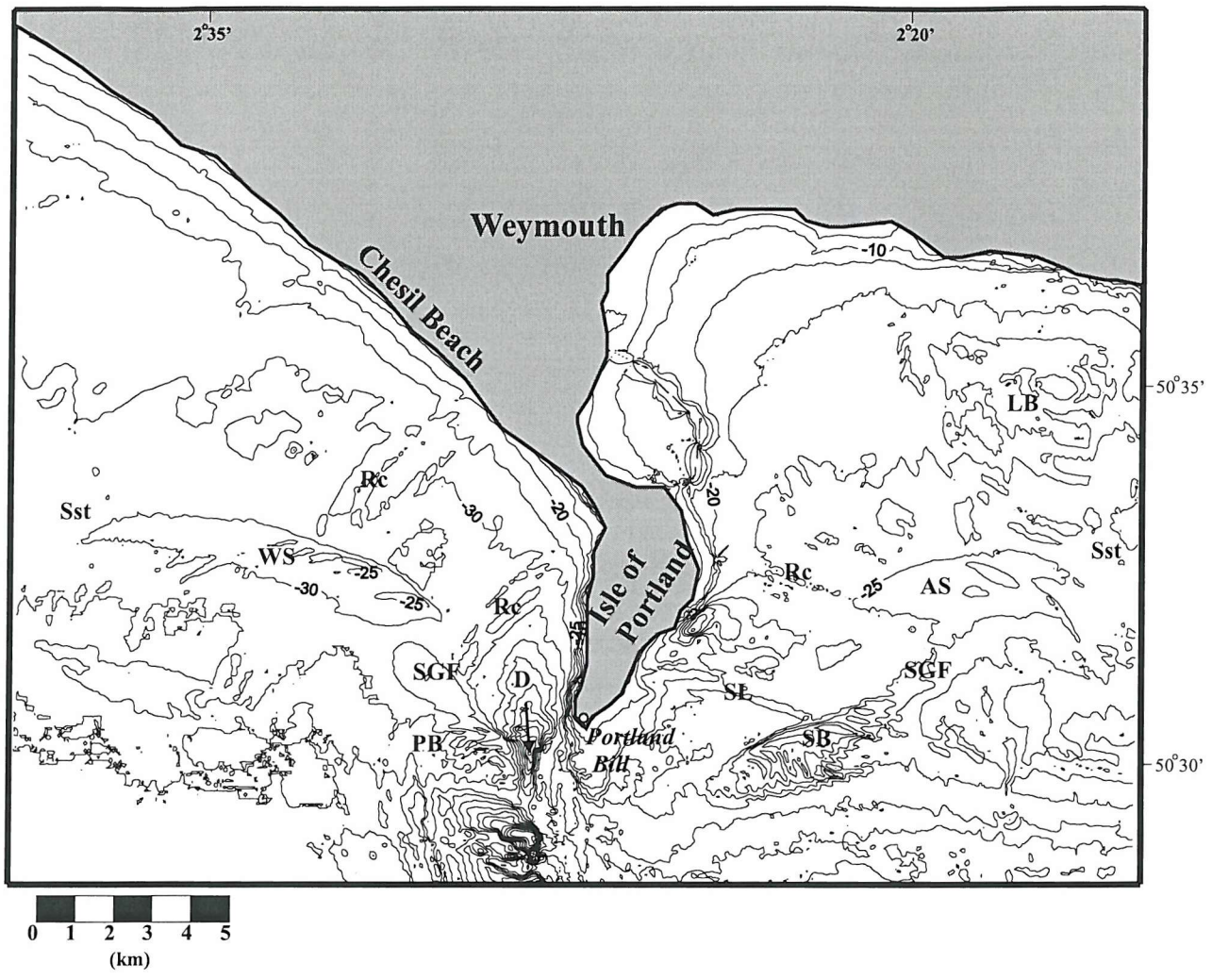

Figure 7.2. Detailed bathymetric map of the area under investigation, based upon UK Hydrographic Office Fair Sheets. Contour interval in metres and reduced to Chart Datum, which is approximately the level of Lowest Astronomical Tide. Key: SB-Shambles Bank; AS-Adamant Shoal; sGF-Sand/Gravel Flat; PB-Portland Bank; WS- West Shoal; Sst – Rippled sand sheet; LB- Lulworth Bank; SL- Shambles Ledge; Rc- Rock outcrop; D – Deep area.

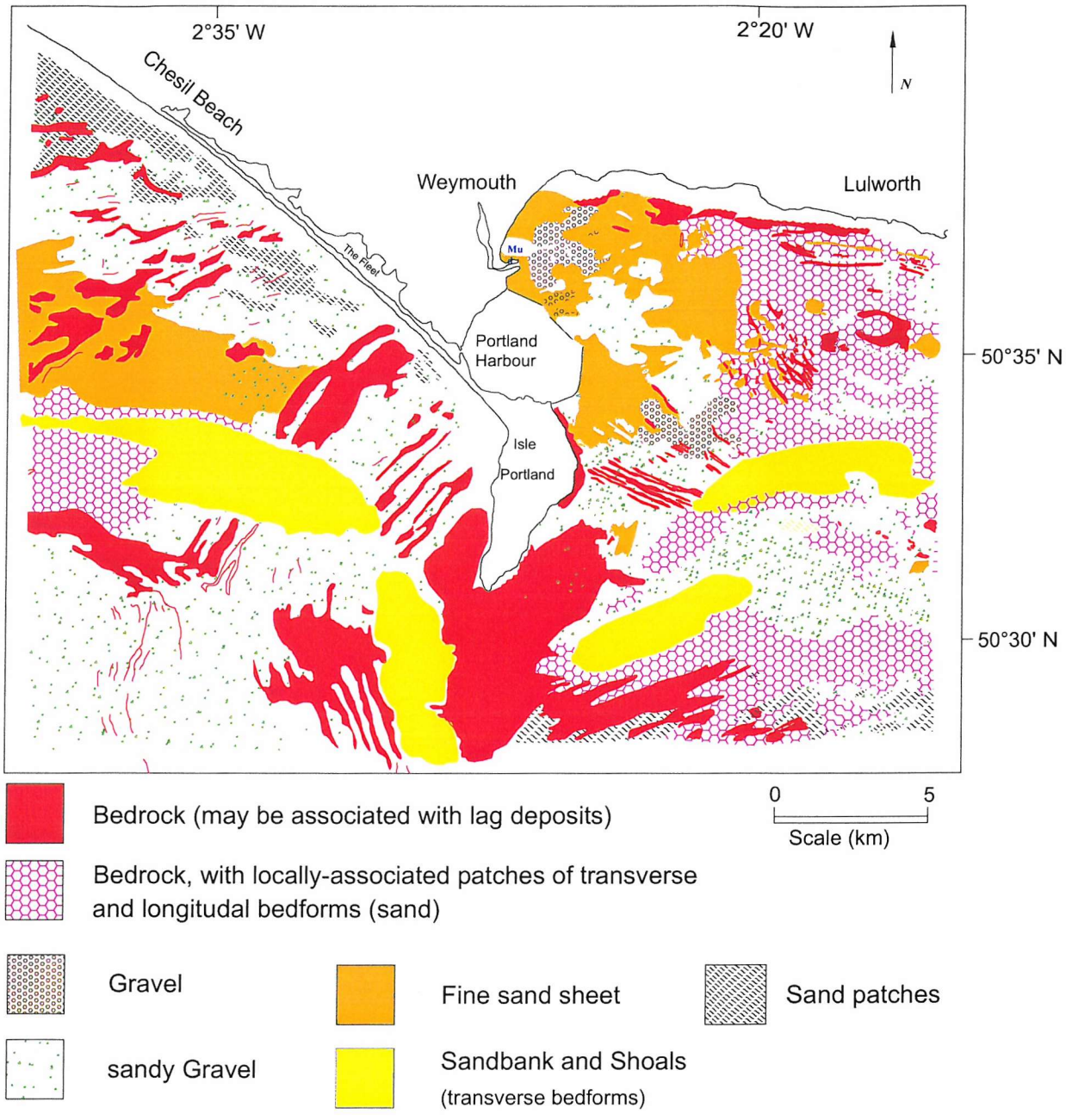

Figure 7.3. Seabed sediment distribution map, based upon sediment samples and side-scan sonar data derived from a compilation of acquired fieldwork and available datasets (Nunny, 1995 and Kenyon, 1994).

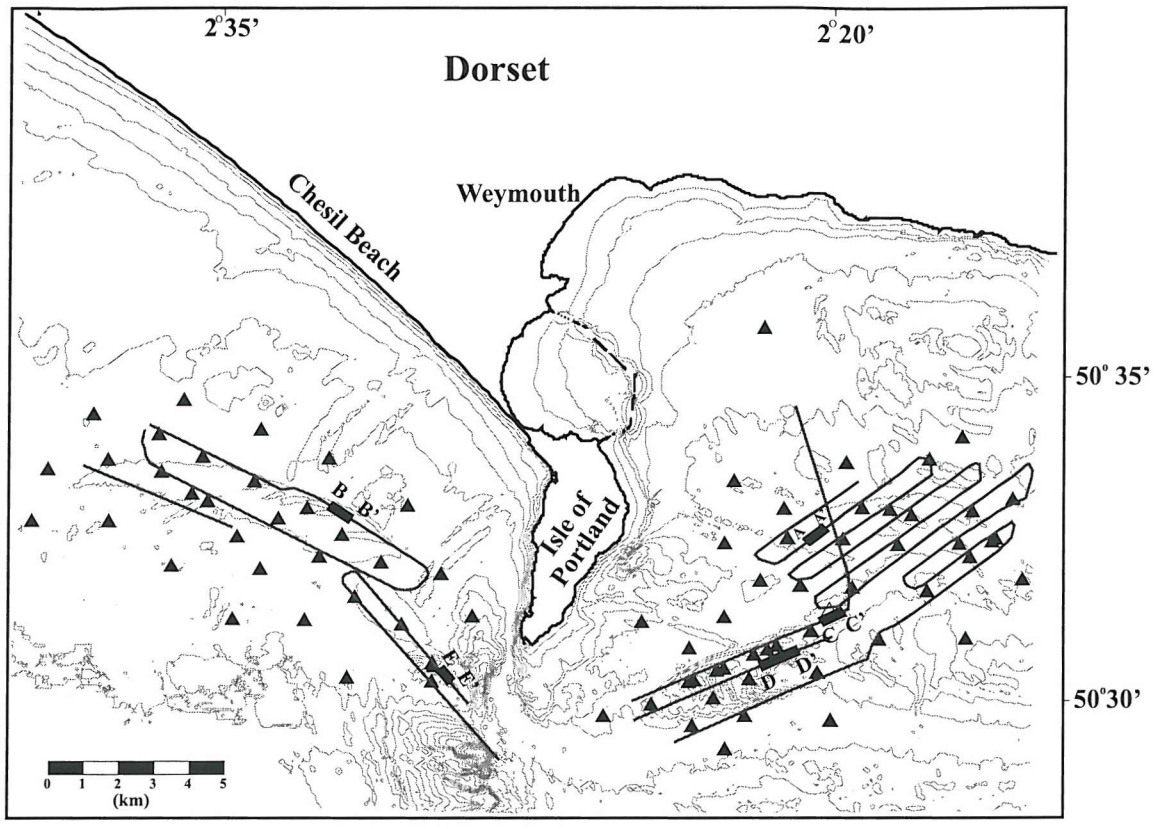

Figure 7.4. Location of seabed sediment samples collected (▲) and side-scan survey tracks (—). Location of the images presented in Figures 6, 7, 8 and 9 (A _ A') are also shown.

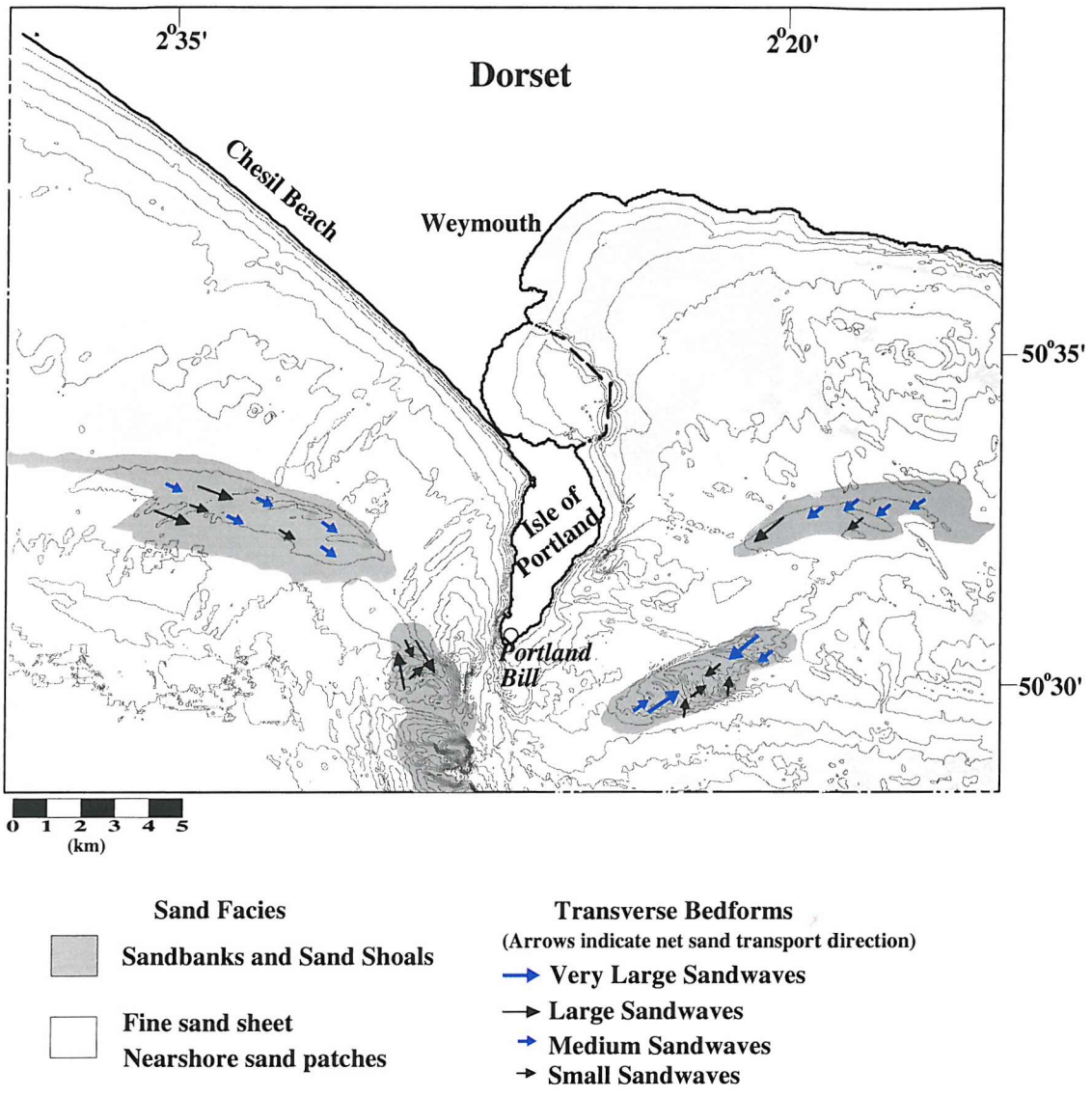

Figure 7.5. Sand distribution areas, in relation to seabed morphology: (a) Towards the headland, the distribution of sands is restricted to the shoal and bank areas; (b) arrows indicate the direction of transverse bedform asymmetry; (c) net sand transport is inferred by assuming the direction of the large and very large sandwaves (see below); and (d) sandwave classification is based upon their wavelength (L) and height (H), following Ashley et al. (1990), i.e. very large (L)100m, H>5m); large (L-10-100m, H-0.75-5m); medium (L-5-10m, H-0.4-0.75m); and small (L-0.6-5m, H-0.075-0.4m).

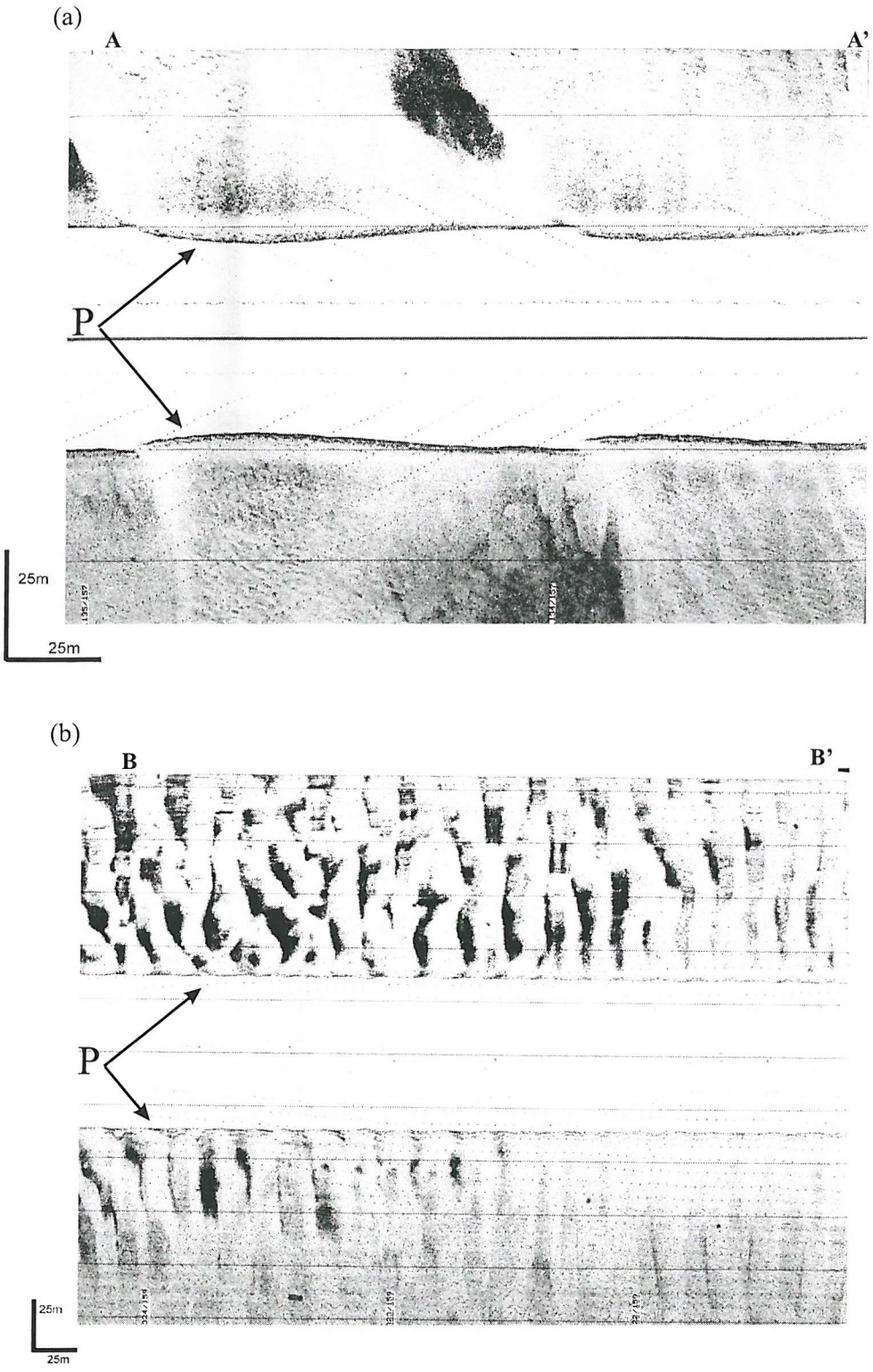

Figure 7.6. Side-scan sonar images of large and medium sandwaves, associated with the sand shoal deposits: (a) Adamant Shoal area, showing 2-D large sandwaves with medium and small sandwaves superimposed (D_{50}=0.55mm; w_s=7 cm s^{-1}); and (b) West Shoal area, showing medium sandwaves (D_{50} =0.26mm; w_s = 4 cm s^{-1}). High values of acoustic backscatter have darker tones in this, and subsequent side-scan images. P is the seabed profile, beneath the sonar fish. For image locations, refer to Figure 7.4.

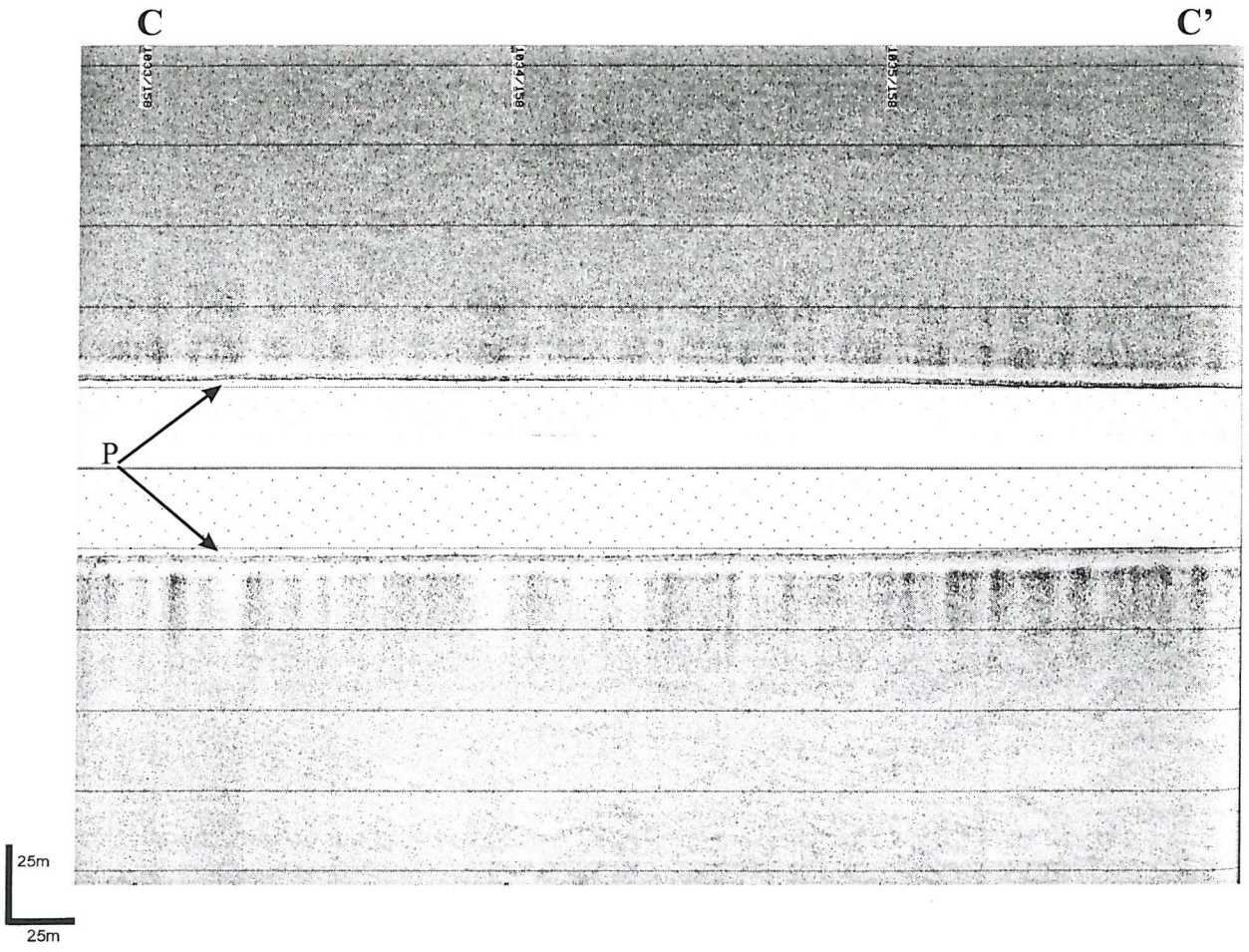

Figure 7.7. Side-scan sonar image of the East sand/gravel flat bed area, showing a flat and uniform seabed (D_{50}=4mm; 55% of gravel and 44% of sand and 1% of mud). For location refer to Figure 7.4.

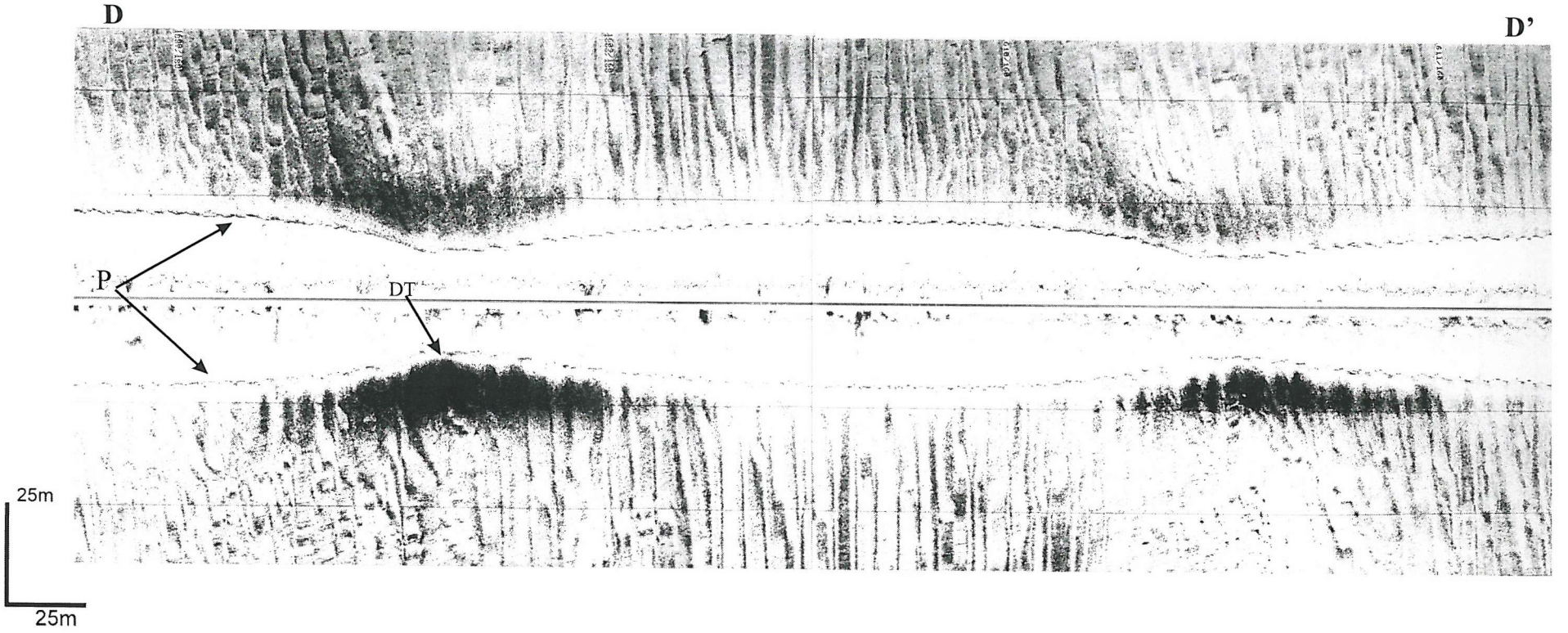

Figure 7.8. Side-scan sonar image, showing the complex pattern of bedforms associated with the Shambles Bank. Very large sandwaves associated with a complex pattern of 2-D and 3-D medium sandwaves (D_{50}= 0.9 mm, w_s= 8.5 cm s^{-1}). The dark tones (DT) in the near range are an artefact due to the sonar fish being close to the seabed. For location, refer to Figure 7.4.

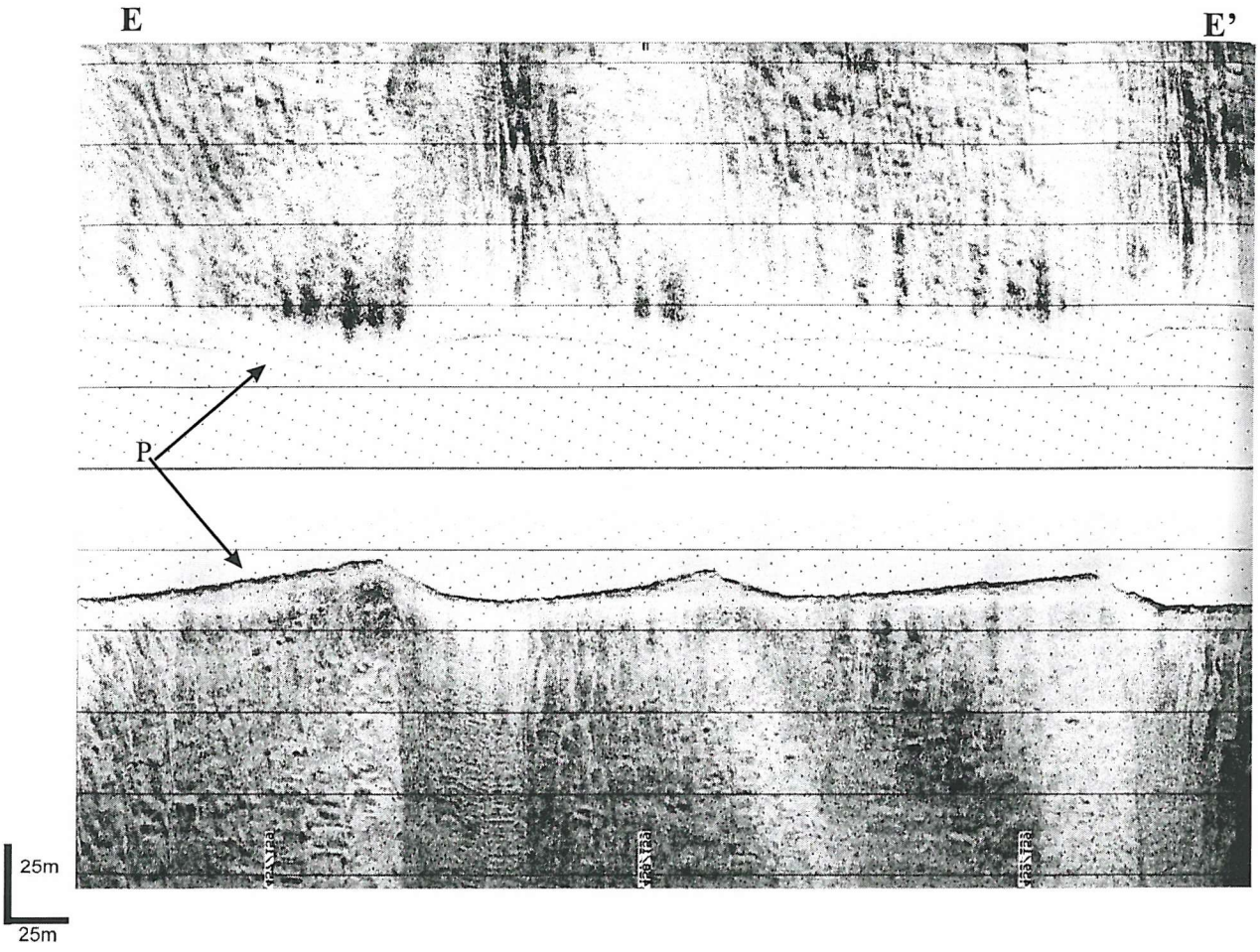

Figure 7.9. Side-scan sonar image of 2-D large sandwaves, on the top of the Portland Bank (D_{50}=0.91mm, w_s =8.25 cm s^{-1}). For location, refer to Figure 7.4.

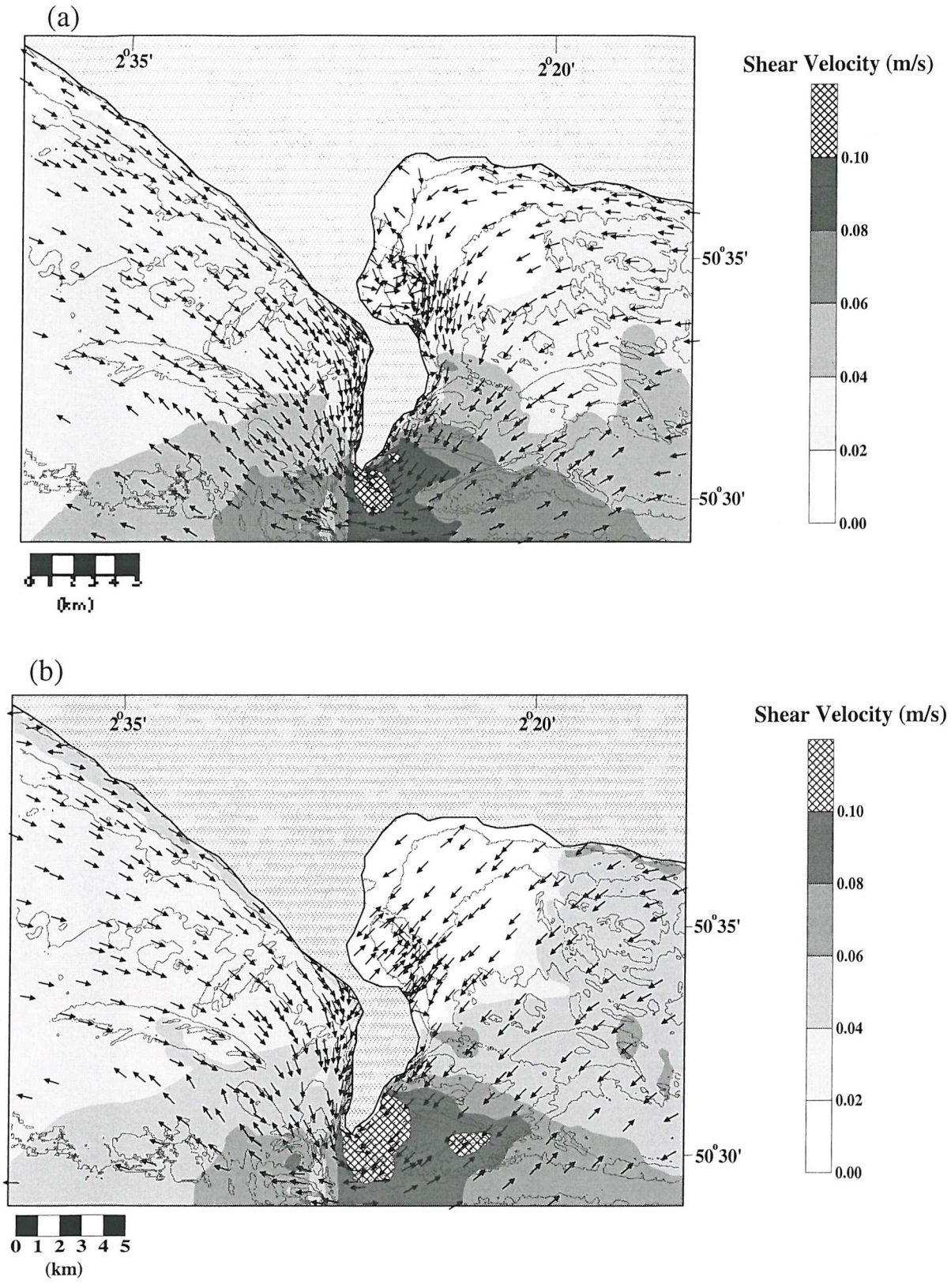

Figure 7.10. Maximum bed shear stress (direction (arrows) and magnitude (shading)) expressed as shear velocity calculated for: (a) currents alone; and (b) combined wave (significant wave condition, see text) and currents. Calculations were undertaken using SEDTRANS92 (Li and Amos, 1995). Note: arrows are not to scale, in terms of magnitude.

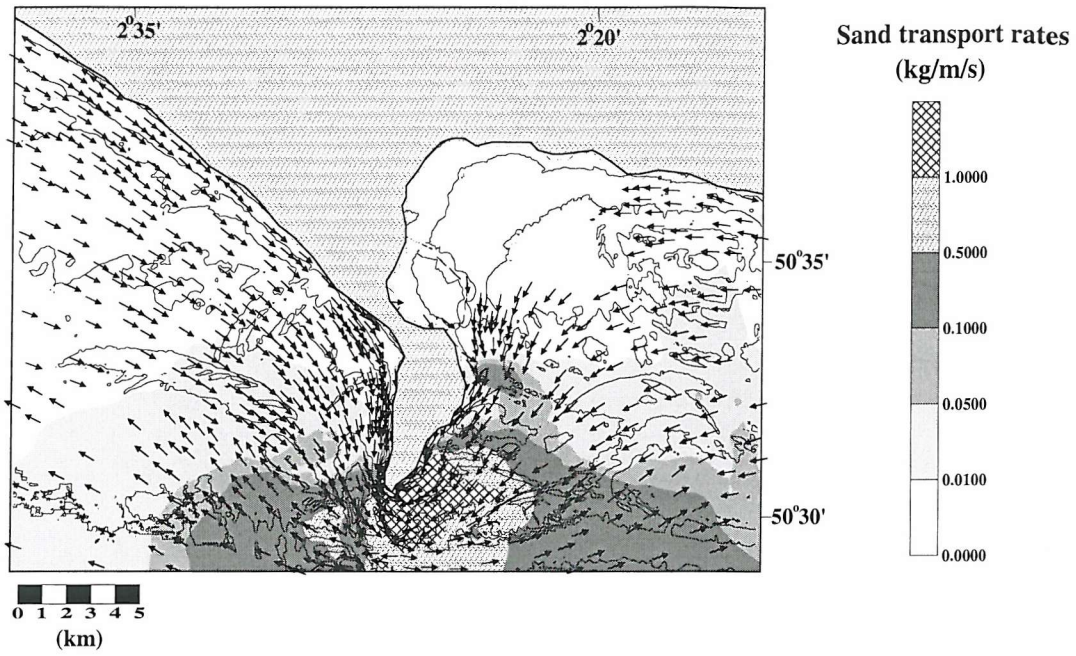

Figure 7.11. Net bedload transport direction (arrows) indicated by maximum bedload (medium sand) transport rates, over a spring tidal cycle (under currents alone). Transport rates are predicted using the algorithm proposed by Gadd et al. (1978). Note: arrows are not to scale, in terms of magnitude.

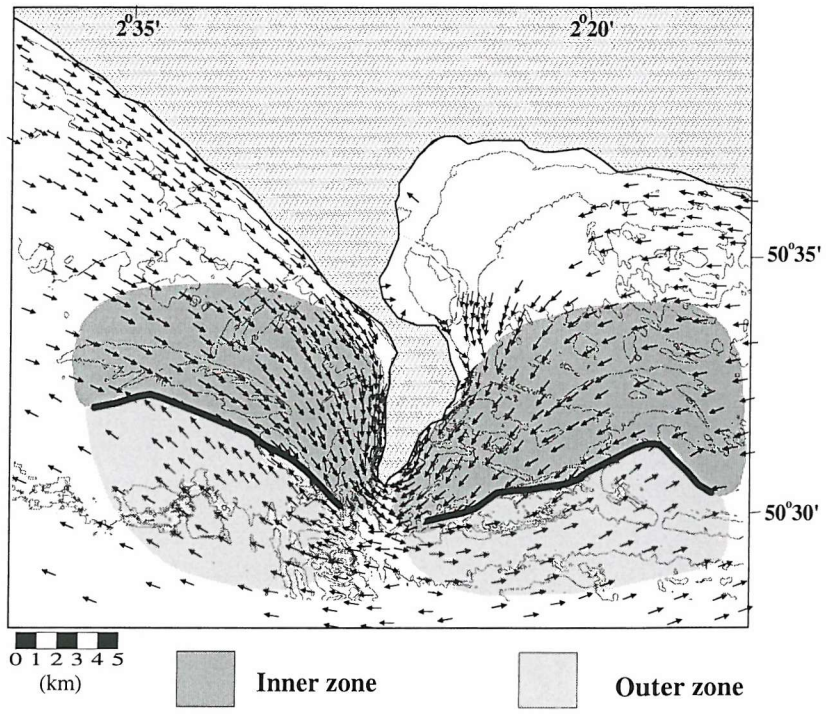

Figure 7.12. Map showing the occurrence of two conceptually-distinct regions of sedimentary processes (shaded), on both sides of the headland: an "inner zone" characterised by increasing bedload transport, towards the headland and an "outer zone" defined by decreasing bedload transport, away from the headland. The boundary between these two zones defines a shear stress/bedload convergent zone (—). Arrows represent maximum bedload sand transport (not to scale).

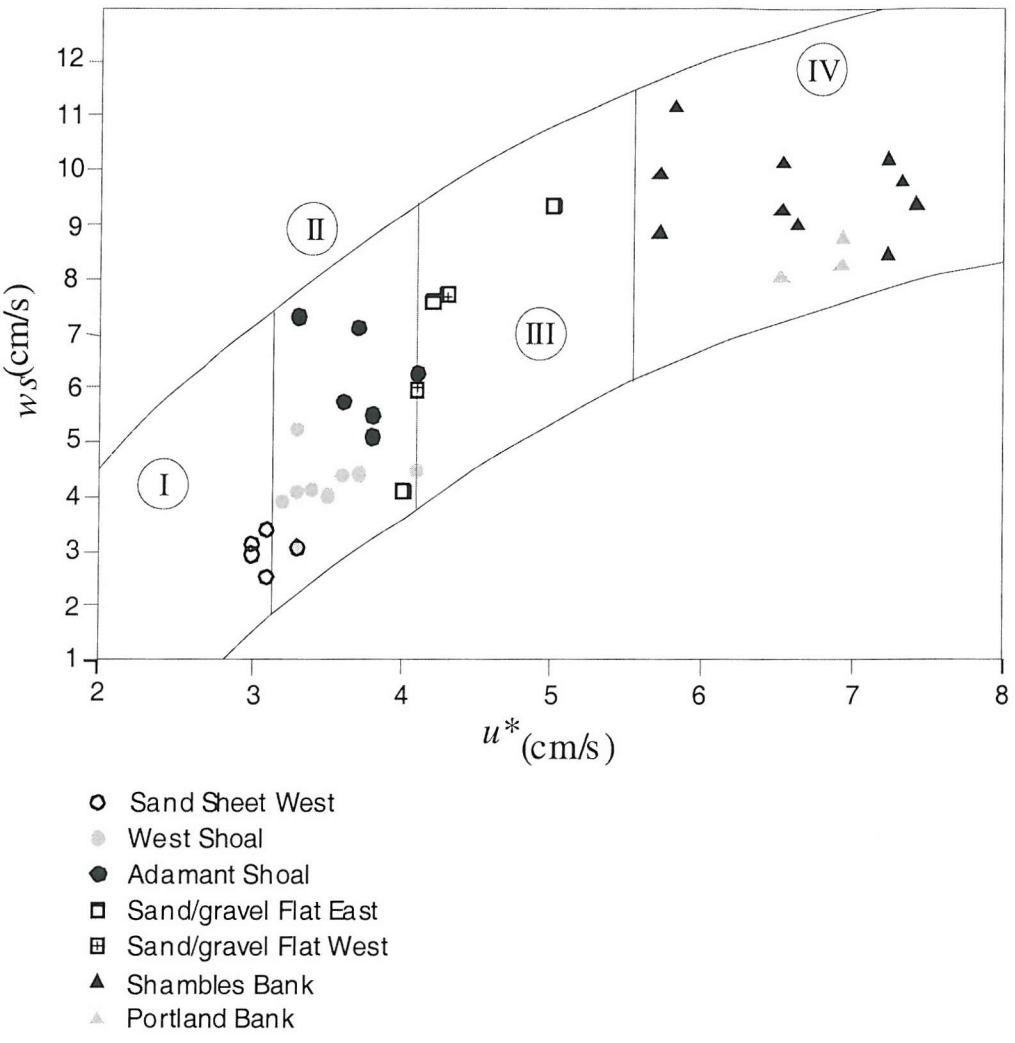

Figure 7.13. Diagram showing the correlation between sand grain settling velocity (w_s) and the maximum shear velocity ($u*$, under currents alone). The maximum shear velocity was calculated using SEDTRANS92 and refers to the location of the seabed sample recovery. (Key to regions: I – rippled sand sheet; II – sand shoals (medium-large sandwaves); III – sand/gravel flat; and IV – sandbanks).

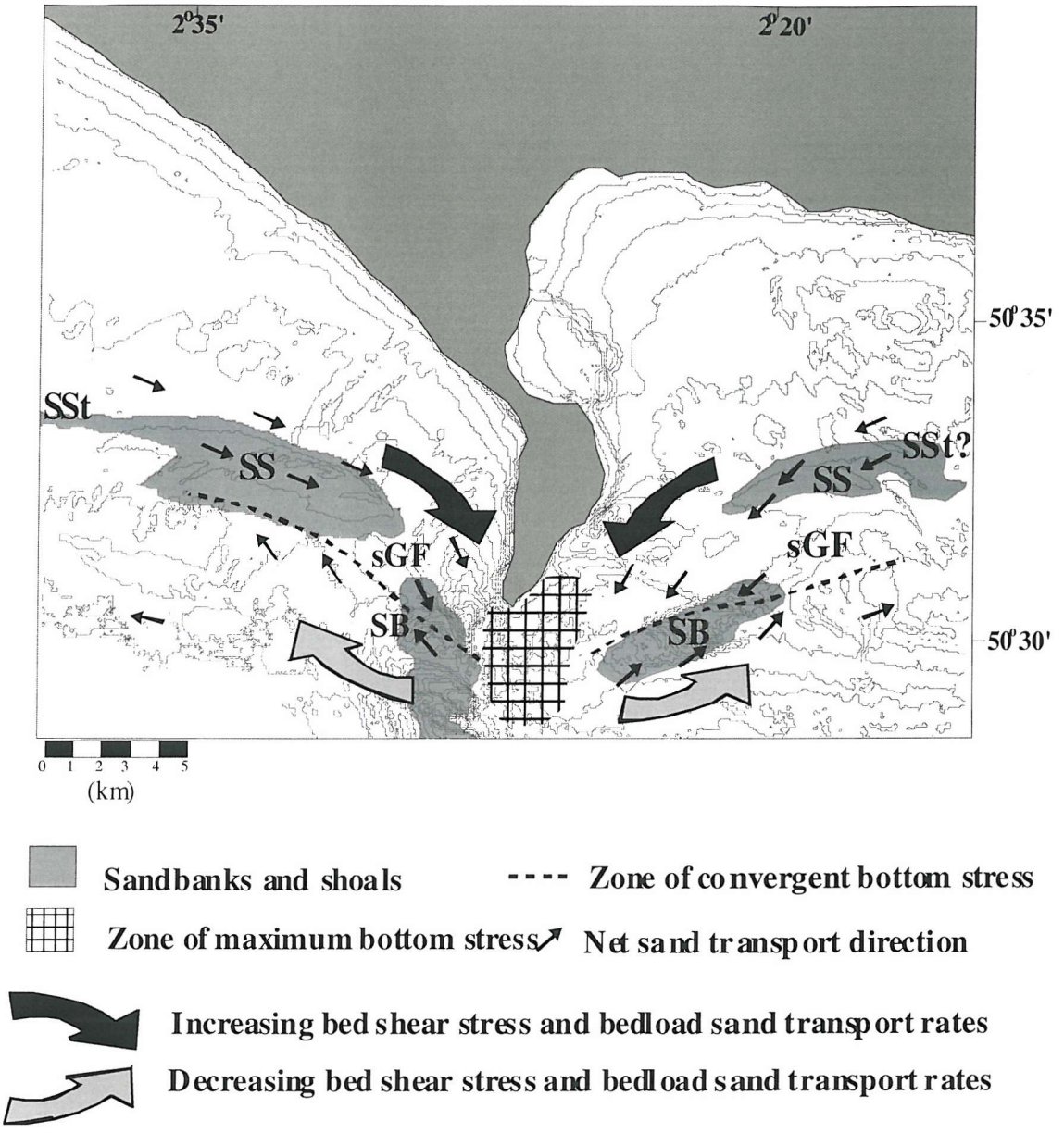

Figure 7.14. Regional concept of headland-associated eddy/bedload convergent zones, derived on the basis of current data, sediment and bedform distribution, shear stress and bedload transport calculations. (Key: SB- sandbank; sGF- sandy Gravel flat; SS- sand shoal; SSt- rippled sand sheet.)

Chapter 8

Bastos, A.C., Collins, M.B. and Kenyon. N.H., 2002. Morphology and internal structure of sand shoals and sandbanks off the Dorset coast, English Channel. Submitted to Sedimentology in July 2002.

Authors	Initiative of the Study	Data Collection and Analysis	Interpretation	Manuscript Preparation
Bastos	70%	100%	80%	80%
Collins	15%	-	10%	10%
Kenyon	15%	-	10%	10%

Chapter 8

Morphology and Internal Structure of Sand Shoals and Sandbanks off the Dorset Coast, English Channel

Abstract

The morphology and internal structure of sedimentary deposits around a coastal headland (Portland Bill, Southern UK) are investigated, using side-scan sonar and high-resolution seismic data sets.

A group of headland-shelf deposits (HSD) are recognised, revealing a fairly symmetrical sigmoidal plan view distribution, on both sides of the headland. These deposits are described, sequentially towards the headland, as: sand shoals, or sand streams (Adamant and West Shoals); sandy/gravel flats, representing sand bypass zones (East and West Flats); and sandbanks, associated with zones of sand convergence (Shambles and Portland Bank). The shoals and banks are the main depocentres.

Morphological and architectural evidence, combined with long-term sedimentary processes and the spatial distribution and nature of the basal reflector (BR), indicates the hydrodynamic and morphological controls on the formation, evolution and maintenance of the deposits. The lower seismic units (SU0 and SU1) of the Shambles Bank consist of a sedimentary core, probably, representing the remains of a similar bank formed in previous periods of high sea-level or an early stage of the bank development under different hydrodynamic conditions. The present morphology of the Shambles Bank is represented by an upper seismic unit (SU3), characterised by large-scale sandwave foresets dipping 6° to 8°.

The elongated Portland Deep, to the west of Portland Bill, constrains the growth of the Portland Bank; whereas, the Shambles Bank, to the east, rests upon a flat and broad basal surface. Thus, the morphology of the basal surface reveals that differential erosion of the seafloor is an important factor controlling the growth and size of the sandbanks.

The morphology and internal structure of the sandbanks, especially of the Shambles Bank, confirms the complex interaction between hydrodynamic and sedimentary processes. Hence, the evolution and maintenance of the banks are more complex than previous predictions based solely upon tidally-induced residual water circulation.

Reference: *Bastos, A.C., Collins, M.B. and Kenyon. N.H., 2002. Morphology and internal structure of sand shoals and sandbanks off the Dorset coast, English Channel. Submitted to Sedimentology in July 2002.*

8.1 Introduction

The floor of the continental shelf is subject to the combined processes of erosion, transport and deposition of sedimentary material. Over a geological time-scale, the shelf surface is considered to be one of dynamic equilibrium (Swift and Thorne, 1991), controlled by physical variables such as: the rate of relative sea-level rise; the level and character of sediment inputs; fluid power; and sediment transport rates and pathways.

During the post-glacial sea-level rise, continental shelf sand deposits are formed by reworking of lowstand (or early transgressive) deposits. A specific type of offshore (highstand) sand deposit is represented by sandbanks (or linear sand ridges and/or sand shoals, as described by various authors). The origin and maintenance of modern (active) shelf sandbanks have been investigated extensively, principally in terms of their morphology and hydrodynamics (reviews in: Pattiaratchi and Collins, 1987; Dyer and Huntley, 1999). Sandbanks are considered to be hydrodynamically-controlled systems, whose formation and maintenance processes are linked to the prevailing hydrodynamic conditions and relative sea-level rise. They are present on tide-dominated shelves (Stride *et al.* 1982) or storm-dominated shelves (Swift and Field, 1981) and can be described as active or moribund sand bodies (Kenyon *et al.*, 1981), depending upon their bathymetric setting in relation to the hydrodynamic forces. Theories for the origin and maintenance of sandbanks usually fall into two broad categories (Dyer and Huntley, 1999): (a) relict features, created during the post-glacial sea-level rise; and (b) formed as a response to the hydrodynamic and sediment regimes, similar to those presently active.

Different mechanisms for sandbank formation and maintenance have been proposed, including: the spiral flow concept (Houbolt, 1968); the bed shear stress stability model (Smith, 1969); lateral migration (Caston, 1972); seabed stability models (Huthnance, 1982 a, b; Hulscher *et al.*, 1993; Trowbridge, 1995; Hulscher, 1996; and Calvete *et al.* 2001); response to standing edge waves (Dolan *et al.*, 1979); and "tidal stirring" (Pingree, 1978 and Pingree and Maddock, 1979).

Conversely, there is a substantial lack of understanding of the internal structure (stratigraphy) of sandbanks (compared, for example, to the modelling of sandbank formation), within the overall context of the understanding of sandbank evolution. The seismic records of the Well

Bank and Smith's Knoll (Norfolk Banks, North Sea), presented by Houbolt (1968), were the first recognition of sandbank structure; these showed relatively gentle (5°) and inclined reflectors, lying parallel to the steepest flank of the bank. Houbolt (1968) observed also that the Well Bank rests upon a flat surface, supporting the concept of hydrodynamically-controlled formation.

More recently, three different types of sandbanks have been recognised from their stratigraphy (Berne *et al.*, 1994 and Berne *et al.*, 1998) and considered as a continuum: (a) the "Houbolt sand accumulation model", or sandbanks resting on a (transgressive) flat surface and related to a convergent pattern of sediment transport (e.g. Well Bank (Houbolt, 1968); Kwintebank in the Southern North Sea (De Moor, 1989); "moribund" East Bank in the North Sea (Davis and Balson, 1992); (b) sandbanks presenting a "core" of older deposits, in which the shape of the banks are associated with erosional processes and the reworking of underlying deposits (or lower stratigraphic units) (e.g. Brown Ridge and the Zeeland Group in the North Sea (Houbolt, 1968; D'Olier, 1981; and Laban and Schuttenhelm, 1981); tidal sand ridges in the East China Sea (Yang and Sun, 1988); Middlekerke Bank in the southern North Sea (Berne *et al.*, 1994)). In this type the sandbank facies would be restricted to the upper seismic units; (c) sandbanks considered as an end member unit, where banks (or ridges) have been sculpted from former lowstand deposits or early transgressive deposits (e.g. Kaiser-I-Hind Bank, Celtic Sea (Berne *et al.*; 1998)) In this type, sandbank formation reflects a reshaping of pre-existing deposits, rather than in response to a bank-growth process.

A particular type of sandbank occurs associated with coastal irregularities or headlands (the *banner banks* of Belderson *et al.* (1982) and Dyer and Huntley (1999)). Their formation is believed to be associated with the development of headland-associated eddies, during the tidal cycle (the "tidal stirring" concept of Pingree (1978)) (Fig. 8.1). Many headland-associated sandbanks are recognised around the British Isles, such as for example: the Skerries Bank (Start Point, English Channel); Stanley and North West Banks (Lundy Island, Bristol Channel); the Devil's Ridge, Tripods and Bastram Shoals (Lleyn Peninsula, Cardigan Bay); the Helwick, Scarweather and Nash Sands (Bristol Channel); the Shambles and Portland Banks (Portland Bill, English Channel); and the King Williams, Ballacash, Bahama and Wart Banks (Isle of Man, Irish Sea). The occurrence of headland-associated sandbanks is also observed around the Channel Islands (Great Bank and du Chateau Bank, Jersey), on the coast of France (Corbiere Bank, St. Malo) and on the Irish coast (Burford and Arklow Banks).

The significance of headland-associated eddies, on sediment transport and deposition around a coastal headland, have been described elsewhere; this is in terms of the occurrence of isolated sandbanks (Pingree, 1978; Pingree and Maddock, 1979; Ferentinos and Collins, 1980; Dyer and Huntley, 1999; Signell and Harris, 2000). However, a recent investigation undertaken around Portland Bill (Dorset, Southern England) has shown that there is a sequence of sedimentary deposits (including sand shoals, flat areas and sandbanks), on both sides of the headland (Bastos *et al.*, 2002). These deposits reflect changes in tidal current speed and sand transport rates towards the headland.

The morphological and architectural characteristics of the headland-associated deposits on either side of Portland Bill have been investigated here, using high-resolution seismic and side-scan sonar data. The principal objective of the present study is to recognise the morphology and internal structure of these deposits and discuss their formation, in terms of the parameters controlling evolution, such as, the prevailing hydrodynamics (tidally and wave-induced currents) and seafloor morphology. The internal structure of the sand deposits is used then to assess the previously proposed concepts of headland-associated sandbank formation, evolution and maintenance.

8.2 Geological/Geomorphological and Hydrodynamic Setting

The study area is located on the inner continental shelf, adjacent to the Isle of Portland, Dorset (Southern UK) (Fig. 8.2). The Isle of Portland separates two embayments, with different morphology: Purbeck Bay, to the east, where the average water depth is 25m and gentle bathymetric gradients are observed near to the coast; and Lyme Bay, to the west, where the average water depth is 35m and steep gradients occur offshore of Chesil Beach (Fig. 8.2).

The seabed morphology around Portland Bill is characterised by zones of non-deposition (or modern rock floor erosion) and sediment accumulation. The seabed consists, predominantly, of a discontinuous veneer of coarse lag deposits and bedrock outcrops, associated with patches of mobile sands. Sand accumulation areas are represented by the Shambles and Portland Banks and the Adamant and West Shoals (Fig. 8.2).

Several parameters have been recognised as influencing the regional sculpture of the seabed, including: differential resistance of the seafloor rocks (Donovan and Stride, 1961a and Stride, 1991); interaction between the tidal currents (and waves) and the coastal headland (Isle of Portland) (Pingree, 1978; Signell and Harris, 2000); and the last Holocene transgression. The seabed morphology is characterised by positive and negative "relief features" including bedrock outcrops, coarse lag deposits and modern shelf deposits (sandbank and shoals) (Fig. 8.3).

The rock floor of the seabed around Portland Bill comprises Upper Jurassic rocks, represented by: Corallian Beds (sandstones and limestones); Kimmeridge Clay (shales with thin layers of limestone); Portland Beds (sandstones and limestones); and Purbeck Beds (limestones) (Donovan and Stride, 1961a) (Fig. 8.4).

Corallian rocks outcrop in the core of the submerged part of the Purbeck Monocline, forming the submarine rock feature called the Lulworth Banks (Fig. 8.3), off the Purbeck coast. Shales, representing the Kimmeridge Clay sequence, are dominant over the shelf area to the east of the Isle of Portland. Thin layers of hard limestones, intercalated in the middle of the shale sequence, form rock ridges on the seafloor (Donovan and Stride, 1961a) (Fig. 8.3).

The northern flank of the Shambles syncline, consisting of sandstones and limestones (Portland Sands and Portland Stone), can be recognised on bathymetric charts as relief features of 25 and 30m deep, forming the Shambles Ledge. Lying transverse to and partly burying the Shambles Ledge, the Shambles Bank is the most prominent sedimentary deposit on this part of the shelf.

Immediately to the west of Portland, the Lyme Bay shelf is characterised by Upper Jurassic rocks, represented by Corallian Beds, Kimmeridge Clay and the Portland Beds (Figs. 8.3 and 8.4). A linear deep area, the Portland Deep, reaching depths of up to 75m, lies almost parallel and immediately to the west of Portland Bill, ending up in a depression about 100m in depth. This linear deep follows the lithological contact between sandstones (Portland Sands) and shales (Kimmeridge Clay). On the adjacent land surface, this contact is observed in the northwestern part of the Isle of Portland, being responsible for a series of landslides due to the distinct lithological characteristics of the sequences. Thus, it is considered that the Portland Deep has been carved in shales, as a result of differential erosion.

The inner continental shelf, shallower than 60m, is subject to semi-diurnal tides with an amplitude of 2m (on spring tides) at Portland Harbour. The tidal currents tend to increase offshore and towards Portland Bill. Spring peak current speeds, near the water surface, range from 0.4 m s^{-1} up to 3.6 m s^{-1}, in the vicinity of Portland Bill. During the tidal cycle, the development of tidal eddies are observed, on both sides of Portland Bill in response to ebb- and flood-dominated flows, respectively. The dominant wave approach over the area is from the southwest with significant wave height of 0.8 m and zero-cross period of 4.5 s; significant wave height exceeding 2.0m over the area occurs for only 10% of the year (Draper, 1991).

8.3 Methods

8.3.1 Data Compilation

Bathymetric and seabed sediment distribution data were compiled using available information and unpublished data sets. A bathymetric map was produced by digitising UK Hydrographic Office Fair Sheets (Fig. 8.3). Seabed sediment and bedform distribution were characterised, initially, on the basis of an extensive compilation of unpublished data sets (Kenyon (1994), for the east of Portland Bill; and Nunny (1995), for the west of Portland Bill); this generated a seabed sediment distribution map for the inner shelf (see also Bastos *et al.*, 2002).

8.3.2 Field data acquisition

Two acoustic surveys were undertaken (Fig. 8.5). A survey of the seabed morphology was undertaken in June, 2000, using a Widescan system (100 kHz). The data were acquired in analogue and digital formats. This survey obtained 100 km of side-scan sonar track and 80 seabed sediment samples.

A survey of seabed morphology, sediment thickness and internal structure of sand deposits was carried out in June, 2001, consisting of side-scan sonar and high-resolution shallow seismic profiling. During this latter survey, a GeoAcoustic side-scan sonar (500kHz) was used, in combination with a 100 Joule Geopulse Boomer 610. The data were acquired in digital (GeoPro 4) and analogue formats, respectively. A total of 105 km of side-scan and seismic profiles were acquired. During both surveys, a GPS Trimble system was used for navigation positioning, giving an approximate 5m accuracy.

8.3.3 Fieldwork data processing

Sediment facies and bedforms were mapped using the side-scan sonar records. The bedform classification adopted here largely follows Ashley *et al.* (1990). However, overall, it was found that the term sandwave is more appropriate to use than dunes. The sandwave classification, based upon their wavelength (L) and height (H), is; very large (L>100m, H>5m); large (L-10-100m, H-0.75-5m); medium (L-5-10m, H-0.4-0.75m); and small (L-0.6-5m, H-0.075-0.4m). Seismic interpretation was based upon internal seismic reflection patterns and the external shape of seismic facies, as described by Mitchum *et al.* (1977). Sediment

thickness was calculated on the basis of the seismic records, assuming an average sound velocity within the sediments of 1600 cm s^{-1}. The depth to the bedrock was obtained by adding the water depth, abstracted from the bathymetric map, to the measured sediment thickness. Note that the water depth is reduced to Chart Datum, i.e. the Lowest Astronomical Tide.

Sediment samples were processed by means of sieving and settling tower techniques, to derive mean grain size (D_{50}) and settling velocity (w_s), respectively. Carbonate content was obtained by subjecting a sub-sample to HCl attack.

The terms sandbank and sand shoal are used in the present investigation, with distinct geomorphological meanings. Sandbanks are described here as the major sand accumulation bodies, being more than 2 km in length and 1 km in width, and with a maximum thickness of around 20 m. They are superimposed with large and very-large sandwaves and linear sand ridges. These superimposed bedforms show a convergent sand transport pattern, towards the bank crest. Sand shoals are more elongated sand bodies, with medium to large sandwaves superimposed. They are smaller in size than the sandbanks, specially in terms of thickness (around 6 to 8 m). There is no indication of sandwave convergence along their crest.

8.4 Results

The data are presented and interpreted in Figures 8.6 to 8.12.

8.4.1 Seismic Results

Analysis of the seismic records has permitted three orders of seismic reflectors to be distinguished: a major unconformity at the top of the Jurassic rocks; first-order reflectors representing an unconformity and seismic facies boundaries; and second-order reflectors.

The major unconformity reflector (BR, basal reflector) is observed in all the seismic sections. The BR is usually a high amplitude reflector, representing the top of the Jurassic rocks; however, in some areas, it could be associated with lag deposits. Moreover, the BR is an unconformity that represents a significant stratigraphic hiatus, observed widely over the English Channel (Curry, 1989; Stride, 1991; and Evans, 1992).

A first-order reflector is defined here as an unconformity and/or a seismic facies boundary. First-order reflectors were recognised here only on the Shambles and Portland Banks and on the West Flat; they are usually erosional surfaces. Three erosional surfaces were recognised for the Shambles (SR1, SR2, SR3) and Portland (PR1, PR2, PR3) Banks. These surfaces are not necessarily synchronous between banks.

Second-order reflectors were recognised and are used here to describe the large-scale internal structure of the deposits. Prograding clinoforms, horizontal/sub-horizontal and chaotic reflectors were recognised.

Basal Reflector

Overall, the depth of the BR varies slightly between the eastern and western areas (Fig. 8.6), showing an average depth of 30 m. An exception for this pattern is the Portland Bank and Portland Deep area, where the BR goes down to about 100 m.

The BR is very irregular when associated with Kimmeridge Clay sequences (Adamant Shoal, East and West Flats and part of West Shoal), because thin layers of resistant limestone within the shale sequence tend to form rock ridges on the seafloor. The BR is considerably flatter to the northwest of the West Shoal, where it is associated with the Corallian Beds sequence;

likewise, underlying the Shambles Bank, where it is associated with the Portland Stone sequence. However, it should be noted that at the northeastern end of the Shambles Bank, the BR forms a knoll along the contact between shales of the Kimmeridge Clay sequence and the sandstones of the Portland Sands sequence (forming the Shambles Ledge) (Figs. 8.4 and 8.6a). Off Portland Bill, the BR outcrops at the seafloor and forms a series of steps, before it descends into the Portland Deep area (Fig. 8.6b). These steps mark the contact between Portland Stone and Portland Sands (according to the interpretation of Donovan and Stride, 1961a).

Despite its irregularity, the BR shows, over most of the area, gentle angles of dip. An exception is the region from the tip of Portland Bill, to the beginning of the West Flat. Over this region, the BR dips abruptly, forming the linear deep area (5° to 6°). In the Portland Bank region, the BR dips relatively strongly (1°) towards the east.

Sediment Thickness

The sediment thickness distribution follows a similar pattern, on both sides of the headland. The thickest deposits are the banks, with an average of 10 m for the Portland Bank (maximum of 19 m) and 15 m for the Shambles Bank (maximum of 22 m). Away from the banks, but following a narrow longitudinal axis towards the NE (eastern deposits) and NW (western deposits), the sandy/gravel flat deposits on both sides show an average thickness of 5 m. The shoals have an average thickness of 6 m, reaching up to 9 m below the crest of the large sandwaves. Seismic profiles across the deposits show that sediment accumulation is confined to these two groups of deposits on either side of the headland.

8.4.2 Superficial Morphology and Architecture

The inner shelf around the Isle of Portland is typically erosive (represented mainly by rock outcrops and lag gravel deposits), with specific areas of sediment accumulation. These areas are referred to, from now on, as headland-shelf deposits (HSD). Two HSD were recognised, showing a fairly symmetrical sigmoidal geometry shape on either side of the headland (Fig. 8.2). The HSD consist of sand shoals, sandy/gravel flats and sandbanks. The shoals and banks are asymmetrical in profile, with the steeper flank facing towards the coast. Only the sandy/gravel flats are symmetrical in profile.

Sediment distribution along the HSD is characterised by siliciclastic and bioclastic sands, bioclastic gravelly-sands and sandy-gravels. In general, a similar sequence of bedforms is

observed on both sides of the headland: medium and large sandwaves on the shoals; a sandwave-free zone on the flats; and very large sandwaves (superimposed with medium and small sandwaves), showing a converging pattern on the sandbanks.

Eastern HSD

The eastern HSD consists of the Adamant Shoal, East Flat and the Shambles Bank. A longitudinal section of the deposits is shown in Fig. 8.6a.

The Adamant Shoal is a sand deposit lying in a mean water depth of 25 m, with thickness ranging from 5 to 7 m; it reaches 10 m thick beneath the larger bedforms. The shoal is aligned sub-parallel to the coastline, presenting a concave-southward arcuate shape.

In terms of modern processes, the shoal could be described as a *sand stream*, composed of coarse to very coarse sands (D_{50} = 0.5-1 mm; w_s = 6-8 cm s^{-1}; carbonate content = 30%) and characterised by a sequence of medium to large sandwaves, generally with an asymmetric profile pointing towards the SW. A veering in the sandwave crest direction occurs, following the shape of the shoal. At its northeastern end, medium to large sandwaves have an almost N-S (340°-160°) crest direction; at its southwestern end, the direction is approximately NW-SE (310°-135°). This pattern is in agreement with the pattern of strongest ebb tidal currents predicted from a hydrodynamic model (TELEMAC-2D, see Bastos *et al.*, 2002) for this area.

A very large (NW-SE) sandwave marks the eastern limit of the shoal (Fig. 8.3). This sandwave is oblique to the northern limit of the shoal, having an asymmetric profile towards SW at its southern end (Fig. 8.7 a). A more symmetric profile is observed towards its northwestern end. It consists of sandy-gravel to gravelly sediments, showing a decrease in grain size towards the NW (following the more symmetric profile). Medium and small sandwaves also occur on the top of the ridge. This feature is also the limit of occurrence of transverse bedforms. The sonographs show that to the south of the sandwave, there is a sandwave-free zone.

Two main kinds of seismic reflectors are identified, forming the internal structure of the Adamant Shoal (Fig. 8.7a). Horizontal to sub-horizontal reflectors are observed at a transitional zone, between the flat area and the shoal; and, large-scale oblique clinoforms occur at the main part of the shoal. In general, the internal structure is characterised by clinoforms dipping (1°-2°) towards the north (Fig. 8.8). The occurrence of erosional surfaces,

truncated by overlying clinoforms, is observed over limited areas ; however, they do not extend more than a few hundred meters. To some extent, the external shape of the Adamant Shoal reflects its internal structure. The only exeption to this pattern is the occurrence of the very large sandwave (Fig. 8.7a); its internal strucutre is marked by medium to high amplitude clinoform reflectors, dipping (7°) towards the SW. These clinoforms truncate an erosional surface, that occurs approximately at the same depth as the surrounding seabed.

The East Flat lies to the south of the Adamant Shoal. It is an area depleted of bedforms (associated with high and homogeneous backscatter patterns, on the sonographs), consisting of lithoclastic/bioclastic gravel and sandy-gravel sediments. The seismic data have revealed that this deposit is, in general, 4 to 6 m in thickness. The internal structure is characterised by parallel and sub-parallel (low amplitude) reflectors. A cross-sectional profile reveals that the deposit is mound-shaped, with internal reflectors following the external shape (Fig. 8.7b).

A sandbank is one end member of the HSD sequence. The Shambles Bank is the most prominent sedimentary deposit of the area. It is an elliptically-shaped bank, with a maximum height of 22m, about 5km in length and 2 km in width. The bank is aligned in a NE-SW direction, sub-parallel to the eastern coast of the Isle of Portland, showing a strongly asymmetric profile, steeper towards the coast (NW).

Distinct morphological, sedimentological and architectural characteristics can be recognised along the Shambles Bank (Fig. 8.9a). The northeastern end of the bank is characterised morphologically by very large sandwaves, with an asymmetric profile steeper towards the SW (ebb-orientated). A total of three sandwaves were recognised. They are about 200 m wide and 6 to 7 m high, with spacing between them of around 500 m. These sandwaves lie oblique to the bank longitudinal axis and their crest direction is 285°-105°. Medium sandwaves are observed on the crest and along the trough, showing crest direction ranging from 300°-120° to 325°-145°. The sandwaves consist of bioclastic sandy-gravels (D_{50} = 2.4 mm).

The southwestern end of the bank is characterised by very large sandwaves, with wavelength of around 300 m and maximum crest heights of 7 m. These sandwaves show flood current-dominated asymmetric profiles (steeper towards the NE). Small- and medium-sized sandwaves are present on the stoss side of the larger sandwaves, usually forming an oblique angle with the major sandwave crest (small and medium sandwave crest direction range from

320°-140° to 300°-120°). Small sandwaves are observed also along the trough, between the larger sandwaves. These have crests perpendicular to the crest of the very large sandwaves. A decrease in sediment grain size is observed along the bank; these sandwaves consist of coarse to very coarse bioclastic sands (D_{50} = 0.9 mm; w_s = 8.45 cm s^{-1}; carbonate content = 80%).

The asymmetry of the very large sandwaves shows a convergent pattern towards the centre of the bank (Fig. 8.6). The central part of the Shambles Bank is characterised by very large symmetric sandwaves and a linear ridge-like feature. This ridge lies sub-parallel to the bank flank (northwestern flank) and almost perpendicular to the very large sandwave crests. This feature is morphologically flat, with small and medium sandwaves superimposed.

Seismic sections have revealed that the Shambles Bank is a sedimentary deposit, lying on top of a flat bedrock erosional surface (BR), dipping gently towards the southwest. The only exception for this BR pattern is the occurrence of a bedrock ridge (Shambles Ledge), which is associated directly with the northeastern end of the bank. The limits of the bank are very clearly shown in the seismic sections (Fig. 8.7c). Apart from its northeastern end, where the bank is linked to the East Flat, the bank is surrounded by bedrock (mussel beds are also present), i.e. the bank is laterally isolated.

Three first-order reflectors were recognised within all the cross sections of the bank. These are numbered sequentially upwards, as SR1, SR2 and SR3. SR1 is a high-amplitude reflector corresponding to an erosional surface (Fig. 8.10); its occurrence is limited to the southeastern flank of the bank. SR2 is a very undulating reflector, observed mainly within the central and southeastern flank of the bank. SR3 is a flat and horizontal reflector, which occurs along the entire bank; this represents the lower bounding surface for the large-scale oblique clinoforms. These reflectors mark the limit of different seismic units (SU0, SU1, SU2, SU3). Only SU3 is observed along the entire bank.

Longitudinal seismic sections show a large-scale *sandwave-climbing pattern* along the bank (Fig. 8.9b). The present morphology of the bank is represented by SU3. This unit is characterised by large-scale foresets, dipping (6°-8°) in the same direction as the lee side of the very large sandwaves. This is similar to the internal structure of the subtidal sandwaves described by Berne *et al.* (1988) and Berne *et al.* (1993). Nevertheless, a lateral facies variation is observed within SU3, from the central part towards the northwestern flank. Large-

scale foresets give place to sub-horizontal reflectors in the central part, with clinoforms along the flank.

The transverse sections reveal a significant contrast in the internal structure of the Shambles Bank. The southeastern flank, consisting mainly of units SU0 and SU1, has a far more complex arrangement of internal reflectors and erosional surfaces, when compared to the simple gently dipping clinoform (Houbolt type) structure observed from the central and northwestern parts of the bank, in units SU2 and SU3.

SU0 and SU1 units, in the southeastern part of the bank, consist mainly of oblique prograding reflectors. They generally dip N to NW, with dip angles decreasing towards the centre of the bank, although some reverse dipping is seen.

Western HSD

The western HSD system consists of the West Shoal, West Flat and the Portland Bank. A longitudinal section of the deposits is shown in Figure 8.6 .

The West Shoal is an elongated sand deposit, lying sub-parallel to the coastline (Chesil Beach), in a water depth of 30 m. The shoal is strongly asymmetric and steeper towards the coast (Fig. 8.7d). Its thickness ranges from 4 to 8 m, showing a significant decrease in sand thickness towards the NW, where it gives way to a rippled sand sheet (thickness < 2 m) (Fig. 8.6b). Mean sand grain size varies along the deposits. From its SE end towards NW, a decrease in D_{50} is observed, from 0.26 mm to 0.18 mm; the carbonate content is about 30% along the entire shoal.

The surface of the shoal is covered in small, medium and large sandwaves. Large sandwaves have a mean wavelength of 200 m and a crest height of 2 m. They have fairly asymmetric profiles, with the steep side dipping towards the southeast. There are complex and variable shapes in the medium and small sandwave-trains, ranging between "straight to sinuous" and "sinuous out of phase" (Allen, 1968). Similar to the Adamant Shoal, a veering of the sandwave crests is present on the West Shoal, as well as a prominent very large sandwave (SW-NE) lying close to the western limit of the shoal (Fig. 8.3). This sandwave is 4 m in height and it does not show a clear asymmetric profile.

Transverse seismic sections display large-scale horizontal to sub-horizontal (low reflectivity) reflectors, which give place gradually to inclined reflectors (clinoforms), dipping at 4° towards the north (Fig. 8.11). This deposit architecture is very similar to the internal structure described by Houbolt (1968), for the Well Bank in the southern North Sea.

The West Flat lies to the southeast of the West Shoal. Similar to the East Flat, this region is depleted of bedforms. It has a uniform high backscatter character in the sonographs and consists of lithoclastic/bioclastic gravel and sandy-gravel sediments. The West Flat is a mound-shaped deposit, with thickness ranging from 4 to 9 m (Fig. 8.7e). A transversal section reveals horizontal and sub-horizontal (low amplitude) reflectors, which tend to incline towards the flanks of the deposit, giving it its mounded-shape (Fig. 8.7e).

A first-order reflector (WR1), bounding two seismic units, was recognised. There is no overlying truncation on this bounding surface and it appears to follow the mound-shape of the deposit. The lower unit (WU1) shows low amplitude reflectors. A sub-unit is characterised by very gently inclined reflectors, dipping towards the N-NW. The upper unit (WU2) shows high amplitude horizontal and sub-horizontal reflectors. The considerably greater thickness of the West Flat, compared to the East Flat, could be explained by the depth and by the dipping of the BR (see above).

The high energy end-member of the West HSD is the Portland Bank. The Portland Bank is an oval-shaped bank, 2.5 km in length and 1 km in width. The morphology, size and location of the deposit all appear to be controlled by the surrounding seafloor morphology, related to the BR (Figs. 8.6 and 8.9a). Deep areas bound the eastern and southern edges of the deposit. Its thickness ranges from 8 to 12 m, but can reach up to 19 m below the crests of the very large bedforms present on the region.

Similar to the Shambles Bank, the Portland Bank is composed of very coarse bioclastic sands (D_{50} = 1.2 mm; w_s = 8.5 cm s^{-1}; carbonate content = 80%). The surface of the Bank is characterised by very large asymmetric sandwaves (with their lee sides dipping towards the southeast). The very large sandwaves present have a mean wavelength of 250 m and a height of 6 m. A convergent pattern of sandwaves is not clearly identifiable along the main axis of the bank. However, large asymmetric sandwaves (ebb-orientated) are present along the western flank of the bank.

The seismic sections reveal three major bounding surfaces (PR1, PR2, PR3, numbered sequentially from the basal reflector to the seabed) (Fig. 8.7f). These surfaces are truncating underlying clinoforms. PR1 is a low-amplitude reflector corresponding to an erosional surface; its occurrence is limited to the northeastern flank of the bank. PR2 is a high-amplitude and undulating reflector. Although it can be traced along the entire length of the bank, it does not appear as a continuous reflector. Like surface SR3 on the Shambles Bank, PR3 is a flat and horizontal reflector that occurs along the entire bank. It is the lower bounding surface for the large-scale oblique clinoforms (PU3). These reflectors (PR1, PR2 and PR3) mark the limit of different seismic units (PU0, PU1, PU2, PU3). Because the bank thickens towards its central part, the seismic units are not observed along the entire bank, apart from SU3.

Longitudinal seismic sections show a large-scale *sandwave-climbing pattern* along the bank, as observed for the Shambles Bank (Fig. 8.9c). Unit PU3, which corresponds to the present day bank, is very similar to unit SU3 described for the Shambles Bank. It has large-scale foresets, dipping 7°-8° in the same direction as the lee side of the very large sandwaves. These sandwave foresets are downlapping against a flat erosional surface (PR3), that truncates the underlying buried sandwave foresets (PU2).

The Portland Bank is steeper towards the coast. A transverse seismic section reveals a very irregular morphology, due to the sinuosity of the very large sandwave crests (Fig. 8.7f). The internal structure corresponds, generally, to sandwave foresets. Units PU0 and PU1 are only observed clearly along the northern flank. Unit PU0 rests on the BR and is characterised by horizontal and sub-horizontal reflectors. Unit PU1 shows high- amplitude reflectors, dipping (5°) towards N-NE. These clinoforms are truncated, on the top, by an undulating erosional surface (PR2). The unit PU2 is characterised by clinoforms (buried sandwaves), dipping in the direction of the lee side of the very large sandwaves; however, on the northern flank the reflectors show a more complex pattern, with clinoforms reversing their dip direction (Fig. 8.7f). The Portland Bank differs from the Shambles Bank not only in size, but in that the dipping basal surface ends in a very deep area (up to approximately 100 m) (Figs. 8.2 and 8.6).

8.5 Discussion and Conclusions

Morphological and high-resolution seismic analysis shows a sequence of interrelated (headland-associated) sedimentary deposits (HSD), on both sides of Portland Bill. Each of the HSD consists of distinct members (shoals, flats and sandbanks). The deposits reflect a fairly symmetrical pattern of sediment transport and deposition around the headland. The HSD are characterised as: (i) being laterally isolated, but longitudinally connected (Figs. 8.6 and 8.7); (ii) having an asymmetric cross-section steeper towards the coast (shoals and banks); and (iii) having two depocentres, of which the sandbanks are the thickest and the high energy end-members.

The shoals are at the lower energy end of the HSD (Bastos *et al.*, 2002). They are elongated sand streams formed by large sandwaves, with asymmetric profiles steeper towards the southern limit of the headland. The sandwave crests, forming the shoals, indicate sand transport veering towards the south (the tip of Portland Bill), following the deviation in the current direction (constrained by the coastal irregularity).

As tidal current speed increases towards the headland, mound-shaped deposits occur, with a flat and homogeneous gravelly bed and with sub-horizontal internal reflectors (the West and East Flats). These deposits may represent a sand bypass zone. In an area of greater tidal current speed, sandbanks occur. They are in an area which is under a more significant influence of the transient eddies, acting as convergent traps for sediments (Fig. 8.12). These convergent traps are shown by the convergence of the very large sandwaves (ebb and flood-orientated), towards the bank crest. The banks consist of very coarse to coarse bioclastic sands (80% carbonate content).

The internal structure of the upper seismic units (SU3 and SP3) shows that the sandwaves climb on top of each other towards the crest of the banks, where they reach their maximum thickness.

The morphological characteristics summarised above indicate hydrodynamic control of the formation, evolution and maintenance of these deposits. The long-term sedimentary processes are interpreted on the basis of the internal structure and are related to the (hydrodynamic) forcing mechanisms for the formation and evolution of the HSD. The transversal asymmetry

of the deposits, together with the occurrence of clinoforms within the internal structure, suggest that the sand shoals and sandbanks have a long-term component of sediment transport towards the coast. Kenyon *et al.* (1981) and Huthnance (1982a) have used sandbank asymmetry as an indicator of net sand transport direction.

Explanations for the possible coastward long-term transport are: (i) long-term wave action and/or the influence of storm waves; (ii) hydrodynamic patterns enhanced by the localised formation of transient eddies and inequalities in current speed and direction, creating a net bank movement towards the coast and consequently, forming an asymmetric profile facing towards the direction of net bank movement (valid for the sandbanks only); and (iii) low rates of marine transgression, i.e. sea-level rise.

Although the formation of headland-associated sandbanks is related to the development of headland eddies (Pingree, 1978; Ferentinos and Collins, 1980; and Signell and Harris, 2000), it is reasonable to consider that the maintenance and long-term dynamics of these banks and shoals are controlled by the combination of the three factors described above, especially the influence of waves. Tidal currents and storm waves represent the controlling-mechanisms acting during the late stages of bank and shoal evolution as represented by the upper units SU3 and SU2 on the Shambles Banks, PU3 on the Portland Bank and the large-scale reflectors in the sand shoals. The dispersive and destructional influence of waves controls the height of sandbanks (Ferentinos and Collins, 1980; Houthuys *et al.*, 1994); moreover, their long-term action forces the banks and shoals to migrate towards the coast. The tidal currents (and associated transient eddies) are responsible for the maintenance of the morphology of the banks and shoals. This is in very good agreement with the stability model, proposed by Huthnance (1982a, b). Sea-level rise is, supposedly, affecting sandbank and sand shoal evolution since the early stages of their formation.

Hitherto, the formation and evolution of HSD have been discussed in terms of the evidence for hydrodynamic control. Although there is a significant symmetry in the regional distribution of these deposits on both sides of the headland, minor length-scale differences can be observed when comparing the deposits individually; this is especially true for the sandbanks. These differences may be partly due to the morphological characteristics of the bedrock, which forms the base (BR) of the sedimentary deposits.

Two significant characteristics of the regional pattern of the BR were recognised: the mean depth of the BR is 5 to 10 m deeper on the west side of Portland; and there are local deeps and rock ridges. The bedrock surface is a controlling-factor for the formation and evolution of the sandbanks (and results in a difference in the size of the banks). The influence of the seabed on the formation and evolution of the sandbanks can be exemplified by the relationship between the Portland Bank and the Portland Deep (Figs. 8.6 and 8.9a). The deep area restricts the growth and development of the Portland Bank. On the contrary, the Shambles Bank lies on top of a resistent and broad basal surface and its northern end is associated with a distinct rock ridge, the Shambles Ledge.

Thus far, morphological-control has been discussed within the context of the BR. However, the Shambles Bank has distinct units in its internal structure, suggesting that the lower units (SU0 and SU1) represent either the remains of a similar bank formed in previous periods with a similar coastal setting but modified in the subsequent period of sea level lowstand or an early stage of the bank development under different hydrodynamic conditions. The absence of any borehole information leads only to speculation of the origin of such units.

Consequently, the lower units (SU0 and SU1) represent a sedimentary core that probably has influenced the growth and shape of the Shambles Bank, during some stage of its evolution when the hydrodynamic conditions were similar to the present. The upper units (SU2 and SU3) show an internal structure, characterised by large-scale sub-horizontal profiles and (steep) dipping clinoforms (SU2) and very large sandwave internal structure and sub-horizontal reflectors (SU3). The distribution of such units reveals that, at some stage during the last transgression, prograding facies (SU2) started developing (dipping towards the NW) onlapping the lower SU0 and SU1 and forming the northwestern flank of the bank (Fig. 8.10c). Along the northwestern flank of the bank, the SU2 reflectors rest directly on the BR (angles of dip range from 4° over the central part to a maximum of 8° at the flank). Subsequently, an erosional event formed the SR3 flat-bounding surface (observed all over the bank), and the present shape of the bank started to develop (SU3).

Recognition of the HSD, together with the subsequent investigation on their internal structure, have revealed that the formation and evolution of a coastal headland-associated sandbank is likely to be related to a larger sedimentary system than assumed previously (Pingree, 1978). This sedimentary system corresponds to a convergence of *sand streams* towards the tip of the headland. Here, the influence of transient eddies controls the formation of a sediment

convergent zone and leads then to the development of sandbanks (Fig. 8.13). Moreover, the characteristics of the basal surface should be considered because it can significantly influence the development of sand bodies, especially their length-scale. The complex morphology and internal structure recognised for the sandbanks, especially the contrast in morphology and internal structure observed along the Shambles Bank, have confirmed that sedimentary processes controlling the evolution and maintenance of these banks are far more complex than predictions related only to residual water circulation.

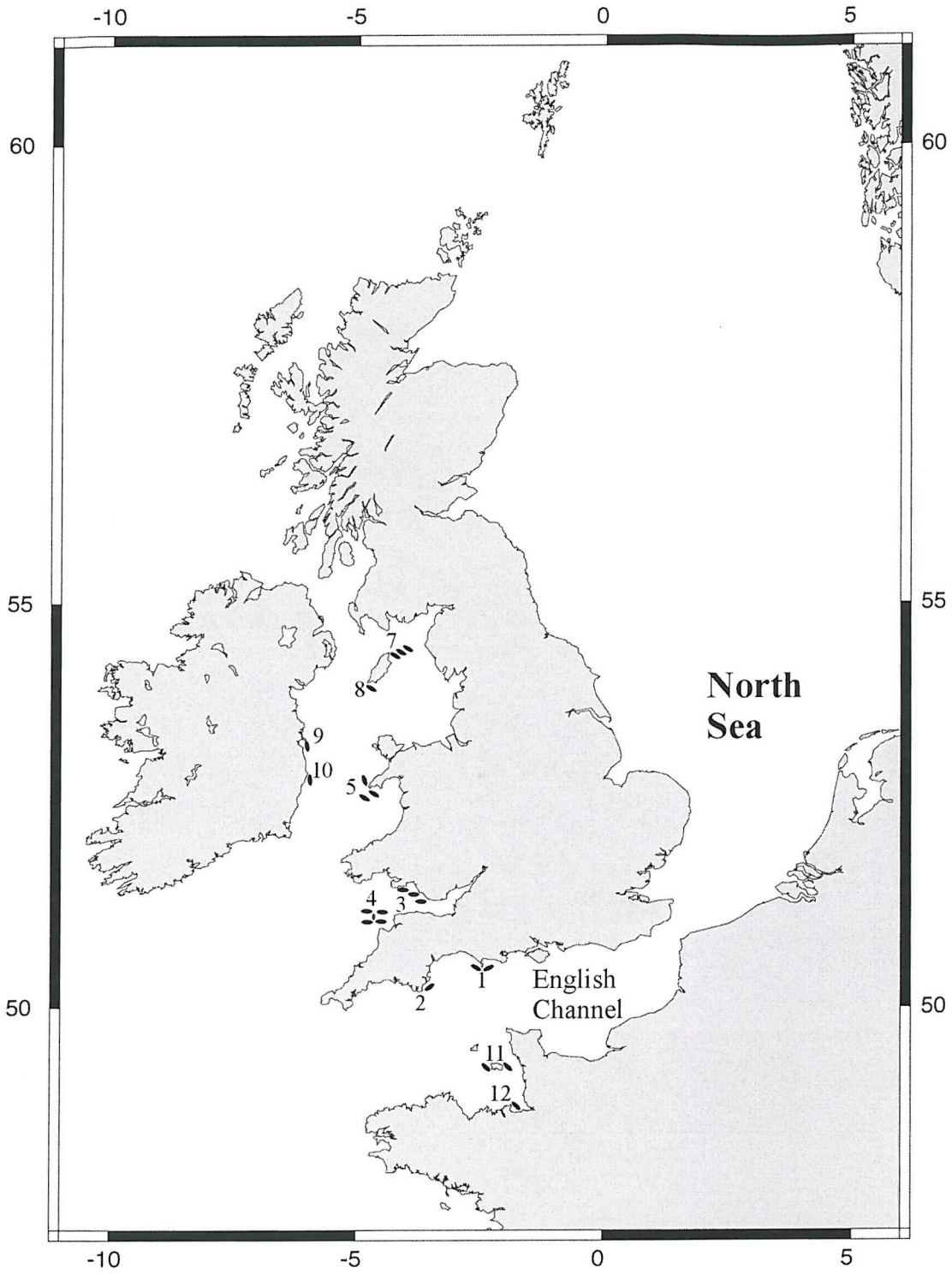

Figure 8.1. Map showing the general location of some examples of headland-associated sandbanks around the UK, Channel Islands, French and Irish coasts. Key: 1- Shambles and Portland Banks; 2 - Skerries Bank; 3 - Helwick, Scarweather and Nash Sands; 4 - Stanley and North West Banks; 5 - Devil's Ridge, Tripods and Bastram Shoals; 7 - King Williams, Ballacash and Bahama Banks; 8 - Wart Banks; 9 - Burford Bank; 10 - Arklow Bank; 11 - Great Bank and du Chateau Bank; 12 - Corbiere Bank.

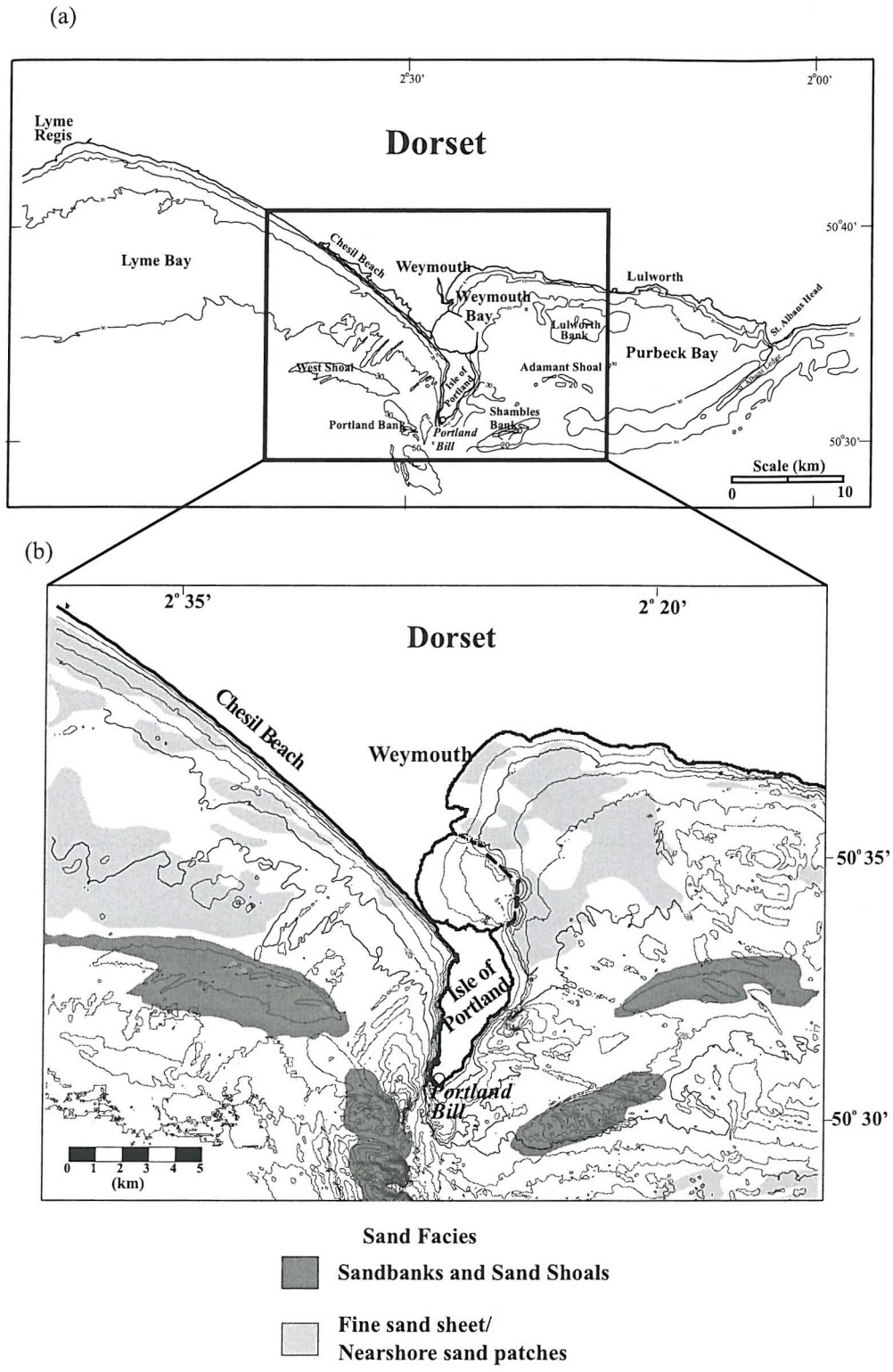

Figure 8.2. (a) Regional setting of Portland Bill and the area under investigation; (b) sand distribution areas, in relation to seabed morphology. The detailed bathymetric map is based upon UK Hydrographic Office Fair Sheets. Contour interval in metres and reduced to Chart Datum. Sand distribution map is based upon sediment samples and side-scan sonar data derived from a compilation of acquired fieldwork and available datasets (Nunny, 1995 and Kenyon, 1994).

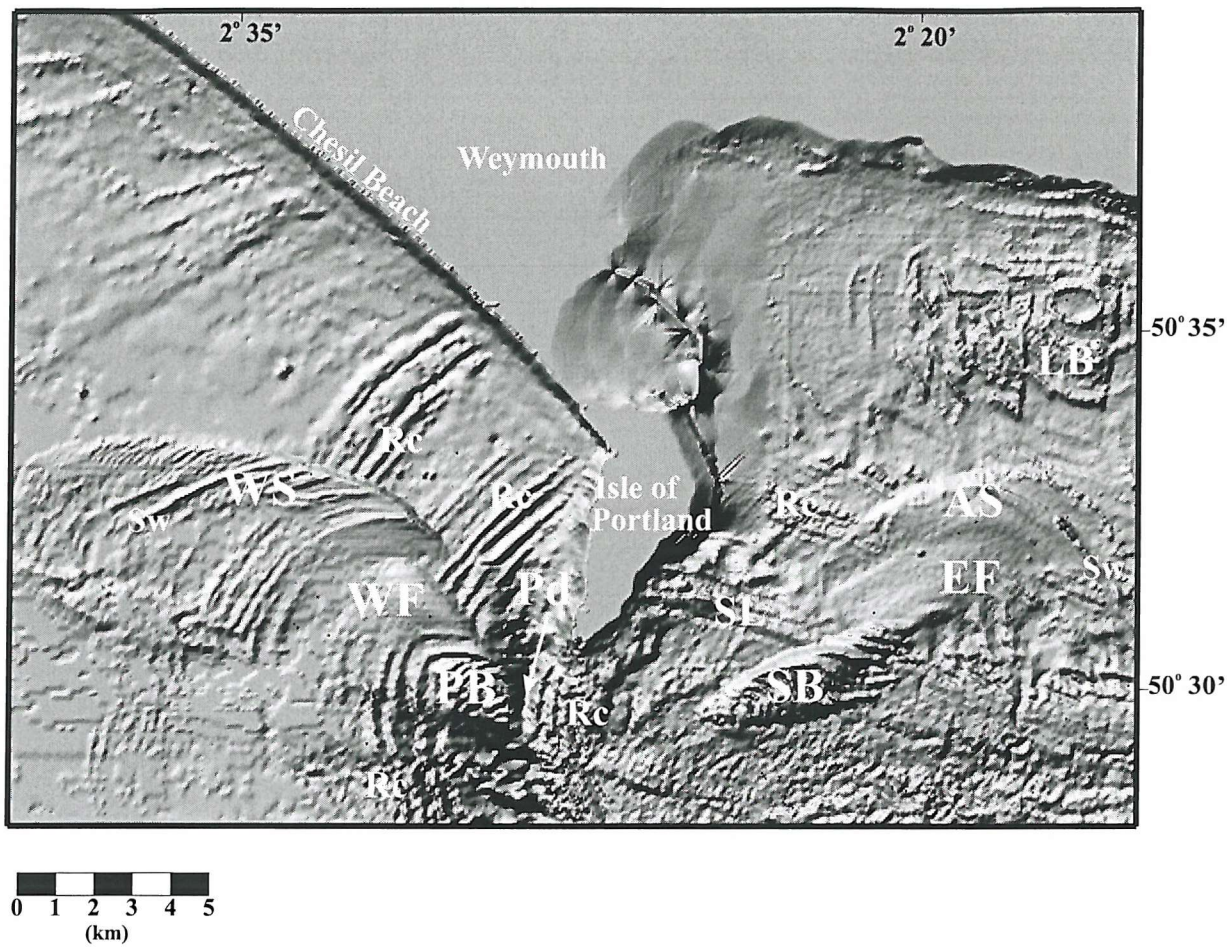

Figure 8.3. Seabed "shaded relief" map of the study area showing the most prominent topographic features (Note: Map derived from a version of the bathymetric chart shown as Figure 2b.). Key: SB-Shambles Bank; AS-Adamant Shoal; EF- East Flat; PB-Portland Bank; WF – West Flat; WS- West Shoal; SSt – Rippled sand sheet; LB- Lulworth Banks; SL-Shambles Ledge; Rc- Rock outcrop; Sw – very large sandwaves; Pd – Portland Deep .

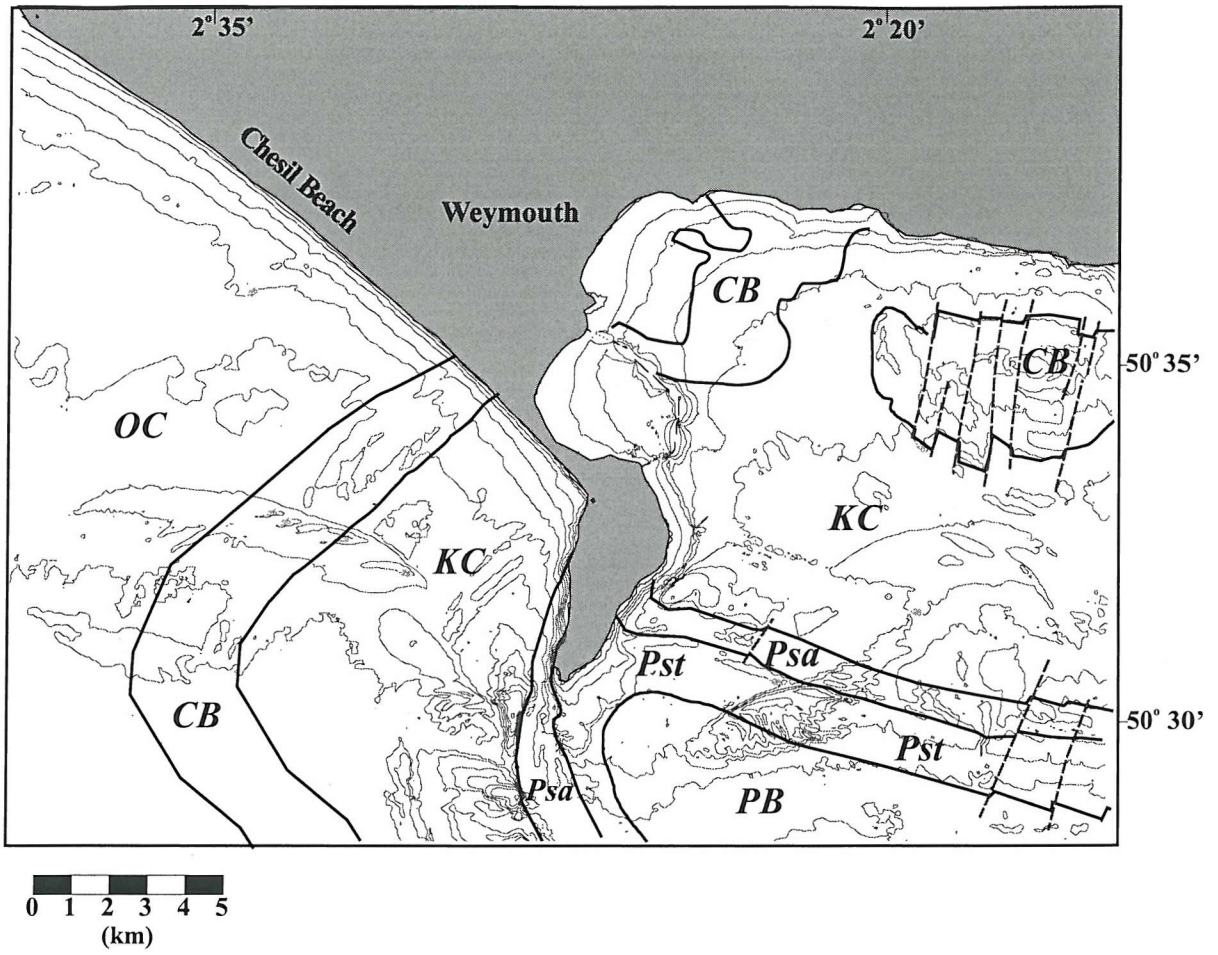

Figure 8.4. Offshore solid geology map, superimposed upon the bathymetry (after Donovan and Stride, 1961a). Key: OC – Oxford Clay, KC – Kimmeridge Clay, CB – Corallian Beds, Pst – Portland Stone, Psa – Portland Sands and PB – Purbeck Beds.

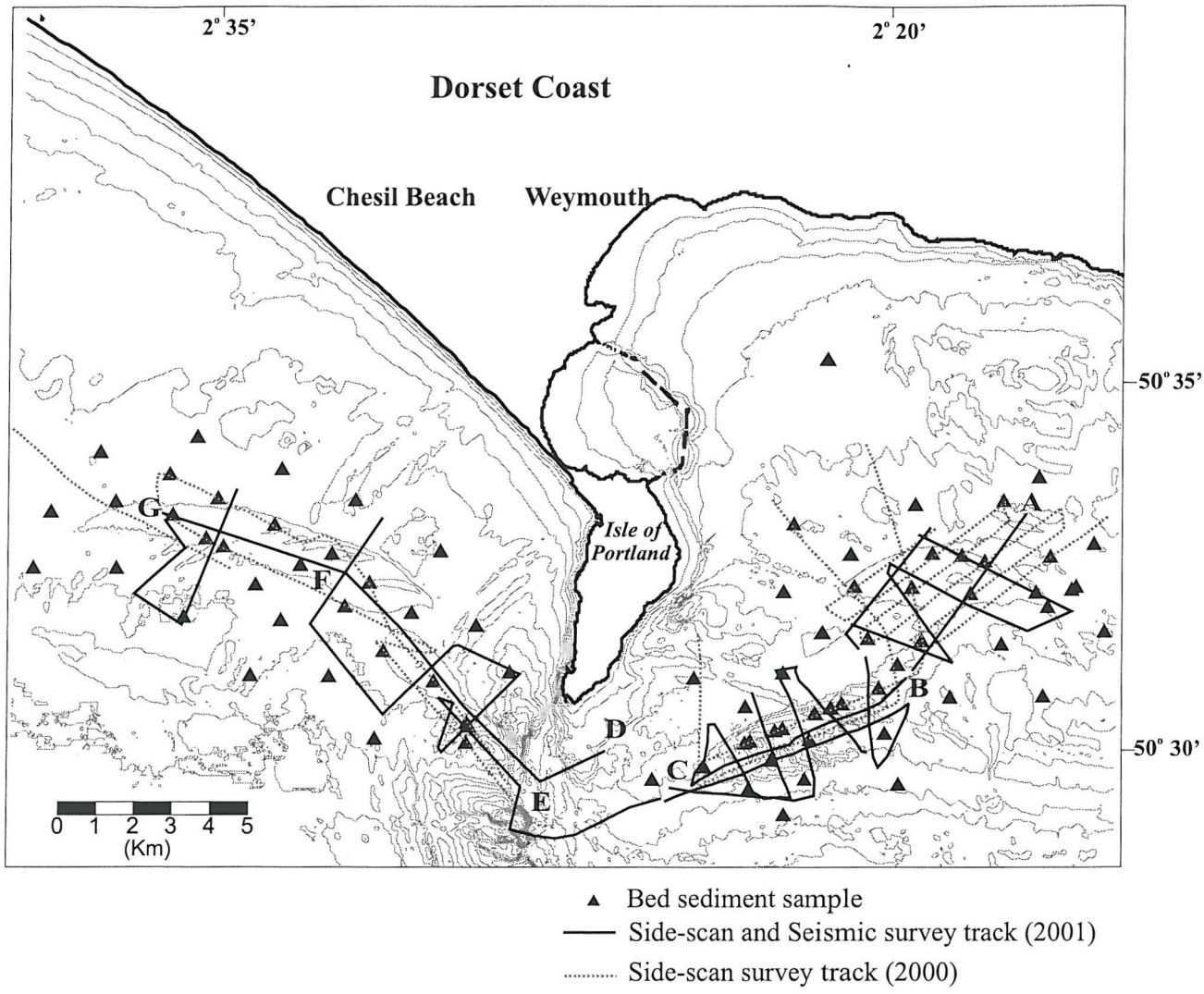

Figure 8.5. Location of the collected seabed sediment samples, side-scan sonar and seismic survey tracks.

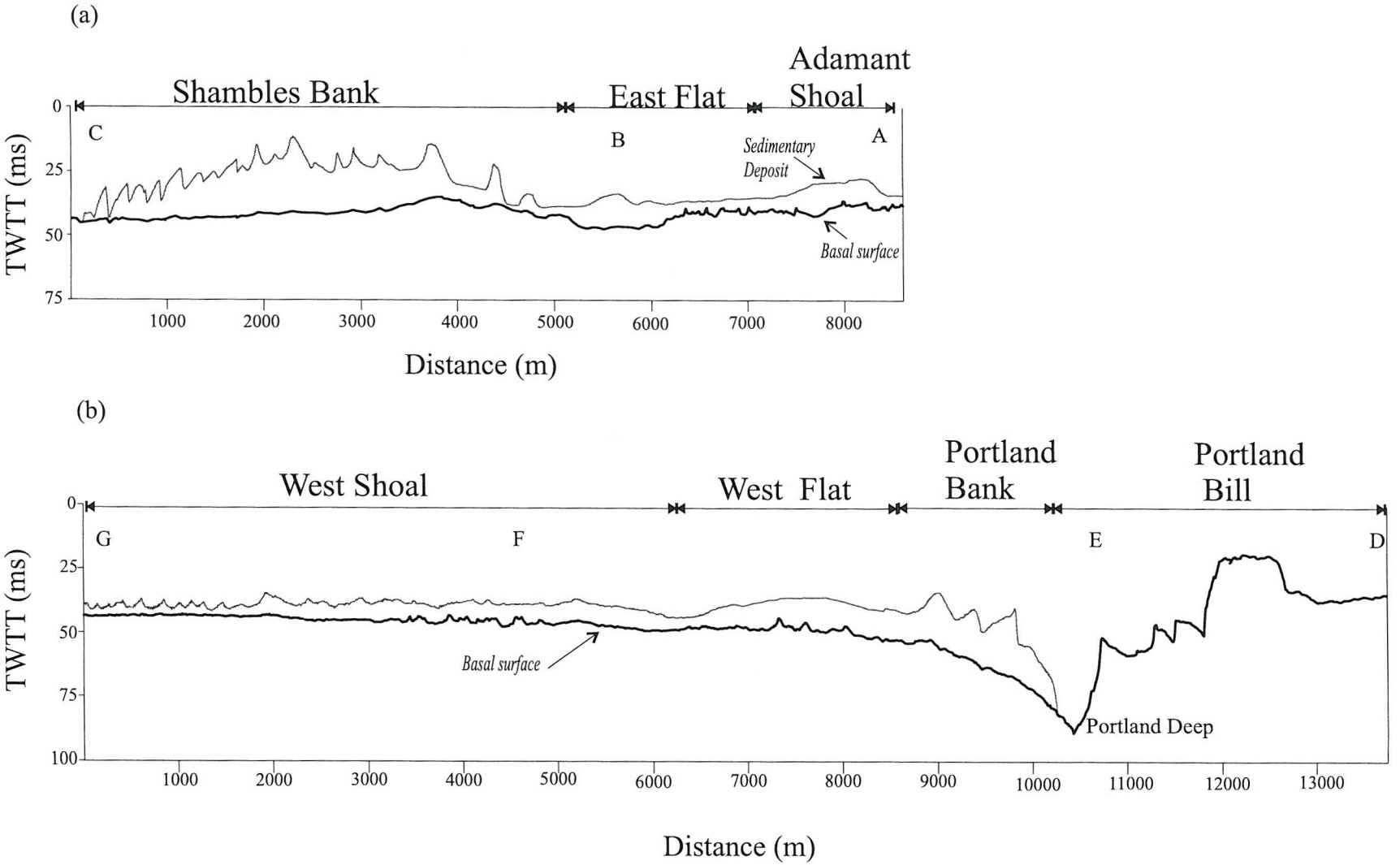

Figure 8.6. Longitudinal section through the deposits showing their thickness and the spatial relation with the basal surface. For location refer to Figure 8.5.

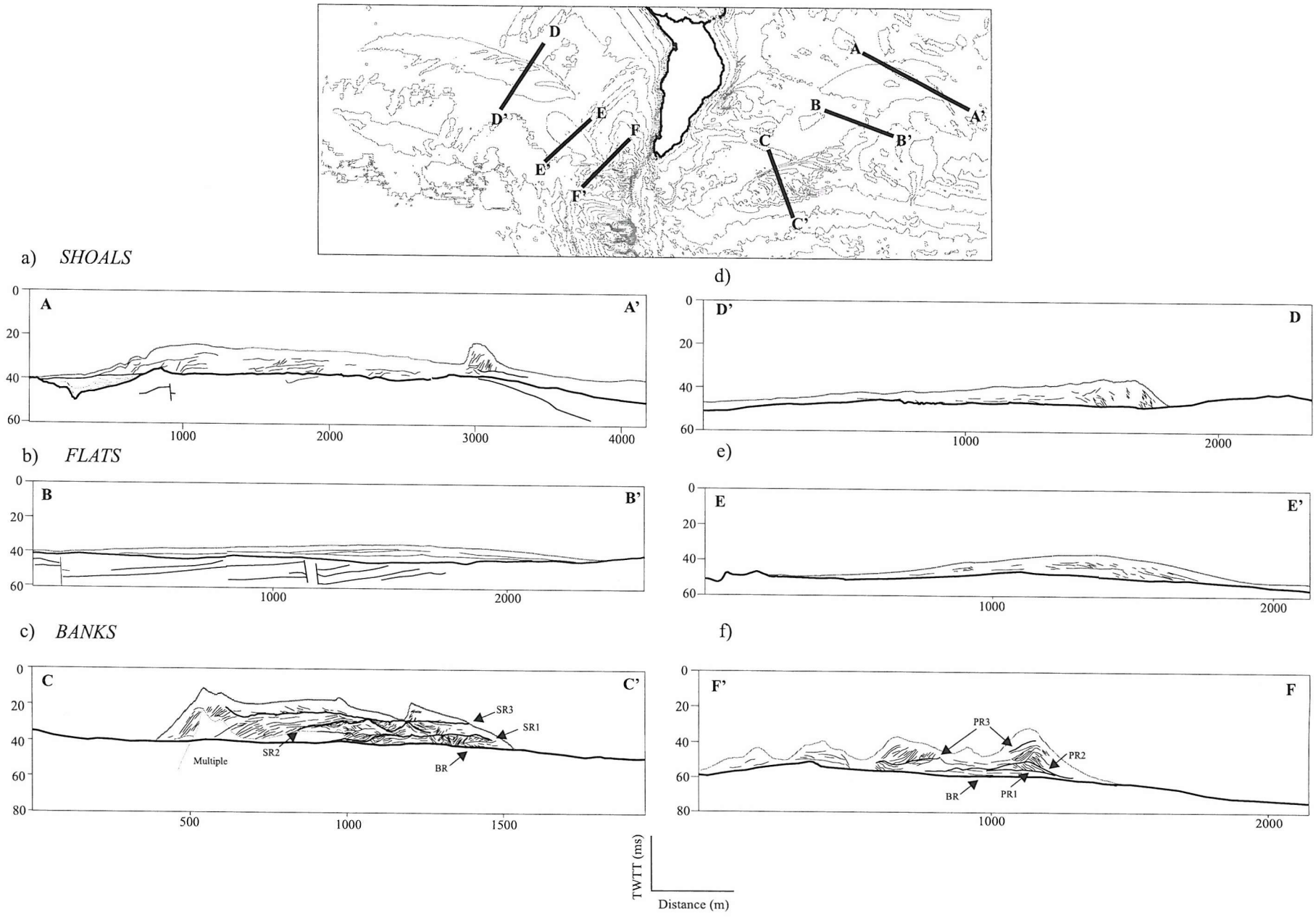

Figure 8.7. Transverse sections showing the architecture and internal structure of the deposits. (a) Adamant Shoal; (b) East Flat; (c) Shambles Bank, showing the three first-order reflectors (SR1, SR2 and SR3); (d) West Shoal; (e) West Flat; and (F) Portland Bank, showing the three first-order reflectors (PR1, PR2 and PR3).

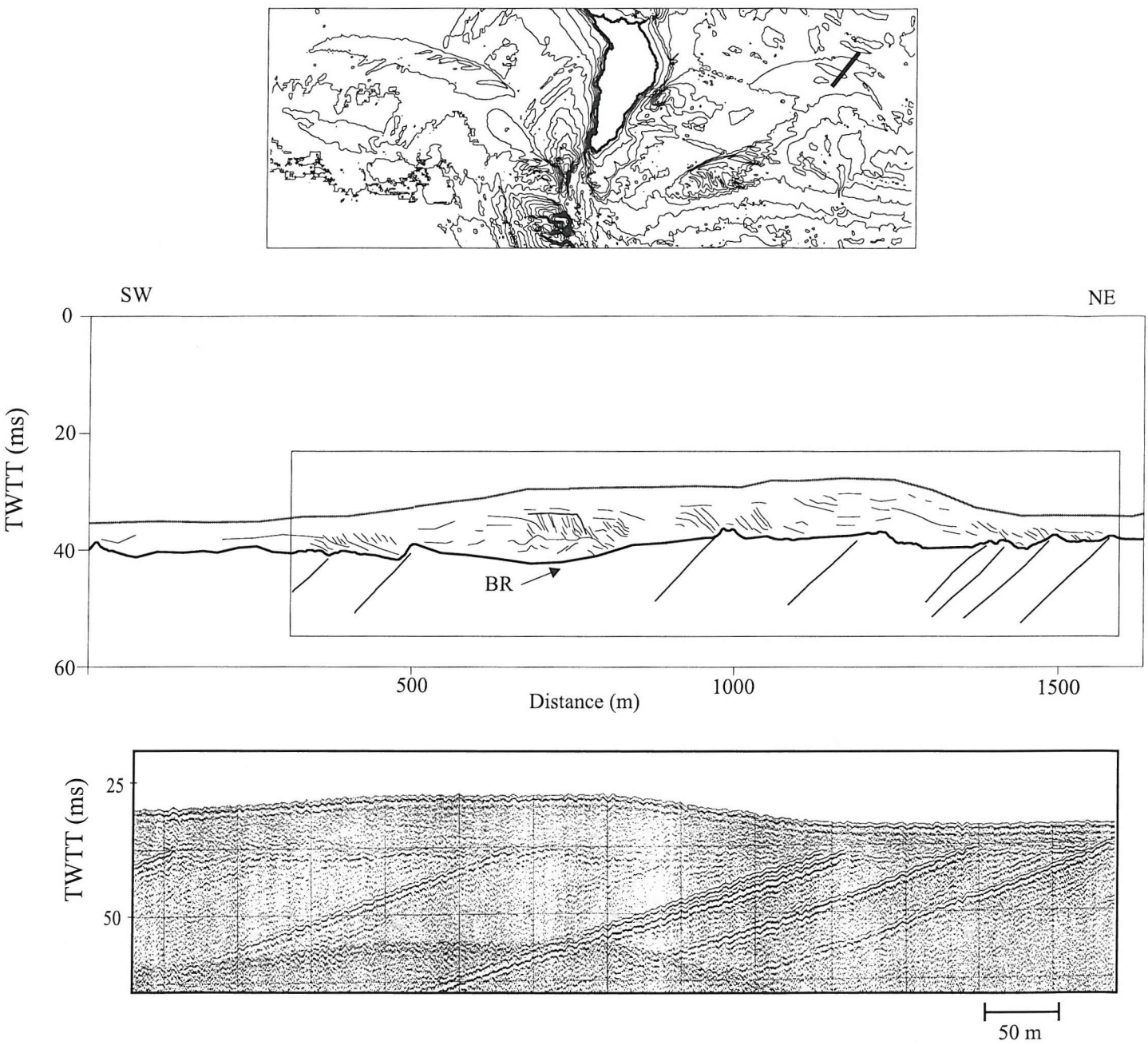

Figure 8.8. Transverse seismic section along the Adamant Shoal, with the corresponding interpretation. The asymmetric profile of the shoal and the occurrence of clinoforms suggest a long-term migration of the shoal towards the coast.

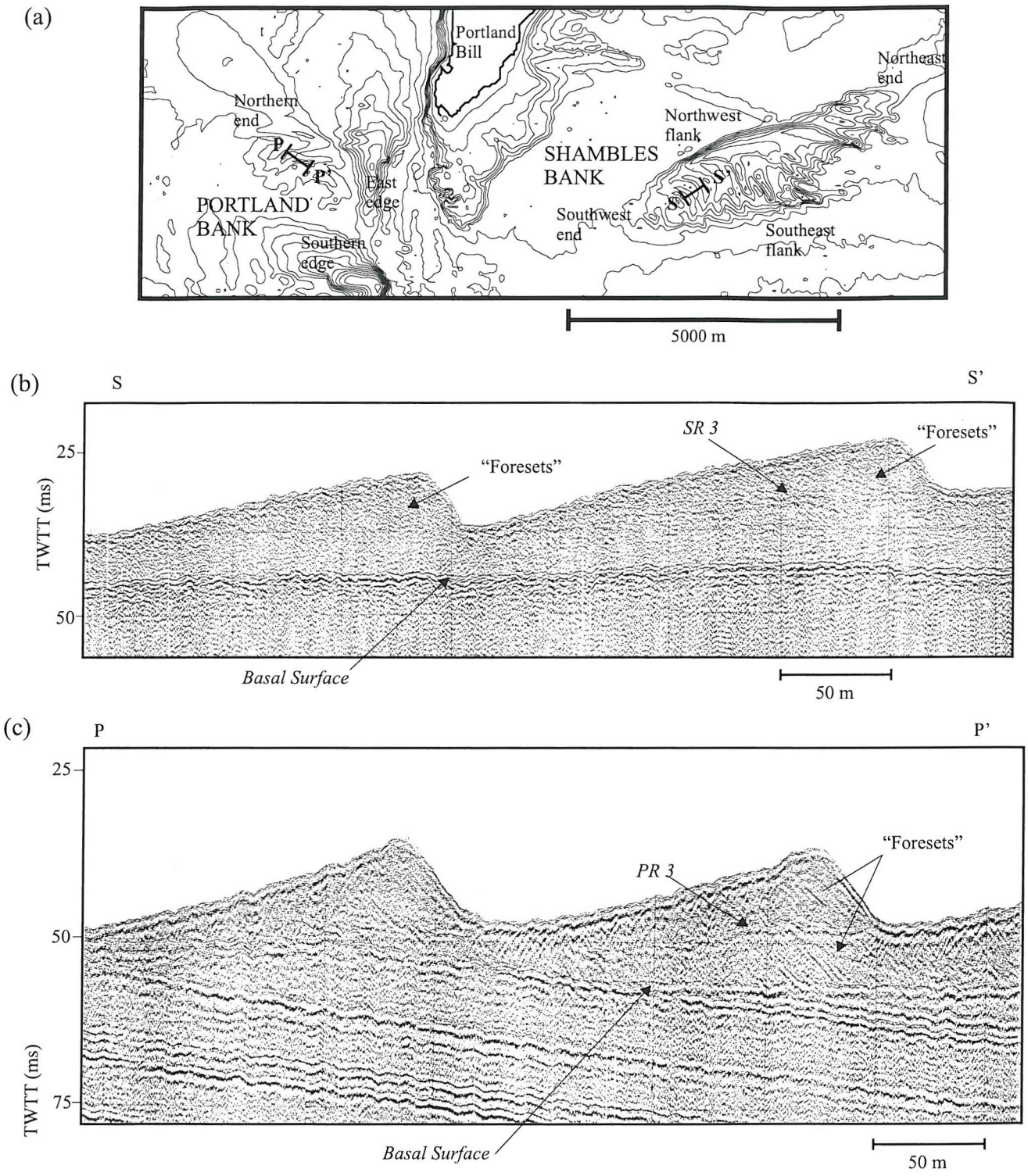

Figure 8.9. Longitudinal seismic sections showing the *sandwave-climbing pattern*. (a) Detailed morphology of the area around the tip of the headland and the location of the seismic profiles; (b) Section along the Shambles Bank, showing a flat horizontal basal surface with very large sandwaves overlying; and (c) Section along the Portland Bank showing an inclined basal surface with very large sandwaves overlying a sequence with foresets.

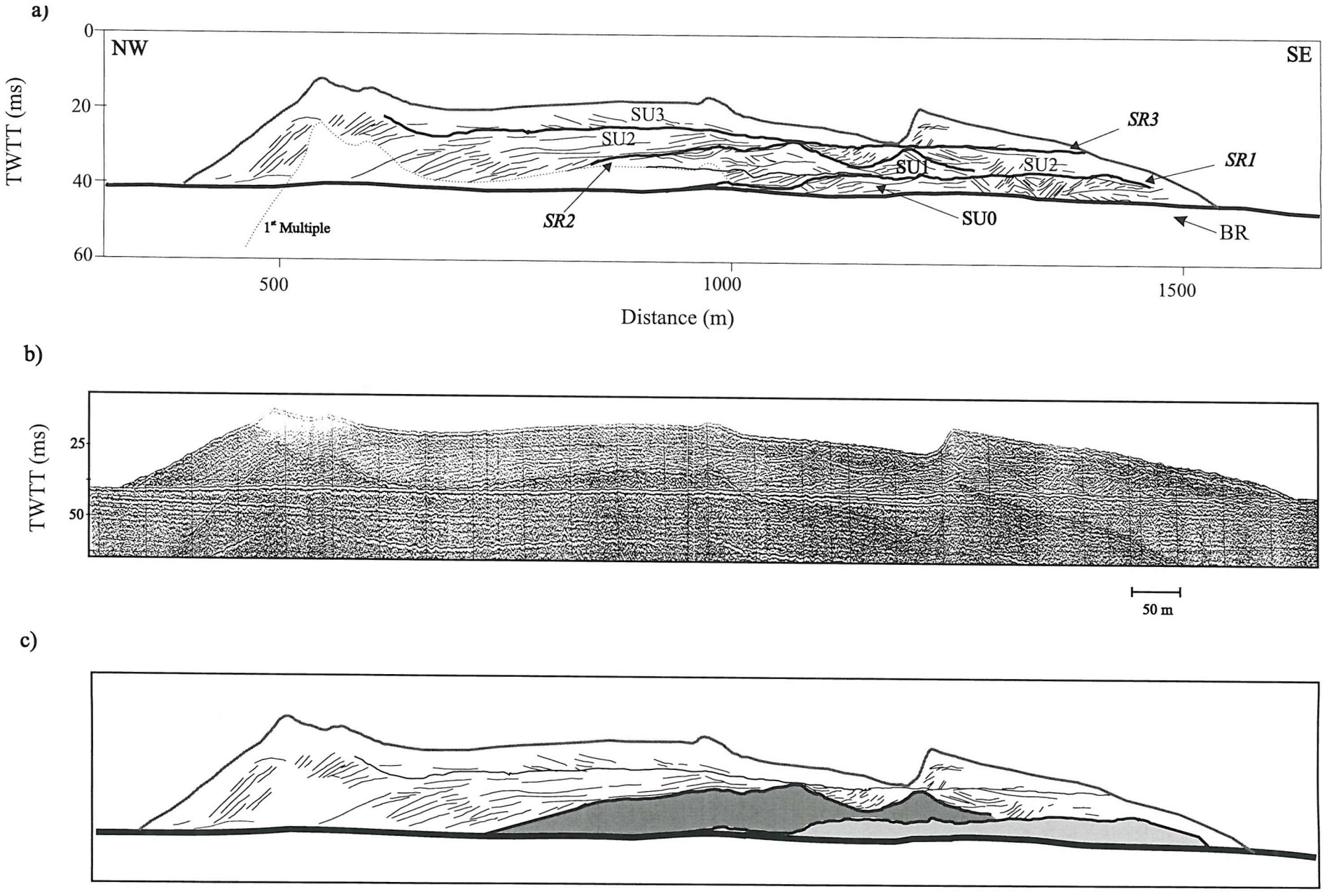

Figure 8.10. Transverse section across the Shambles Bank: (a) seismic section interpretation showing the bounding surfaces and seismic units; (b) transverse seismic section (for location refer to Figure 7); and (c) interpretation of the seismic units regarding their characteristics in relation to the bank evolution.

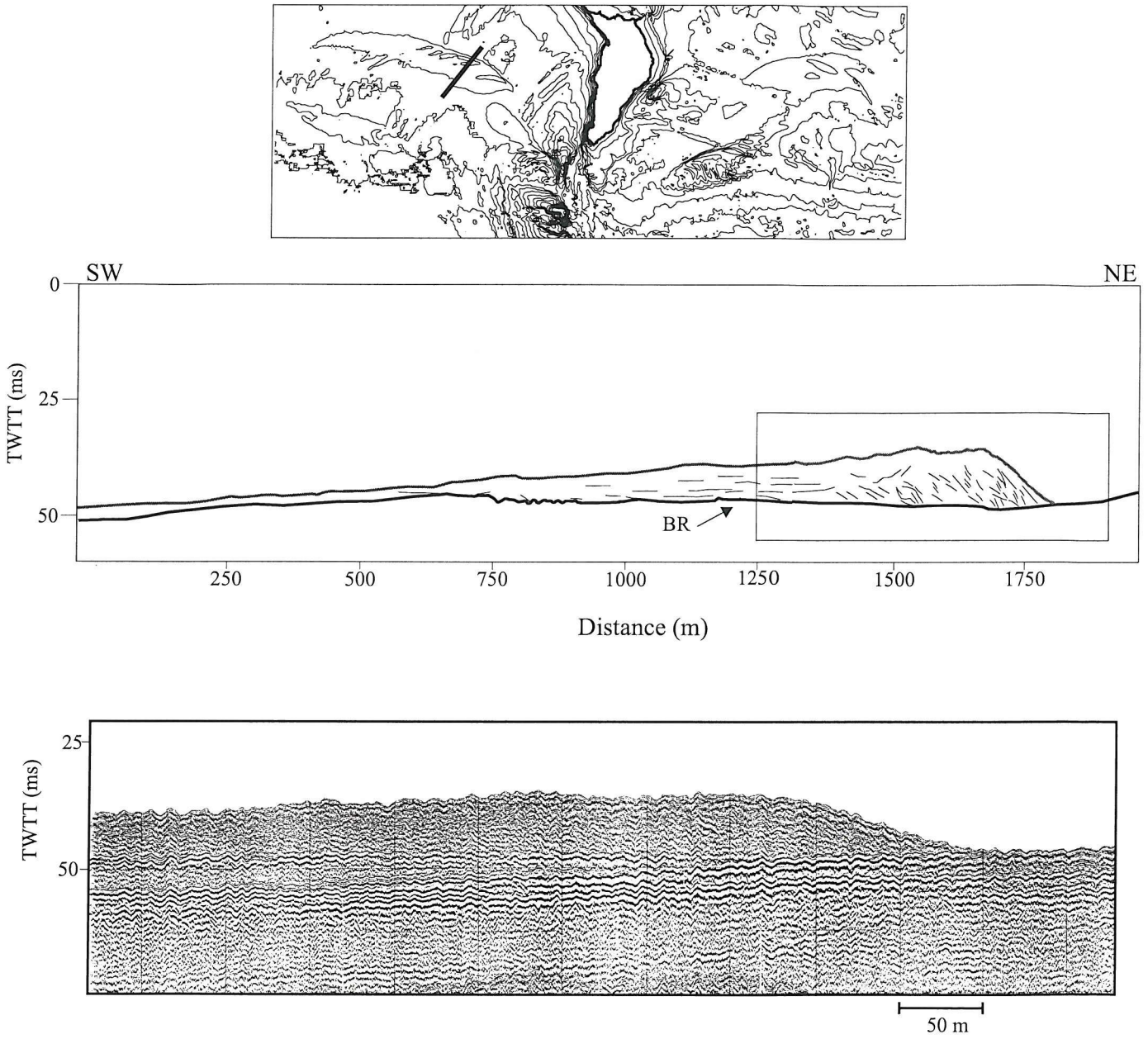

Figure 8.11. Transverse seismic section across the West Shoal. The asymmetric profile of the shoal and the occurrence of clinoforms observed over this section suggest long-term migration of the shoal towards the coast, as for the Adamant Shoal (refer to Fig. 8.8)

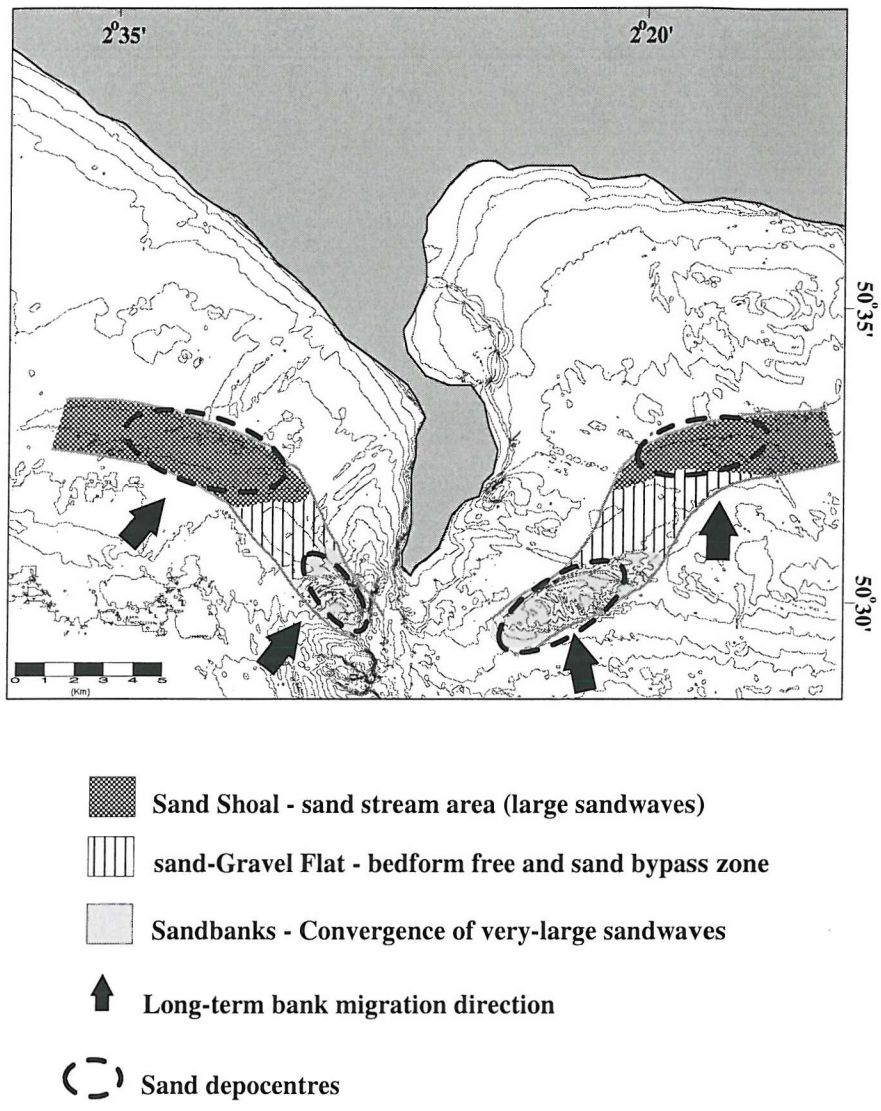

Figure 8.12. Regional distribution of the headland-associated sedimentary deposits (HSD), indicating the occurrence of two depocentres and the long-term bank migration direction.

Chapter 9

Conclusions and Recommendations for Future Research

9.1 Synthesis

The present study has investigated the sedimentary processes and deposits associated with a coastal headland. A range of different scientific approaches was undertaken, in order to develop and expand upon the scientific understanding of such processes and deposits: (a) numerical modelling (including tidally-induced flow, sand transport and wave refraction); (b) *in situ* hydrodynamic data collection; and (c) geophysical surveys and sediment sampling, including mapping of the seabed facies and bedform distribution (using side-scan sonar) and identification of the internal structure of the deposits (using an high-resolution seismic profiler).

The collection and collation of the scientific data during the present research, has permitted a comprehensive and critical review of the existing knowledge to be undertaken; this led to the formulation of an integrated (generic) conceptual model of sedimentary processes and deposits, associated with headlands.

A review of existing published information has revealed that various studies have been undertaken, in order to investigate the formation and evolution of tidally-induced eddies around headlands (Pingree, 1978; Pingree and Maddock, 1979; Ferentinos and Collins, 1980; Zimmerman, 1981; Robinson, 1983; Signell and Geyer, 1991; and Davis *et al.*, 1995). However, the influence of such headland-associated eddies, on the sedimentary processes (erosion, transport and deposition), had been considered originally only from a physical oceanography perspective (Pingree, 1978; Ferentinos and Collins, 1980), or using numerical models of an idealised coastline geometry and tidal forcing (Signell and Harris, 2000).

The sedimentological implication of the development of such eddies has been described elsewhere, in terms of the occurrence of sandbanks associated with headlands. The formation of such banks can be explained by, for example, the "tidal-stirring" concept (Pingree, 1978); this suggests that headland-associated sandbanks are formed within the central part of residual eddies. Moreover, this concept predicts the occurrence of asymmetric sandbanks associated

with headlands i.e. sandbanks of different scales, when the Coriolis effect (or planetary vorticity) is significant, compared to inertial and pressure gradient forces (Pingree, 1978). However, for an idealised situation, it has been observed elsewhere that the Coriolis force did not compare strongly to the relative vorticity of the residual circulation. Instead, the formation of such sandbanks was found to be related to patterns of bed shear stress and sediment flux during a tidal cycle (Signell and Harris, 2000).

It would appear that the existing concepts describing the formation of headland-associated sandbanks have not considered the process of sand transport around headlands; likewise, they have underestimated the importance of the morphological/sedimentological characteristics of the seabed. Against this background, the present research has attempted to fulfil these gaps in existing knowledge, by investigating sedimentary processes and deposits associated with a coastal headland.

The results obtained have shown that the process of sand dispersal, around a coastal headland, can be described in terms of a general conceptual model; this combines sand transport processes and the distribution of sedimentary deposits. The model defines the occurrence of two "sand mobile" (inner and outer zones) zones, with differing directions of bedload transport rate gradients. The boundary between these two zones defines a bedload convergence zone, which is associated with the occurrence of the sandbanks, on both sides of the headland. At the tip of the headland, a scour zone (or zone of maximum erosion) occurs; this is associated with bedrock exposed on the seabed.

Within this conceptual model, net bedload (sand) transport patterns were identified as being related to instantaneous gradients in the bed shear stress and bedload transport rates, during the flood and ebb flows, rather than the averaged (residual) flow. During the evolution of the tidally-induced transient eddies, no current-induced bedload eddy is formed. Most of the bedload transport occurred during the period of maximum flood and ebb flows, when gradients in the bed shear stress and transport rates are also at maximum.

The distribution of sedimentary deposits over the inner continental shelf under investigation was used also to define a model for sand dispersal around the headland. A sequence of sedimentary deposits, described as headland-shelf deposits (HSD), was observed; these were found to be associated with a complex suite of bedforms and sedimentary facies. Such deposits have a reasonably symmetrical sigmoidal plan-view distribution, on both sides of the

headland; they are described, sequentially, towards the headland, as: sand shoals, or "sand streams" (the Adamant and West Shoals); sandy/gravel flats, representing sand bypass zones (the East and West Flats); and sandbanks, associated with zones of sand convergence (Shambles and Portland Banks). The HSD are isolated laterally, but are connected longitudinally. Both shoals and banks have an asymmetric cross-section steeper towards the coast, being the main depocentres over the area.

Sediment input to the shelf seems to be associated with coastal (cliff/beach) erosion and/or seabed sediment reworking and erosion of the (rock) seabed. Hence, in relation to the limited input of siliciclastic sediment presently, the surficial sediments of the area appear to be enriched constantly by the breakdown of skeletal debris; this is observed clearly on the Shambles and Portland Banks, where the nature of the sediments (80% carbonate content, associated with shell debris) is indicative of erosion of the surrounding seabed

These findings, described above, combined with the interpretation of the internal structure of the deposits, influence considerably the understanding of headland-associated sandbank formation and maintenance processes. Hence, the occurrence of headland-associated sandbanks is likely to be related to a larger sedimentary system, than assumed previously. The sandbanks are the high-energy end-members of a HSD sequence. The formation of the sandbanks was found (within the present investigation) to be the result of the strong convergent component of sand transport, induced by instantaneous gradients in bedload transport rates throughout the tidal cycle. The complex morphology and internal structure recognised for the sandbanks (especially the Shambles Bank) have confirmed that sedimentary processes controlling the evolution and maintenance of these banks are far more complex, than predictions related only to residual water circulation.

Based upon the observational data and the outputs obtained from numerical modelling, it was found that the processes of maintenance of a headland-associated sandbank can be described in terms of a combination of two different hydrodynamic and sediment dynamic processes, acting during the different phases (ebb and flood) of the tidal cycle. Within the context of the present study, it has been identified that the "tidal stirring" (Pingree, 1978), or the formation of transient eddies, control the sedimentary processes during the flood phase; the sandbank-induced bottom friction, as described by Huthnance's "stability model" (Huthnance, 1982), controls the sedimentary processes during the ebb flow. The maintenance of the sandbank can

be described in terms of an anticlockwise sand transport pattern around the bank, or a bedload convergence zone, along the crest.

In the particular case study presented here, the occurrence of asymmetric sandbanks (the Shambles and Portland Banks) adjacent to the headland was observed. One possible explanation for such development of asymmetric sandbanks could be the influence of storm wave activity, on either side of the headland. However, despite the observation that storm waves (Hs > 2 m; Tz >10 s) could disturb significantly the seabed over the area (they can, potentially, disturb a medium-grained sand bed, in water depths of up to 35m), no major difference in wave action was observed when comparing the (refracted) wave height distribution over the inner continental shelf, on both sides of the headland.

Nonetheless, around Portland Bill, the association of the distinct characteristics of the coastal geometry (headland geometry), seabed morphology (bathymetry) and solid geology (differential erosion) can be considered further, important, controlling parameters on sandbank formation and evolution around the Isle of Portland. A detailed analysis of the results for net bedload transport shows that the net transport rates are not distributed symmetrically around the headland tip, as would be expected for a situation where the length-scales (headland scale, tidal excursion and bottom friction) have, approximately, the same magnitude. The elongated Portland Deep, located to the west of the headland, constrains the growth of the Portland Bank; conversely, the Shambles Bank, to the east, rests upon a flat and broad basal surface. Such an interpretation has broader implications and applications in modelling the formation of headland-associated sandbanks, elsewhere.

Finally, the sedimentary processes associated with coastal headlands are characterised by a reasonably symmetric sequence of sedimentary deposits, associated with a complex suite of bedforms and sedimentary facies. The occurrence of such facies and deposits is controlled by instantaneous gradients in bed shear stress and sediment transport rates; these are related to the transient development of headland-eddies and the associated bedload transport. Hence, the use of residual circulation to describe patterns of sediment movement and deposition is most inappropriate, for this particular case. Moreover, because the formation and development of transient eddies is associated with a bottom frictional torque induced by increased velocity near the headland, the headland geometry and the seabed morphology are influencing, also, the spatial distribution of bed shear stress and sediment transport rates; these (headland

geometry and seabed morphology) may play a significant role in the formation and evolution of the resultant sedimentary facies and deposits (HSD), associated with headlands.

An integrated analysis of sediment dynamics, morphology and architecture of sedimentary deposits, together with spatial distribution and nature of the bedrock, indicates the hydrodynamic and morphological controls on the formation, evolution and maintenance of HSD.

9.2 Concluding Remarks and Recommendations

Overall, the results have shown that, in order to propose concepts for the formation and evolution of any sedimentary deposit, it is important to investigate and understand the associated sediment transport patterns; likewise, to characterise the sedimentary deposits and their regional context. The application of different scientific methods has provided results that have contributed, in different ways and perspectives, to a conceptual model derived on the basis of the results of the present study. This model has provided a sedimentological perspective on the formation and occurrence of headland-associated deposits, including sandbanks; investigation into its applicability to other settings is now required.

In spite of the advances made in the present research to this subject area, scientific questions remain. A summary of some of the unresolved problems, together with recommendations for future research, are outlined below.

(1) The physical parameters controlling the formation of asymmetric sandbanks require investigation, in a more quantitative manner, to complement the observations introduced and interpreted here. For example, examine the influence of the scale and geometry of the headland, on the formation of the sandbanks.
(2) For the specific area investigated here, the development and use of a morphodynamic model would permit the influence of different parameters, considered to be controlling the formation of asymmetric sandbanks, to be examined.
(3) The effect of waves on the development of tidally-induced transient eddies is still unclear; this needs to be assessed, probably in association with field data, in order to predict changes in the sand transport pathways.

(4) The dynamics of sandbanks and shoals, under the influence of combined (tidally- and wave-induced) flows requires further analysis, incorporating field observations. The collection of wave and current data, over and adjacent to the deposits, would permit a more comprehensive understanding to be developed of the influence of waves on the associated sand transport patterns.

(5) For the HSD studied here, a major gap in knowledge still remains associated with the collection of sedimentary cores; these should provide an improved interpretation of the stratigraphy of the deposits.

(6) Although the proposed conceptual model for sand transport around coastal headlands is capable of being extrapolated to other coastal areas, the presence of a sequence of sedimentary facies (as described here) has still to be verified elsewhere.

REFERENCES

Allen, J.R.L., 1968. *Current Ripples*. North-Holland, Amsterdam, 433pp.

Allison, R.J., 1991. *The Coastal Landforms of West Dorset*. Geologists' Association, London.130pp.

Amos, C.L., Bowen, A.J., Huntley, D.A. and Lewis, C.F.M., 1988. Ripple generation under the combined influences of waves and currents on the Canadian continental shelf. *Continental Shelf Research*, 8(10), 1129-1153.

Amos, C.L., Barrie, J.V. and Judge, J.T., 1995. Storm-enhanced sand transport in a macrotidal setting, Queen Charlotte Islands, British Columbia, Canada. In: *Tidal Signatures in Modern and Ancient Sediments* (Ed) Flemming, B. W. and Bartholoma, A. Blackwell Science, 53-70.

Ashley, G.M. et al., 1990. Classification of large-scale subaqueous bedforms: A new look at an old problem. *Journal of Sedimentary Petrology*, 60(1), 160-172.

Bagnold, R. A., 1963. Beach and nearshore processes. Part 1. Mechanics of marine sedimentation. In: *The Earth Beneath the Sea, Vol.* 3, (Ed). Hill, M. N. Wiley-Interscience,New York. 507-528

Bastos, A.C., Kenyon, N.H. and Collins, M.B., 2002. Sedimentary processes, bedforms and facies, associated with a coastal headland: Portland Bill, Southern UK. *Marine Geology* 187 (3-4), 235-258.

Belderson, R.H., 1986. Offshore tidal and non-tidal sand ridges and sheets: Differences in morphology and hydrodynamic setting. In: Knight, R.J. and McLean, J.R. (Ed.). *Shelf Sands and Sandstones*. Canadian Society of Petroleum Geologists, Memoir II, pp 293-301.

Belderson, R. H. and Stride, A. H., 1966. Tidal current fashioning of a basal bed. *Marine Geology*, 4, 237-257.

Belderson, R. H., Johnson, M. A., and Kenyon, N. H., 1982. Bedforms: In: *Offshore Tidal Sands: Processes and Deposits*, (Ed.) Stride, A. H.. Chapman and Hall,London, pp 27-57.

Bell, P., 2000. *Environmental Law*. Blackstone Press Ltd. 250pp

Berne, S., Lericolas, G., Marsset, T., Bourillet, J.F., and De Batist, M., 1998. Erosional offshore sand ridges and lowstand shorefaces: Examples from tide- and wave-dominated environments of France. *Journal of Sedimentary Research*, 68 (4), 540-555.

Berne, S., Trentesaux, A., Stolk, A., Missiaen, T., and de Batist, M., 1994. Architecture and long term evolution of a tidal sandbank: The Middelkerke Bank (southern North Sea). *Marine Geology,* 121, 57-72.

Berne, S., Castaing, P., Le Drezen, E. and Lericolas, G., 1993. Morphology, internal structure and reversal of asymmetry of large subtidal dunes in the entrance to Gironde Estuary (France). *Journal of Sedimentary Research*, 65(5), 780-793.

Berne, S., Auffret, J.P. and Walker, P., 1988. Internal structure of subtidal sand waves revealed by high-resolution seismic reflection. *Sedimentology*, 35, 5-20.

BGS, 1983a. Seabed sediments. Portland Sheet. British Geological Survey, Keyworth.

BGS, 1983b. Portland sheet. Solid geology. 1:250000 series. Keyworth, British Geological Survey.

Bijker, E.W., 1967. The increase in bed shear due to wave motion. *Proceedings of 10th Conference Coastal Engineering*, ASCE, 1, 57-72.

Boersma, J. R. and Terwindt, J. H. J., 1981. Neap-spring tide sequences of intertidal shoal deposits in a mesotidal estuary. *Sedimentology,* 28, 151-170.

Brampton, A., Evans, C.D.R. and Velegrakis, A.F., 1998. South Coast Mobility Study: West of the Isle of Wight. Construction Industry Research and Information Association (CIRIA) Report PR65. 201 pp.

Bray, M. J., 1997. Episodic shingle supply and the modified development of Chesil Beach, England. *Journal of Coastal Research*, 13(4), 1035-1049.

Bray, M. J., 1992. Coastal sediment supply and transport. In: *The Coastal Landforms of West Dorset*, (Ed) Allison, R.J.. Geologists' Association, London, 94-115.

Bray, M. J., Carter, D.J., and Hooke, J.M., 1995. Littoral cell definition and budgets for central southern England. *Journal of Coastal Research, 11,* (2)381-400.

Brown, C.B., 1950. In: *Engineering Hydraulics,* (Ed.) Rouse, H., Wiley, New York, 1039pp

Cacchione, D.A. and Drake, D.E., 1990. Shelf sediment transport . In: *The Sea*, Vol.9, Ocean Engineering Science, (Ed.) LeMehaute, B. and Hanes, D.M., John Wiley & Sons, New York, 729-774.

Cacchione, D.A., Drake, D.E., Ferreira, J.T. and Tate, G.B., 1994. Bottom stress estimates and sand transport on northern California inner continental shelf. *Continental Shelf Research*, 14(10/11), 1273-1289.

Calvete, D., Walgreen, M., De Swart, H.E., and Falques, A., 2001. A model for sand ridges on the shelf: Effect of tidal and steady currents. *Journal of Geophysical Research*, 106 (C5), 9311-9325.

Carr, A.P. and Blackley, M.W.L., 1974. Ideas on the origin and development of Chesil Beach, Dorset. Proc. *of the Dorset Natural History and Archaeological Society*, 95, 9-17.

Carr, A.P. and Blackley, M.W.L., 1973. Investigations bearing on the age and development of Chesil Beach, Dorset, and the associated area. *Trans. Inst. Brit. Geogr.*, 58, 99-111.

Carr, A.P., 1969. Size grading along a pebble beach: Chesil Beach, England. Journal *Sedimentary Petrology*, 39, 297-311.

Caston, V.N.D., 1972. Linear sandbanks in the southern North Sea. *Sedimentology*, 18, 63-78.

Christoffersen, J.B. and Jonsson, I.G., 1985. Bed friction and dissipation in a combined current and wave motion. *Ocean Engineering*, 12(5), 387-423.

Collins, M.B., Shimwell, S.J., Gao, S., Powell, H., Hewitson, C., and Taylor, J.A., 1995. Water and sediment movement in the vicinity of linear sandbanks: The Norfolk Banks, southern North Sea. *Marine Geology*, 123, 125-142.

Collins, M.B. and Rigler, J.K., 1982. The use of settling velocity in defining the initiation of motion of heavy mineral grains under unidirectional flow. *Sedimentology*, 29, 419-426.

Cowel, P.J. and Thom, B.G., 1994. Morphodynamics of Coastal Evolution. In: *Coastal Evolution: Late Quaternary shoreline morphodynamics,* (Ed) Carter, R.W.G. and Woodroffe, C.D. Cambridge Univ. Press, 33-86.

Curry, D., 1989. The rock floor of the English Channel and its significance for the interpretation of marine unconformities. *Proceedings Geological Association*, 100(3), 339-352.

Davies, P.A., Dakin, J.M. and Falconer, R.A., 1995. Eddy formation behind a coastal headland. *Journal of Coastal Research*, 11(1), 154-167.

Davies, A.G., Soulsby, R.L. and King, H.L., 1988. A numerical model of the combined wave and current bottom boundary layer. *Journal of Geophysical Research*, 93(C1), 491-508.

Davis, R.A. and Balson, P.B., 1992. Stratigraphy of a North Sea tidal sand ridge. *Journal of Sedimentary Research*, 62, 116-121.

De Moor, G. (1989) Maintenance of the Flemish Banks. In: *The Quaternary and Tertiary Geology of the Southern Bight, North Sea* (Eds J.P. Henriet and G. de Moor), Ministry of Economic Affairs – Belgium Geological Society, Bruxelles, 185-228.

De Vriend, H.J., 1990. Morphological Processes in Shallow Tidal Seas. In: *Residual Currents and Long Term Transport*, (Ed) Cheng, R. T. Springer Verlag, 276-301.

Dewez, S., Clabaut, P., Vicaire, O., Beck, C., Chamley, H. and Augris, C., 1989. Transits sedimentaires resultants aux confins Manche-mer du Nord. *Bulletin de la Societe Geologique de France*, 5, 1043-1053.

Dolan, R., Hayden, B. and Felder, W., 1979. Shoreline periodicities and linear offshore shoals. *Journal of Geology,* 87, 393-402.

D'Olier, B. (1981) Sedimentary events during the Flandrian sea-level rise in the south-west corner of the North Sea. In*: Holocene Marine Sedimentation in the North Sea Basin* (Ed) S.D. Nio, R.T.E. Schuttenhelm and T.C.E van Weering), *Special Publication International Association of Sedimentologists*, 5, 221-227.

Donovan, D. T. and Stride, A. H., 1961(a). An acoustic survey of the seafloor south of Dorset and its geological interpretation. *Phil. Trans. Royal Soc London*, 244(712), 299-330.

Donovan, D. T. and Stride, A. H., 1961(b). Erosion of a rock floor by tidal sand streams. *Geological Magazine*, 48(5), 393-398.

Drake, D.E. and Cacchione, D.A., 1992. Wave-current interaction in the bottom boundary layer during storm and non-storm conditions: observations and model predictions. *Continental Shelf Research*, 12, 1331-1352.

Draper, L., 1991. Wave Climate of the Brtish Isles. HMSO, London.

Draper, L., 1977. Waves at Shambles Light Vessel, Portland Bill, during 1968. In: *A Voyage of Discovery* (Ed) Angel, M. Pergamon Press, Oxford, pp 429-438.

Dyer, K. R. and Huntley, D. A., 1999. The origin, classification and modelling of sandbanks and ridges. *Continental Shelf Research*, 19, 1285-1330.

Dyer, K.R. and Soulsby, R.L., 1988. Sand transport on the continental shelf. *Annual Reviews in Fluid Mechanics*, 20, 295-324.

Dyer, K. R., 1986. *Coastal and Estuarine Sediment Dynamics*. Chichester: John Wiley. 342 p.

Dyer, K. R., 1980. Velocity profiles over a rippled bed the threshold of movement of sand. *Estuarine Coastal Marine Science*, (10)181-199.

Ebersole, B.A., Cialone, M.A., and Prater, M.D., 1986. Regional Coastal Processes Numerical Modeling System Report 1 RCPWAVE-A Linear Wave Propagation Model for Engineering Use. Technical Report CERC-86-4, US Army Engineer Waterway Experiment Station, Vicksburg.

Einstein, H.A., 1950. The bedload function for sediment transportation in open channel flows. Soil Cons. Serv. U.S. Dept. Agric. Tech. Bull.

Emery, K.O., 1952. Continental shelf sediments off southern California. *Bulletin Geological Society of America*, 63, 1105-1108.

Engelund, F. and Hansen, E., 1972. A monograph in sediment transport in alluvial streams. Technical Press, Copenhangen. 62pp.

Evans, G., 1992. Some aspects of continental shelf sedimentation: a discussion on "The rock floor of the English Channel and its significance for the interpretation of marine unconformities" by Curry (1989) and "Growth and burial of the English Channel unconformity" by Stride (1990). *Proceedings Geological Association*, 103, 155-158.

Ferentinos, G. and Collins, M. B., 1980. Effetcs of shoreline irregularities on a rectilinear tidal current and their significance in sedimentation processes. *Journal of Sedimentary Petrology*, 50(4), 1081-1094.

Flemming, B.W., 1980. Sand transport and bedform patterns on the continental shelf between Durban and Port Elizabeth (Southeast African continental margin). *Sedimentary Geology*, 26, 179-205.

Folk, R.L., 1980. *Petrology of Sedimentary Rocks*. Hemphill Publishing Company, Austin, Texas (USA). 182pp.

Fredsoe, J., 1984. Turbulent boundary layer in wave-current motion. *Journal Hydraulic Engineering*, 110, 1103-1120.

Fredsoe, J. and Deigaard, R., 1992. *Mechanics of Coastal Sediment Transport*. 3rd Ed. Advanced Series on Ocean Engineering, Vol. 3, World Scientific Publishing, London. 369pp.

Fry, V.A. and Aubrey, D.G., 1990. Tidal velocity asymmetries and bedload transport in shallow embayments. *Estuarine, Coastal and Shelf Science*, 30(5), 453-473.

Gadd, P. E., Lavelle, J. W., and Swift, D. J., 1978. Estimate of sand transport on the New York shelf using near-bottom current meter observations. *Journal of Sedimentary Petrology*, 48, 239-252.

Geyer, W. R., 1993. Three-dimensional tidal flow around headlands. *Journal of Geophysical Research*, 98(C1), 955-966.

Geyer, W. R. and Signell, R. P., 1990. Measurements of tidal flow around headland with a shipboard Acoustic Doppler Current Profiler. *Journal of Geophysical Research*, 95(C3), 3189-3197.

Grant, W.D. and Madsen, O.S., 1986. The continental shelf bottom boundary layer. *Annual Reviews Fluid Mechanics*, 18, 265-305.

Grant, W.D. and Madsen, O.S., 1982. Movable bed roughness in unsteady oscillatory flow. *Journal of Geophysical Research*, 87(C1), 469-481.

Grant, W.D. and Madsen, O.S., 1979. Combined wave and current interaction with a rough bottom. *Journal of Geophysical Research*, 84(C4), 1797-1808.

Green, M.O., Vincent, C.E., McCave, I.N., Dickson, R.R., Rees, J.M. and Pearson, N.D., 1995. Storm sediment transport: observations from the British North Sea shelf. *Continental Shelf Research*, 15(8), 889-912.

Grochowski, N. T. L. and Collins, M. B., 1994. Wave activity on the seabed of the English Channel: A note. *Journal of Marine Biological Association UK*, (74)739-742.

Grochowski, N. T. L., Collins, M. B., Boxall, S. R., and Salomon, J. C., 1993. Sediment transport predictions for the English Channel, using numerical models. *Journal Geological Society of London*, 150, 683-695.

Guy, H.P., Simons, D.B. and Richardson, E.V., 1966. Summary of alluvial channel data from flume experiments, 1956-61. U.S. Geological Survey Professional Paper, 426-I. 96pp.

Hamblin, R.J.O., Crosby, A., Balson, P.S., Jones, S.M., Chadwick, R.A., Penn, I.E., and Arthur, M.J., 1992. *The Geology of the English Channel*. UK Offshore Regional

Report 10. British Geological Survey, Her Majesty's Stationary Office, London. 106pp.

Hardcastle, P. J. and King, A. C., 1972. Chesil Beach sea wave record. *Civil Eng. Pub. Works Rev.*, 67, 299-300.

Harris, P. T., Pattiaratchi, C., Collins, M. B., and Dalrymple, R. W., 1995. What is a bedload parting? In: *Tidal Signatures in Modern and Ancient Sediments* (Ed) Flemming, B. W. and Bartholoma, A. Blackwell Science, pp 3-18.

Hawkins,A.B. and Sebbage,M.J.,1972. The reversal of sand waves in the Bristol Channel. *Marine Geology*, 12, M7-M9.

Heathershaw, A.D., 1988. Sediment transport in the sea, on beaches and in rivers: Part I-fundamental principles. *Journal of Naval Science*, 14(3), 154-170.

Heathershaw, A. D., 1981. Comparisons of measured and predicted sediment transport rates in tidal currents. *Marine Geology*, 42, 75-104.

Heathershaw, A. D. and Hammond, A. D. C., 1980. Secondary circulation near sandbanks and in coastal embayments. *Deutsche Hydrographische Zeitschrift*, 33(4), 135-151.

Hervouet, J. M., 1991. TELEMAC, a fully vectorised finite element software for shallow water equations. HE43/91-27, Electricite de France.

Hjulstrom, F., 1939. Transportation of detritus by moving water. In: *Recent Marine Sediments*, (Ed) Trask, P.D., Thomas Murby. 5-31.

Houbolt, J.J.H.C., 1968. Recent sediments in the southern bight of the North Sea. *Geologie Mijnbouw*, 47, 245-273.

House, M.R., 1983. *Geology of the Dorset Coast*. Geologists' Association Guide, London.

Houthuys, R. Trentesaux, A., De Wolf, P., 1994. Storm influences on a tidal sandbank's surface (Middelkerke Bank, southern North Sea). *Marine Geology*, 121, 23-41.

HR Wallingford, 1998. Durlston Head to Portland Bill Shoreline Management Plan. Report EX 3824, HR Wallingford. Wallingford, UK. 25pp.

Hulscher, S.J.M.H., 1996. Tide-induced large-scale regular bed form patterns in a three-dimensional shallow water model. *Journal of Geophysical Research*, 101, 207270-20744.

Hulscher, S.J.M.H. and van den Brink, G.M., 2001. Comparison between predicted and observed sand waves and sand banks in the North Sea. *Journal of Geophysical Research*, 106 (C5), 9327-9338.

Hulscher, S.J.M.H., De Swart, H.E. and De Vriend, H.J., 1993. The generation of offshore tidal sand banks and sand waves. *Continental Shelf Research*, 13, 1183-1204.

Huthnance, J.M., 1982(a). On one mechanism forming linear sand banks. *Estuarine Coastal Marine Science*, 14, 79-99.

Huthnance, J.M., 1982(b). On the formation of sand banks of finite extent. *Estuarine Coastal Marine Science*, 15, 277-299.

Huynh-Thanh, S. and Temperville, A., 1991. A numerical model of the rough turbulent boundary layer in combined wave and current interaction. In: *Sand transport in Rivers, Estuaries and the Sea*, (Ed.) Soulsby, R.L. and Bettess, R., Balkema, Rotterdam, 93-100.

Imasato, N., 1983. What is tide-induced residual current? *Journal of Physical Oceanography*, 13, 1307-1317.

Johnson, D.W., 1919. *Shore processes and shoreline development*. John Wiley & Sons, New York. 583pp.

Johnson, M. A., Kenyon, N. H., Belderson, R. H., and Stride, A. H., 1982. Sand Transport. In: *Offshore Tidal Sands: Processes and Deposits*, (Ed) Stride, A. H.. Chapman and Hall, London, pp 58-94.

Jonsson, I.G., 1966. Wave boundary layers and friction factors. *Proc. 10th Conference Coastal Engineering*, Tokyo, Japan. 127-148.

Kachel, N.B. and Sterneberg, R.W., 1971. Transport of bedload as ripples during an ebb current. *Marine Geology*, 10, 229-244.

Kapsdali, M.S. and Dyer, K.R., 1986. Threshold conditions for sand movement on a rippled bed. *Geo-Marine letters*, 6, 161-164.

Kenyon, N. H., 1994. Evaluation of seabed character and sediment processes in Weymouth Bay (UK). Technical Report Amoco. 25pp.

Kenyon, N. H. and Stride, A. H., 1970. The tide-swept continental shelf sediments between the Shetland Isles and France. *Sedimentology*, 14, 159-173.

Kenyon, N. H., Belderson, R. H., Stride, A. H., and Johnson, M. A. ,1981. Offshore tidal sandbanks as indicators of net sand transport and as potential deposits. In: *Holocene Marine Sedimentation in the North Sea Basin,* (Ed) S.D. Nio, R.T.E. Schuttenhelm and T.C.E van Weering), *Special Publication International Association of Sedimentologists*, 5, 257-268.

Komar, P.D., 1976. *Beach Processes and Sedimentation*. New Jersey: Prentice-Hall. 429 p.

Komar, P.D. and Clemens, K.E., 1986. The relationship between a grain's settling velocity and threshold of motion under unidirectional currents. *Journal Sedimentary Petrology*, 56, 258-266.

Komar, P.D. and Li, Z., 1986. Pivoting analyses of the selective entrainment of sediments by shape and size with application to gravel threshold. *Sedimentology*, (33)425-436.

Komar, P.D. and Miller, M.C., 1973. The threshold of sediment movement under oscillatory water waves. *Journal Sedimentary Petrology*, (43)1101-1110.

Komar, P.D. and Miller, M.C., 1975. On the comparison between the threshold of sediment motion under waves and unidirectional currents with a discussion of the practical evaluation of the threshold. *Journal Sedimentary Petrology*, (45)362-367.

Laban, C. and Schuttenhelm, R.T.E. (1981) Some new evidence on the origin of the Zealand Ridges. In: *Holocene Marine Sedimentation in the North Sea Basin,* (Ed) S.D. Nio, R.T.E. Schuttenhelm and T.C.E van Weering, *Special Publication International Association of Sedimentologists*, 5, 239-245.

Lanckneus, J., van Lancker, V., Moerkerke, G., van den Eynde, D., Fettweis, M., de Batist, M., and Jacobs, P., 2001. Investigation of the natural sand transport on the Belgian continental shelf. BUDGET, Final Report. Federal Office for Scientific, Technical and Cultural Affairs (OSTC), Belgium. 104pp.

Lanckneus, J., and de Moor, 1995. Bedforms on the Middelkerke Bank, southern North Sea. In: *Tidal Signatures in Modern and Ancient Sediments* (Ed) Flemming, B. W. and Bartholoma, A. Blackwell Science, 33-51.

Lanckneus, J., De Moor, G. and Stolk, A., 1994. Environmental setting, morphology and volumetric evolution of the Middelkerke Bank (southern North Sea). *Marine Geology*, 121, 1-21.

Larsonneur, C. Bouysse, P. and Auffret, J.P. 1982. The superficial sediments of the English Channel and its Western Approaches. *Sedimentology*, 29, 851-864.

Leeder, M.R., 1999. *Sedimentology and Sedimentary Basins: from Turbulence to Tectonics.* Blackwell Science, Oxford. 591pp.

Li, M. Z., Amos, C. L. and Heffler, D.E., 1997. Boundary layer dynamics and sediment transport under storm and non-storm conditions on the Scotian shelf. *Marine Geology*, 141, 157-181.

Li, M. Z. and Amos, C. L., 1995. SEDTRANS92: A sediment transport model for continental shelves. *Computers & Geosciences*, 21(4), 533-554.

Li, Z. and Komar, P.D., 1986. Laboratory measurements of pivoting angles for application to selective entrainment of gravel in a current. *Sedimentology*, 33, 413-423.

Liu, H.K., 1957. Mechanics of sediment ripple formation. *Journal Hydraulic Div.*, 83, 1-23.

Maa, J.P.Y. and Hobbs, III., 1998. Physical impact of waves on adjacent coasts resulting from dredging at Sandbridge Shoal, Virginia. *Journal of Coastal Research*, **14** (2), 107-113.

MacDonald, N.J. and O'Connor, B.A., 1996. Changes in wave impact on the Flemish coast due to increased means sea level. *Journal of Marine Systems*, 7, 133-144.

Maddock, L. and Pingree, R.D., 1978. Numerical simulation of the Portland tidal eddies. *Estuarine and Coastal Marine Science*, 6, 353-363.

McCave, I.N. and Langhorne, D.N., 1982. Sandwaves and sediment transport around the end of a tidal sand bank. *Sedimentology*, 29, 95-110.

Middleton, G.V. and Southard, J.B., 1984. *Mechanics of Sediment Movement.* SEPM Short Course N3, Tulsa, Oklahoma, USA. 401pp.

Miller, M.C., McCave, I.N., and Komar, P.D., 1977. Threshold of sediment motion under unidirectional currents. *Sedimentology,* 24, 507-527.

Mitchum, R.M., Vail, P.R. and Sangree, J.B. (1977) Stratigraphic interpretation of seismic reflection patterns in depositional sequences. In: *Seismic Stratigraphy – Application to Hydrocarbon Exploration,* (Ed) C.E. Payton), *American Association of Petroleum Geologists*, Memoir 26, 117-133.

Nikuradse, J., 1933. Stromungsgesetze in rauhen Rohren. VDI Forschungsheft 361, Berlin. English Translation: Laws of flow in rough pipes. National Advisory Comm. Aeronautics, Tech. Mem. 1292 (translated in 1950).

Nittrouer, C.A. and Wright, L.D., 1994. Transport of particles across continental shelves. *Reviews of Geophysics*, 32 (1), 85-113.

Nunny, R. S., 1995. The physical environment: sediments, Vol. 2. Lyme Bay Environmental Study, Technical Report Kerr-McGee Oil (UK). 75pp.

Off, T. ,1963. Rhythmic linear sand bodies caused by tidal currents. *Bulletin American Association Petroleum Geology,* 47, 324-341.

Owen, P.R., 1964. Saltation of uniform grains in air. *Journal of Fluid Mechanics*, 20(2), 225-242.

Paphitis, D., Collins, M.B. Nash, L.A., and Wallbridge, S., 2002. Settling velocities and entrainment thresholds of biogenic sands (shell fragments) under unidirectional flow. *Sedimentology*, 49, 211-225.

Paphitis, D., 2001. Sediment movement under unidirectional flows: an assessment of empirical thresholds curves. *Coastal Engineering*, 43, 227-245.

Pattiaratchi, C. and Collins, M.B., 1988. Wave influence on coastal sand transport paths in a tidally dominated environment. *Ocean and Shoreline Management*, 11, 449-465.

Pattiaratchi, C. and Collins, M. B., 1987. Mechanisms for linear sandbank formation and maintenance in relation to dynamical oceanographic observations. *Progress in Oceanography,* 19, 117-176.

Pattiaratchi, C. and Collins, M. B., 1985. Sand transport under the combined influence of waves and tidal currents: an assessment of available formulae. *Marine Geology*, 67, 83-100.

Pattiaratchi, C., James, A., and Collins, M. B., 1986. Island wakes and headland eddies: A comparison between remotely sensed data and laboratory experiments. *Journal of Geophysical Research*, 92(C1), 783-794.

Pingree, R. D., 1978. The formation of the Shambles and other banks by tidal stirring of the seas. *Journal of the Marine Biological Association U K*, 58, 211-226.

Pingree, R. D. and Griffiths, D. K., 1979. Sand transport paths around the British Isles resulting from M2 and M4 tidal interactions. *Journal Marine Biology Association UK*, 59, 497-513.

Pingree, R. D. and Maddock, L., 1979. The tidal physics of headland flows and offshore tidal bank formation. *Marine Geology*, 32, 269-289.

Pond, S. and Pickard, G.L, 1983. *Introductory Dynamical Oceanography. 2nd Ed.*, Butterworth Heinemann Ltd. 329 p.

Powell, H.J., 1996. Water and sediment movement in the vicinity of linear sandbanks: the Norfolk Banks, southern North Sea. Unpublished PhD Thesis, University of Southampton, Dept. Oceanography. 250pp.

Pugh, D.T. 1987. *Tides, Surges and Mean Sea-Levels*. Chichester: John Wiley and Sons. 472p.

Robinson, I. S., 1981. Tidal vorticity and residual circulation. *Deep Sea Research*, 28A, 195-212.

Robinson, I. S., 1983. Tidally induced residual flows. In: *Physical Oceanography of Coastal and Shelf Seas*, 35, (Ed) Johns, B. Elsevier,Oxford, pp 321-356.

Shepard, F.P., 1932. Sediments on continental shelves. *Bulletin Geological Society of America*, 43, 1017-1034.

Shields, A., 1936. Anwendung der Ahnlichkeits-Mechanik und der Turbulenzforschung auf die Geschiebebewegung. Preussische Versuchsanstalt fur Wasserbau und Schiffbau, Berlin. 26pp. Translation: Application of similarity principles and turbulence research to bedload movement. Translated by Ott, W.P. and van Uchelen, J.C. WM Keck Lab. Of Hydraulics and Water Resources, Report 167, 26pp.

Signell, R. P. and Geyer, W. R., 1991. Transient eddy formation around headlands. *Journal of Geophysical Research*, 96(C6), 2561-2575.

Signell, R. P. and Harris C. K., 2000. Modeling sandbank formation around tidal headlands. In: *Proceedings 6th International Conference Estuarine and Coastal Modelling*, (Ed.) Spaulding, M.L. and Blumberg, A.F. New Orleans, LA, November 1999. ASCE Press.

Sleath, J.F.A., 1991. Velocities and shear stresses in wave-current flows. *Journal of Geophysical Research*, 96 (C8), 15237-15244.

Sleath, J.F.A., 1984. *Seabed Mechanics*. John Wiley & Sons Inc. New York, USA. 335pp.

Smith, J. D. , 1977. Modelling of sediment transport on continental shelves. In: *The Sea, Vol. 6*, (Ed) Goldberg, E.D., McCave, I.N., O'Brien, J.J., and Steele, J.H. Wiley-Interscience, New York, 539-576.

Smith, J.D., 1969. Geomorphology of a sand ridge. *Journal of Geology*, 77, 39-55.

Snedden, J.W. and Dalrymple, R.W., 1999. Modern shelf sand ridges: from historical perspective to a unified hydrodynamic and evolutionary model. In: Isolated Shallow Marine Sand Bodies: Sequence Stratigraphic Analysis and Sedimentological Interpretation, (Ed) Bergman, K.M. and Snedden, J.W. SEPM Special Publication, Tulsa, USA. pp 13-28.

Soulsby, R.L., 1997. *Dynamics of Marine Sands*. Thomas Telford, London. 249pp.

Soulsby, R.L., 1995. Bed shear stresses due to combined waves and currents. In: *Advances in Coastal Morphodynamics*, (Ed.) Stive, M.J.F., de Vriend, H.J., Fredsoe, J., Hamm, L., Soulsby, R.L., Teisson, C. and Winterwerp, J.C. Delft Hydraulics, Netherlands, 4.20-4.23.

Soulsby, R.L., 1993. Modelling of coastal processes. *Proceedings 1993 MAFF Conference of River and Coastal Engineers*, Loughborough, UK, 111-118.

Soulsby, R.L., 1983. The bottom boundary layer of shelf seas. In: *Physical Oceanography of Coastal and Shelf Seas*, 35, (Ed) Johns, B. Elsevier,Oxford, pp 189-266.

Sternberg, R. W., 1972. Predicting initial motion and bedload transport of sediment particles in the shallow marine environment: In: *Shelf sediment transport, processes and pattern,* (Ed)Swift, D. J., Duane, D. B., and Pilkey, O. H. Dowden, Hutchison and Ross, Inc., Stroudsburg, Pennsylvania. pp61-83.

Sternberg, R.W., 1968. Friction factors in tidal channels with differing bed roughness. Marine *Geology*, 6, 243-260.

Stride, A. H., 1963. Current-swept sea floors near the southern half of Great Britain. *Quarterly Journal Geological Society*, 119, 175-199.

Stride, A.H., 1990. Growth and burial of the English Channel unconformity. *Proceedings Geological Association*, 101(4), 335-340.

Stride, A. H., Belderson, R. H., Kenyon, N. H. and Johnson, M. A., 1982. Offshore tidal deposits: sand sheet and sand bank facies: In: *Offshore Tidal Sands: Processes and Deposits*, (Ed) Stride, A. H. Chapman and Hall, London. 58-94.

Stride, A. H., Belderson, R. H. and Kenyon, N. H., 1972. Longitudinal furrows and depositional sand bodies of the English Channel. *Mem B R G M*, (79)233-240.

Sugimoto, T., 1975. Effect of boundary geometries on tidal currents and tidal mixing. *Journal of the Oceanographical Society of Japan*, 31, 1-14.

Sunamura, T., 1993. *Geomorphology of Rocky Coasts*. Wiley, Chichester, 302pp.

Swart, D.H., 1976. Predictive equations regarding coastal transport. *Proceeding 15th Conference Coastal Engineering*, ASCE, 1113-1132.

Swift, D. J. ,1975. Tidal sand ridges and shoal-retreat massifs. *Marine Geology*, 18, 105-134.

Swift, D. J., 1970. Quaternary shelves and the return to grade. *Marine Geology*, 8, 5-30.

Swift, D.J.P. and Thorne, J.A. (1991) Sedimentation on continental margins, I: a general model for shelf sedimentation. In: *Shelf Sands and Sand Bodies: Geometry Facies and Sequence Stratigraphy* (Ed) D.J.P. Swift, G.F. Oertel, R.W. Tillman and J.A. Thorne. *International Association of Sedimentologists Special Publication*, 14, 3-31.

Swift, D.J.P. and Field, M.E., 1981. Evolution of a classic sand ridge field: Maryland sector, North American inner shelf. *Sedimentology*, 28, 461-482.

Swift, D. J., Stanley, D.J. and Curry, J.R., 1971. Relict sediment on continental shelves: a reconsideration. *Journal Geology*, 79, 322-346.

Tee, K., 1976. Tide-induced residual current, a 2-D nonlinear numerical tidal model. *Journal of Marine Research*, 34, 603-628.

Terwindt, J. H. J. and Brouwer, M. J. N., 1986. The behaviour of intertidal sandwaves during neap-spring tide cycles and the relevance for paleoflow reconstruction. *Sedimentology*, 33, 1-31.

Tessier, B., Corbau, C., Chamley, H. and Auffret, J.P., 1999. Internal structure of shoreface banks revealed by high-resolution seismic reflection in a macrotidal environment (Dunkerque Area, Northern France). *Journal of Coastal Research*, 15 (3), 593-606.

Trowbridge, J.H., 1995. A mechanism for the formation and maintenance of shore-oblique sand ridges on storm-dominated shelves. *Journal of Geophysical Research*, 100 (C8), 16071-16086.

Van Rijn, L.C., 1993. *Principles of Sediment Transport in Rivers, Estuaries and Coastal Seas*. Aqua publications, Amsterdam. 620pp.

Van Veen, J., 1935. Sandwaves in the Southern North Sea. *International Hydrology Review*, 12, 21-29.

Vianna, M.L., Solewicz, R., Cabral, A.P. and Testa, V., 1991. Sandstream on the northeast Brazilian Shelf. *Continental Shelf Research*, 11(6), 509-524.

West, I.A., 2001. *West's Geology Resources* –Internet site: www.soton.ac.uk/~imw/index.htm School of Ocean and Earth Sciences, Southampton University, UK. version: U29.05.02.

Whitehouse, R.J.S., 2001. Understanding the behaviour and engineering significance of offshore and coastal sandbanks. HR Wallingford, Report SR 512. 30pp.

Wiberg, P.L. and Rubin, D. M., 1989. Bed roughness produced by saltating sediment. *Journal of Geophysical Research*, 94(4), 5011-5016.

Wiberg, P.L. and Smith, J.D., 1983. A comparison of field data and theoretical models for wave-current interactions at the seabed on the continental shelf. *Continental Shelf Research*, 2, 147-162.

Williams, J.J., MacDonald, N.J., O'Connor, B.A. and Pan, S., 2000. Offshore sandbank dynamics. *Journal of Marine Systems*, 24, 153-173.

Williams, J.J. and Rose, C.P., 2001. Measured and predicted rates of sediment transport in storm conditions. *Marine Geology*, 179, 121-133.

Wolanski, E., Imberger, J., and Heron, M., 1984. Island wakes in shallow coastal waters. *Journal of Geophysical Research*, 89, 10553-10569.

Wright, L. D. ,1995. *Morphodynamics of Inner Continental Shelves.* CRC Press,Boca Raton.241pp.

Yalin, M.S., 1972. *Mechanics of sediment transport.* Pergamon Press, Oxford. 290p.

Yang, C. and Sun, J., 1988. Tidal sand ridges on the East China Sea shelf. In: *Tide-Influenced Sedimentary Environments and Facies,* (Ed) P.L. de Boer *et al.* Reidel Publishing Co., Dordrecht, 23-38.

Zimmerman, J. T. F., 1981. Dynamics, diffusion and geomorphological significance of tidal residual eddies. *Nature*, 290, 549-555.